MOTION AND FORCE CONTROL OF FLEXIBLE JOINT ROBOT MANIPULATORS

by

ATEF TANIOUS MASSOUD MOSSAD, B. Sc. Hons. (Mech. Eng.), M. Sc.

A Thesis

Submitted to the School of Graduate Studies

in partial Fulfillment of the Requirements

for the Degree

Doctorate of Philosophy

McMaster University

MOTION AND FORCE CONTROL OF FLEXIBLE JOINT ROBOT MANIPULATORS

DOCTOR OF PHILOSOPHY (1994) McMASTER UNIVERSITY

(Mechanical Engineering) Hamilton, Ontario, Canada

TITLE: Motion and Force Control of Flexible Joint Robot Manipulators

AUTHOR: Atef Tanious Massoud Mossad
B. Sc. Hons. (Mech. Eng.) (Cairo University)
M. Sc. (Mech. Eng.) (Cairo University)

SUPERVISOR: Dr. Hoda A. ElMaraghy

NUMBER of PAGES: xv, 198

ABSTRACT

Excitation of lightly damped drive system resonances severely limits the performance of most current robotic manipulators. Also, many industrial applications require the control of the contact forces in order to execute contact tasks properly. This dissertation discusses the development and experimental verification of advanced high performance control algorithms in order to control the position and contact force of nonlinear manipulators with flexibilities which reside in the drive systems. An experimental two–link planar manipulator has been designed and constructed to test the control algorithms. The developed manipulator exhibits damped drive system resonances and highly nonlinear and coupled dynamics.

Several techniques for controlling the position and force of flexible joint robot manipulators are developed and evaluated. A collocated Proportional–Derivative controller is implemented to demonstrate the limitation of such a controller which is commonly used for industrial robots. Then, a fourth order feedback linearizable model is constructed and analyzed. A feedback linearization controller is designed, simulated and implemented in the joint space as a preliminary investigation of the feedback linearization performance. Results proved a tracking performance superior to that of the PD controller and support applying feedback techniques for position and force control.

Two model–based position and force control approaches based on feedback linearization concept are developed, simulated and implemented. The dynamic hybrid controller deals with the contact with rigid environments while the impedance control deals with performing free and/or contact with compliant environment motions. The results indicate excellent performance in tracking the position and regulating the contact force. These two approaches serve as basic structure for the design of robust and adaptive controllers.

A robust sliding mode controller is designed, simulated and implemented to maintain the model–based tracking performance in the presence of payload variations and other parametric uncertainty. The problem is formulated by using the feedback linearizable model and the constraint imposed by the contact environment, to characterize the disturbance caused by parametric uncertainty in the system. In addition, the effect of parametric uncertainty on computing the unmeasured state elements is included in the analysis and the design of the robust controller. Results indicate that the controller obtains an excellent tracking performance in the presence of parametric uncertainty. This controller solves the problem of the necessity of the exact state of the feedback linearizable system for feedback. In addition, a specific relation between the uncertainty bounds and the achievable accuracy is derived. Another alternative to deal with parametric uncertainty is an adaptive cascade controller which is developed, simulated and implemented. It consists of a direct adaptive controller for the rigid dynamics and a Model Reference Adaptive Controller (MRAC) for the flexible dynamics. Results indicate good force tracking with slow position response. The cascade approach requires extremely fast actuator to achieve the feedback linearization results. A robust sliding mode observer is developed in order to estimate the unmeasured state elements of the feedback linearizable system in case of parametric uncertainty. This observer is useful for the successful application of adaptive feedback linearization algorithms. An adaptive feedback linearization control algorithm combined with the sliding mode observer is developed and simulated. The formulation enables designing adaptive laws using the original system state and the angular accelerations instead of the state of the feedback linearizable system and characterizing the stability of the overall system. The simulation results show the ability of the control algorithm to achieve position and force tracking by robust estimation of the state vector and updating of the robot parameters.

ACKNOWLEDGEMENT

I would like to thank my supervisor, Dr. Hoda A. ElMaraghy, for her guidance and support throughout the course of this research. I would like also to express my gratitude to the members of my supervisory committee Dr. N. H. Sinha and Dr. D. S. Weaver.

I am very grateful to Dr. Hoda ElMaraghy, the Mechanical Engineering Department, and McMaster University for the Research Scholarships, the Teaching Assistantships and the Scholarships I have received for financial support. I would like to thank the Mechanical Engineering Department secretaries Louise Perry, Jane Mah, Maryanne Hazelwood and Betty Bedell–Ryc and the FMS secretary Barbara Nethercot.

I would like to thank the System Manager and Programmer, Todd Pfaff, for his assistance in maintaining the software and providing the nice programming environment. I also appreciate the cooperation of Stacy Joseph, the Electrical Engineering summer trainee, in assisting during the course of the real time programming.

There are many people who helped in designing and building the experimental setup. I would like to thank Ron Lodewyks, Dr. W. H. ElMaraghy, Dr. K. Jankowski and Dr. Ahmed Zaki for their contributions during the design stage of the experimental robot. I appreciate the assistance and help of the technicians Ron Lodewyks, Joe Verhaege and Dave Schick. I would like to thank the machinist who manufactured the robot Jim McLaren

I appreciate the discussions and exchange of information with my friend and colleague Dr. Ahmed Zaki during the four and half years of this research.

Finally, I dedicate this work to my great parents, sisters and, brothers (I love you all).

TABLE OF CONTENTS

MOTION AND FORCE CONTROL OF FLEXIBLE JOINT ROBOT MANIPULATORS

LIST OF FIGURES

LIST OF TABLES

CHAPTER 1

INTRODUCTION

1.1 MOTIVATIONS

Robots as machines which can assist or replace humans in performing tedious and hazardous tasks have long been a dream of mankind. The application of robots in industry is increasing around the world. The science of robotics is still progressing to achieve better performance and to employ robots in many new and sophisticated applications. The progress in computers, sensors, materials, mechanical design, and control theories is continually leading to great developments and advances in robotics.

There are two main motivations for the research presented in this dissertation; joint flexibility in the mechanical arm and the need for controlling the contact forces and moments of the end effector. These are described in detail in the following three sections.

1.1.1 Joint Flexibility

Sweet et al. and Good et al. [111,33] have investigated the problem of robotic manipulation. Experimentally, they identified several aspects that limit the performance of a typical robot manipulator. One of the main aspects is the unmodelled dynamics, especially the flexibilities of the mechanical arm. For the particular manipulator tested, a resonance frequency of approximately 9 Hz was observed due to the joint torsional flexibility. Rivin [90] studied several robots and determined many sources of flexibility such as harmonic drives,

belts, chains, torsional shafts, gear reducers, etc. He also revealed that 80 to 98% of the flexibility in these robots resided in the drive system rather than in the links. Therefore, consideration of the joint flexibility in modelling and control can contribute to a better performance much more than link flexibility for most industrial robots. Even for direct drive robots when a link is remotely driven to increase the payload of the robot, the transmission mechanism introduces flexibility [24].

The existence of the flexibility at the robot joints causes lightly damped oscillations if the resonant modes are excited. Usually, this happens because the resonant frequencies, due to joint flexibility, have low values and hence they are inside the control bandwidth. Of course, joint flexibility decreases end–point accuracy. The worst effect is that it can cause control instability [26,27]. Limiting the control bandwidth to avoid exciting the resonant modes was suggested by Christian and Seering [14], but this limits the robot performance.

1.1.2 The Need for Force Control

The tasks performed by a robot manipulator can be classified into two categories. In the first one, the robot moves in free space carrying a load or manipulating some object. In this case, position control is adequate to perform the task successfully. While in the second class, the robot end effector comes into contact with an external environment. Tasks such as these appear in many industrial processes such as assembly, debburing, grinding, and the like. For these contact tasks position control is not adequate. For example, a very slight position error could lead to extremely large forces of interaction with disastrous consequences. Therefore, it is necessary to control the contact forces and moments at the end–effector in order to achieve a better task execution.

1.1.3 Position and Force Control for Flexible Joint Robot Manipulators

It was found that joint flexibility can deteriorate force trajectories at the interaction with an environment by limiting the control bandwidth and causing control instability. Although the problems of position control for flexible joint robots and position and force control for rigid robots have been studied separately, there is a lack in both theoretical and experimental efforts to investigate the combined problem which is controlling position and force for flexible joint robots. However, it is more critical to account for joint flexibility when dealing with force control rather than with pure position control [26,27].

1.2 OBJECTIVE AND APPROACH

The objective of the research reported in this dissertation was to investigate the control of position and force for mechanical manipulators in those cases where joint flexibility adversely affects performance, to develop new control strategies to improve performance, and to verify those strategies experimentally.

The approach followed in this research was to build an experimental robot manipulator which truly exhibits the problems which industrial robots have due to joint flexibility, develop a number of control algorithms which aim at controlling position and force for robots with joint flexibility, and experimentally test and validate these control algorithms.

1.3 CONTRIBUTIONS

The reported research makes the following contributions to the field of robotics and control:

1–An experimental robot setup was established to test various control algorithms consist-

ing of a mechanical arm and a real–time control system. The mechanical arm is a modular two–link planar direct drive manipulator designed and built to exhibit most of the problems which industrial robots have due to joint flexibility. Joint flexibility is designed–in using helical torsional springs which can be replaced to change the flexibility characteristics. The links can also be changed. The arm is equipped with four encoders to read the angular positions of the two motors and the two links and a force/torque sensor at the end effector. A sine–sweep test was performed on the experimental robot with the result that the obtained dynamic parameters closely matched those computed during the design stage. The real–time control system consists of a digital signal processing card and a number of input/output boards for communication with the motors and reading the different sensors. The real–time code was written in C language in a modular fashion to allow different users to use the experimental setup.

2– A collocated proportional–plus–derivative (PD) controller was implemented on the experimental robot. The limitations of this collocated controller to have the links track a desired angular position were demonstrated.

3– A feedback linearization controller was designed and implemented on the experimental robot in both the joint and task spaces. The experimental results reveal that the feedback linearization technique enabled good tracking to be achieved for the links angular positions and the end–point position. The response is much better in comparison with the PD controller. These results support the use of the nonlinear feedback linearization technique as the inner loop for controlling the position and force for flexible joint robots.

4– A dynamic hybrid control approach to control the position and force for flexible joint robots constrained by rigid environments was developed, simulated and implemented on the

experimental robot. This is a model–based feedback linearization algorithm. The control law is designed to linearize the system, decouple it into a position and a force subsystems using a constraint frame, and impose a desired closed loop characteristic for each subsystem. The simulation and experimental results demonstrate the success of this control algorithm in achieving good tracking for both the position and force trajectories.

5– **An impedance control** approach to control the position and/or force for flexible joint robots was developed, simulated and implemented on the experimental robot. This is also a model–based feedback linearization algorithm. The simulation and experimental results demonstrate the success of the controller to regulate the contact force and control the position of the end–point. The ability of the controller to perform both contact and free motions and to switch between these tasks was also demonstrated.

6– **A robust sliding mode control** algorithm was developed, simulated and implemented on the experimental robot. The robust controller is meant to account for the mismatch in the closed loop due to parameter uncertainty. A fourth order and a second order sliding surfaces are defined for the position and force subsystems respectively. The control law is composed of two terms; the first is similar to the that of the dynamic hybrid control scheme which would achieve exact linearization and perfect tracking if the robot parameters are known, the second is a switching term which is derived to have the position and force subsystems reach and remain on their sliding surfaces. Simulation and experimental results demonstrate good tracking and stable response despite 52.7% uncertainty in the links inertia parameters.

7– **A robust nonlinear sliding mode observer** for the feedback linearizable system was developed and tested. This observer requires the measurement of the links angular position only. In cases where the flexible joint robot parameters are uncertain, the main obstacle in implementing the feedback linearization technique is the necessity of the full state of the

feedback linearizable system for the feedback. Using this observer enables development and testing of many control algorithms which require the full state of the feedback linearizable system for the feedback.

8– **An adaptive cascade control** algorithms was developed, simulated and implemented on the experimental robot. The cascade controller consists of a direct adaptive control algorithm for the rigid dynamics (links subsystem) and a Model Reference Adaptive Control algorithm for the flexible dynamics (motors subsystem). The rigid dynamics controller generates desired motor angular positions in order that the end–point tracks desired position and force trajectories despite parametric uncertainty in the rigid dynamics model. The flexible dynamics controller is responsible for tracking the desired motors angular position while rejecting disturbance imposed on the motors subsystem by parametric inaccuracy. Simulation results indicated a good performance while experimental results indicated a good tracking for the force trajectory and a slow stable position tracking response for 52.7% parametric uncertainty.

8– **An adaptive feedback linearization control** approach was developed and simulated. The control algorithm consists of a nonlinear feedback control law which uses the estimated parameters and states, a robust nonlinear observer and an adaptation law. In this control algorithm the parameters and states are updated simultaneously. The conditions under which the closed loop, composed of the robot, the controller, the observer and the adaptation law is stable, are obtained. Simulation results indicated the good performance of the control algorithm.

1.4 OVERVIEW OF THE THESIS

The dissertation is divided into 8 chapters and 3 appendices. Included in chapter 1 is the motivation, objective, research approach, a list of contributions, and this overview of the thesis.

Chapter 2 presents a review of the related research topics, including modelling of robots with flexible joints, position control for flexible joint robots, position and force control for rigid robots, position and force control for flexible joint robots, and experimental results reported in the literature regarding the control of flexible joint robots. This chapter concludes with several key issues directly related to the considered problem.

In chapter 3 a description of the experimental two–link flexible joint robot manipulator is presented. This includes the design of the mechanical arm and the real–time control system.

In chapter 4 two dynamic models of the experimental flexible joint robot are presented and the identification of the adopted model parameters is described.

Chapter 5 contains the development of the feedback linearizable fourth order model which is used for the development of 4 control algorithms. The design of nonlinear feedback controllers, based on the feedback linearizable model, is presented. Experimental comparison between the nonlinear feedback and PD controllers are presented.

Chapter 6 describes the development of two model–based nonlinear control approaches to control the position and force for flexible joint robots, namely the dynamic hybrid and the impedance control approaches. The dynamic hybrid control algorithm deals with the case where the robot is interacting with a rigid environment. A nonlinear feedback control law has been designed which decouples the system into a position and a force subsystems using a constraint frame, linearizes the system, and imposes a desired closed loop char-

acteristic for each of the position and force subsystem independently. The impedance control algorithm deals with the compliant motion case. A fourth order desired target impedance is designed in the task space and a nonlinear feedback control law is designed which linearizes the system and imposes the desired target impedance. Simulation and experimental results are presented.

Chapter 7 describes the development of one robust and two adaptive control algorithms to achieve position and force tracking in case of parametric uncertainty in flexible joint robots. Section 7.2 describes the design of a robust sliding mode controller and the simulation and experimental results. Section 7.3 describes the design of an adaptive cascade controller which consists of a direct adaptive algorithm for the rigid dynamics and a Model Reference Adaptive Control algorithm for the flexible dynamics. Simulation and experimental results are presented. Finally, section 7.4 describes the development of an adaptive feedback linearization algorithm. Also, the design of a robust observer is presented. The adaptive controller is composed of the robust nonlinear sliding mode observer, a nonlinear feedback control law, and an adaptation law. Simulation results are presented.

The dissertation is concluded in chapter 8 with introduction, conclusions and future research.

The thesis includes three appendices. Appendix A contains description of the mechanical manipulator, actuators and sensors. Appendix B describes the kinematics of the two–link manipulator. Appendix C describes velocity estimation and filtering.

The following commercial software packages have been used during the research: MATRIXx and xmath [46], I–DEAS [93] and MACSYMA [112].

CHAPTER 2

LITERATURE SURVEY AND REVIEW

In this chapter, the cited literature deals exclusively with research related to the control of manipulators with flexible joints. General reviews of the literature on dynamics and control of manipulators can be found in [17,106,107]. The literature on position and force control of manipulators with flexible joints is reviewed under five categories: modelling, position control of flexible joint robots, position and force control for rigid robots, position and force control for flexible joint robots, and experimental results concerning flexible joint robots. Finally, the key issues related to the considered problem are discussed.

2.1 MODELLING

Modelling of manipulators with lumped elasticity in the drive system is straightforward in simple cases. Methods of modelling rigid manipulators can be extended with additional actuator dynamics which include flexibility of the drive system. Two different dynamic models describing flexible joint robot manipulators were cited in the literature.

In the first model, which one can refer to as the more exact model, the equations describing this model are two sets; the first set of equations describes the links system dynamics and the second set describes the actuators system dynamics. The two systems are coupled dynamically by the rotors inertias and statically by the stiffness of the joints. This model has been used by a few researchers studying flexible joint robots such as [18,19,68,69].

Spong [104] developed the second model in which the kinetic energy of each rotor is assumed to be only due to its own rotation. This assumption would be true only if all rotors

are housed in a common stationary base. Practical designs show many cases in which some of the actuators are fixed to moving links. Thus, rotor kinetic energy is due to its own rotation and the rotation of the link holding its stator. The result of this assumption is that the links and actuators systems are only statically coupled by the stiffness of the joints. This simplified model reduces to rigid manipulator model when joint stiffness values tend to infinity. The second model has been used extensively by most researchers studying flexible joint robots such as [6,30,42,45,50,58,64,66,97,104,114,119].

2.2 POSITION CONTROL OF FLEXIBLE JOINT ROBOTS

2.2.1 Computed–Torque Methods

The computed torque method is very well known for control of rigid manipulators. This is a general term which includes a number of methods for decoupling and linearizing nonlinear systems, such as robots, for control purposes. Other similar methods include inverse dynamics, feedback decoupling, resolved acceleration, nonlinear model matching, and nonlinear dynamic feedback. A decoupling and linearizing control algorithm is generally designed to compute the exact torques needed to be applied at each motor to make the manipulator appear to posses linear multi–variable response characteristics for which a simple linear controller is then designed. The first of these methods appears to have been developed originally for rigid robots by Freund [31] and Bejzcy [5].

The extension of the computed–torque control methods to manipulators with flexible joints has been difficult because no longer does each joint in the manipulator have an actuator to directly apply the decoupling and linearizing torques; for joints are separated from their actuators by the dynamics of the flexible drive. In other words, the model of rigid manipulators is feedback linearizable while the flexible joint manipulator model is not.

However, using feedback linearization techniques, the model of the flexible joint robot can be transformed to a new system which can be decoupled and linearized. Progress has been reported in the last few years on approximate and exact computed–torque solutions for flexible joint robot manipulators by DeLuca et al. [10], Uhlik [114], Forrest–Babcock [30], Khorasani [57], Marino and Spong [70], Jankowski and Van Brussel [50], Spong [104] and Hung [45].

2.2.2 Singular–Perturbation Methods

The singular–perturbation technique is a mathematical method for spectrally separating a nonlinear system into slow and fast subsystems to which appropriate control techniques can be applied. This approach has been used for control of flexible joint manipulators. Ficolo et al. [28] proposed the use of the singular–perturbation techniques for the case of weakly elastic joint robots in which elastic dynamics are very fast compared to the slow, rigid–body dynamics.

In [29] the application of the Model Reference Adaptive Control (MRAC) to the slow rigid–body dynamics and Variable Structure Control Systems (VSCS) to the fast flexible dynamics was proposed. In [69] standard computed–torque control methods to the rigid–body dynamics and linear regulator and tracking methods to the fast elastic dynamics were applied. Readman and Belanger [89] proposed velocity feedback to stabilize the fast dynamics. Khorasani and Spong [58], Hung [45], and Marino and Nicosia [69] proposed similar design in which they applied the computed–torque for the slow dynamics and a corrective controller to damp the fast dynamics.

An adaptive version of this controller has been proposed by Ghorble et al. [32], Hung [45], and Marino and Nicosia [69]. Other adaptive control approaches have been proposed. Mrad and Ahmad [81] derived an adaptive control law based on an energy motivated

Lyapunov function and a linear parametrization model of the links subsystem. An adaptive control strategy, based on an approximate linear model, was proposed by Tomi et al. [113]. Uhlik [114] proposed estimation algorithms for the unknown payloads but the the stability of the combined system was not considered. Han [34] applied an adaptive feedback linearization for position control in the joint space.

Other approaches, similar to the singular–perturbation approach, are those in which the flexible joint robot is regarded as being composed of the links subsystem and the motors subsystem. Lee et al. [64] proposed decoupling to obtain a desired motor angular position instantaneously which is then used to design an optimal controller for the motors subsystem. Lin et al. [68] considered the model in which dynamic coupling between the links and the motors subsystems is not neglected. They proposed Proportional–Integral–Derivative (PID) controllers for the rigid (links) subsystem and for the vibrational (motors) subsystem independently. In addition, a control term is added to the PID controllers to stabilize the overall system. Kiranski et al. [61] suggested the measurement of the torque/force on the output shaft of the elastic reduction unit (joint flexibility) in order to compensate for the flexible dynamics effects. The measured, or computed, signal is filtered then used by a linear controller. Widmann and Ahmad [119] presented a modified position control algorithm in which they introduced feedforward compensation of the joint torques and considered the problem of selecting the control gains to minimize the structural mode excitation. Recently, Hsu and Guenther [44] presented cascade controller for position control in the joint space. They proposed Slotine and Li's adaptive algorithm for the link subsystem and a variable structure controller for the motors subsystem.

2.2.3 State Estimation

The task of designing observers for robot manipulators is important for successful implementation of some control algorithms which require unmeasured states for feedback. The problem of estimating unmeasured states of a robot is inherently related to nonlinear state estimation. Misawa and Hedrick [79] summaries a number of nonlinear observers for nonlinear systems. The development of robust sliding mode observers for nonlinear systems by Slotine et al. [100] found successful application to rigid robot manipulators to estimate the joints angular velocities [11].

For flexible joint robot manipulators, state estimation is more important due to the fact that the system states are double those of equivalent rigid robots while the measurements remains the same. Hernandez and Barbot [37] designed a sliding mode observer [11] for the slow dynamics of a singularly–perturbed flexible joint robot. Hollars [42] applied constant gain extended Kalman filter to estimate the state of an experimental two–link manipulator with flexible joints. Recently, ElMaraghy and Massoud [25] developed a nonlinear robust sliding mode observer for the feedback linearizable model of flexible joint robot manipulators

2.3 POSITION AND FORCE CONTROL FOR RIGID ROBOTS

The research area concerning the problem of controlling contact forces when a robot end effector interacts with some external environment is very rich. Whitney [118] surveyed most of the proposed control approaches and An and Hollerbach [2] analyzed and compared some of these control approaches. A recent survey of force control approaches can be found in [117]. Enhancement of these techniques is continuously being reported by considering parameters uncertainty and designing adaptive algorithms.

In general, the environment with which the robot end effector comes into contact can be classified as: i) rigid and ii) compliant environments. In the first class, the environment is assumed to be perfectly rigid. The force normal to the constraint environment is not doing any work and the end effector cannot move in an arbitrary manner as its motion is constrained. As a result, kinematic constraints are imposed on the manipulator motion. This type of contact is usually referred to as contact with rigid environment, or constrained motion. The other class of contact deals with tasks in which the environment is not perfectly rigid, therefore, some deformation of the environment occurs and the force is doing work. This type of contact is referred to as compliant motion.

Force control approaches can be categorized according to the above classification as the consideration of the type of the environment plays an important role in the dynamic model and hence in the design of the force control algorithms. Thus, force control approaches are classified into two: first, those in which the environment is rigid (constrained motion), and second, those in which the environment is compliant or no kinematic constraints are used in the design of the force control algorithm.

In the constrained motion case, the constraints imposed by the environment on the motion of the manipulator are considered in the dynamic model. The incorporation of the constraints into the dynamic model allows to decouple the degrees of freedom of the system exactly into degrees of freedom for the force directions and the rest of the degrees of freedom for the motion directions. The theoretical framework for the constrained motion was developed by McClamroch and Wang [76]. Once the system is decoupled using the constraints into the equation of motion, different approaches can be applied to control the contact force and the motion. For example, McClamroch and Wang [76] designed a computed–torque controller for the position subsystem in the joint space and a proportional controller for the force subsystem. Krishnan and McClamroch [62] applied a linear quadratic optimal regulator for

the linearized nonlinear differential–algebraic equations. Also, Mills and Goldenberg [78] designed a linear controller for the linearized model. Yoshikawa [122] applied nonlinear feedback to linearize the decoupled system, then designed a servo controller for each of the force and position subsystems.

For the compliant motion case, or when no kinematic constraints are considered, several control approaches have been proposed. Raibert and Craig [88] adopted the development of Mason [71] to develop the hybrid control approach. In this approach, a selection matrix is designed to determine which degrees of freedom are to be used for position control and which are to be used for force control. Then for each of these two sets of degrees of freedom a separate controller is designed. Some researchers have presented extensions and modifications to this basic hybrid control approach where the dynamics are taken into consideration. Khatib [55,56] formulated the dynamic model in the cartesian space then compensated for these dynamics. This approach allows direct control of the contact force and motion in the cartesian space. The resolved acceleration force control approach [95] and the idea presented by DeLuca [20] are similar to Khatib's approach.

Another interesting force control approach is the impedance control developed by Hogan [39]. The basic principal of the impedance control approach is that the controller does not attempt to regulate the position error nor the resulting force, but rather it regulates the interaction between the position error and the resulting force by specifying a desired relation or impedance.

A second order impedance is usually specified for rigid robot manipulators. This approach represents a generalization for the compliant force control problem as more design parameters are used to specify a desired relation between the position error and the force. Therefore, a wide variety of the contact characteristics can be obtained. Many researchers have adopted this approach when dealing with force control such as [40,38,120,52,53]. In

these efforts many issues related to impedance control such as robustness, limitations, and experimentation have been addressed.

2.4 POSITION AND FORCE CONTROL FOR FLEXIBLE JOINT ROBOTS

Most of the developed force control approaches were based on the assumption that the robot arm is rigid.,i.e., no consideration was given to the structural flexibility of the mechanical arm while developing those force control approaches. Little work has been carried out for controlling the position and force for flexible joint robot manipulators, although the need for force control and compensation for the joint flexibility effects are important and justified [13,26,27,33,111]. This is the subject of the research reported in this thesis.

Spong [105] applied the idea of integral manifold and corrective control to a singularly perturbed system. He aimed at extending force control approaches for rigid robots to the case of flexible joint. Mills [77] also applied the idea of composite control to a singular perturbation model considering the constrained motion case. Krishnan and McClamroch [62] applied a linear quadratic optimal regulator to a linearized constrained model. Jankowski and ElMaraghy [47,48,49] proposed an algorithm for coordinate reduction and feedback linearization hybrid position and force control. Han et al. [35] applied a composite controller to a singular perturbation constrained flexible joint robot. The rigid dynamics controller was an adaptive algorithm similar to Slotine and Li's algorithm with modifications for force control.

2.5 EXPERIMENTAL RESEARCH EFFORTS

Experimental setups are needed to test and validate many of the developed control algorithms. Most of the theoretical and simulation results do not reflect all the actual prob-

lems in flexible robotic systems, such as state measurements, real–time computation, modelling simplifications and experimental identifications. Finally, an experimentally validated control algorithm proves its potential success for real world implementation and application.

Many experimental setups have been constructed in many universities and research centers to investigate modelling and control of flexible link robot manipulators [8,83,84,12,85,36,15,124]. However, very few experimental setups have been constructed to investigate the same problems for robots exhibiting joint flexibilities. This is surprising because most industrial robots suffer from joint flexibility rather than link flexibility which is more prominent in space application.

Hung [45] built a single–link flexible joint robot. Joint flexibility is introduced by a set of linear extension springs. The main design criterion for this robot is that the minimum value of the resonant frequency due to joint flexibility is about 5.5 Hz and the maximum value is about 20 Hz. This value can be changed by changing the number of springs. The results achieved from this work are: 1) experimental verification of the feedback linearization control for flexible joint robots in the joint space, 2) experimental verification of a modified version of the computed–torque control method, and 3) experimental verification of a modified version of Slotine and Li [101] adaptive control algorithm. Jankowski and Van Brussel [50] implemented the inverse dynamics control approach to a two–link planar robot. Joint flexibility was introduced only in the first joint by means of two linear compression springs.

While the research on the single–link flexible joint manipulators has provided much insight into the behavior and control of such a system, it is still a Single–Input–Single–Output (SISO) system. The dependency of the inertia matrix on the configuration and the coupling it introduces do not exist in the single–link case.

Hollars [42] built a two–link SCARA type manipulator with flexible joints. The flexibility is introduced by using linear tension springs in the driving belts. The robot is semi

direct–drive, the gear ratios are 5.9 and 2.44 at the shoulder and elbow, respectively. The two resonant frequencies for this manipulator are about 9.15 and 11.5 Hz. He implemented three control algorithms: 1) Collocated PID demonstrated the bandwidth limitation, poor rejection of disturbances and large steady–state end–point positioning errors, 2) Linear–Quadratic–Gaussian (LQG) resulted in improvement of about four times in bandwidth and steady state error over those for the collocated PID was obtained at or near the configuration specific model of the manipulator. Observations showed that the LQG rapidly loses performance as the arm geometry or payloads mass vary from the design point and deteriorates to instability for some geometries and payload masses, and 3) Constant–Gain Extended Kalman Filter (CGEKF), with a Linear–Quadratic–Regulator (LQR) showed improvements in disturbance rejection and stability over the entire work space.

Uhlik [114] used the same experimental setup to evaluate two control algorithms. First, he designed and implemented the computed–torque approach in the joint space. This nonlinear feedback controller resulted in improvement in the robustness, positioning error, and stability. The second control algorithm is an adaptive controller in which he implemented different parameter estimation techniques to identify an unknown payload mass. Experiments showed that the successful parameter estimation helped maintaining stability for some unknown mass and achieve good tracking performance.

From the above summary, one can easily see that the problem of controlling position and force while considering joint flexibility still needs further theoretical and experimental exploration. Preliminary theoretical and experimental work achieved during the research in this dissertation was published under joint authorship in [72,25,75,22,23].

2.6 KEY ISSUES

After examining the current state of research on the control of flexible joint robots, several key issues emerged as the primary motivation for the research reported here: experimental testing, nonlinear control, state estimation, and robustness considerations.

1. Experimental Testing

None of the cited position and force control algorithms for flexible joint robots has been experimentally tested. Experimental implementation and testing are urgently required to evaluate different control algorithms as simulation and analytic studies do not include many practical issues.

2. Nonlinear Control

Most of the cited control algorithms use the singular perturbation method for flexible joint robots. This method makes it easier to extend control approaches developed for rigid robots to control the slow dynamics, then to design a separate controller to damp the fast dynamics. However, these control algorithms relay on the fundamental assumption of weakly elastic joints which are close to rigid robots. Thus, they do not ensure the same performance for different flexibility characteristics. There is a need to develop nonlinear control algorithms which are not sensitive to the flexibility characteristics and to establish a basic structure for subsequent robustness considerations.

3. State Estimation

There have been less efforts to consider the problem of building state estimators for flexible joint robot manipulators. Most simulation studies make the assumption that all desired states are available from noise–free sensors. Thus, practical issues regarding state estimation for implementation need to be considered.

4. Robustness Considerations

No consideration was given to the robustness of the control algorithms developed for position and force control of flexible joint robot manipulators. Most of the cited adaptive position control algorithms are based on the singularly–perturbed model. There is a need to develop robust and adaptive control algorithms for models other than those satisfy the singular perturbation requirements of weak elastic joints.

CHAPTER 3

THE EXPERIMENTAL TWO–LINK ROBOT MANIPULATOR

The experimental two–link robot manipulator with flexible joints serves as a test bed for new control concepts developed for robots which suffer from joint flexibility problem. This chapter describes objectives, the procedure followed for the design of the manipulator, the real–time control system, and an overview of the experimental setup.

3.1 THE MECHANICAL ARM

3.1.1 Objectives and Conceptual Design

The main objectives considered during the design are:

1– Resonant frequencies: the robot should simulate the actual problem of joint flexibility by having resonant frequencies less than 10 Hz due to joint flexibility.

2– Modularity: the robot should be modular and allow changing the joints and/or links.

3– Sensors: the robot should be equipped with the necessary sensors to allow implementation of various nonlinear control algorithms in free and constrained motions.

4– High performance: obtain the maximum end point acceleration and the forces possible.

The designed robot has two degrees of freedom which are sufficient to study position and force control problems and it exhibits the interesting nonlinear and highly coupled dynamics characteristics of many manipulators. The joints are revolute with parallel axes of rotation. They are parallel to the gravity field and driven by direct drive motors. The arm resembles the first two degrees of freedom of SCARA type robots. The advantages of such

design are: the design is optimized for fast pick and place operations, it reduces the motor torque requirements due to gravity loading, and the vertical actuation action is dynamically decoupled from the horizontal links. This design has been chosen for the experimental robot because it represents a large number of industrial robots, leads to a very compact design and construction, and enables introducing joint flexibility in one element. As a result, it is easy to change the joint stiffness and a wide range of joint flexibility can be investigated. There is a trade off between link lengths, rigidity, and work space. After considering the motor sizes, the requirements for force control, the characteristics of commercial robots, and the energy characteristics [3], the link lengths were chosen to be 0.4 and 0.35 m for the first and second joints, respectively. Direct drive motors were chosen to allow isolating the effects of joint flexibility rather than introducing problems associated with high gearing such as back-lash. The friction still exists in direct drive motors and needs to be considered. Moreover, direct drive robots are more suitable for force control applications.

3.1.2 Manipulator Structure

Figure 3.1 shows a solid model of the experimental manipulator with the base. The two links are connected by revolute joints which provide motion in the horizontal plane. The first link is 0.4 m and the second link is 0.35 m. The first joint range of motion is 360 degrees while the second is about 190 degrees. Therefore, the work space is a planar annular ring, as shown in figure 3.2. The minimum reach of the manipulator is 0.5 m and the maximum reach is 0.75 m.

The design proceeded as follows. First the links and joints were designed to meet the main objectives. This yielded a rough estimate of the masses and inertia parameters which were used to choose the motors. Then the solid modeler , I–DEAS [93], was used to detail the design and obtain an accurate estimate of the parameters. The performance of the robot, in terms of the link accelerations and the forces that the robot can exert on an environ-

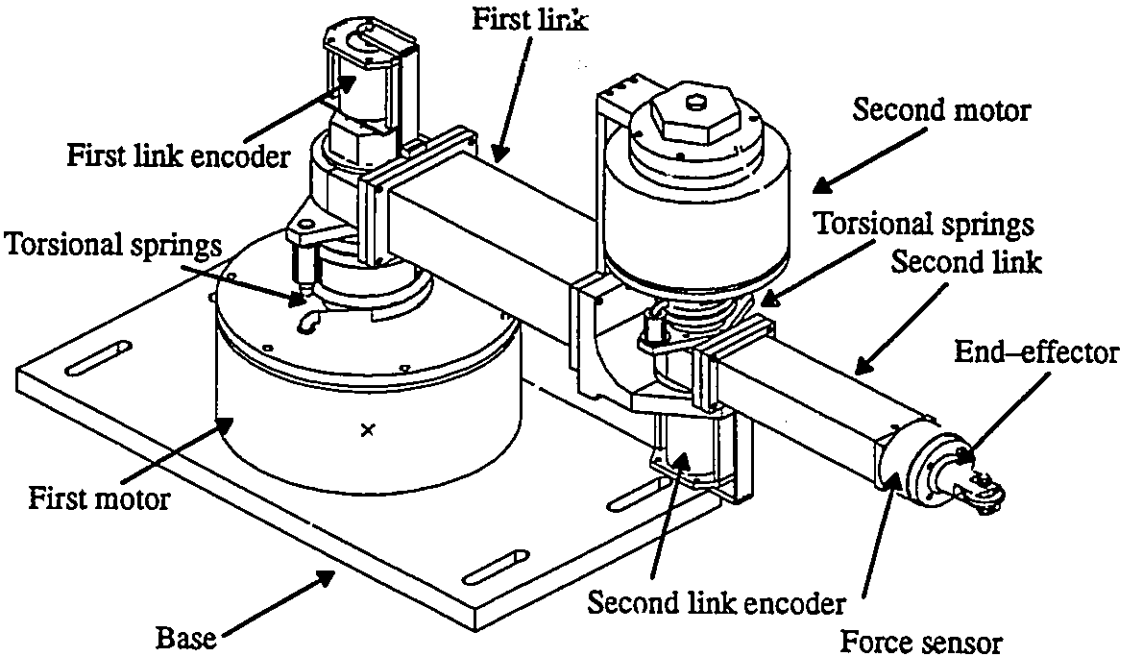

Fig. 3.1 Solid model of the experimental robot

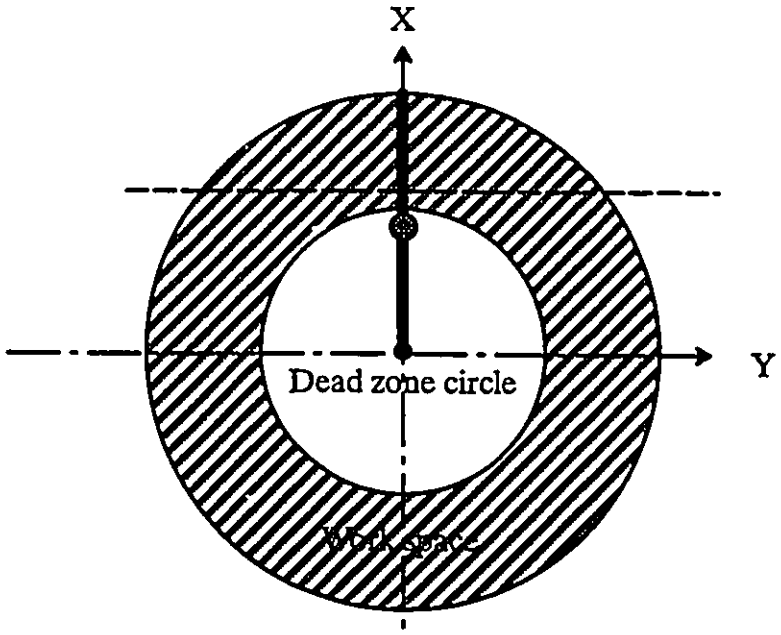

Fig. 3.2 The experimental robot work space

ment, was evaluated. A modified version of the computed–torque was used in the simulation. This process was repeated several times until the design objectives were satisfied.

3.1.2.1 Design of the Rigid Links

The links design preceded the joints design because the links parameters are required to design the joints. In designing the links, the objective is to minimize their weight in order to obtain a greater performance from the same motors. This objective is limited by the following constraints: a) safe working stresses must be ensured, b) minimum vertical tip deflection is desired, and c) the resonant frequencies due to link flexibilities should be much greater than those due to joint flexibilities.

For the purpose of satisfying the main objective and the first two constraints, the arm is approximated by a cantilever with concentrated loads. Regarding the third constraint, the link flexibilities are approximated using the lumped mass stiffness approach. Although, only the first vibrational mode of each link was included, it was sufficient to guarantee that the lowest resonant frequency, due to links flexibility, can be chosen to be much greater than the joint resonant frequencies. Hence, the dominant vibration behavior is due to joint flexibility in the bandwidth of interest. Thus, this design yields rigid links. It is interesting to notice that all three constraints have the effect of increasing the weight, i.e., increasing the links rigidity, increasing the strength, decreasing the vertical tip defection, and increasing the links resonant frequencies. Both steel and aluminum of solid and hollow cross sections were considered [90]. After several iterations the optimum parameters that satisfy the objective and the constraints were determined. In the final design, the links are made of aluminum with hollow rectangular cross sections. The choice of rectangular cross section was due to the consideration of having the manipulator operate in a vertical plane. In such configuration, the loads which the structure components have to withstand are more than those when operating in the horizontal plane due to gravity loading. The maximum vertical tip deflection at the end point is 0.015 mm when the payload is 10.0 kg and the robot operates in a horizontal plane. The lowest resonant frequency from the links flexibility is greater than 120 Hz.

3.1.2.2 Design of the Flexible Joints

Although robots differ in size, speed, power and payload, the effect of the flexibilities in the drive system is the same. They lead to very low resonant frequencies. For many industrial robots these resonant frequencies are less than 10 Hz. Therefore, the objective in designing the flexible joints was to have resonant frequencies, due to joint flexibilities, be less than 10.0 Hz. Different experimental flexible joint robots [42,43,50] were studied and many ideas were considered to introduce and control the joint flexibility. The idea implemented here is to use helical torsional springs. In this design, the construction is very compact. Also, a wide range of flexibility can be obtained by employing different springs. At each joint two identical and concentric helical torsional springs are used to achieve the same behavior in both directions of rotation.

Referring to Chapter 4, for the dynamic model and the computation of the natural frequencies, the inertia matrix is maximum when the arm is fully extended. This configuration corresponds to the minimum natural frequencies for particular joint stiffness values. The characteristic equation yields an expression for the natural frequencies as a function of the inertial parameters and the joint stiffness values. An expression for the tip deflection in the working plane is obtained as a function of the joint stiffness values and the contact forces. Using these two expressions, the optimum flexibility ranges were extracted to allocate the natural frequencies as desired and to minimize the tip deflection in the working plane.

A detailed mechanical design of the robot was produced using I–DEAS [93] solid modelling package. Figure 3.1 shows a graphical model of the robot produced by I–DEAS. The advantages of using a solid modeler in the design are: 1) accurate estimation of the robot dynamic parameters, such as masses, inertia, ...etc., especially for complicated constructions (as shown in table 1) can be obtained, 2) ease of design modifications during design iterations, and 3) reliable detailed design information and drawings for manufacturing can be

produced. As mentioned earlier a modified version of the computed torque approach was used to evaluate the performance. The maximum tip acceleration is 4.75 g (the gravity acceleration), which indicate that high performance was achieved by this design.

Table 1 Robot parameters from design

	First Link	Second Link
Length (m)	0.4000	0.3500
Center of mass (m) measured from the joint axis of rotation.	0.3007	0.1505
Mass (kg)	10.756	1.859
Moment of inertia ($kg.m^2$) about a vertical axis passing through the centre of mass.	0.2269	0.0429
Joint stiffness (N.m/rad)	198.49	51.11

3.2 THE REAL–TIME CONTROLLER

3.2.1 The Controlled System

In a rigid robot, the angular position of the link is seen to be the same as that of its driving motor scaled only by the gear ratio. However, in a flexible joint robot, the link angular position is a generalized variable of interest. It differs from the motor angular position by the value of the joint angular deflection. Also, most of the control algorithms developed to date for flexible joint robots assume the availability of, at least, the link angular position. For these two considerations, it is necessary to measure both the link and motor angular positions, i.e. before and after the flexibility. For each joint, the angular position of the motor is measured using the built in optical encoder. The link angular position is measured using an optical encoder located after the flexible joint in such a way that it measures the absolute angular position of the link. The motor angular velocities are available as analog signals from

the motors servo controllers. A Force/Torque sensor is mounted at the end effector of the robot to implement force control algorithms. This sensor provides resolved 3 cartesian forces and their 3 cartesian moments. The force sensor controller provides the six signals as analog or digital through the optional Input/Output board. For the current configuration, analog signals are used. The two actuators are direct drive DC motors. The peak torques of these motors are 100.0 and 30.0 N.m, for the first and second motors, respectively. The servo controllers allow controlling the motors in one of three modes: position, velocity or torque mode. The torque mode is used for the identification and control considered in this research.

In summary, the manipulator system has two inputs, commanded voltage signals to the motors, and twelve outputs; four angular positions of the two links and the two motors, two angular velocities of the two motors, six force and torque components in cartesian space.

3.2.2 The Real–Time Control System

The dSPACE real–time control hardware [21] consists of a Texas Instruments TM320C30 DSP, rated at 33 MFLOPS and a number of I/O controllers in an ISA expansion chassis as shown in figure 3.3. The expansion chassis is connect to a 33 MHz 486 PC through a passive ISA bus extension. The DSP and the I/O controllers are also connected to a local PHS–bus. The I/O controllers are a 32 channel A/D 16 bit board, a 5 channel D/A 12 bit board, a 5 channel 24 bit incremental encoder board, and a 32 line Digital Input/Output board.

The A/D board is used to measure the 3 forces and the 3 moments from the force sensor board analog port and the 2 motor velocities from the motors servo controllers. The D/A board is used to output the commanding analog signal to the motors servo controllers for any of the velocity or the torque control modes. The incremental encoder board is used to read the 4 encoders in the robot. The Digital Input/Output board is used for controlling

the motors servo controllers, controlling the motors in the position mode, controlling the brake, and reading a number of limit switches. The PC host is connected to a SUN workstation through a TCP/IP Ethernet network. This feature helps data and code transfer between the PC and the network.

The real–time code was written in C language in a modular fashion to allow users to test their control algorithms on the experimental robot. Full description of the real–time code can be found in [74]. It consists of two programs: one running on the DSP and another on the PC host. The real time DSP program is responsible for reading the sensory input from the I/O controllers, computing control algorithm, and transferring data between the DSP, PC and the motors servo controllers. The PC host program transfers data to and from the DSP, displays and stores data, and provides a front–end user interface to control the process.

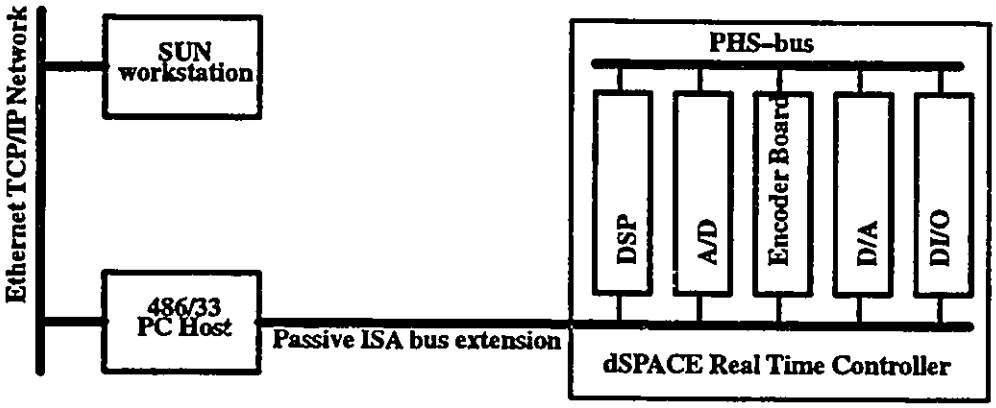

Fig. 3.3 The real–time control system hardware

3.3 SUMMARY

The design objectives of the experimental two–link manipulator with flexible joints were met by the presented design. Chapter 4 describes the analytic dynamic models of the experimental robot manipulator developed for the identification and control purposes.

The basic characteristics of the robot manipulator hardware are summarized as follows:

– The robot is a two–link SCARA manipulator operating in the horizontal plane.

– Joint flexibility has been specially isolated and exaggerated by introducing two helical torsional springs between the rotor and the link for each of the two joints, while the links and base of the manipulator are very rigid. With the current springs used, the manipulator has two resonant frequencies of 5.2 and 7.5 Hz, when it is fully extended.

– The manipulator is modular in the sense that the links and or joints can be changed.

– The manipulator motors has Coulomb friction which can be compensated for by feedback control.

– The manipulator is equipped with 4 encoders to measure the angular positions of the links and motors. Motors angular velocities and contact forces and moments are available through the motors servo controllers and the force sensor controller, respectively.

– The real–time control system can run complicated algorithms such as the computed torque in the task space at speed of 1.0 KHz.

CHAPTER 4

DYNAMIC MODELLING AND IDENTIFICATION

This chapter describes analytical models developed for the experimental flexible joint robot manipulator and the experimental identification. Firstly, modelling considerations and assumptions are examined. Then, the kinematic models describing the position, velocity, acceleration, and third and fourth derivatives of the position are described. Two dynamic models are developed which describe the dynamic behavior of the manipulator followed by investigation of its dynamic characteristics. The experimental identification technique, used to identify the dynamic model parameters, is described. This chapter concludes with a summary of the main features of the dynamic model of the experimental flexible joint robot manipulator.

4.1 MODELLING CONSIDERATIONS AND ASSUMPTIONS

The main issue considered while developing the dynamic models of the experimental manipulator was that the system is Multi–Input–Multi–Output (MIMO) and highly nonlinear. Whether the dynamic model is used to investigate the dynamic characteristics, or to develop and implement control algorithms, the full nonlinear model should be developed and understood, then allowable simplifications may be used. There is a trade–off between modelling and control, i.e. for a very simple model one needs to develop a sophisticated controller to account for the incomplete representation of the system, while for a comprehensive model a simple controller can, if available, achieve a remarkable performance. Flexible link

robots are distributed parameters systems while flexible joint robots can be accurately modelled with lumped stiffness parameters at the joints.

The following are the assumptions adopted for development of the experimental manipulator dynamic models:

1. The links are perfectly rigid , thus the system flexibility is only due to joint flexibilities. Therefore, there are only four generalized coordinates necessary to completely describe the position of any point on the mechanism; two for the links and two for the motors.
2. Joint torque is linear in the joint deflection.
3. The axes of rotation of all actuators are parallel to each other as well as to the gravity direction.
4. The center of mass of each link lies in its vertical plane of symmetry.
5. The masses of the springs are included with the appropriate rotors and links, assuming that the center of mass of the spring remains constant relative to its fixed ends.
6. The only source of nonlinear friction is the Coulomb friction at the motors, all other sources of friction are linear viscous.
7. The rotors are symmetric about their axes of rotation.
8. The motors are pure torque sources.

4.2 KINEMATICS

For a two–link rigid robot, only two generalized coordinates are sufficient to describe the position of any point on the mechanism. However, when the joints are flexible and the links are rigid, four generalized coordinates are necessary; two to describe the rigid links motion and two to describe the motion of the motors. There are four coordinate frames used. First, a cartesian reference frame (XYZ) is established. It is fixed to the base of the robot as shown in figure 4.1 and defined by the three coordinates X,Y, and Z. The other three coordi-

nate spaces are defined relative to this reference frame. For the experimental manipulator, four generalized coordinates form the joint coordinate space. These coordinates are the angular positions of the two links and the two motors. They are represented by q_1, q_2, q_{m1}, q_{m2}. Each is measured relative to the reference frame as shown in figure 4.1. With regard to the development and implementation of force control, two other frames are defined. The constraint frame presented in Chapter 6 and force/torque sensor frame presented in appendix B. The transformation between these two frames and the reference frame are presented in Chapter 6 and appendix B.

There are various relationships between these four coordinate spaces which are extremely important to the experimental work on the two–link flexible joint robot. The joint coordinate space is used for the development of the dynamic model used in the control algorithms. The reference frame, the constraint frame, and the force/torque sensor frame are used for motion and force control development and implementation. It is important to note that motion of the rigid links is described only by two coordinates in any of the coordinate spaces as the actuators are kinematically decoupled from the links by the flexible joints. Twenty one kinematic relations between the four coordinate frames are required. These transformations apply to flexible joint and rigid two–link manipulators and are classified into 3 groups:

A– Ten transformations between the joint space frame and the reference frame are given by:

1. Forward kinematics refers to the transformation from the joint space coordinate to the reference frame.
2. Inverse kinematics refer to the transformation from the reference frame to the joint space.
3. Forward Jacobian transforms velocities in the joint space to velocities in the reference frame.

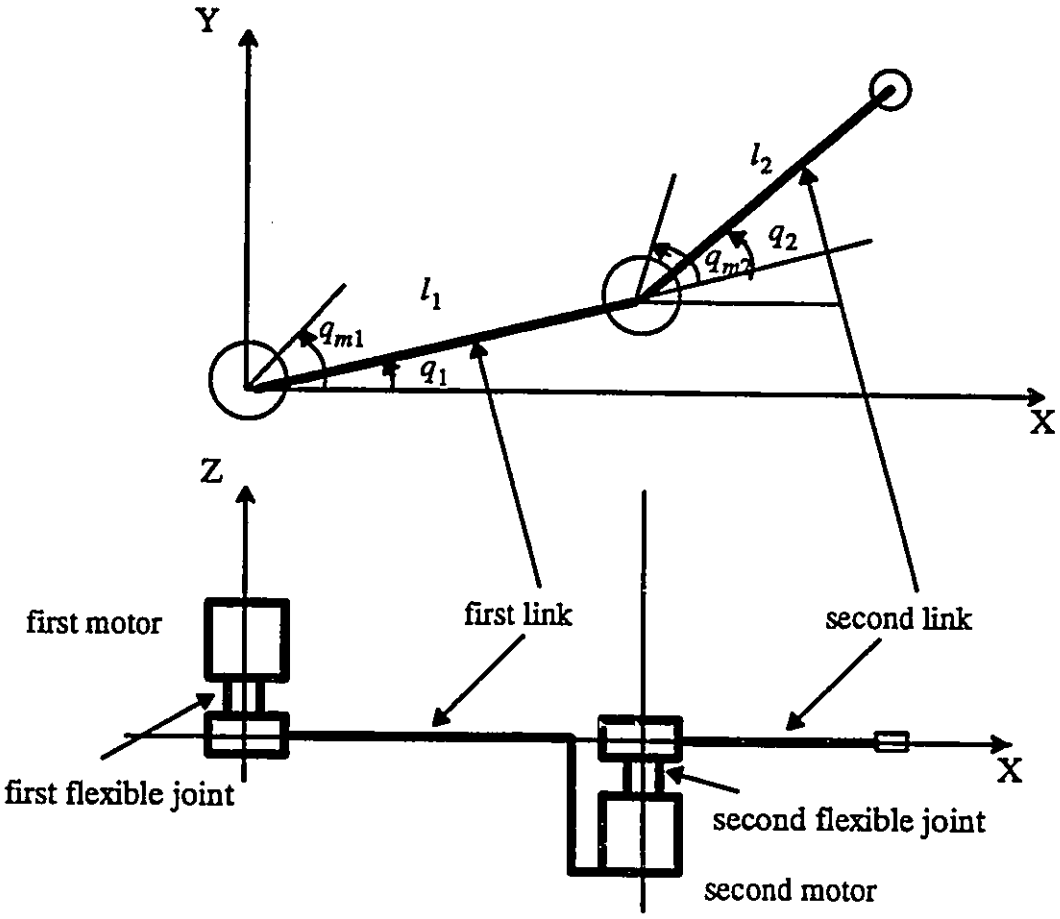

Fig. 4.1 Kinematic model of the experimental robot

4. Inverse Jacobian transforms velocities in the reference frame to velocities in the joint space.

5,6,7 Second, third and fourth derivative Jacobians transform acceleration, jerk and jerk first derivative from joint space to the reference frame.

8,9,10 Inverse second, third and fourth derivatives Jacobians transform accelerations, jerk and jerk first derivative from the reference frame to the joint space.

B– Ten transformations between the constraint frame and the reference frame are given by:

1. Transformation of position vector from the reference frame to the constraint frame.

2. Transformation of position vector from the constraint frame to the reference frame.

3. Rotation of the velocity vector from the constraint frame to the reference frame.

4. Inverse rotation, which transforms velocity vector from the reference frame to the constraint frame.

5,6,7 Transformations of the acceleration, jerk and jerk first derivative from the constraint frame to the reference frame.

8,9,10 Inverse transformations of the acceleration, jerk and jerk first derivative from the reference frame to the constraint frame.

C– One transformation between the force/torque sensor frame and the constraint frame: the transformation of the force vector from the force/torque sensor frame into the force vector in the constraint frame.

4.3 DYNAMIC MODELS

Two full nonlinear dynamic models of the experimental two–link flexible joint robot are developed in this section. The dynamic characteristics of the two models are then investigated and compared.

4.3.1 Model 1

In addition to the eight stated assumptions, another fundamental assumption is adopted for model no. 1: it is stated that a rotor rotational kinetic energy is mainly due to its own rotation. This is not true for all rotors in a robot manipulator since in many design configurations a rotor rotational kinetic energy is dependent upon the velocity (or velocities) of the link (s) carrying the motor of that rotor. However, the result of this assumption is a model which still includes the effect of joint flexibility and has the main structural description of the relationship between the parameters and the variables of the flexible joint manipulator system. This model was developed by Spong [104]. It has since been used by most researchers studying the control problems of flexible joint robot manipulators.

Figure 4.2 shows a model of the experimental two–link flexible joint robot manipulator. The joint space coordinates are used to describe the configuration of the manipulator.

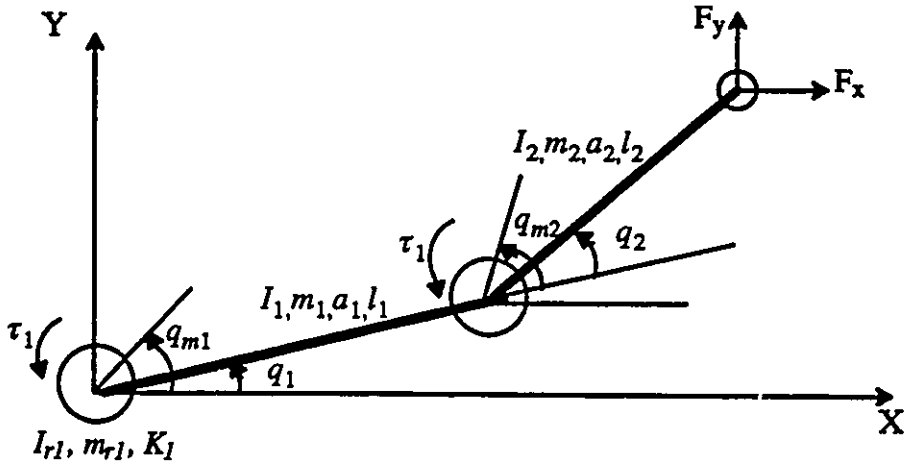

Fig. 4.2 Coordinates and parameters of the experimental robot dynamic models

The symbols shown in figure 4.2 are defined as follows:

q_i the angular position of link i

q_{mi} the angular position of motor i

I_{ri} the moment of inertia of rotor i about its axis of rotation

m_{ri} the mass of rotor i

k_i the effective torsional stiffness of joint i

I_i the moment of inertia of link i about an axis passing through its center of mass

m_i the mass of link i

l_i the length of link i measured between the corresponding joints

a_i the distance from the axis of rotation of joint i to the center of mass of link i

τ_i the input torque from motor i at joint i

Standard Euler–Lagrange equations were used to derive the nonlinear equation of motion in the following standard matrix form:

$$D(q)\,\ddot{q} + C(q,\dot{q}) + B_l\,\dot{q} - K(q_m - q) = -J^T F \qquad (4.3.1)$$

$$I_m\,\ddot{q_m} + B_m\,\dot{q_m} + F_c + K(q_m - q) = T \qquad (4.3.2)$$

where the following $2x1$ vectors are defined as:

$q = \begin{bmatrix} q_1 \\ q_2 \end{bmatrix}$ the links angular position vector

$q_m = \begin{bmatrix} q_{m1} \\ q_{m2} \end{bmatrix}$ the motors angular position vector

$\tau = \begin{bmatrix} \tau_1 \\ \tau_2 \end{bmatrix}$ the input torque vector

$F = \begin{bmatrix} F_x \\ F_y \end{bmatrix}$ the contact force vector expressed in the reference frame

$F_c = \begin{bmatrix} f_{c1} \\ f_{c2} \end{bmatrix}$ the Coulomb friction vector

$C(q,\dot{q}) = \begin{bmatrix} -d_3\,(2\dot{q_1} + \dot{q_2})\,\dot{q_2}\sin q_2 \\ d_3\,\dot{q_2}^2 \sin q_2 \end{bmatrix}$ the Coriolis and centrifugal forces vector

and the following $2x2$ matrices are defined as:

$D(q) = \begin{bmatrix} d_1 + 2d_2\cos(q_2) & d_3 + d_2\cos(q_2) \\ d_3 + d_2\cos(q_2) & d_3 \end{bmatrix}$ the manipulator inertia matrix

$K = \begin{bmatrix} K_1 & 0 \\ 0 & K_2 \end{bmatrix}$ the joint stiffness matrix

$I_m = \begin{bmatrix} I_{m1} & 0 \\ 0 & I_{m2} \end{bmatrix}$ the motors inertia matrix

$B = \begin{bmatrix} b_1 & 0 \\ 0 & b_2 \end{bmatrix}$ joints viscous friction matrix

$B_m = \begin{bmatrix} b_{m1} & 0 \\ 0 & b_{m2} \end{bmatrix}$ the motors viscous friction matrix

where

$$d_1 = I_1 + I_2 + m_1 a_1^2 + m_{r2} l_1^2 + m_2 (l_1^2 + a_2^2)$$

$$d_2 = m_2 \, l_1 a_2$$

$$d_3 = I_2 + m_2 a_2^2$$

By inspecting the flexible joint manipulator equations of motion, equations (4.3.1) and (4.3.2), it can be seen that the first equation describes the links system dynamics and the second equation describes the motors system dynamics. These two systems are coupled statically due to the flexibilities at the joints. The links system equation of motion resembles the equation of motion of the equivalent rigid robot. However, there is a fundamental difference, the actuator input torques are replaced by the stiffness forces. The nonlinearities in this dynamic model are a result of the dependency of the manipulator inertia matrix on the configuration, the nonlinear elements forming the Coriolis and centrifugal forces vector and the Coulomb friction vector.

4.3.2 Model 2

In this model, no assumption is implied regarding the rotational kinetic energy of the rotors. Only assumptions 1 to 8 are adopted. For the experimental manipulator, the assumption regarding the kinetic energy of rotors affects only the second rotor. The true kinetic energy of the second rotor is given by:

$$K.E.)_{rotor2} = \frac{1}{2} m_{r2} \dot{q}_1^2 + \frac{1}{2} I_{r2} (\dot{q}_{m2}^2 + \dot{q}_1^2) \qquad (4.3.3)$$

instead of the approximated value, used to derive model 1, which is

$$K.E.)_{rotor2} = \frac{1}{2} m_{r2} \dot{q}_1^2 + \frac{1}{2} I_{r2} \dot{q}_{m2}^2 \qquad (4.3.4)$$

It is clear from the above two expressions for the kinetic energy, that the assumption regarding the kinetic energy removes the dependency of the second rotor kinetic energy on the first link angular velocity.

Following the same procedure as for the first model, the equations of motion for model 2 are:

$$D(q)\,\ddot{q} + \Lambda\ddot{q_m} + C(q,\dot{q}) + B\dot{q} - K(q_m - q) = -J^T F \qquad (4.3.5)$$

$$\Lambda^T\ddot{q} + I_m\,\ddot{q_m} + B_m\dot{q_m} + K(q_m - q) = U \qquad (4.3.6)$$

where $\Lambda = \begin{bmatrix} 0 & I_{r2} \\ 0 & 0 \end{bmatrix}$.

By inspecting model 2, given by equations (4.3.5) and (4.3.6), one can see that the links and motor systems are coupled both dynamically and statically. This model has been used less often in studying control problems for flexible joint robots. It is more difficult to use model 2 to develop control approaches compared with model 1 owing to the dynamic coupling.

4.3.3 Dynamic Characteristics

In this section, the dynamic characteristics of the two models are studied and compared. The aim of the comparisons is to investigate the effect of approximating the rotor kinetic energy rather than using the true expression. The bases used in the comparisons are the natural frequencies and frequency response functions. Comparisons and evaluations are performed using the manipulator parameters as identified in section 4.4.

4.3.3.1 Natural Frequencies

For both models, the undamped natural frequencies can be obtained from the following characteristic equation with its own inertia matrix.

$$\det\left[\,K_s - \omega^2 M_s\,(q)\,\right] = 0 \qquad (4.3.7)$$

where $K_s = \begin{bmatrix} K & -K \\ -K & K \end{bmatrix}$, for model 1 $M_s = \begin{bmatrix} D(q) & 0 \\ 0 & I_m \end{bmatrix}$

and for model 2 $$M_s = \begin{bmatrix} D(q) & \Lambda \\ \Lambda & I_m \end{bmatrix}$$

The effect of the joints flexibilities on the manipulator natural frequencies is investigated by considering a wide range of joints flexibilities. This effect was considered during the robot design to select natural frequencies in order that the experimental robot would exhibit the problems which industrial robots suffer from due to the flexibilities in their drive systems. Figure 4.3 shows plots of the manipulator undamped natural frequencies as they vary with the first joint stiffness for specific values of the second joint stiffness for both models. First, it can be seen that the natural frequencies of the two models have the same pattern, i.e., neglect of the dynamic coupling in the model 1 does not change the characteristic behavior and the values of the natural frequencies of both models are very close to each other. Second, it is interesting to see the effect of the first joint stiffness as it divides the plot into two regions. Increasing the first joint stiffness in any of the two regions, results in increasing only one of the two natural frequencies but the other natural frequency remains almost constant. The natural frequency is increased as the second joint stiffness changes to a higher value. Figure 4.4 (a and b) clearly illustrates the natural frequencies of both models as they vary with the first joint stiffness for the particular value of 31.27 N.m/rad of the second joint stiffness. The maximum error in the natural frequencies, due to neglecting of the dynamic coupling is less than 1.3 %.

The effect of the second rotor inertia on the manipulator undamped natural frequencies follows. It is observed from figure 4.5 that the second rotor moment of inertia affects only the second natural frequency. Increasing this moment of inertia decreases the second natural frequency and increases the difference between the two models. However, for the wide range of the second rotor moment of inertia considered, the difference between the two models is very small.

4.3.3.2 Frequency Response Functions

It is necessary to linearize the system to permit frequency response analysis. The required linearized models should maintain the fundamental effect resulting from assuming that the kinetic energy of the rotor is only due to its own rotation. The manipulator at the particular configuration where it is fully extended is considered to establish these linearized models. The following two assumptions are also required. First, for a very small change in the links position vector, the manipulator inertia matrix remains constant. Second, for very small changes around this configuration, the Coriolis and centrifugal force vector can be neglected because the sine term, which appears as a multiplication factor in the Coriolis and centrifugal force vector elements, is zero. The Coulomb friction at the motors is neglected. Based on these assumption the following linear model can be obtained.

$$M_s \ddot{X} + C_s \dot{X} + K_s X = f \qquad (4.3.8)$$

where $X = \left[q_1 \; q_2 \; q_{m1} \; q_{m2} \right]^T$, $f = \left[f_1 \; f_2 \; u_1 \; u_2 \right]^T$

and the damping matrix is defined as $C_s = \begin{bmatrix} B & 0 \\ 0 & B_m \end{bmatrix}$

Taking the Laplace transform of equation (4.3.8) with zero initial conditions, the following transfer function model results.

$$X(s) = \left[M s^2 + C s + K \right]^{-1} \; F(s) = G(s) \; F(s) \qquad (4.3.9)$$

where $G(s)$ is the transfer function matrix. The frequency response functions can be obtained by replacing s by $j\,\omega$, where $j = \sqrt{-1}$. The two models were then compared by evaluating the different frequency response functions. Of particular interest, and importance, are the frequency response functions relating the angular acceleration (or velocity) to the motor torques, $G_{33}(s)$ (frequency response function from the first motor acceleration to the first motor torque) and $G_{44}(s)$ (frequency response function from the second motor acceleration

to the second motor torque) as it is used in the identification. Results of the comparison revealed that the two models have almost the same response. Figures 4.6 and 4.7 show frequency response functions $G_{33}(s)$ and $G_{44}(s)$ for the two models.

Based on the comparisons between the two models, one can conclude that the effect of approximating the second rotor rotational kinetic energy, results in a very small change in the dynamic model. The model also retains the basic characteristics of the system regarding the joint flexibility. Thus, the adoption of model 1 for the development and implementation of control algorithms is justified.

4.4 IDENTIFICATION

Accurate estimation of the model parameters is important for accurate control of the robot motions. First, it can be used to provide the link/load parameters for nonadaptive model–based controllers, such as the computed torque method (feedback linearization) or the feedforward+PD method [1]. Second, it may be used to generate reasonable initial parameter estimates for adaptive robot controllers. If the robot picks up a very heavy load, direct application of adaptive control with large parameters uncertainty may result in large initial tracking errors or actuator saturation. The problem becomes more severe in force control because the initial error may result in very early instability.

The solid modelling of the mechanical arm enabled a very accurate estimate of the inertias, masses, and center of masses to be obtained. These estimates are as reliable as the physical measurements of those parameters. In addition, solid modelling has another feature which physical measurements do not have. It is the ability to construct subassemblies then obtain their inertial properties. It would be impossible in reality to isolate and measure properties of such subassemblies. Thus, if one can obtain accurate estimates of the damping and stiffness parameters of the robot, the complete parameters set would be available, and control

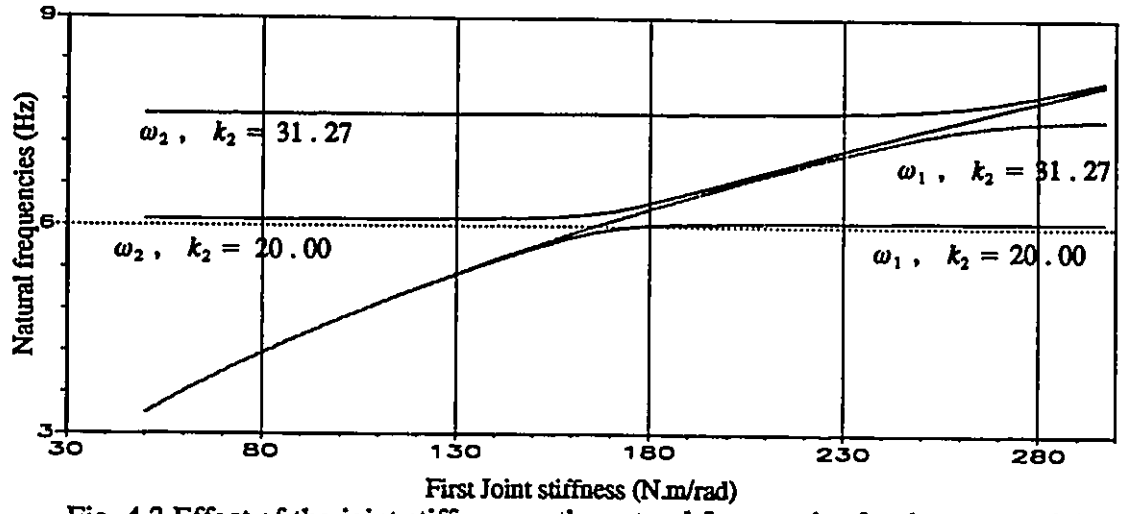

Fig. 4.3 Effect of the joint stiffness on the natural frequencies for the two models

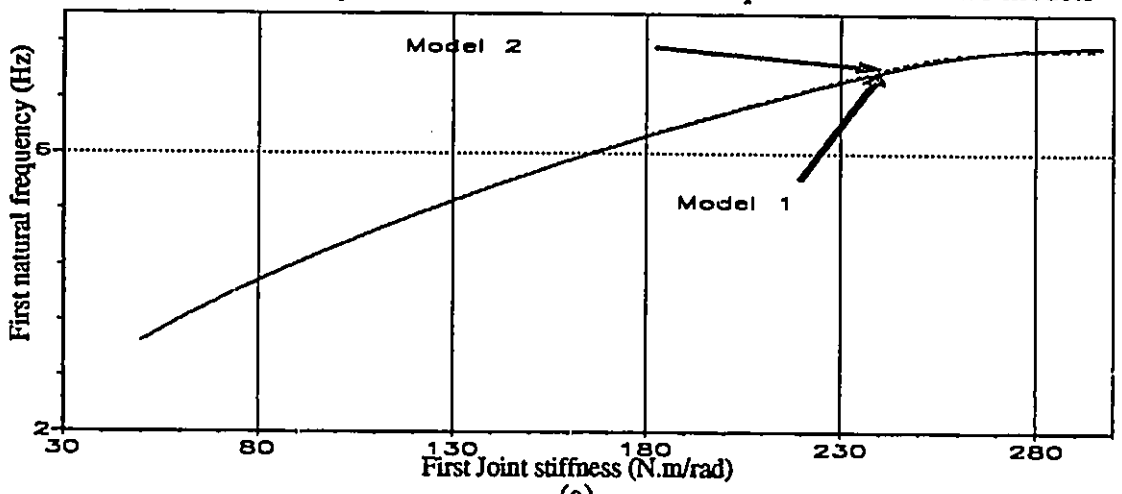

(a)

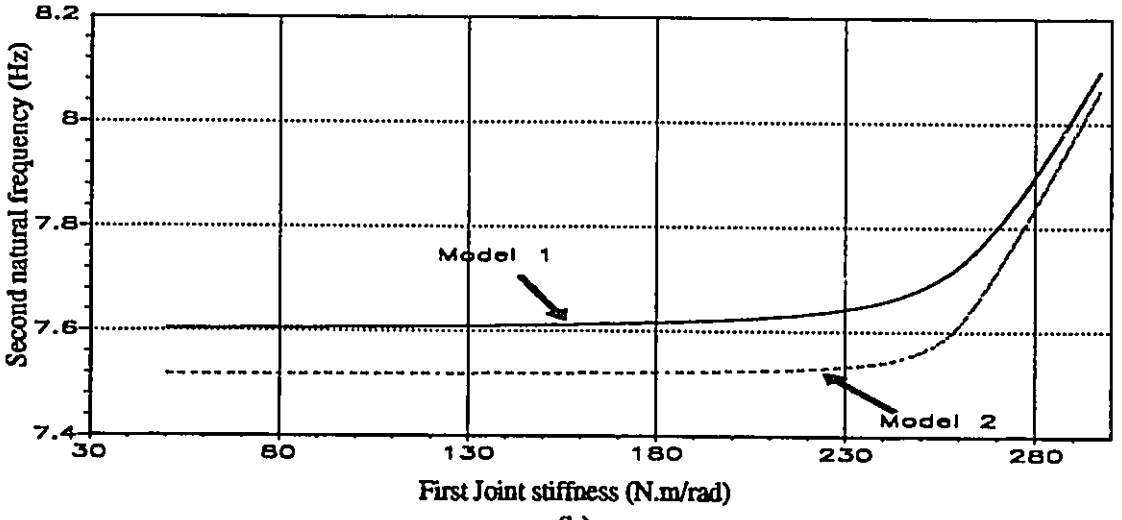

(b)

Fig. 4.4 Effect of the first joint stiffness on the natural frequencies for the two models

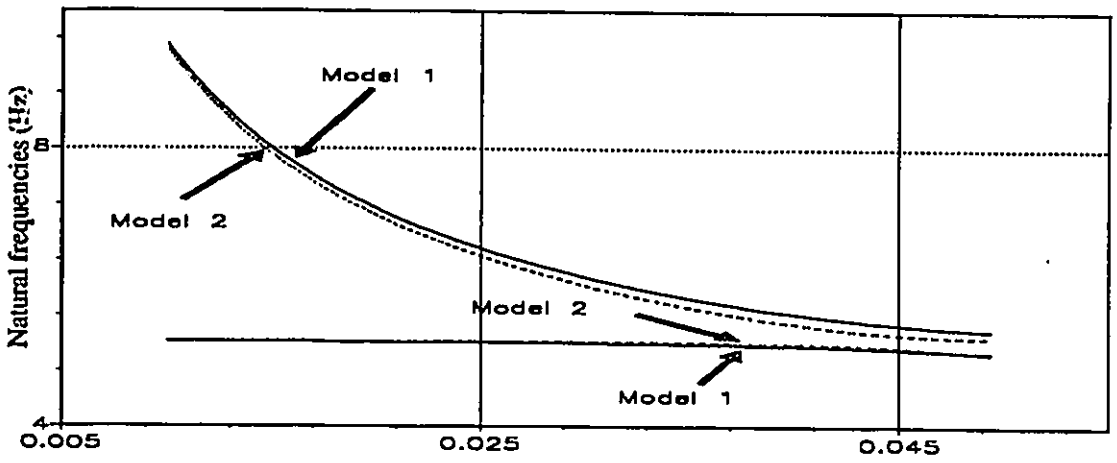

Fig. 4.5 Effect of the second rotor inertia on the natural frequencies for the two models

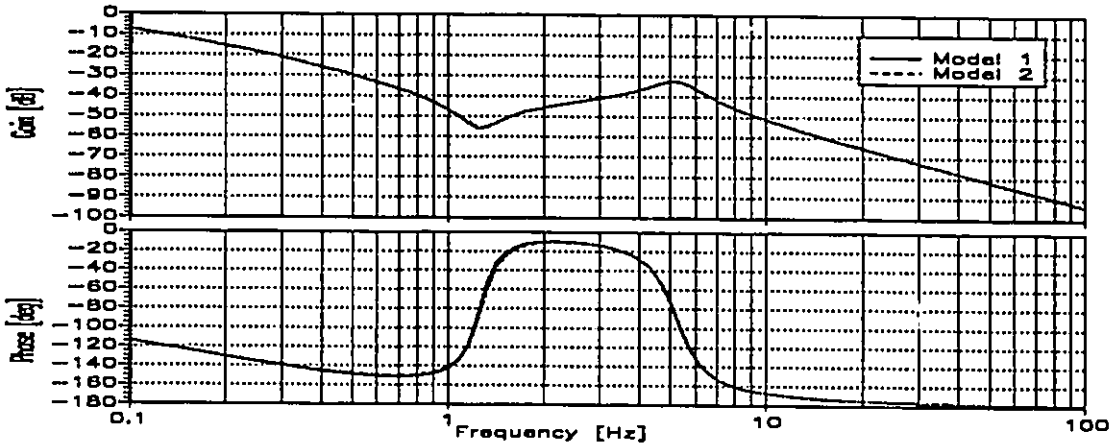

Fig. 4.6 Frequency response function $G_{33}(s)$ for the two models

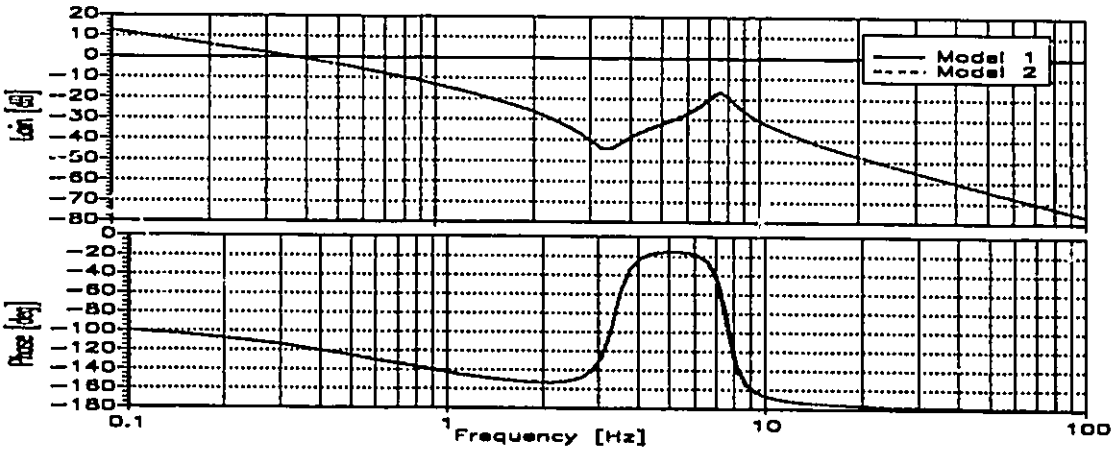

Fig. 4.7 Frequency response function $G_{44}(s)$ for the two models

design can then proceed. However, another identification scheme was performed in which all the parameters were to be identified. Later, the parameters computed form the solid modelling are compared with those from the experimental identification.

4.4.1 Identification Approach and Model

The task of identifying the parameters of the dynamic model given by equation (4.3.1) and (4.3.2) is difficult as the system is nonlinear Multi–Input–Multi–Output (MIMO). It can be noted, by inspecting the dynamic model, that the total number of parameters is 13 (5 inertial, 6 damping, and 2 stiffness). Once these parameters are available, the dynamic model is completely known. Thus, the goal of the identification process is to obtain accurate values for these 13 parameters.

To simplify the identification process, each link and its driving motor are considered separately. This consideration decomposes the experimental manipulator to two Single–Input–Multi–Output (SIMO) systems. The only nonlinearity in each of these two systems is the Coulomb friction in the motors. The Coulomb friction is neglected in these two systems and is to be determined by a separate identification process. Therefore, the experimental manipulator system can be decomposed into two Single–Input–Multi–Output linear systems. The first system is the first joint (the first motor and the first link) and the second system is the second joint (the second motor and the second link). Each of these two systems is a single–link flexible joint manipulator. Figure 4.8 shows a sketch of such a manipulator system.

The following procedures are performed in order to obtain and identify the two systems. First, constrain the first system by clamping the first link to the fixed table, and thus the second system is isolated and identifiable. To identify the first system, the brake of the second motor is applied. Hence, the second system is considered as an extra mass added to

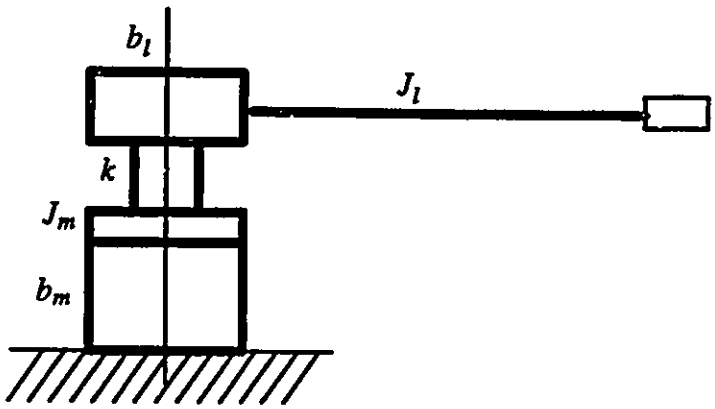

Fig. 4.8 A single–link flexible joint manipulator

the end of the first link. The order of the identification is to identify the second system first then identify the first system. This approach can be applied to the general case of six degrees of freedom manipulators. Hollars [42] used a similar technique to identify a two–link planar flexible joint manipulator. The two linear systems were obtained by considering the manipulator when the relative angle between the two links is 90° and hence the manipulator system is decoupled. The Coulomb friction and the Coriolis and centrifugal force vector were neglected, and thus two linear systems were obtained. Kang et al. [51] performed a similar identification for a two–link direct drive planar robot manipulator. They obtained the identification models by disassembling the robot and identifying each motor/link dynamics.

The following state space model represents either of the two systems discussed above.

$$\dot{x} = A\,x + B\,u$$
$$y = C\,x \qquad (4.4.1)$$

where

$$x = \begin{bmatrix} q_m \\ \dot{q}_m \\ q \\ \dot{q} \end{bmatrix},\quad A = \begin{bmatrix} 0 & 1 & 0 & 0 \\ -k/J_m & -b_m/J_m & k/J_m & 0 \\ 0 & 0 & 0 & 1 \\ k/J_l & 0 & -k/J_l & -b_l/J_l \end{bmatrix},\quad B = \begin{bmatrix} 0 \\ 1/J_m \\ 0 \\ 0 \end{bmatrix} \text{ and}$$

$$C = [0\ 1\ 0\ 0]$$

where q_m, $\dot{q}_m$, q, and $\dot{q}$ are the motor angular position and angular velocity and the link angular position and angular velocity, respectively. k is the joint torsional stiffness. J_m and J_l are the effective inertias of the rotor and the link, respectively. τ is the applied motor torque. The model of a single–link flexible joint robot given by equation 4.4.1 is used as the identification model.

4.4.2 Experimental Identification

At this stage, it is possible to use time or frequency domains identification. After consideration of both alternatives [92,96], the frequency response is used. This enables gaining insight into the dynamic characteristics of the system, which time domain identification would not provide. A collocated transfer function with the motor torque as the input and the motor velocity as the output is chosen for the experimental identification because i) a collocated transfer function contains plant zeros not present in a noncollocated transfer function, and ii) the angular velocity is available directly from the motor servo controller. From the state space model given by equation 4.4.1 the transfer function matrix is defined by:

$$G\ (s) = C\ (sI - A)^{-1}\ B \qquad (4.4.2)$$

For each joint subsystem, the following transfer function can be extracted:

$$g\ (s) \doteq \frac{\dot{q}_m(s)}{u(s)} = \frac{s^2 + 2\ \zeta_z\ \omega_z\ s + \omega_z^2}{J_m\ (s + d)\ (\ s^2 + 2\ \zeta_p\ \omega_p\ s + \omega_p^2\ )} \qquad (4.4.3)$$

The identification of the robot is reduced to the identification of two transfer functions. Each of these transfer functions is with its own coefficients given by equation (4.4.3). The robot parameters are related to the transfer function coefficients by a set of algebraic equations. The two transfer functions were identified by using sine sweep tests for each of the two joints, then the robot parameters were extracted. The inertia coupling term d_3 cannot be extracted

as it is included in both J_l's, thus its value is obtained by matching the resonant frequencies of the manipulator dynamic model with the experimental resonant frequencies.

For each of the two transfer functions, the sine sweep excitation signal has a frequency band of 0.5 to 20.0 Hz, the total test period is 10.23 seconds, and the sampling frequency is 100.0 Hz [92]. This specific frequency band is selected as it contains all the zeros and poles of the two transfer functions and it is not desirable to introduce other dynamics into the identification process. The amplitudes of the excitation signals were chosen to ensure exciting the resonant frequencies of the system in the allowable range of the resulting link motions.

Figures 4.9 and 4.10 respectively show plots of the measured and identified frequency response functions for the first and second joints. The magnitude and phase of the frequency response function are shown for frequencies up to 20.0 Hz. The problem was formulated so as to minimize the error of the complex frequency response [67]. The transfer functions identified were obtained by using the weight least squares technique. The theoretical fit is reasonably good for the magnitude, however, it is poor for the phase due to the Coulomb friction nonlinearities at the motors which were neglected in the identification model. The test and procedure of fitting a theoretical model to the frequency response measurements were repeated several times. Most of the tests gave similar results, only one is chosen because, in this type of frequency response identification, no benefits would result from averaging.

Table 4.1 lists the transfer functions parameters which were identified. The experimental robot manipulator exhibits the joint flexibility problem. Specifically, it has two resonant frequencies at 5.2 and 7.5 Hz and the cantilever vibration frequency of the manipulator is 1.7 Hz. The true linear damping coefficients are probably less than those obtained if Coulomb friction could be isolated. Table 4.2 lists the robot parameters from the solid modelling

and the experimental frequency response identification. The values shown indicate excellent correlation between the two approaches used to obtain the robot dynamic model parameters. Only the joint stiffness constants are smaller than their designed values

Joint stiffness identification

When the robot parameters were extracted from the frequency response functions identification, it was found that the joint stiffness constants are smaller than their designed values as can be noted in table 4.2. This difference could be due to the fact that the helical torsional springs end with extended arms (for torque transmission and construction purposes), and hence the joint effective stiffness accounts for both the coils and the extended arms while the designed stiffness was only based on the coils. The joint stiffness constants were identified statically by constraining the link and commanding its driving motor to apply a specific torque. For each joint 10 measurements (5 in each direction of rotation) of the applied torque and the resulting motor rotation were recorded. The least squares fitting of the data provided average values of the joint stiffness constants. These values are 135.46 and 31.34 N.m/rad for the first and second joints, respectively, thus agreeing with values obtained from the experimental frequency response identification.

Coulomb friction identification

It is true that direct drive motors eliminate backlash, however, friction still exists. In the frequency response identification carried out, the Coulomb friction in the motor was neglected, and only viscous friction was considered. Initial control experiments, PD and feedback linearization in the joint space, indicated that the motors have Coulomb friction which must be considered in the dynamic model. For each joint, the Coulomb friction was identified by recording the commanded torque at which the rotor started rotating. Several measurements were acquired in both directions of rotation for many configurations of the robot work space, then an average value for the Coulomb friction was identified. Table 4.3

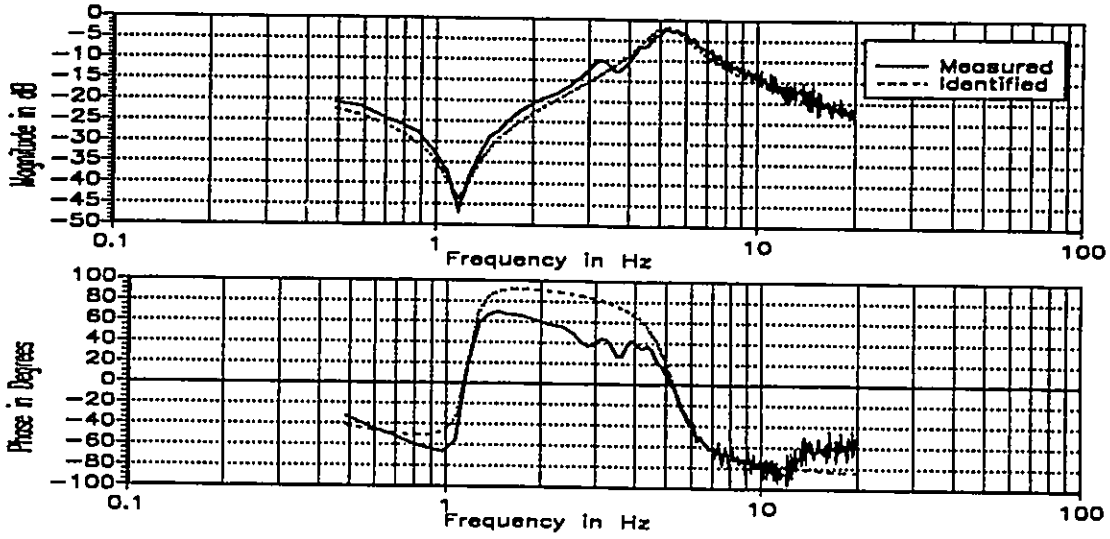

Fig. 4.9 Measured and identified transfer function of joint 1

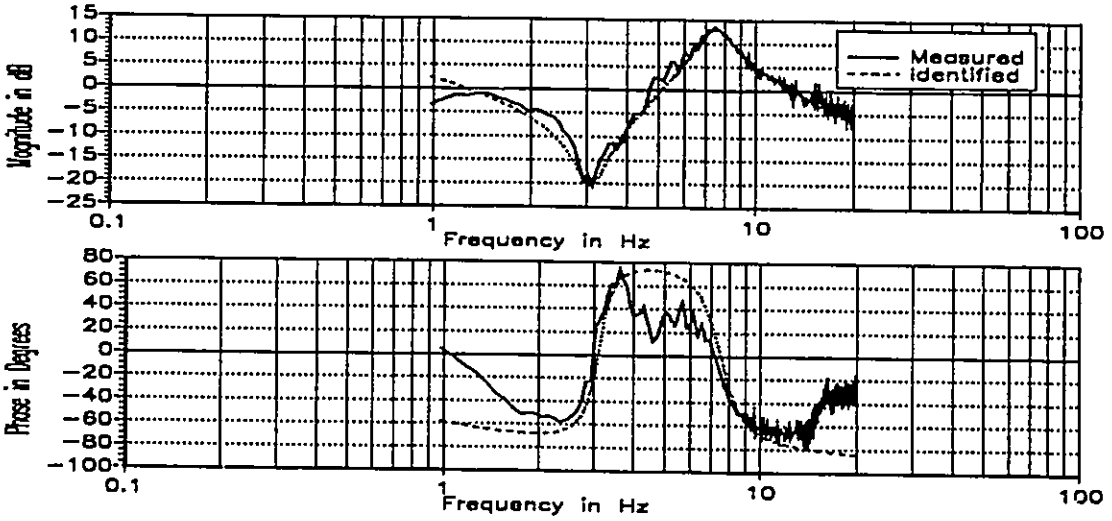

Fig. 4.10 Measured and identified transfer function of joint 2

lists the identified Coulomb friction values and the values supplied by the manufacturer together with their percentage of the motors maximum torques. The values identified are smaller than those supplied, however, their percentages suggest that their effect should be considered. Compensation for the Coulomb friction is presented in Chapter 5.

4.4.3 Model Validation

Model validation is performed in three separate stages. First, validation of the identified transfer functions. Second, a comparison between the robot parameters from the frequency response identification and from the solid modelling. Third, and most important, studying the tracking errors and performance of experimentally implemented model–based controllers .

Frequency response function

For each of the two transfer functions, the estimated and measured velocities were compared. The results indicated that the model is reasonably good in generating a response very close to that measured. However, the residual magnitudes were unsatisfactory. Inspection of the bode diagrams in figures 4.9 and 4.10 clearly shows the phase lag in the experimentally measured frequency response when compared with the theoretical fit. This phase lag could be attributed to the Coulomb friction in the motors, this was evident in the linear decaying of the measured velocities. Another model is constructed in which the Coulomb friction nonlinearity was combined, as a feedback loop, with linear transfer function as shown in figure 4.11.

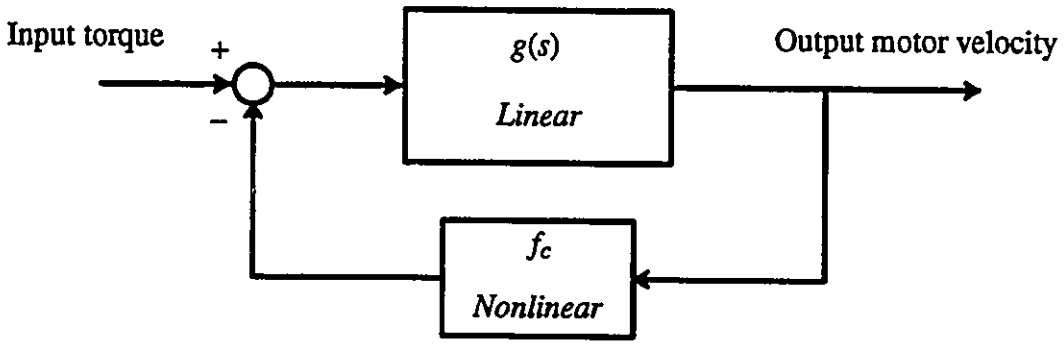

Fig. 4.11 Joint nonlinear model

The estimated velocity from this model is more consistent with the measured velocity than that estimated from the joint linear transfer function alone. Moreover, the maximum

error between the estimated and measured velocities was significantly reduced when Coulomb friction was included in the model. As indicated by Sinha and Kuszta [96] the model is considered to be suitable if the responses of the plant and the model are sufficiently close. How the responses are close can be quantified in terms of the sequence of the residuals. A model is considered satisfactory if the residuals form a white noise with zero mean, and has a small a variance as possible. The test used here for the velocity residuals is that suggested by Stoica [108]. The test is to satisfy, for 95% confidence, the following inequality:

$$N \sum_{i=0}^{m} \varrho_i^2 \leq (m + 1.65\sqrt{2m}) \qquad (4.4.3)$$

where ϱ_i is the i^{th} correlation coefficient, N is the total number of measurement points, and m is the number of points over which the summation is taken. This condition was satisfied for both models of the joints. For the first joint model 250 points are used and gave 248.3377 $\leq$ 286.895. While for the second joint model, the inequality is satisfied for the total number N, as 1041.7 $\leq$ 1098.7. The reason for the critical satisfaction of the condition for the second joint model is because Coulomb friction amplitude is not constant with the velocity as proposed in the nonlinear model. However, the value obtained in the separate Coulomb friction identification is an upper bound. Besides the observed nature of the Coulomb friction, other possible sources of error include the noise in the measured velocity and ripples in the motor output torque. Based on the results of these tests, the joint models are satisfactory. The comparison of the robot parameters from the frequency response identification and from the solid modelling, as listed in table 4.2, serves as another validation for the frequency response identification.

Robot dynamic model

Since the purpose of estimating the robot parameters is to use them for control, the

best test for verifying the quality of the estimates is to use them in a robot controller. Thus, the experimental performance of the model–based controllers can be used to validate the robot dynamic model and parameters' estimation. This is because, model–based controllers require the knowledge of the true system parameters in order to perform in a stable and acceptable manner. In conclusion, the experimental results obtained from the model–based controllers, in which the experimentally identified parameters were adopted, presented in Chapters 5 and 6, simply mean that the identified parameters are satisfactory for the control purpose.

Table 4.1 Transfer function parameters

	First joint	Second joint
ω_z rad/sec (Hz)	7.38 (1.7)	19.47 (3.1)
ς_z	0.060	0.075
ω_p rad/sec (Hz)	32.75 (5.2)	47.12 (7.5)
ς_p	0.143	0.116
d rad/sec	1.717	3.68
J_m kg.m^2	0.1224	0.0168

Table 4.2 Robot parameters from Design and Sine Sweep Identification

	I–DEAS	Sine Sweep
l_1 (m)	0.400	
l_2 (m)	0.350	
d_1 (kg.m^2)	2.110	2.087
d_2 (kg.m^2)	0.223	0.216
d_3 (kg.m^2)	0.085	0.084
b_1 (N.m.s/rad)		2.041
b_2 (N.m.s/rad)		0.242

Continued Table 4.2 Robot parameters from Design and Sine Sweep Identification

b_{m1} (N.m.s/rad)		1.254
b_{m2} (N.m.s/rad)		0.119
k_1 (N.m/rad)	198.49	125.56
k_2 (N.m/rad)	51.11	31.27
I_{m1} (kg.m^2)	0.1226	0.1224
I_{m2} (kg.m^2)	0.017	0.0168

Table 4.3 Motors Coulomb friction

	First motor	Second motor
F_c identified (N.M) % of the max. torque	3.2 3.2	1.2 4.0
F_c supplied (N.M) % of the max. torque	5.0 5.0	2.0 6.6

4.5 SUMMARY

In this chapter, the kinematic and dynamic models of the experimental two–link flexible joint robot manipulator are presented, together with the identification approach and experimentations. The dynamic characteristics of the two dynamic models developed for the flexible joint robot were studied and compared. The results of the comparison justifies the use of model 1 where the links and the motors systems are only statically coupled. The dynamic model parameters obtained from the experimental identification closely match those obtained during the design using solid modelling. In addition, the presented identification approach enabled studying the dynamic characteristics of the experimental manipulator which, in turn, ensured that the design objectives were satisfactorily achieved. For each of the two joints, joint stiffness and Coulomb friction were identified separately.

CHAPTER 5

PRELIMINARY CONTROL

This chapter describes the design and implementation of the PD controller, commonly used for industrial robotic applications. A fourth order feedback linearizable model of the flexible joint manipulator is derived and its properties are presented. A nonlinear feedback linearization controller is designed, based on the full nonlinear fourth order model, simulated, and implemented on the experimental robot in the joint space. Simulation and experimental results of the PD and nonlinear feedback linearization controllers are presented.

5.1 INTRODUCTION

It was both interesting and worthwhile to design and test PD control for the experimental flexible joint robot manipulator. The reasons are: i) the PD controller is commonly used for industrial robots and thus it was interesting to investigate and evaluate its performance and potential for further application in controlling the position and force for flexible joint robots, ii) the PD controller is one of many independent joint control algorithms in which all the coupling terms between the links are neglected, and iii) it requires very simple computation makes it attractive for experimental implementations. Hollars [42] verified bandwidth limitations as presented earlier by Book [7] for flexible robots. The analysis of a general model of a single–link flexible joint showed that an absolute limit on the achievable bandwidth exists and is equal to one–half the cantilever frequency of the system with direct drive and impedance matched drive trains.

5.2 PD CONTROL

5.2.1 PD controller Design

The PD controller design is based on a linear model of the experimental flexible joint robot which was used in the identification and in equation 4.4.1. The critical issue is whether to use link or motor states for the feedback. The output to be controlled is, of course, the link angular position. If one defines the output matrix to include both the link and motor angular positions, then there are two open loop transfer functions between the input torque and the outputs. These two transfer functions are given by the following two equations:

$$G_l(s) \doteq \frac{q_l(s)}{u(s)} = \frac{K_l}{s\,(s+d)\,(s^2 + 2\,\zeta_p\,\omega_p\,s + \omega_p{}^2)} \qquad (5.2.1)$$

$$G_m(s) \doteq \frac{q_m(s)}{u(s)} = \frac{K_m\,(s^2 + 2\,\zeta_z\,\omega_z\,s + \omega_z{}^2)}{s\,(s+d)\,(s^2 + 2\,\zeta_p\,\omega_p\,s + \omega_p{}^2)} \qquad (5.2.2)$$

The case of noncollocated feedback control limits the allowable used gains. In other words the noncollocated controller is unstable for high gains which can be seen from its root–locus analysis. Thus, the case of collocated feedback control was considered. In this case, the motor angular position and velocity are used to implement the PD control law. Therefore, the PD control law for each joint is given by:

$$u = K_p\,(q_d - q_m) + K_v\,(\dot{q}_d - \dot{q}_m) \qquad (5.2.3)$$

where q_d and $\dot{q}_d$ are the desired link angular position and velocity respectively, and K_p and K_v are the proportional and derivative feedback gains respectively. The controlled joint system can be represented as in figure 5.1 when the motor angular position only is used in the feedback. When the motor angular velocity only is used, the system can be represented as in figure 5.2. The design of the gains for the PD controller is based on the root locus analysis.

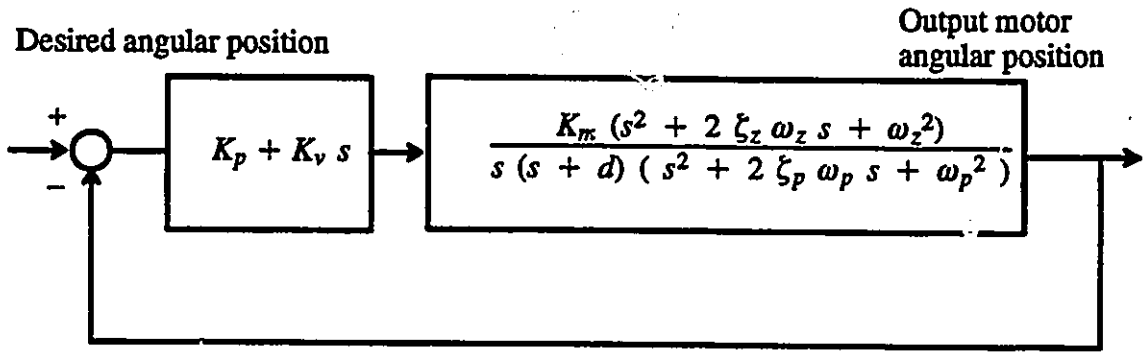

Fig. 5.1 PD joint control with position measurement

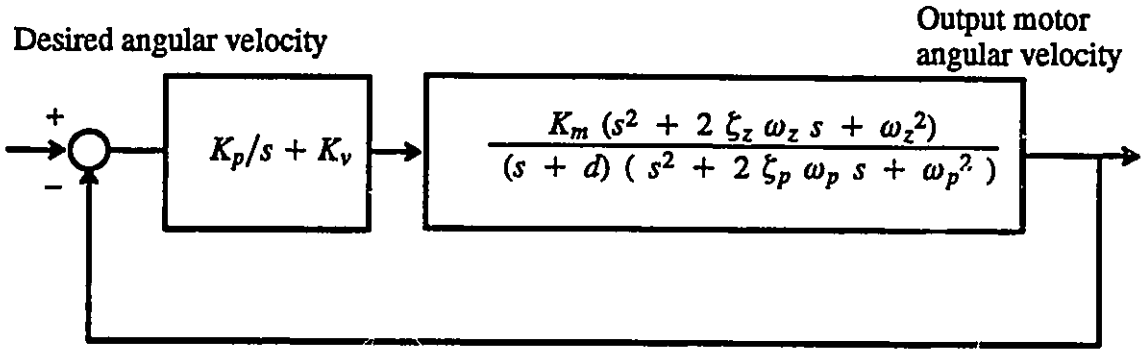

Fig. 5.2 PD joint control with velocity measurement

Figures 5.3 and 5.4 show the root loci of the closed loop system for the first and second joints when motor velocity is used to close the loop.

Inspecting the root loci clearly shows that the system is stable for all values of the derivative feedback gain. However, the presence of the open loop zeros near the imaginary axis may result in poor performance. Lyapunov stability criterion can be used to prove that the pure PD feedback for a passive structure is stable when the phase loss due to sensor dynamics, actuator dynamics, and digital implementation time delay are neglected. Table 5.1 lists the PD controller feedback gains corresponding to the root loci design presented in figures 5.3 and 5.4.

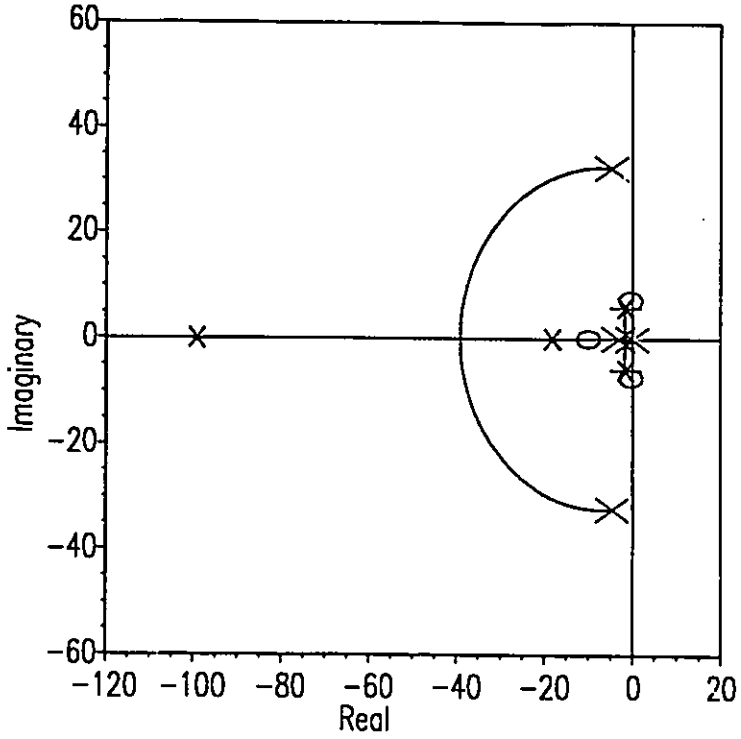

Fig. 5.3 root locus under PD control for joint1

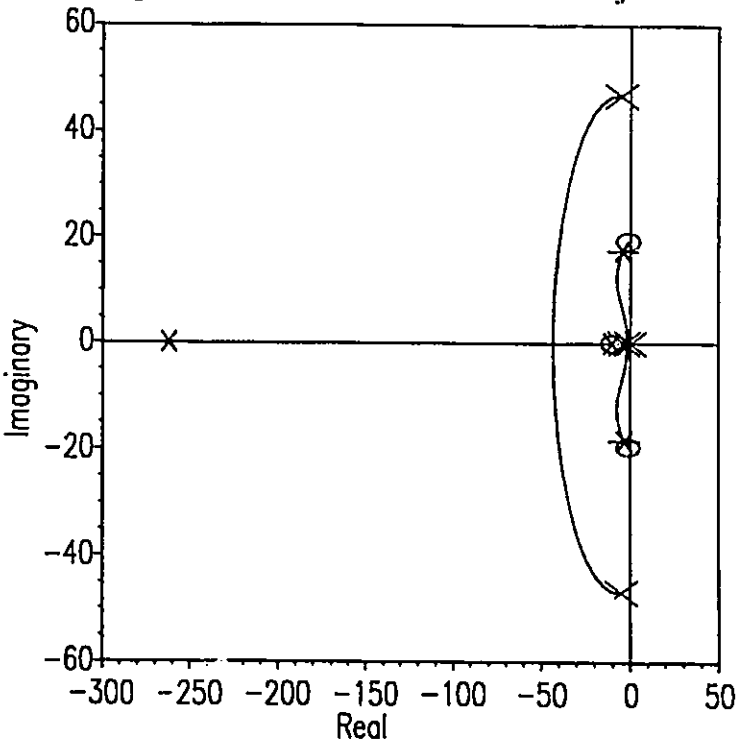

Fig. 5.4 root locus under PD control for joint 2

Table 5.1 PD controller gains

	First Joint	Second Joint
K_p	133.0	13.3
K_v	45.0	4.5

5.2.2 Implementation Issues

5.2.2.1 Trajectory generation

Through efforts and studies made concerning trajectory generation for robot manipulators, a close relation has been found between the trajectory and the controller which must be considered during trajectory design. For the feedback linearization controller, presented in section 5.3, the fourth order derivative of the desired angular position should be smooth and continuous. Thus at least a fifth–order polynomial function is necessary for the desired position. To ensure this requirement and to have a base for comparing the PD with the feedback linearization, a smooth trajectory of a ninth–order polynomial is selected. It requires few more computations than the fifth–order polynomial. The trajectory generation function for simulation and real–time control codes requires only two parameters; the total motion time and the total travel to completely specify the trajectory up to the fourth derivative. Figures 5.5 and 5.6 show the desired position, velocity, and acceleration for one second rise time step.

5.2.2.2 Coulomb friction compensation

It is necessary to compensate for the Coulomb friction at the motors in order to enhance the motors performance. After modelling the Coulomb friction, the feedback linearization approach is used to feedback a Coulomb–friction cancelling torque signal which can be combined with other controllers. When a slightly smaller level of friction, about 85%, is used for the Coulomb friction compensation the response of the joint was reasonably im-

proved. For stiction compensation, a small dead band around the zero velocity is combined with the Coulomb feedback torque. The amplitude of the stiction compensation in this dead band is a little smaller than that which starts the rotor motion. A standard method of reducing the stiction effect in a system is never to let the friction surfaces come to rest with respect to each other as demonstrated experimentally by Hollars [42]. This can be achieved by applying a high frequency torque signal called "dither" to the motors to keep the contact surfaces oscillating at a very small amplitude. However, this technique was not implemented because the stiction level is not constant for all configurations and the dither signal, when applied at low stiction configuration, would result in an undesirable high amplitude of oscillations. Therefore, the Coulomb friction is compensated for by the following torque signal which combines the dead band as well:

$$\tau_c = \begin{cases} F_{cr}\, sgn(\dot{q}_m) & |\dot{q}_m| \geq 0.015 \\ F_{ct}\, sgn(\dot{q}_m) & |\dot{q}_m| < 0.015 \end{cases} \qquad (5.2.4)$$

where F_{cr} and F_{ct} are 85% and 95% of the Coulomb friction identified in Chapter 4.

5.2.3 Simulation Results

All controllers developed in this thesis have been simulated to evaluate their performance prior to experimental testing. In the simulations, the PD controller was applied to the full nonlinear model as described by equations 4.3.1 and 4.3.2. The desired trajectory for each of the two joints is a 0.75 rad smooth step in one second as presented in section 5.2.2.1. Figures 5.7 and 5.8 show plots of the desired angular position, and the actual motor and link angular positions for the two joints. Figures 5.9 and 5.10 show plots of the desired angular velocity and the actual motor and link angular velocities. The performance specifications of any controller are accuracy, stability and speed of response. The PD controller meets the stability specification but the transient and steady state response are not acceptable because of the clear significant overshoot and the slow speed of response. Another important criterion

to consider in the evaluation is the response of not only the motors (flexible system) but also the links (rigid system). The main issue in the collocated PD controller is that it aims at controlling the motor state, not the link state. Although, for a typical robot manipulator, all the tasks can only be performed by the links motion. Thus, even if the PD controller would perfectly track the desired angular position and velocity this does not ensure in any manner the acceptable control of the links simply because the motors and the links are connected by the joint finite stiffness. Tracking of the motor to achieve tracking of the links would only be reliable if the joint is perfectly rigid. In conclusion, the PD controller may give acceptable performance for rigid robots but not for flexible joint robots.

5.2.4 Experimental Results

The PD controller was implemented on the experimental robot. The sampling frequency was 1 KHz and the Coulomb friction compensation was combined with the control law. The desired trajectory is the same as that used in the simulation. Figures 5. 11 and 5.12 show plots of the desired angular position and the measured angular positions of the motor and the link for the two joints. Figures 5.13 and 5.14 show the desired and measured angular velocities for the two joints. There are agreements between the simulation and the experimental performance of the PD controller including: i) the clear overshoot, ii) the slow speed of response, and iii) the long settling time. These performance characteristics identify the unacceptable performance. Coulomb friction compensation enhanced the response of the motor, however, the links still lag the desired trajectory. Different root locus–based designs were tested and led to the observation that increasing the ratio of the proportional gain to the derivative gain reduces the overshoot and increases the speed of response. However, the performance remained unacceptable.

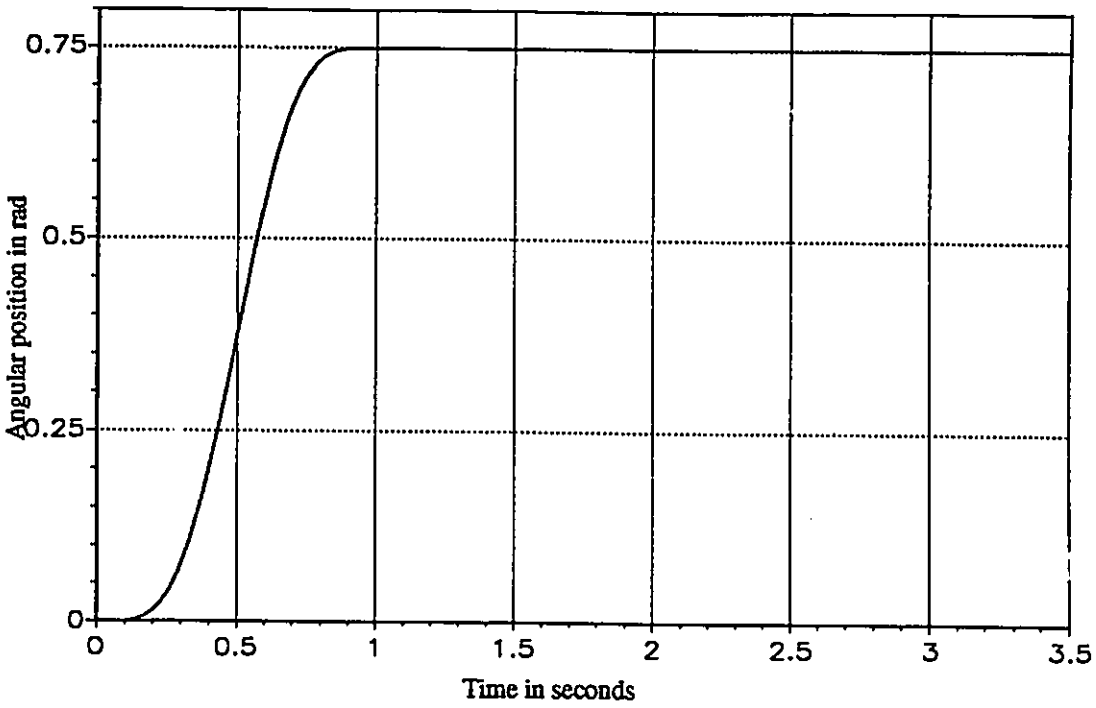

Fig. 5.5 Desired position trajectory

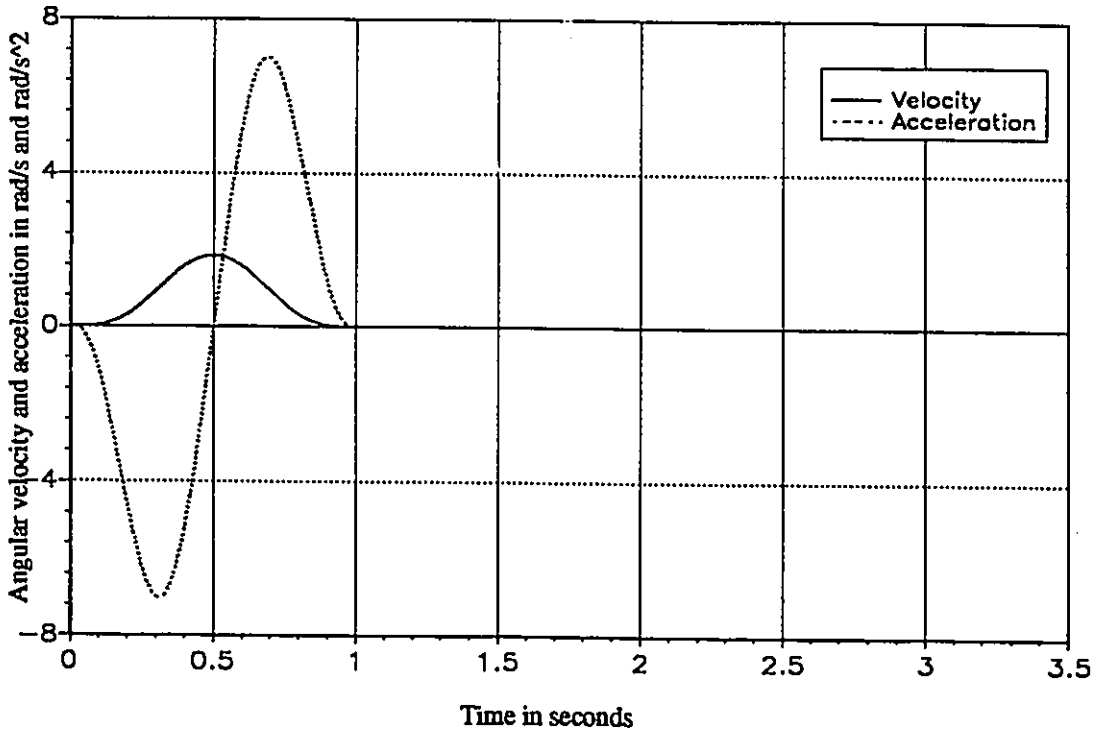

Fig. 5.6 Desired velocity and acceleration trajectories

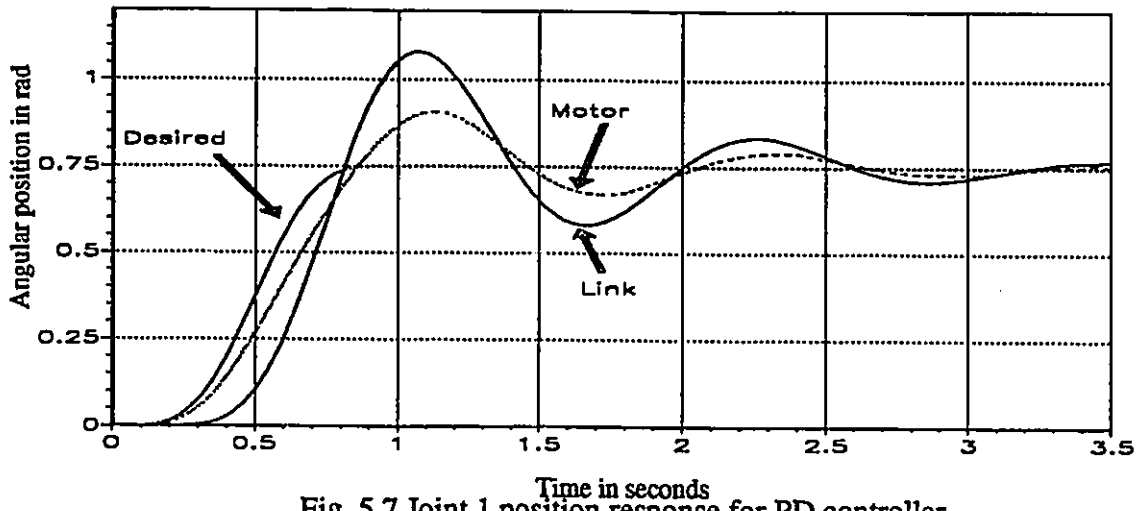

Fig. 5.7 Joint 1 position response for PD controller

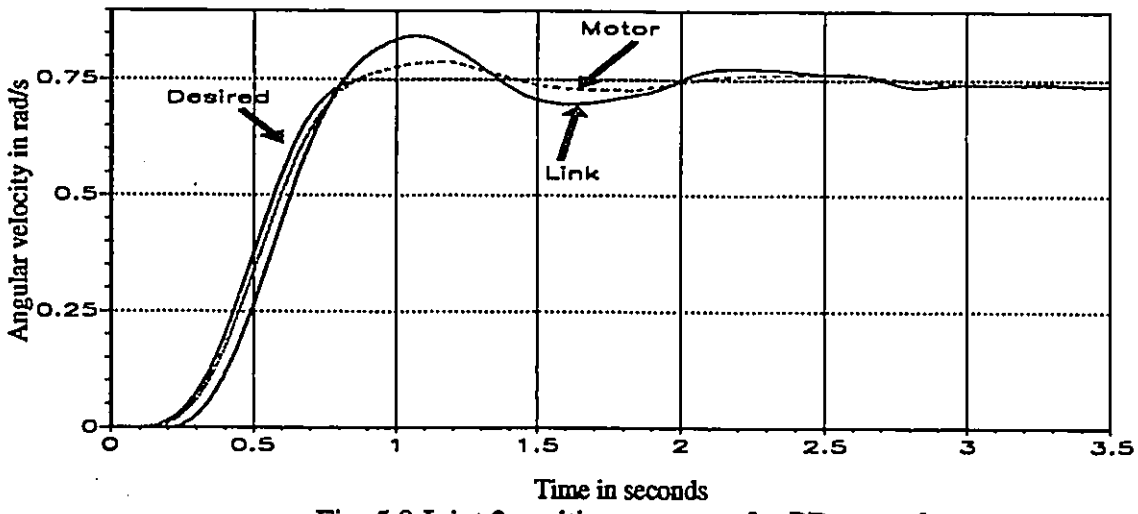

Fig. 5.8 Joint 2 position response for PD control

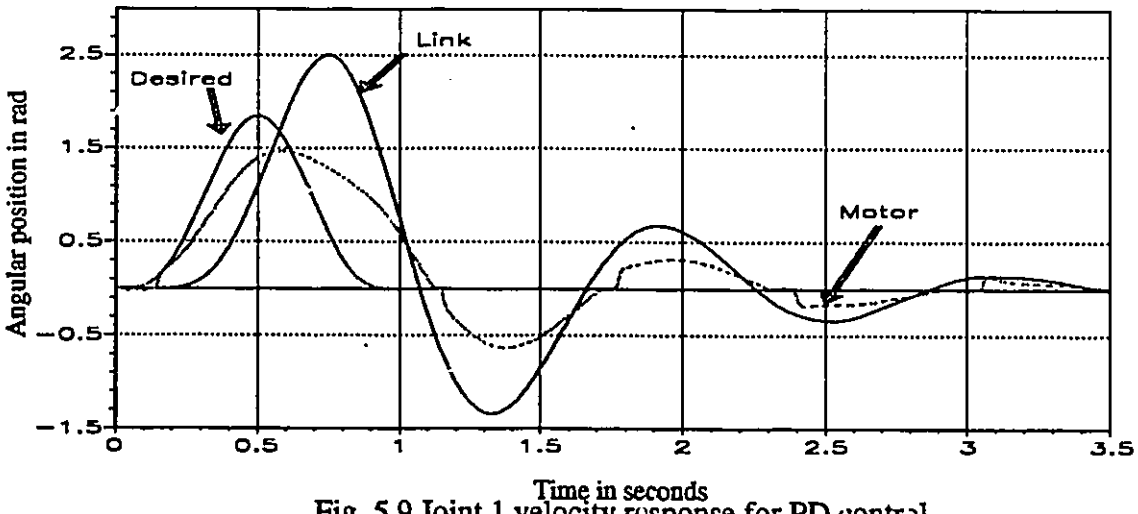

Fig. 5.9 Joint 1 velocity response for PD control

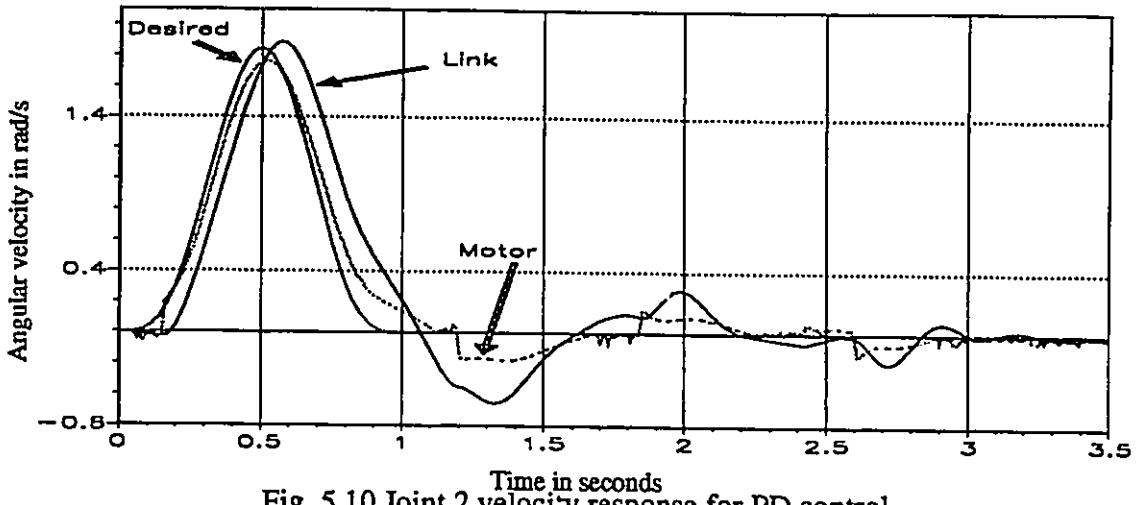

Fig. 5.10 Joint 2 velocity response for PD control

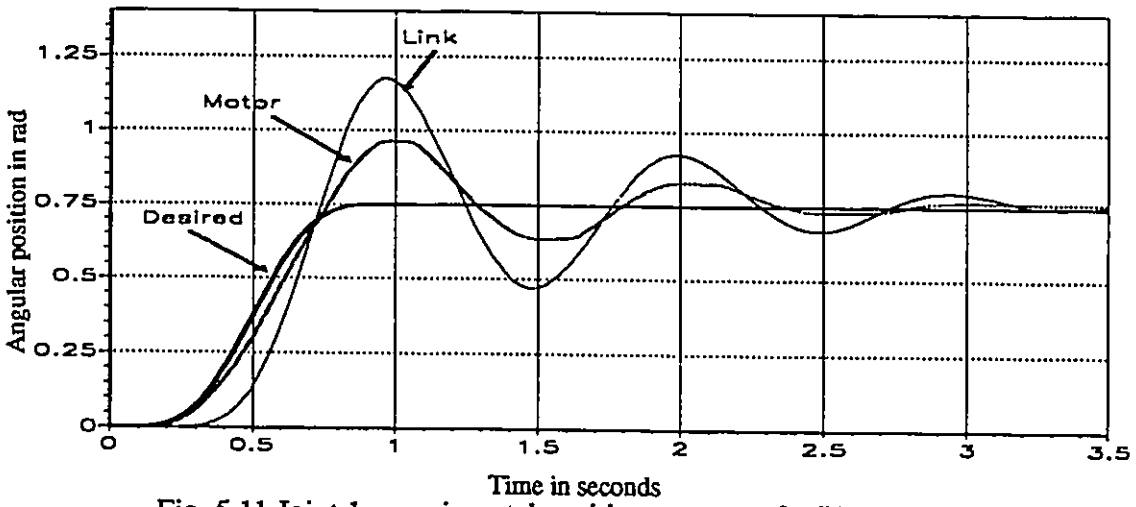

Fig. 5.11 Joint 1 experimental position response for PD controller

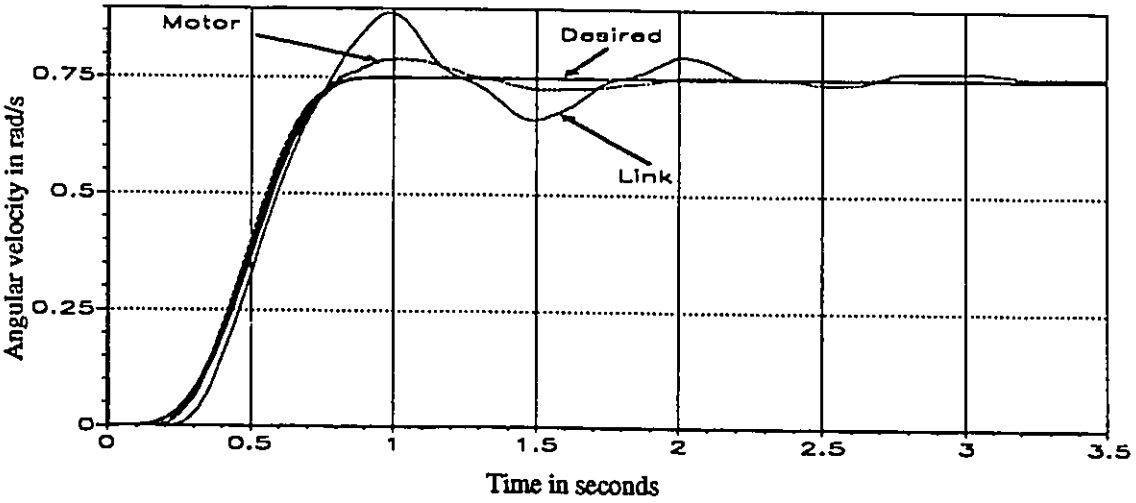

Fig. 5.12 Joint 2 experimental position response for PD control

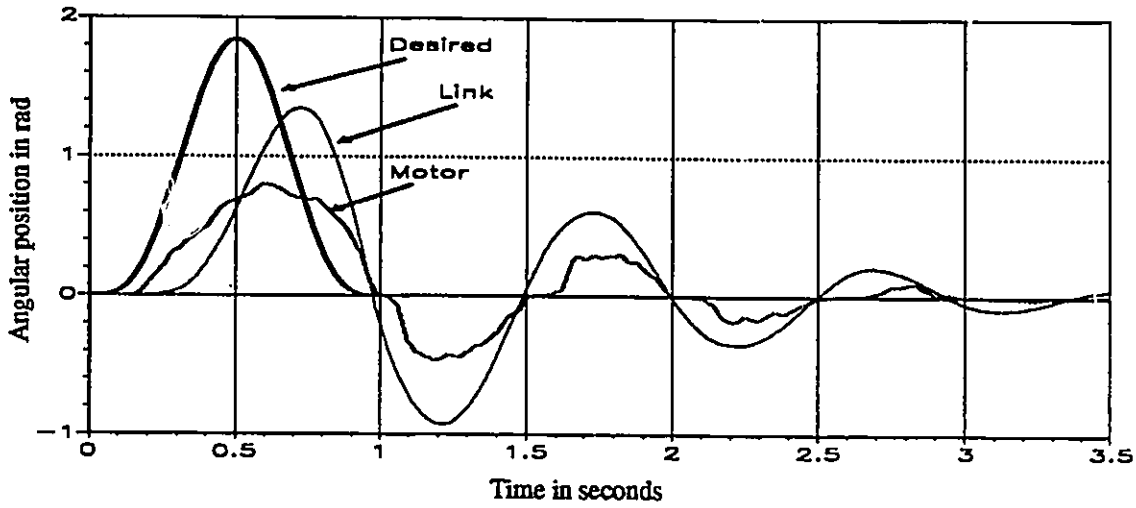

Fig. 5.13 Joint 1 experimental velocity response for PD control

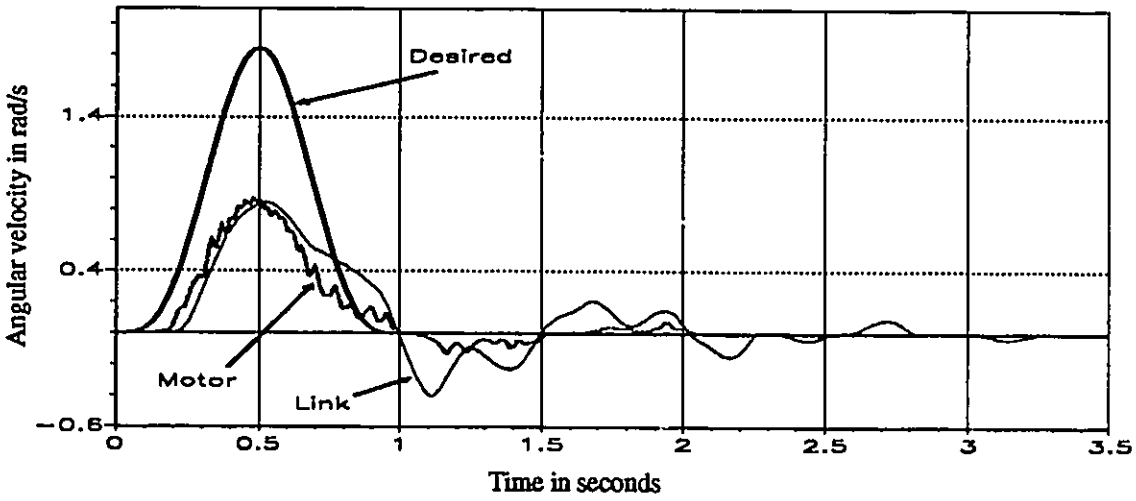

Fig. 5.14 Joint 2 experimental velocity response for PD control

5.3 FEEDBACK LINEARIZATION CONTROL

In this section, the feedback linearization control approach is presented. First, the basic concept is discussed followed by the application of the approach to flexible joint robots. Finally, design, simulation and experimentation of the feedback linearization for the experimental robot in the joint space are presented .

5.3.1 Basic Concept

The basic idea of the feedback linearization approach is to construct a nonlinear control law as an inner loop control which, in the ideal case, exactly linearizes the nonlinear system after a suitable state space change of coordinates. A second stage, or outer loop control in the new coordinates, is then designed to satisfy traditional control design specifications such as tracking, disturbance rejection, and so forth. In some cases, a nonlinear system has the structure which allows to judge whether it is feedback linearizable or not just by inspection. For example, if the nonlinear system state space equation has the following structure [54]:

$$\dot{x} = A\,x + B\,\beta^{-1}(x)\,[u - \alpha(x)] \qquad (5.3.1)$$

where A is nxn, B is nxp, the pair (A, B) is controllable, and the functions $\alpha : R^n \rightarrow R^p$ and $\beta : R^n \rightarrow R^{pxp}$ are defined in a domain $D \subset R^n$ that contains the origin. The matrix $\beta(x)$ is assumed to be non–singular for every $x \in D$. Then the system can be linearized via the state feedback

$$u = \alpha(x) + \beta(x)\,\nu \qquad (5.3.2)$$

where ν is a new input that can be designed as

$$\nu = -K\,x \qquad (5.3.3)$$

such that the matrix $A - BK$ is Hurwitz. The overall nonlinear stabilizing control is:

$$u = \alpha(x) - \beta(x)\ K\ x \qquad (5.3.4)$$

When the nonlinear system does not have the structure of equation 5.3.1 it does not mean that the system is not feedback linearizable. The state equation might have the structure of equation 5.3.1 with another choice of the state variables. The following theorem formally defines feedback linearizable systems.

Theorem 1 [110]:

The nonlinear system

$$\dot{x} = f(x) + g(x)\ u \qquad (5.3.5)$$

where $x \in R^n$ and $u \in R^m$ with $f(x)$ and $g(x)$ are smooth vector fields on R^n and $f(0) = 0$, is feedback linearizable if and only if there exists a region U containing the origin in R^n in which the following two conditions hold:

1– The vector fields $\{\ g,\ ad_f(g), \ldots,\ ad_f^{n-1}(g)\ \}$ are linearly independent in U

2– The set $\{\ g,\ ad_f(g), \ldots,\ ad_f^{n-2}(g)\ \}$ is involutive in U.

$ad_f(g)$ is the Lie Bracket of $f(x)$ and $g(x)$ which is denoted by $[f, g]$ and is defined by $ad_f(g) = [f, g] = \frac{\partial g}{\partial x} f(x) - \frac{\partial f}{\partial x} g(x)$. Also, $ad_f^k(g) = [f, ad_f^{k-1}(g)]$ by induction.

The two conditions are equivalent to finding the coordinate transformation such that in the new coordinate variables the state equation has the structure of equation 5.3.1. In other words, the existence of the state transformation and the nonlinear control law (equation 5.3.2), when applied to the nonlinear system, results in a linear controllable system which satisfies the above two conditions.

For example, given a nonlinear system

$$\dot{y} = f(y) + g(y)\ u \qquad (5.3.6)$$

where $f: U \to R^n$ and $g: U \to R^{n \times p}$ are sufficiently smooth on a domain $U \in R^n$ is said to be feedback linearizable if there exists a diffomorphism $T: U \to R^n$ such that $D = T(U)$

contains the origin and the change of variables $x = T(y)$ transforms the above system into the form of equation 5.3.1 with (A, B) controllable and $\beta(x)$ is non–singular for all $x \in D$. The structure of the feedback linearization control approach can be best illustrated by figure 5.15.

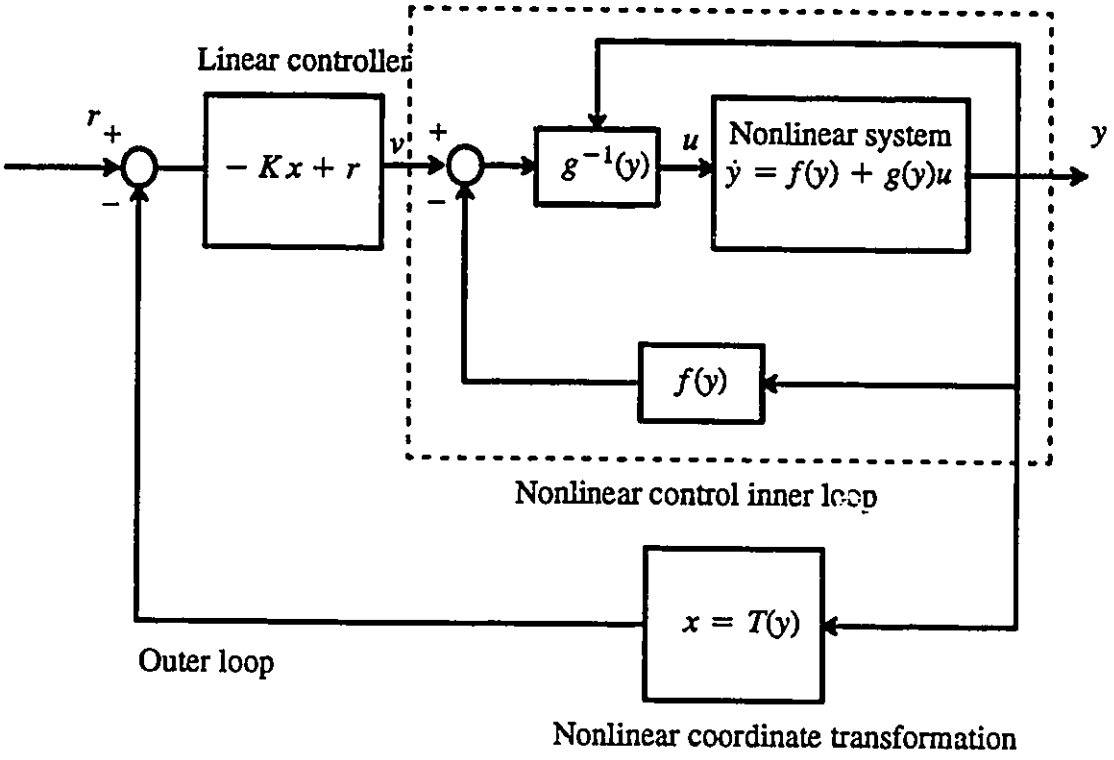

Fig. 5.15 Structure of the feedback linearization approach

Related Issues

There are several important issues to be considered when using the feedback linearization methodology to ensure obtaining the full advantage of this strong nonlinear control approach.

1– State transformation:

Consideration should be given to the availability of the new state as it is required for the feedback. If the new state is not available through direct measurements it can be com-

puted from the nonlinear coordinate transformation. This introduces the second issue, regarding the knowledge of the system parameters. The exact new state can be obtained only if the original full state is available and the parameters of the system are exactly known.

2– Exact parameters:

Knowledge of the exact parameters of the system is necessary to achieve exact linearization by the inner control loop and to compute the new state (in case it is difficult to measure). These two main issues are critical to the applicability of the feedback linearization approach. They are considered in detail in Chapter 7 of the thesis.

5.3.2 Fourth Order Feedback Linearizable Model

The computed–torque or feedback linearization control has been very popular for rigid robots. The advantages of this control approach over its linear counterpart are that it utilizes the full nonlinear model of the robot manipulator in a way which enables decoupling and linearizing the system in the whole work space and specifying desired characteristics to the decoupled linear subsystems. The positions and velocities of the motors and links and the exact parameters of the manipulator are required to achieve exact decoupling and linearization. If these two requirements are met the computed–torque performance would be superior to linear control methods. Moreover, if there is some uncertainty in the robot parameters, the computed–torque satisfies the matching conditions which makes it possible to design robust outer loop controllers.

These attractive advantages can be obtained if the feedback linearization is applied to the flexible joint robot manipulators. Several researchers have considered this approach. Forrest–Barlack [30] developed the fourth order feedback linearizable model and consequently applied computed torque for a two–link flexible joint robot. Hung[45] applied the method to a single–link flexible joint robot. Uhlik [114] applied the idea of feedback linearization in the frame of the inverse dynamics to an experimental two–link flexible joint robot

manipulator. A model describing a rigid robot has the structure making it possible to directly apply feedback linearization. However, for the flexible joint robots model, when the state vector consists of the motor and link angular positions and velocities (equations 4.3.1 and 4.3.2), is not feedback linearizable. Spong [104] showed that the new coordinates required to transform the system into a feedback linearization model are the link angular position, velocity, acceleration, and jerk. The existence of such coordinate transformation and linearizing feedback control, satisfy the feedback linearizability conditions.

We considered next the construction of the fourth order feedback linearizable model. First, the model of the two–link flexible joint robot interacting with an external environment is given by:

$$D(q)\,\ddot{q} + C(q,\dot{q}) + B_l\,\dot{q} - K(q_m - q) = -J^T F \qquad (5.3.7)$$

$$I_m\,\ddot{q_m} + B_m\,\dot{q_m} + F_c + K(q_m - q) = \tau \qquad (5.3.8)$$

By inspecting the above model, it is clear that the input torques are not related directly to the link state vector or to the forces at the end–effector. Thus, it is not straightforward to design the control inputs so that the end–effector would track a specific position or force trajectories. Another issue to note is that the nonlinearities in the rigid dynamics (links system) is not within the reach of the control inputs, thus linearization, by cancelling these nonlinearities, is not possible. Finally, it is not clear how to design the control inputs to decouple the degrees of freedom of links system. These three limitations directly result from the fact that the model is not feedback linearizable. These limitations can be eliminated by transforming the system given by equations 5.3.7 and 5.3.8 to a feedback linearizable form. A first step is to construct the state transformation, as follows:

given the old state vector $y = [\ q\ ,\ \dot{q}\ ,\ q_m\ ,\ \dot{q_m}\ ]^T$, the new state vector is defined to be $x = [\ q\ ,\ \dot{q}\ ,\ \ddot{q}\ ,\ \overset{3}{q}\ ]^T$. One can see that the motor state has been replaced by the acceleration and jerk of the link. By solving the link system equation for the motor angular position

the following results:

$$q_m = K^{-1}[\, D(q)\ddot{q} + c(q,\dot{q}) + B\dot{q} + J^t F\,] + q \qquad (5.3.9)$$

differentiating the above equation w.r.t. time, the motor angular velocity and acceleration results:

$$\dot{q}_m = \frac{d}{dt}\, K^{-1}\,[\, D(q)\ddot{q} + c(q,\dot{q}) + B\dot{q} + J^t F\,] + q \qquad (5.3.10)$$

$$\ddot{q}_m = \frac{d^2}{dt^2}\, K^{-1}[\, D(q)\ddot{q} + c(q,\dot{q}) + B\dot{q} + J^t F\,] + \ddot{q} \qquad (5.3.11)$$

substituting into the motor equation of motion, 5.3.8, the following fourth order model results:

$$M(q)\,\overset{4}{q} + h_p(q,\dot{q},\ddot{q},\overset{3}{q}) + h_f(q,\dot{q},\ddot{q},F,\dot{F}) + N(q)\,J^T\,\ddot{F} = \tau \qquad (5.3.12)$$

where $M(q) = I_m\, K^{-1}\, D(q)$ and $N(q) = I_m\, K^{-1}\, J^T$. $h_p(q,\dot{q},\ddot{q},\overset{3}{q})$ is 2x1 vector where each element is a nonlinear function of the new state vector and $h_f(q,\dot{q},\ddot{q},F,\dot{F})$ is 2x1 vector where each element is a nonlinear function of the new state vector, except the jerk, and the contact force and its first derivative. Assuming that the Coulomb friction nonlinearity can be compensated for independently from the new state vector thus it is not present in equation 5.3.12. Now, the model of the flexible joint robot given by equation 5.3.12 has the following two properties:

1. the matrix $M(q)$ is invertible for all q,

2. all the nonlinearities in the system are in the reach of the control input.

Rewriting the fourth order model in the state space form:

$$\dot{x} = A\,x + B\,M^{-1}(x_1)\,[\tau - f(x)] \qquad (5.3.13)$$

where:

$$A = \begin{bmatrix} 0 & I & 0 & 0 \\ 0 & 0 & I & 0 \\ 0 & 0 & 0 & I \\ 0 & 0 & 0 & 0 \end{bmatrix}, \qquad B = \begin{bmatrix} 0 \\ 0 \\ 0 \\ I \end{bmatrix}$$

and $f(x) = h_p(q, \dot{q}, \ddot{q}, \overset{3}{q}) + h_f(q, \dot{q}, \ddot{q}, F, \dot{F}) + N(q)\, J^T\, \ddot{F}$

I is the 2x2 identity matrix and 0 is the 2x2 zero matrix. The system given by equation 5.3.13 has the feedback linearizability structure similar to that in equation 5.3.1.

The construction of the fourth order procedures are summarized below:

1– The original system given by equation 5.3.7 and 5.3.8, which can be written in the following state space form; is not feed back linearizable.

$$\dot{y} = f(y) + g(y)\, \tau \qquad (5.3.14)$$

2– The coordinate transformation:

$$x \equiv \begin{bmatrix} x_1 \\ x_2 \\ x_3 \\ x_4 \end{bmatrix} = T(y) = \begin{bmatrix} y_1 \\ y_2 \\ T_3(y_1 y_2 y_3) \\ T_4(y_1, y_2, y_3, y_4) \end{bmatrix} \qquad (5.3.15)$$

where: $T_3(y_1, y_2, y_3) = D^{-1}(y_1)\left[\, K(y_1 - y_3) - J^T(y_1)\, F - c(y_1, y_2) - By_2 \,\right]$

$$T_4(y_1, y_2, y_3, y_4) = \frac{d}{dt}\{D^{-1}(y_1)\left[\, K(y_1 - y_3) - J^T(y_1)\, F - c(y_1, y_2) - By_2 \,\right]\}$$

is used to transform the system given by equation 5.3.14 to a feedback linearizable system. The inverse transformation $y = T^{-1}(x)$ is defined as

$$y \equiv \begin{bmatrix} y_1 \\ y_2 \\ y_3 \\ y_4 \end{bmatrix} = T^{-1}(y) = \begin{bmatrix} x_1 \\ x_2 \\ T_3^{-1}(x_1 x_2 x_3) \\ T_4^{-1}(x_1, x_2, x_3, x_4) \end{bmatrix} \qquad (5.3.16)$$

where: $T_3^{-1}(x_1, x_2, x_3) = \quad K^{-1}\left[\, D(x_1)x_3 + c(x_1, x_2) + Bx_2 + Kx_1 + J^T(x_1)\, F \,\right]$

$$T_4^{-1}(x_1, x_2, x_3, x_4) = \frac{d}{dt}\{K^{-1}\left[\, D(x_1)x_3 + c(x_1, x_2) + Bx_2 + Kx_1 + J^T(x_1)\, F \,\right]\}$$

3– The feedback linearizable system is given by:

$$\dot{x} = A\ x + B\ M^{-1}(x_1)\ [\tau - f(x)] \qquad (5.3.17)$$

Properties of the fourth order model:

Two important properties of the derived feedback linearizable system that play an important role in describing the behaviour of the system are now discussed.

1. The presented feedback linearization is global.

   This can be seen from the inverse transformation which is well defined and differentiable everywhere and hence the feedback linearization for the system holds globally.

2. The system is pure feedback linearizable. This yields the following two properties: the system is minimum phase and has no zero dynamics. The fact that the system has no zero dynamics can be easily seen when one computes the relative degree, which in this case is equal the the dimension of the system. Therefore, there is no internal dynamics, otherwise one has to ensure the stability of the internal dynamics in addition to the linear input–output stabilization.

5.3.3 Feedback Linearization in the Joint Space

In this section, design, simulation and experimental results of the feedback linearization in the joint space for the experimental flexible joint robot are presented. The case considered here is that when the robot parameters are known. Consideration of parameters uncertainty is presented in Chapter 7.

5.3.3.1 Controller Design

The experimental robot dynamic model given by equation 5.3.7 and 5.3.8 is transformed to the fourth order model given by equation 5.3.13 using the coordinate transformation given by equation 5.3.16. When the robot is not interacting with any external environment then the fourth order model would reduced to:

$$M(q)\ \overset{4}{q} + h_p(q, \dot{q}, \ddot{q}, \overset{3}{q}) = \tau \qquad (5.3.18)$$

The nonlinear linearizing inner loop control is designed as:

$$\tau = \hat{M}(q)\ v + \hat{h}_p(q, \dot{q}, \ddot{q}, \overset{3}{q}) \qquad (5.3.19)$$

where $\hat{M}(q)$, $\hat{h}_p(q, \dot{q}, \ddot{q}, \overset{3}{q})$, $\hat{\ddot{q}}$ and $\hat{\overset{3}{q}}$ are the estimates of $M(q)$, $h_p(q, \dot{q}, \ddot{q}, \overset{3}{q})$, $\ddot{q}$ and $\overset{3}{q}$. Note that the effect of computing the acceleration and jerk is included in the nonlinear vector estimation. Assuming that accurate robot parameters are known, one can compute the new state vector x by using the coordinate transformation given by equation 5.3.15. These two required terms can then be computed for feedback. Thus:

$$\hat{M}(q) \approx M(q) \text{ and } \hat{h}_p(q, \dot{q}, \hat{\ddot{q}}, \hat{\overset{3}{q}}) \approx h_p(q, \dot{q}, \ddot{q}, \overset{3}{q}) \qquad (5.3.20)$$

The application of the inner control described by equation 5.3.19 to the robot model given by equation 5.3.18 results in the following closed loop:

$$\overset{4}{q} = v \qquad (5.3.21)$$

Assuming that the desired trajectory is continuous and smooth up to the fourth derivative, the outer loop input $v \in R^2$ can be designed as:

$$v = \overset{4}{q^d} + K_{p3}\ (\overset{3}{q^d} - \overset{3}{q}) + K_{p2}\ (\ddot{q}^d - \ddot{q}) + K_{p1}\ (\dot{q}^d - \dot{q}) + K_{p0}\ (q^d - q) \qquad (5.3.22)$$

where K_{p3} , K_{p3} , K_{p3} , and K_{p3} are constant 2x2 positive diagonal matrices and $q^d, \dot{q}^d, \ddot{q}^d, \overset{3}{q^d}$ and $\overset{4}{q^d}$ are the desired angular position vector and its first four derivatives respectively. Thus the overall control law is given by:

$$\tau = \hat{M}(q)\ [\overset{4}{q^d} + K_{p3}\overset{3}{e_q} + K_{p2}\ddot{e}_q + K_1\dot{e}_q + K_{p0}e_q] + \hat{h}_p(q, \dot{q}, \ddot{q}, \overset{3}{q}) \qquad (5.3.23)$$

where $e_p = q^d - q$ is the angular position error vector, the following error equation then

results:

$$\overset{4}{e}_q + K_{p3}\overset{3}{e}_q + K_{p2}\ddot{e}_q + K_1\dot{e}_q + K_{p0}e_q = 0 \qquad (5.3.24)$$

The above error equation can be written in the following state space form:

$$\dot{Z} = A_1 Z \qquad (5.3.25)$$

where $Z = \left[z_1\ z_2\ z_3\ z_4\right]^T \equiv \left[e_q\ \dot{e}_q\ \ddot{e}_q\ \overset{3}{e}_q\right]^T$

and $A_1 = \begin{bmatrix} 0 & I & 0 & 0 \\ 0 & 0 & I & 0 \\ 0 & 0 & 0 & I \\ -K_{p0} & -K_{p1} & -K_{p2} & -K_{p3} \end{bmatrix}$

It is now clear that the gain matrices can be designed to allocate the closed loop poles as desired. A specific characteristic frequency and damping ratio can be independently assigned to each link. If it is desired that all the links have the same closed loop performance then the gain matrices are:

$$K_{p0} = I\ \omega_p{}^4, K_{p1} = 4\ I\ \zeta_p\omega_p{}^3, K_{p2} = I\ (4\zeta_p + 2)\omega_p{}^2 \text{ and } K_{p3} = 4\ I\ \zeta_p\omega_p$$

where ω_p and ζ_p are the scalar characteristic frequency and damping of the closed loop respectively. I is the 2x2 identity matrix. When the desired characteristic frequency is 35.0 rad/s and the damping ratio is 1.0 for both joints the elements of the gain matrices are given in the following table.

Table 5.2 Feedback linearization controller gains

	First Joint	Second Joint
K_{p0}	1500625.0	1500625.0
K_{p1}	171500.0	171500.0
K_{p2}	7350.0	7350.0
K_{p3}	140.0	140.0

5.3.3.2 Simulation Results

Simulations were carried out to evaluate the response of the system for tracking a trajectory identical to that used with the PD controller. The full nonlinear model of the experimental robot (equation 5.3.7 and 5.3.8) was used in the simulation with a sampling frequency of 1 KHz. In order to be consistent with the physical experimental implementations, the angular positions and velocities of the motors and links are assumed to be available to the controller, while the angular acceleration and jerk of the links are computed from the dynamic model or, more specifically, from the coordinate transformation. Included in the model is Coulomb friction and its corresponding compensation which is combined with the nonlinear control law. The desired characteristic frequency is 35.0 rad/s and the desired damping ratio is 1.0. Thus, it is desired that the joints behave as a fourth order critically damped system. Figures 5.16 and 5.17 show plots of the link desired angular position and the actual angular positions of the link and the motor for both joints. Figure 5.18 shows angular position tracking errors for both joints. Figures 5.19 and 5.20 show plots of the link desired angular velocity and the actual angular velocities of the link and the motor for both joints. Figure 5.21 shows angular velocity tracking errors for both joints. Inspecting these response tracking plots indicate the superiority of the feedback nonlinear controller over the PD controller. In particular the responses show excellent tracking characteristics for the desired states to be controlled which are the link angular position and velocity. It is interesting to see clearly how the motor angular state has evolved with the objective of forcing the link to track the reference trajectory. Thus, the nonlinear feedback linearization control law is not aimed at damping the vibration of the motor but is continuously aiming at finding the required motor torques to shape the motors' dynamic behavior so that the linear characteristics can be achieved for the rigid dynamics (the links system).

5.3.3.2 Experimental Results

The feedback linearization control was implemented on the experimental robot at a sampling frequency of 1 KHz. The measured variables are the angular positions of the links and the motors and the angular velocities of the motors. The links angular velocities are computed by using 5 points numerical differentiation as presented in appendix C. The robot parameters obtained from the frequency response identification are used to compute the angular acceleration and jerk and the nonlinear terms for feedback. The desired trajectory is the same as that used in the simulation.

Figures 5.22 and 5.23 show plots of the desired angular position and the measured angular positions of the link and the motor for both joints. Figure 5.24 shows the angular position tracking errors for both joints. Similarly, figures 5.25 and 5.26 show plots of the desired angular velocity and the measured angular velocities of the link and the motor for both joints. Figure 5.27 shows the angular velocity tracking errors for both joints. The response obtained from experiments proves that the control law managed to linearize the system (inner loop) and to impose the desired characteristics for the linear system (outer loop). The maximum position tracking error is less than 0.01 rad for joint 1 and is less than 0.018 for joint 2. The maximum velocity tracking error is less than 0.09 rad/s for joint 1 and is less than 0.2 rad/s for joint 2. The residuals are due to the imperfection in the identified parameters, the delay caused by the digital implementation of the continuous control law, and the noise in the measurements. However, the tracking response obtained from the feedback linearization control encourages its use as an inner loop for position and force tracking control problem. Figure 5. 28 shows the joint deflection ($q - q_m$) for both joints. One clearly notices the smooth stretch in the elastic joints caused by the feedback linearization which indicates the rate of energy transfer between the flexible and rigid systems. This figure also indicates the stability of the rigid and the flexible dynamics.

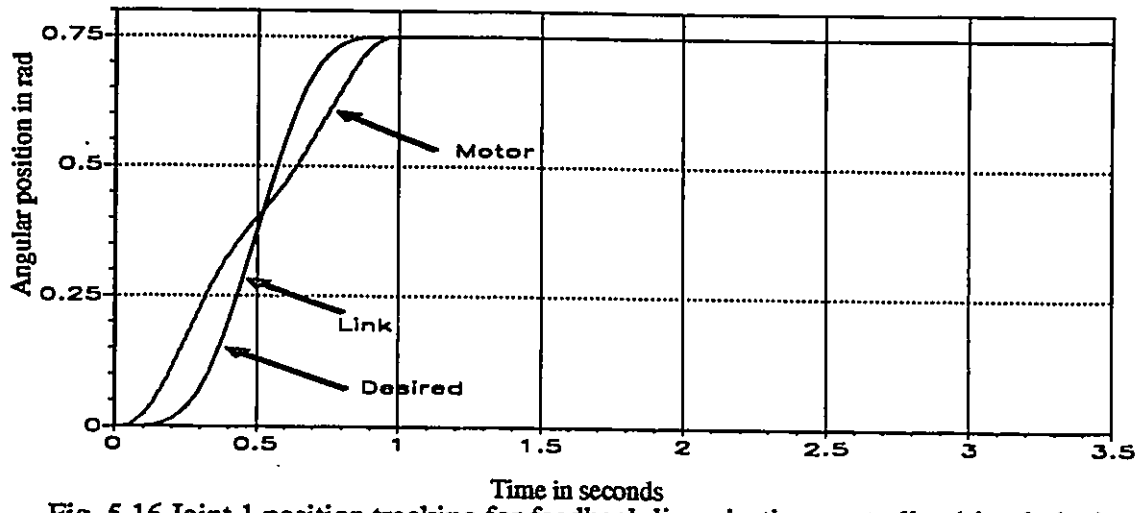

Fig. 5.16 Joint 1 position tracking for feedback linearization controller (simulation)

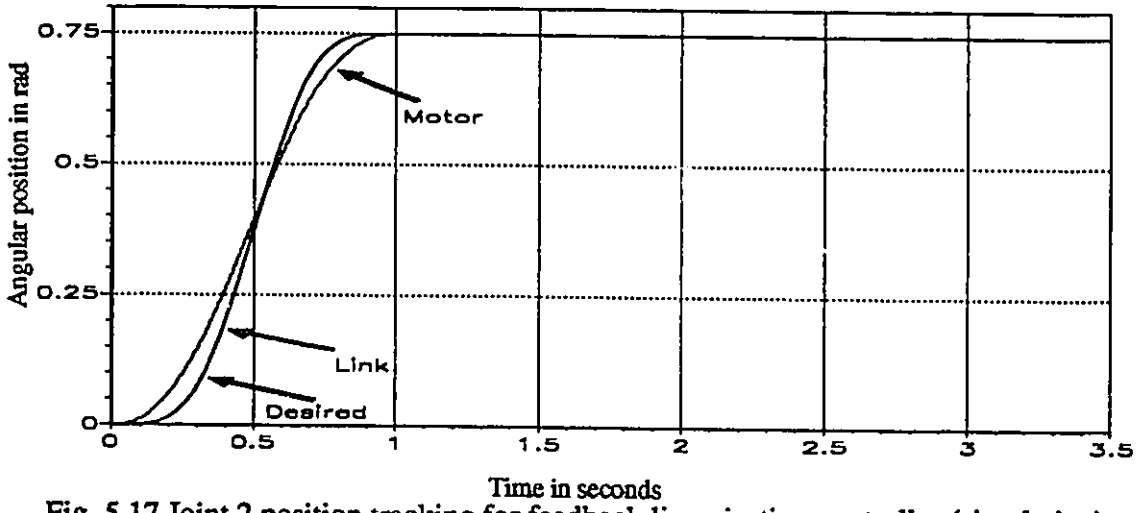

Fig. 5.17 Joint 2 position tracking for feedback linearization controller (simulation)

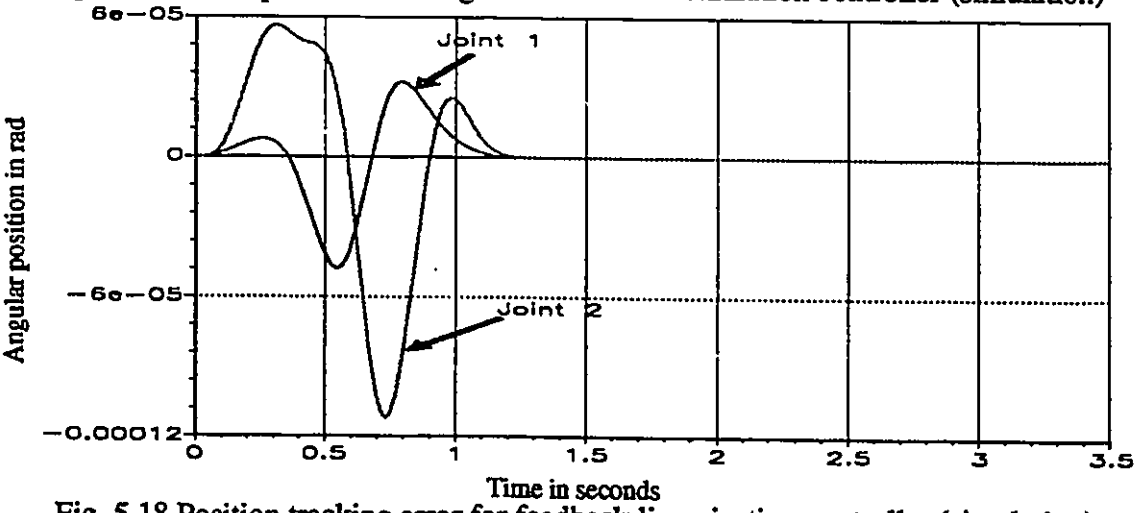

Fig. 5.18 Position tracking error for feedback linearization controller (simulation)

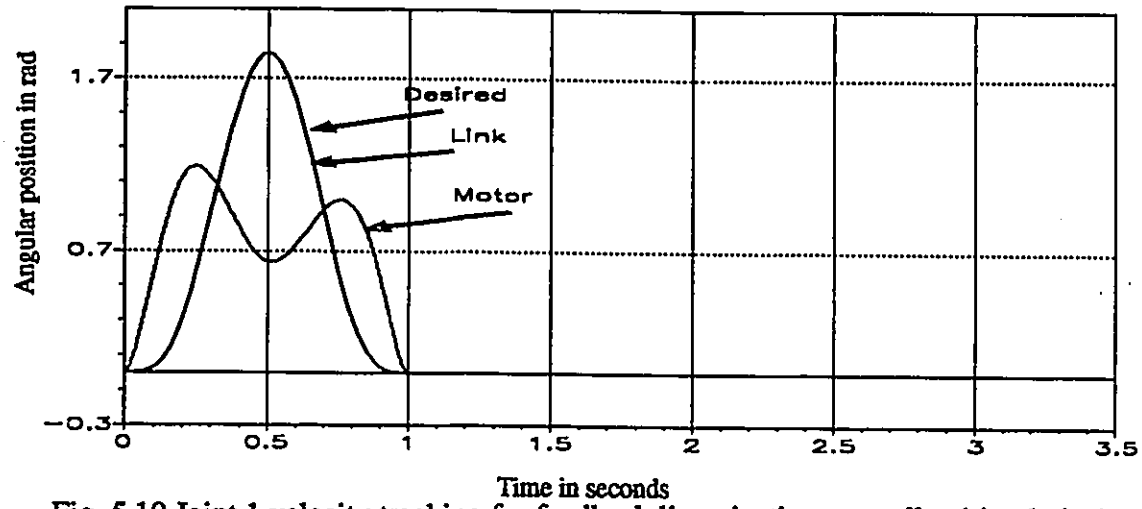

Fig. 5.19 Joint 1 velocity tracking for feedback linearization controller (simulation)

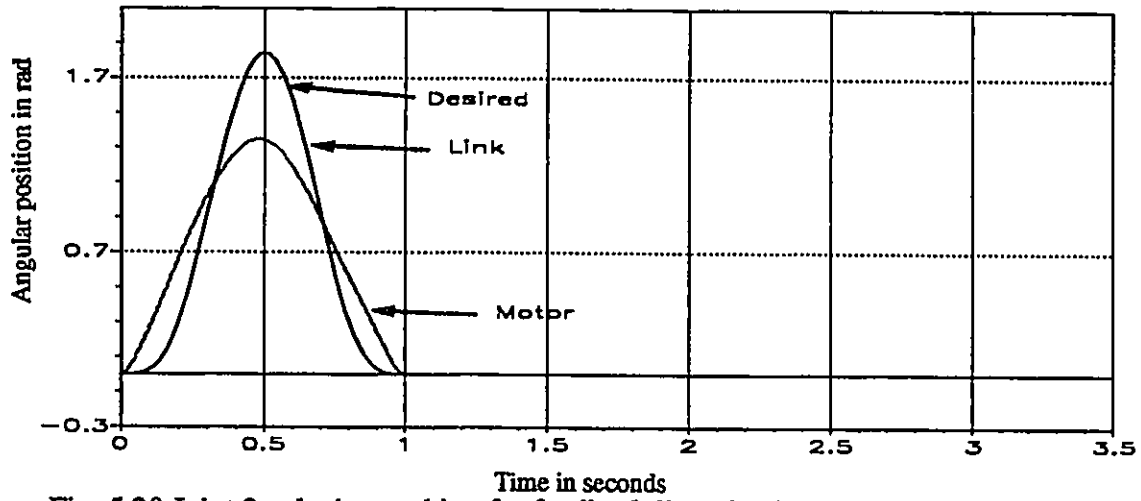

Fig. 5.20 Joint 2 velocity tracking for feedback linearization controller (simulation)

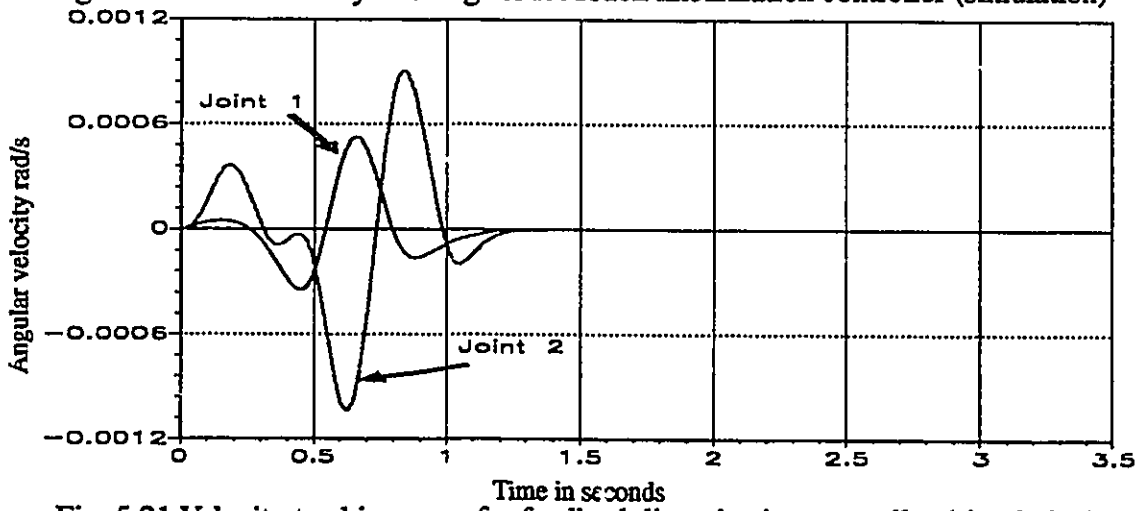

Fig. 5.21 Velocity tracking error for feedback linearization controller (simulation)

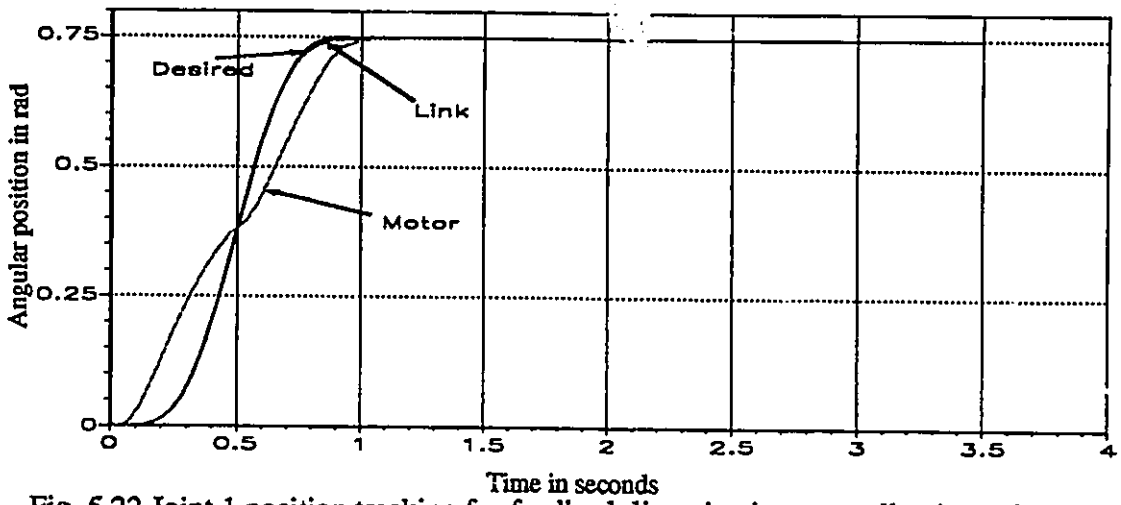

Fig. 5.22 Joint 1 position tracking for feedback linearization controller (experimental)

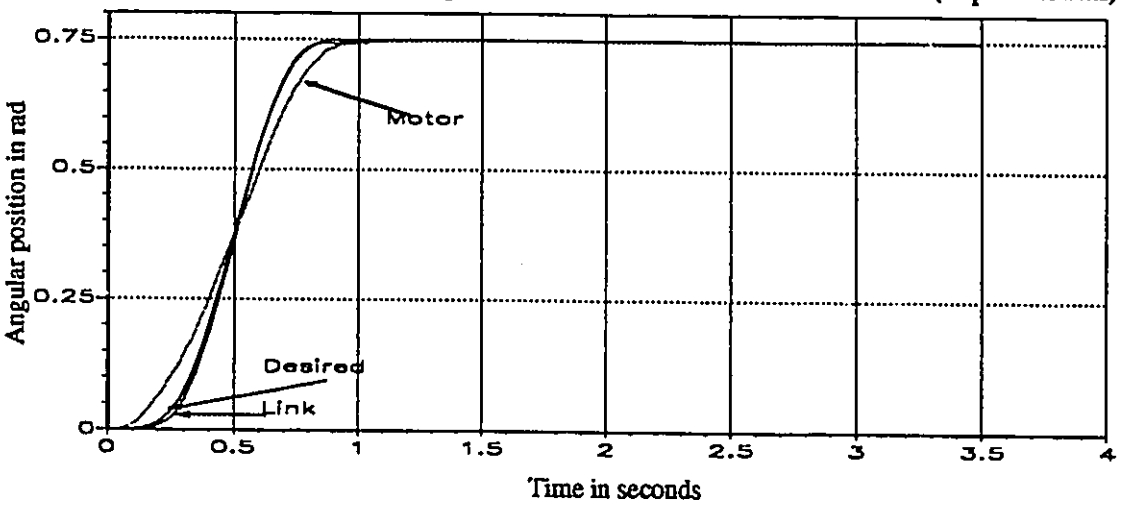

Fig. 5.23 Joint 2 position tracking for feedback linearization controller (experimental)

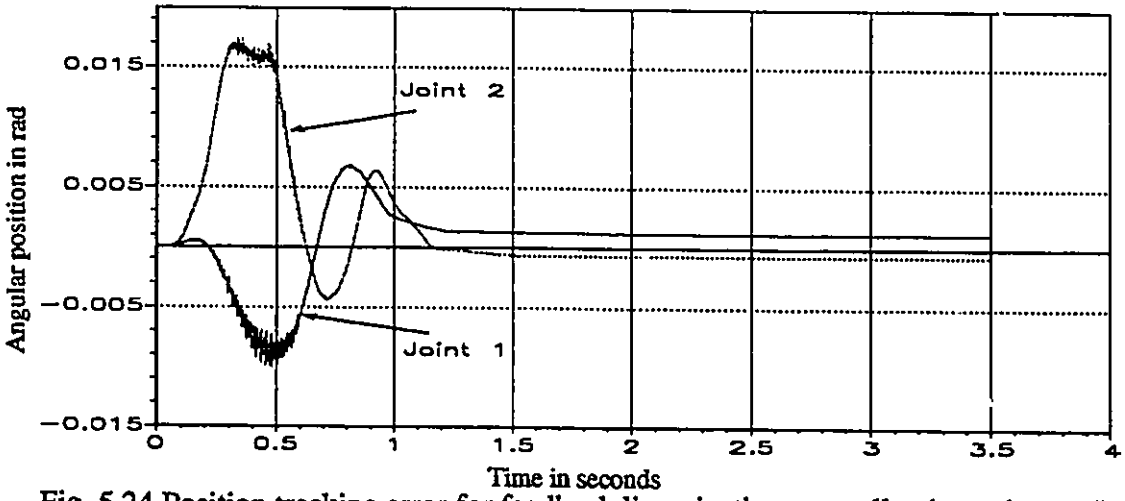

Fig. 5.24 Position tracking error for feedback linearization controller (experimental)

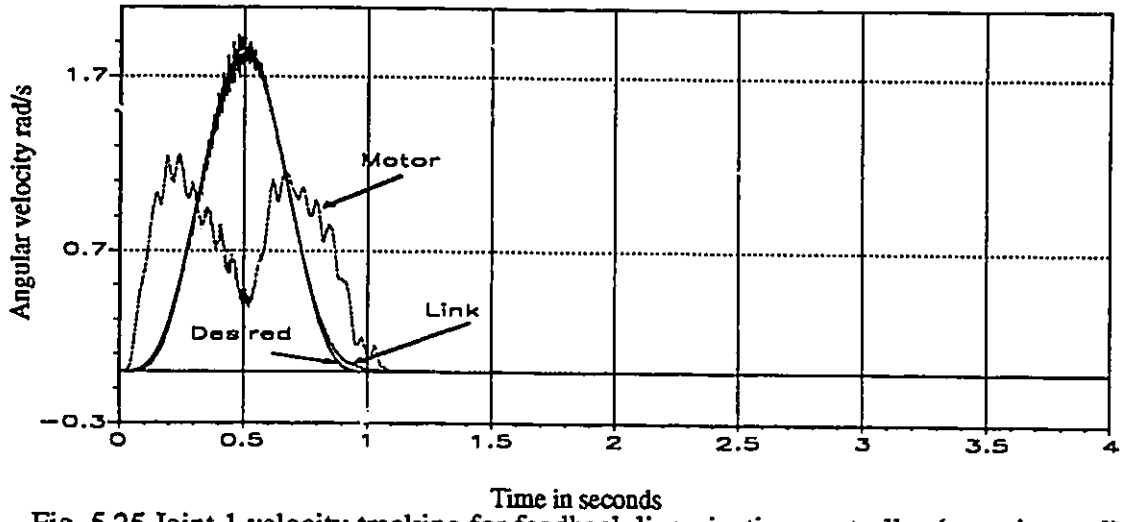

Fig. 5.25 Joint 1 velocity tracking for feedback linearization controller (experimental)

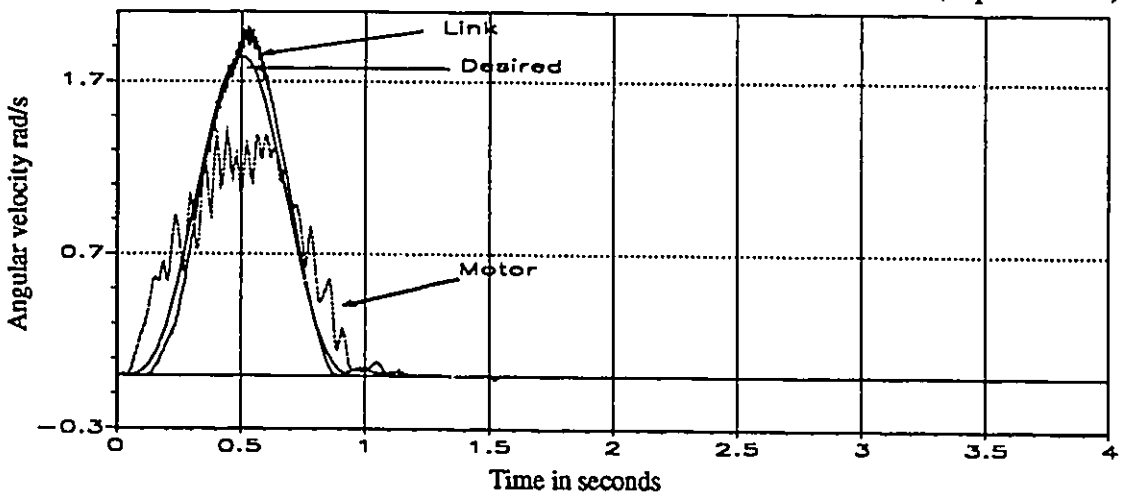

Fig. 5.26 Joint 2 velocity tracking for feedback linearization controller (experimental)

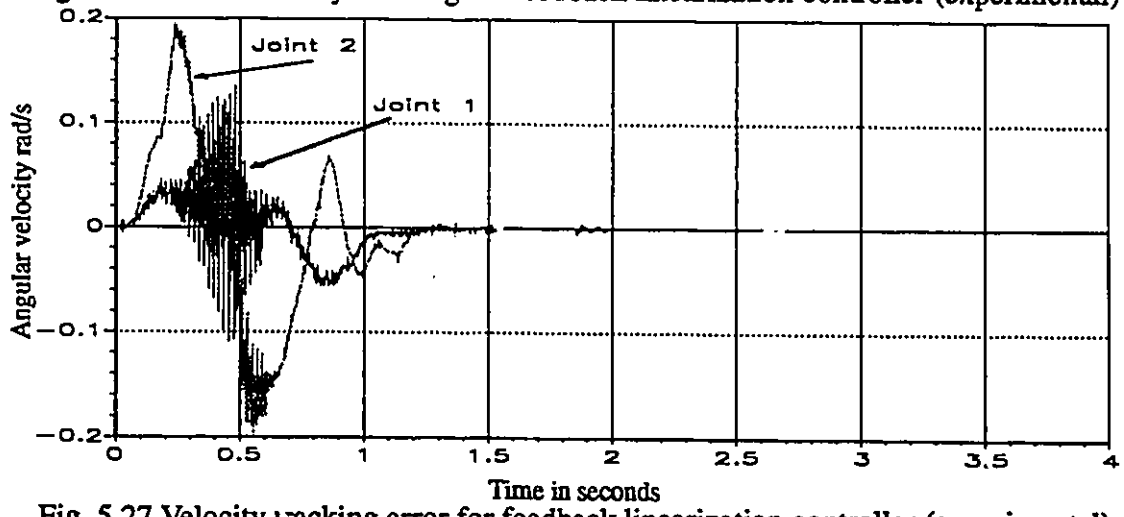

Fig. 5.27 Velocity tracking error for feedback linearization controller (experimental)

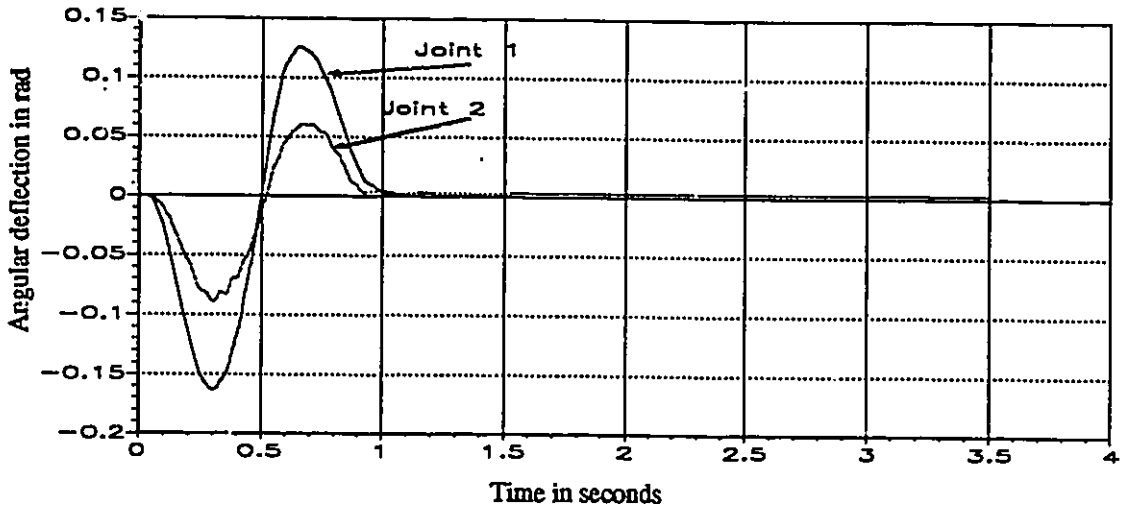

Fig. 5.28 Joint deflection for feedback linearization controller (experimental)

5.4 SUMMARY

A collocated PD controller was designed, simulated, and implemented on the experimental robot. The results showed that the performance of the PD controller is unsatisfactory for flexible joint robots. A fourth order feedback linearization model of the flexible joint robot manipulator was derived. A nonlinear feedback linearization controller was designed, based on the full nonlinear fourth order model of the robot manipulator, simulated, and implemented on the experimental robot in the joint space. Simulation and experimental results obtained indicated the superior performance of the feedback linearization in achieving excellent tracking performance. Thus, the application of the feedback linearization in the inner loop for position and force control for flexible joint robot manipulator is expected to yield good performance.

CHAPTER 6

MODEL–BASED POSITION AND FORCE CONTROL

In this chapter, two different position and force control approaches for flexible joint robot manipulators are presented. Both approaches utilize the feedback linearization results presented in Chapter 5. The dynamic hybrid controller, deals with contact with rigid environments while the impedance controller, deals with contact with compliant environment and transition to/from contact and free motions.

6.1 INTRODUCTION

As described in Chapter 2, robotic applications can be categorized into two classes. The first class concerns the non–contact, e.g. unconstrained motion in the free work–space. In these tasks, the robot's own dynamics have a significant influence upon its performance. This class includes a limited number of typical robotic tasks in practice such as pick–and–place, spray painting or welding. On the other hand, many complex advanced robotic applications such as assembly and machining require the manipulator's end–effector to come into contact with external objects, exert certain forces upon them and/or move along their surfaces. This class of robotic applications are referred to as contact tasks. Contact tasks are characterized by dynamic interaction between the robot and environment. This interaction significantly affects the performance of the robotic control system. Therefore, the interaction forces have to be controlled in order to achieve successful and proper completion of contact tasks. A typical contact task depends on the specific requirements, but in all cases, in

realizing a contact task the robot has to perform three kinds of motion: 1) gross motion, related to the robot motion in free space, 2) compliant motion, related to the robot interaction with an environment, and 3) interference or approach motion, representing all transitions between gross and compliant motions. In addition, robotic compliant motion control can be classified into two categories. First, control approaches which take into account the constraints imposed on the robot motion in designing the controller. The other class includes approaches in which transformation matrices, to decompose the contact tasks, are used to describe and incorporate the contact into the controller. In this research, attention is focussed on performing the compliant motion taking into account the flexibility of the manipulator drive systems.

6.2 DYNAMIC HYBRID CONTROL

6.2.1 Basic Concept

A dynamic hybrid control approach is presented to control the position and force of flexible joint robot manipulators constrained by rigid environments. First, a constraint frame is constructed based on the development by Yoshikawa [121]. In this frame, the directions normal to the constraint surfaces are directions in which forces are to be directly controlled, while the directions complementing the normal directions are those in which positions are to be controlled. Therefore, the constraint frame decouples the system degrees of freedom into a force subsystem and a position subsystem. The construction of the constraint frame is a realization of the fact that the end–effector cannot penetrate the contact surface, thus the robot's degree of freedom normal to the constraint surfaces are lost. The transformations from the joint space into the constraint frame are crucial for specification of the motion and force trajectories in the constraint frame and the realization of the control torques in the joint space. If the constraint surface and the robot parameters are known and the angular posi-

tions and velocities of the links and motors are measured a nonlinear feedback controller can be designed to linearize the system, to decouple the degrees of freedom into a force subsystem and a position subsystem, and to impose desired closed loop characteristics for each of the force and position subsystems independently.

6.2.2 Constraint Frame for Decoupling

Rigid robots are second order systems, therefore, it is sufficient to transform the link angular acceleration and the contact force into the constraint frame in order to obtain the decoupled systems. However, for a flexible joint robot, which is a fourth order system, one requires to transform the fourth derivative of the link angular position vector and the second derivative of the contact forces into the constraint frame in order to obtain the decoupled systems. The required transformations are derived based on the construction of the constraint frame presented next.

Assuming there are m $(m \leq 6)$ independent constraint frictionless surfaces, each is holonomic and is given by an algebraic equation in the reference frame as

$$\phi_i(X) = 0 \qquad i = 1, 2, \ldots . m \qquad (6.2.1)$$

where X is the end–effector position vector in the reference frame. Differentiating the constraint equation w.r.t. time the equation describing the end–effector velocity in the reference frame results in:

$$R_f \dot{X} = 0 \qquad (6.2.2)$$

where $R_f = [e_{m+1}, e_{m+2}, \ldots e_6]^T$ and $e_{m+i} = (\frac{d\phi_i(X)}{dX}) / \| \frac{d\phi_i(X)}{dX} \|$ is a unit vector normal to the constraint surface $\phi_i(x) = 0$. Assuming that there is a set of vectors $(e_1, e_2, \ldots \ldots, e_{6-m})$ such that e_i, $i = 1, 2, \ldots, 6 - m$ are of unit length, differentiable functions of X, mutually independent and are independent of $(e_{m+1}, e_{m+2}, \ldots \ldots, e_6)$, then the following

two matrices can be defined:

$$R_p = [e_1, e_2, \ldots\ldots, e_{6-m}]^T \qquad (6.2.3)$$

$$R = \begin{bmatrix} R_p \\ R_f \end{bmatrix} = [e_1, e_2, \ldots\ldots, e_6]^T \qquad (6.2.4)$$

The matrix R_f represents the coordinate axes normal to the constraint surfaces, while the matrix R_p represents the coordinate axes which complement R_f. The coordinate system with its origin at the current end–effector position X and with the unit bases $(e_1, e_2, \ldots\ldots, e_6)$ defines the constraint frame. The rotation matrix R, composed of R_p and R_f is the velocity transformation matrix from the reference frame into the constraint frame and is given by:

$$\dot{X}_t = R\,\dot{X} \qquad (6.2.5)$$

where X_t is the end effector position vector in the constraint frame. The higher order transformations are obtained by differentiating the velocity transformation given by the above equation to yield:

$$\ddot{X}_t = R\,\ddot{X} + \dot{R}\,\dot{X} \qquad (6.2.6)$$

$$\overset{3}{X}_t = R\,\overset{3}{X} + 2\,\dot{R}\,\ddot{X} + \ddot{R}\,\dot{X} \qquad (6.2.7)$$

$$\overset{4}{X}_t = R\,\overset{4}{X} + 3\,(\ddot{R}\,\ddot{X} + \dot{R}\,\overset{3}{X}) + \overset{3}{R}\,\dot{X} \qquad (6.2.8)$$

The intermediate forward kinematic transformations can be used to find the overall transformation from the joint space in the constraint frame. Therefore, the transformation of the link position vector fourth derivative into the constraint frame is given by:

$$\overset{4}{q} = J^{-1}\,[\,R^{-1}\,(\,\overset{4}{X}_t - a_x\,) - a_q] \qquad (6.2.9)$$

where:

$$a_q = 3\,(\,\dot{J}\,\overset{3}{q} + \ddot{J}\,\ddot{q}\,) + \overset{3}{J}\,\dot{q}$$

$$a_x = 3 (\dot{R} \overset{3}{\dot{X}} + \ddot{R} \ddot{X}) + \overset{3}{R} \dot{X}$$

It should be noted that:

$$\overset{4}{X}_t = \begin{bmatrix} \overset{4}{P} \\ 0 \end{bmatrix} \qquad (6.2.10)$$

where P is the $(6-m)$x1 end–effector position vector tangential to the constraint surfaces. The above equation states that the end–effector velocity and its higher order derivatives normal to the constraint surfaces are zero because the end–effector cannot penetrate the constraining surfaces.

6.2.3 Constraint Contact Force

In this section, the transformation of the contact forces from the reference frame into the constraint frame is derived. Also, a general expression of the contact force in the constraint frame is presented. The end–effector velocity expressed in the reference frame $\dot{X}$, can be expressed as a 6–dimensional vector V consisting of translational velocity along each axis and rotational velocity about each axis as:

$$V = T \dot{X} \qquad (6.2.11)$$

where T is a $6x6$ transformation matrix. It can be shown that the contact force in the reference frame and in the constraint frame are related by the following relationship:

$$F = (R_f T^{-1})^T f_f = L f_f \qquad (6.2.12)$$

where $L = (R_f T^{-1})^T$ and $f_f \in R^m$ represents the contact force vector F in terms of the unit vector L which is normal to the constraint surfaces. The contact force f_f is the negative equivalent of the Lagrangian multipliers λ, i.e. $f_f = -\lambda$. Equation 6.2.12 gives the contact force vector F at the tip of the end–effector expressed in the reference frame due to the force vector f_f which is normal to the constraint surfaces. The transformations of the first

and second derivatives of the contact force vector can be obtained by differentiating equation 6.2.12 to give:

$$\dot{F} = L \dot{f}_f + \dot{L} f_f \qquad (6.2.13)$$

$$\ddot{F} = L \ddot{f}_f + 2 \dot{L} \dot{f}_f + \ddot{L} f_f \qquad (6.2.14)$$

The force second derivative can be rewritten as:

$$\ddot{F} = L \ddot{f}_f + a_f \qquad (6.2.15)$$

where $a_f = 2 \dot{L} \dot{f}_f + \ddot{L} f_f$

It should be noted that equations 6.2.12 to 6.2.15 do not prescribe how to obtain the force vector and its first two derivatives but enables transformation of these vectors from the constraint frame into the reference frame. The contact force f_f can be computed by using the constraint and the rigid dynamics of the robot to give:

$$f_f = (R_f J D^{-1} J^T L)^{-1} [R_f J D^{-1} h_1 + R_f \dot{J} \dot{q} + \dot{R}_f J \dot{q}] \qquad (6.2.16)$$

The above equation illustrates the fact that the contact forces are not independent variables but are functions of the robot state (angular positions and velocities) and the kinematic characteristics of the constraint surfaces. The first derivative of the contact force can be computed by differentiating the above equation to yield:

$$\dot{f}_f = \frac{d}{dt}[(R_f J D^{-1} J^T L)^{-1} [R_f J D^{-1} h_1 + R_f \dot{J} \dot{q} + \dot{R}_f J \dot{q}]]$$

(6.2.17)

6.2.4 The Nonlinear Feedback Controller

In this section a nonlinear feedback controller is designed to achieve position and force tracking for a flexible joint manipulator constrained by a rigid environment. The design is based on the basic concept of the feedback linearization presented and evaluated in Chapter 5. The controller utilizes the feedback linearizable model given by equation 5.3.12 and the results of the constraint frame presented in sections 6.2.2 and 6.2.3 as follows. First, the flexible joint robot manipulator model given by equations 5.3.7 and 5.3.8 is transformed to the fourth order feedback linearizable model given by equation 5.3.12 by using the coordinate transformation of equation 5.3.16. Then, the transformations of the fourth derivative of the link angular position vector, equation 6.2.9, and the second derivative of the contact force, equation 6.2.15, are substituted in the fourth order feedback linearizable mode to give the following decoupled system:

$$M\,J^{-1}\,[\,R^{-1}\,(\,\overset{4}{X}_t - a_x\,) - a_q\,] + h_p\,(q,\dot{q},\ddot{q},\overset{3}{q}) + h_f(q,\dot{q},\ddot{q},F,\dot{F}) + N\,J^T\,(\,L\,\ddot{f} + a_f\,) = \tau \qquad (6.2.18)$$

The goal of the control law is: i) to linearize the nonlinear system, described by the above equation, by cancelling the nonlinear terms $h_p\,(q,\dot{q},\ddot{q},\overset{3}{q})$ and $h_f(q,\dot{q},\ddot{q},F,\dot{F})$, and ii) to utilize the decoupling achieved by the constrained frame to impose desired closed loop characteristics for each of the decoupled linear position and force subsystems. Thus, the control law is designed as described by the following equation:

$$\tau = \hat{M}\,J^{-1}\,[\,R^{-1}\,(\,\overset{4}{X}^*_t - \hat{a}_x\,) - \hat{a}_q\,] + \hat{h}_p\,(q,\dot{q},\ddot{q},\overset{3}{q}) + \hat{h}_f\,(q,\dot{q},\ddot{q},F,\dot{F}) + \hat{N}\,J^T\,(\,L\,\ddot{f}^* + \hat{a}_f\,) \qquad (6.2.19)$$

where $\overset{4}{X}^*_t = \begin{bmatrix} \overset{4}{P}^* \\ 0 \end{bmatrix}$, $\overset{4}{P}^*$ is $(6-m)$ x 1 vector of new input to the position subsystem and

$\ddot{f}$ is m x 1 vector of new inputs to the force subsystem. $\hat{M}$, $\hat{N}$, $\hat{h}_p\ (q,\dot{q},\ddot{q},\overset{3}{q})$, $\hat{h}_f\ (q,\dot{q},\ddot{q},F,\dot{F})$, $\hat{a}_q$, $\hat{a}_x$ and $\hat{a}_f$ are the estimated values of M, N, $h_p\ (q,\dot{q},\ddot{q},\overset{3}{q})$, $h_f\ (q,\dot{q},\ddot{q},F,\dot{F})$, a_q, a_x and a_f respectively. It should be noted that the effect of computing the new state elements $\ddot{q}$ and $\overset{3}{q}$ is included in all terms which depend on these two vectors. Assume that, as in the joint space case, the robot parameters are accurately known. In addition, the angular positions and velocities of the links and motors are measured. The results of these two assumptions are: 1) the new state vector of the linearizable system can be computed by using the coordinate transformation, and 2) an accurate estimation of the nonlinear terms required by the linearizing control law. Thus:

$$\left.\begin{aligned}\hat{\ddot{q}} &\approx \ddot{q}\\ \hat{\overset{3}{q}} &\approx \overset{3}{q}\end{aligned}\right\} \quad \text{state estimation} \qquad (6.2.20)$$

$$\left.\begin{aligned}\hat{M} &\approx M\\ \hat{N} &\approx N\end{aligned}\right\} \quad \text{decoupling matrices estimation} \qquad (6.2.21)$$

$$\left.\begin{aligned}\hat{h}_p\ (q,\dot{q},\ddot{q},\overset{3}{q}) &\approx h_p\ (q,\dot{q},\ddot{q},\overset{3}{q})\\ \hat{h}_f\ (q,\dot{q},\ddot{q},F,\dot{F}) &\approx h_f\ (q,\dot{q},\ddot{q},F,\dot{F})\end{aligned}\right\} \text{nonlinear vectors estimation} \qquad (6.2.22)$$

$$\left.\begin{aligned}\hat{a}_q &\approx a_q\\ \hat{a}_x &\approx a_x\\ \hat{a}_f &\approx a_f\end{aligned}\right\} \quad \text{kinematic transformations estimation} \qquad (6.2.23)$$

The control law given by equation 6.2.19 together with the approximations given by equations 6.2.20 to 6.2.23, when applied to the constrained flexible joint robot given by equations 5.3.7, 5.3.8 and 6.2.1, result in the following closed loop system:

$$\overset{4}{P} = \overset{4}{P^*} \tag{6.2.24}$$

$$\ddot{f}_f = \ddot{f}^* \tag{6.2.25}$$

The nonlinear control law linearizes the system by cancelling the nonlinear terms, uses the constraint frame transformation to decouple the system to the position and force subsystems, and finally imposes a desired closed loop characteristic in each subsystem.

Outer Loop Design

Assume that the desired position trajectory is continuous and smooth up to the fourth derivative and the desired force trajectory is also continuous and smooth up to the second derivative. Then, a characteristic frequency and damping can be achieved for each subsystem as follows. By choosing the input $\overset{4}{P^*} \in R^{6-m}$ as in the following equation

$$\overset{4}{P^*} = \overset{4}{P^d} + K_{p3}\,(\overset{3}{P^d} - \overset{3}{P}) + K_{p2}\,(\ddot{P}^d - \ddot{P}) + K_{p1}\,(\dot{P}^d - \dot{P}) + K_{p0}\,(P^d - P) \tag{6.2.26}$$

where K_{p3} , K_{p3} , K_{p3} , and K_{p3} are $(6-m)$x$(6-m)$ constant positive diagonal matrices and $P^d, \dot{P}^d, \ddot{P}^d, \overset{3}{P^d}$ and $\overset{4}{P^d}$ are the desired position and its first four derivatives, respectively, then, the following error equation results:

$$\overset{4}{e_p} + K_{p3}\overset{3}{e_p} + K_{p2}\ddot{e}_p + K_1\dot{e}_p + K_{p0}e_p = 0 \tag{6.2.27}$$

where $e_p = P^d - P$ is the position error vector. The same procedure are followed for the force subsystem, the force input $\ddot{f}^* \in R^m$ is designed as:

$$\ddot{f}^* = \ddot{f}^d + K_{f1}(\dot{f}^d - \dot{f}) + K_{f0}(f^d - f) \tag{6.2.28}$$

where K_{f0} and K_{f1} are mxm constant positive diagonal matrices and $f^d, \dot{f}^d$ and $\ddot{f}^d$ are the desired normal force and its first two derivatives, respectively. Then the following error equa-

tion results:

$$\ddot{e}_f + K_{f1}\dot{e}_{f1} + K_{f0}e_f = 0 \qquad (6.2.29)$$

where $e_f = f^d - f$ is the force error vector. The closed loop poles for each subsystem can be allocated as desired with the choice of the gain matrices. For the position and force subsystem the gains are designed as follows $K_{p0} = I\omega_p^4$, $K_{p1} = 4I\zeta_p\omega_p^3$, $K_{p2} = I(4\zeta_p + 2)\omega_p^2$ and $K_{p3} = 4I\zeta_p\omega_p$, also $K_{f0} = I\omega_f^2$ and $K_{f1} = 2I\zeta_{fp}\omega_f$. where ω_p, ζ_p, ω_f, and ζ_f are the characteristic frequency and damping ratio of the position and force closed loops, respectively. I 's are the identity matrices of dimensions $(6-m)$x$(6-m)$ for the position gains and mxm for the force gains. The overall system closed loop can be written in the following state space form:

$$\dot{Z} = A_1 Z \qquad (6.2.30)$$

where $$Z = \begin{bmatrix} z_1 & z_2 & z_3 & z_4 & z_5 & z_6 \end{bmatrix}^T \equiv \begin{bmatrix} e_q & \dot{e}_q & \ddot{e}_q & \overset{3}{e}_q & e_f & \dot{e}_f \end{bmatrix}^T$$

and $$A_1 = \begin{bmatrix} 0 & I & 0 & 0 & 0 & 0 \\ 0 & 0 & I & 0 & 0 & 0 \\ 0 & 0 & 0 & I & 0 & 0 \\ -K_{p0} & -K_{p1} & -K_{p2} & -K_{p3} & 0 & 0 \\ 0 & 0 & 0 & 0 & 0 & I \\ 0 & 0 & 0 & 0 & -K_{f0} & -K_{f1} \end{bmatrix}$$

6.2.5 Implementation Issues

6.2.5.1 Task Description

Figure 6.1 shows the experimental flexible joint robot constrained by a rigid straight wall. The robot end–effector has a roller to satisfy the assumption that the wall is frictionless. The wall is made of a steel plate which is rigidly fixed to the table of the robot by two L–shaped legs. The task used in the experiment is to move 0.4 m (starting from point

A to point B) in the Y direction according to a smooth desired position trajectory while applying a desired force normal to the wall in 1.5 seconds. Then, return to the initial point in another 1.5 seconds. The amplitude of the force is 12.0 N.

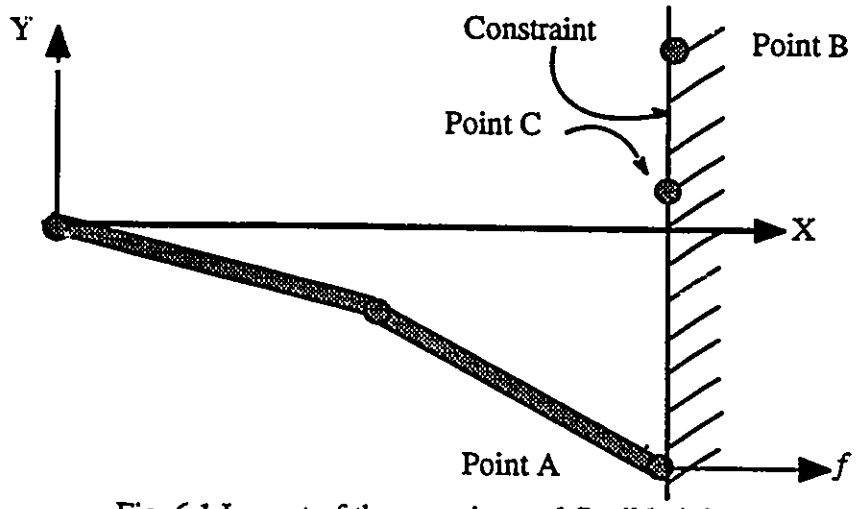

Fig. 6.1 Layout of the experimental flexible joint robot constrained by a straight wali

6.2.5.2 Controller Realization

The overall control law can be obtained by substituting the outer loop control inputs given by equations 6.2.26 and 6.2.28 into the inner loop control law given by equation 6.2.19. The realization of the overall nonlinear feedback control law proceeds as follows:

step 1: Given the angular positions and angular velocities of the links and motors, and the contact force, compute the links accelerations using the corresponding state transformation equations.

step 2: Compute the force first derivative using the links equation of motion.

step 3: Compute the links jerk using the corresponding state transformation equations.

step 4: Compute the position in the constraint frame using the constraint frame transformations.

step 5: Compute the nonlinear terms and evaluate the overall controller.

6.2.6 Simulation Results

Simulations were carried out to evaluate the dynamic hybrid control approach for tracking force and position trajectories as described in section 6.2.5.1. The full nonlinear model of the experimental robot (equation 5.3.7 and 5.3.8) together with the constraint (equation 6.2.1) were used in the simulation when the sampling frequency is 1 KHz. To be consistent with the physical experimental implementations, the angular positions and velocities of the motors and links are assumed to be available for the controller, while the angular acceleration and jerk of the links are computed from the dynamic model or, more specifically, from the coordinate transformation. For the position subsystem, the desired characteristic frequency, ω_p, is 32.0 rad/s and the desired damping ratio, ζ_p, is 1.0, while for the force subsystem, the desired characteristic frequency, ω_f, is 70 rad/s and the damping ratio, ζ_f, is 1.0. Thus, it is desired that the position subsystem behaves as a fourth order critically damped system and the force subsystem behaves as a second order critically damped system. The bandwidth of the force subsystem is chosen to be greater than the position subsystem because the output variable that the force controller is controlling is much faster than the output variable the position controller is controlling. Another fundamental reason for choosing the force controller to be faster than the position controller is that the stability of the overall controller is more sensitive to force tracking response than to position error. The ratio of the force control bandwidth to the position controller bandwidth that best insures stability and tracking was found experimentally to be greater than 2.0. Figures 6.2 and 6.3 show plots of the desired position and velocity trajectories in the direction tangential to the constraining wall, Y–direction. Figure 6.4 shows plot of the desired normal force, X–direction. Figures 6.5, 6.6 and 6.7 show the position, velocity and force tracking errors, respectively. These figures demonstrate the excellent performance of the dynamic hybrid controller in achieving good tracking for both the position and the force subsystems. The position and velocity

tracking errors are related to the force trajectory. These are maximum at higher amplitudes of the tracking force. Figures 6.8 and 6.9 show plots of the motors and links angular positions and angular velocities during the presented tracking to gain insight into the behaviour of the dynamic hybrid controller. As in the joint space implementation of the feedback linearization, the clear stretch in each joint is shaping the motor response so that the links system would achieve the desired tracking performance for both position and force.

6.2.7 Experimental Results

The dynamic hybrid controller was implemented on the experimental flexible joint robot. The sampling frequency was 1 KHz. The conditions of the measurements are as described in the simulation results section. The robot parameters obtained from the frequency response identification were used in implementing the dynamic hybrid control algorithm. The task is the same as described in section 6.2.5.1 and as used in the simulation. The gains used in the experiment are the same as in the simulation. Many experiments were performed on the experimental robot with different position and force amplitudes. The results of one experiment are presented in figures 6.10 to 6.16. Figures 6.10 and 6.11 show position tracking and its corresponding error in the Y–direction. Figures 6.12 show the force tracking in the X–direction. Figures 6.13 and 6.14 show the velocity tracking and its error in the Y–direction. From these figures, one observes that the controller managed to decouple the system into the position and the force subsystem and to track both desired position and force trajectories. The maximum error in the position tracking is less than 5.0 mm which is 1.25% of the position amplitude. Also, the maximum error in the velocity tracking is less than 0.06 m/s which is about 9.0% of the velocity amplitude. The error in the velocity tracking is due to noise in the computation of the velocity from the encoder measurements and to the noise in and nature of the contact force. The position and velocity errors approach zero at the end of the trajectory which indicates the stability of the controller. The residual error in the posi-

tion tracking at the end of the motion can be attributed to the friction force in the direction tangential to the wall which was found to be less than 0.6 N when the normal force amplitude is 12.0 N. Force tracking is quite acceptable despite the chattering which can be attributed to the hard contact between the end–effector roller and the steel wall. This chattering of the contact force also affected the velocity. Also, the chattering of the contact force and the noise in the velocity signals directly affected the estimation of the angular acceleration and jerk. However, the controller was able to maintain stability and good tracking performance. Figures 6.15 and 6.16 show plots of the motors and links angular positions and velocities, which indicate how the motors state are evolved such that the links subsystem achieve position and force tracking.

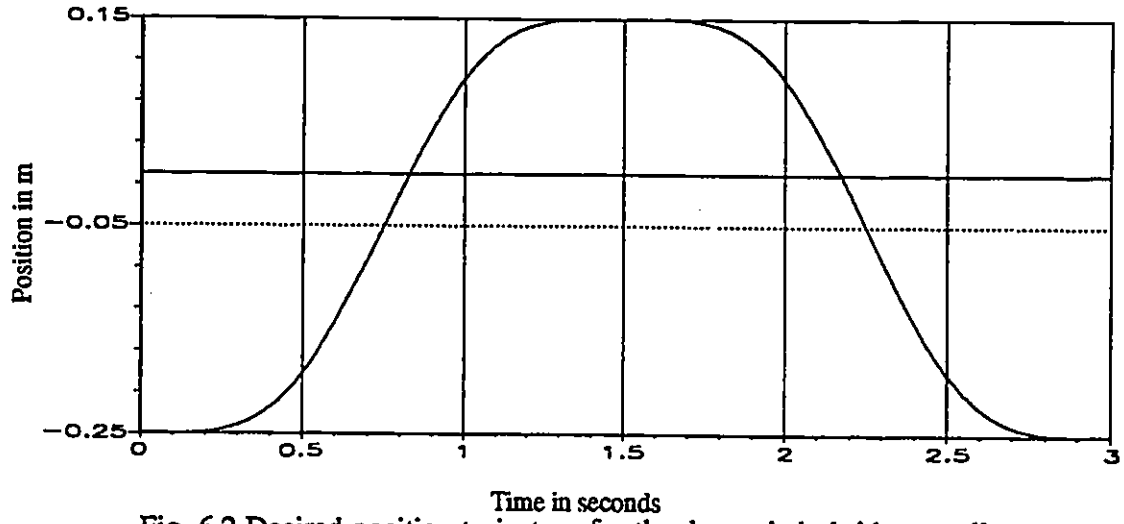

Fig. 6.2 Desired position trajectory for the dynamic hybrid controller

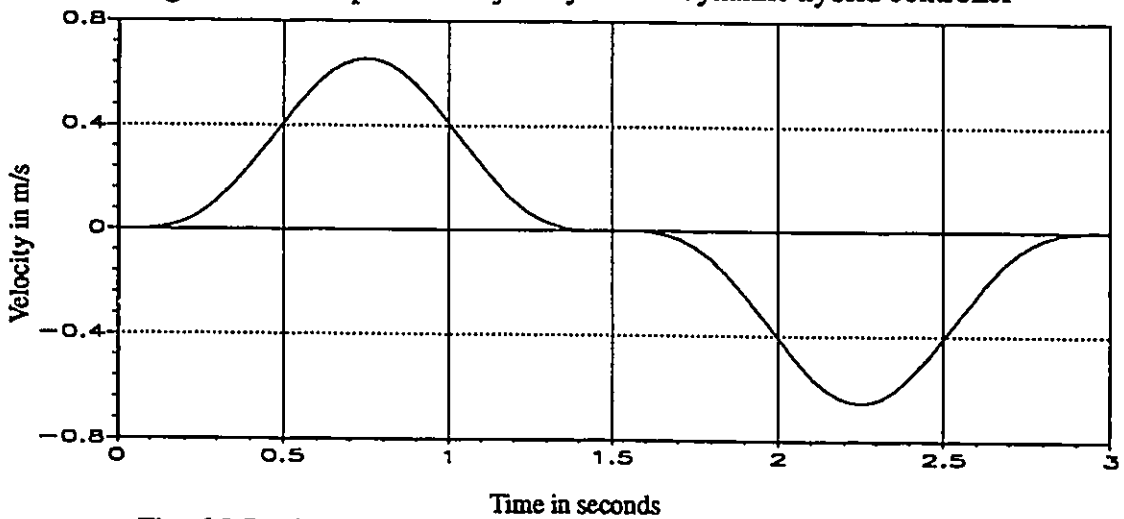

Fig. 6.3 Desired velocity trajectory for the dynamic hybrid controller

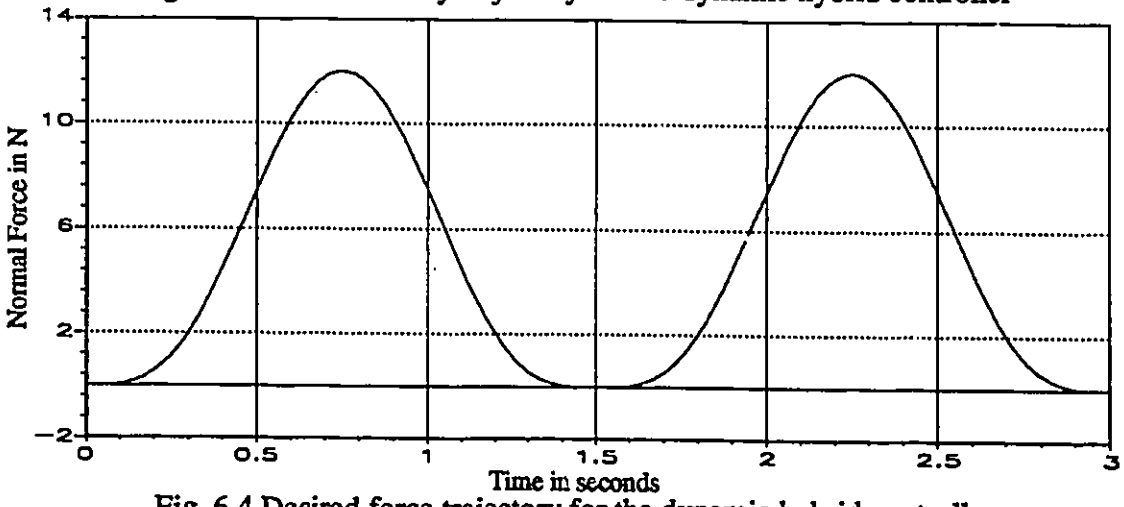

Fig. 6.4 Desired force trajectory for the dynamic hybrid controller

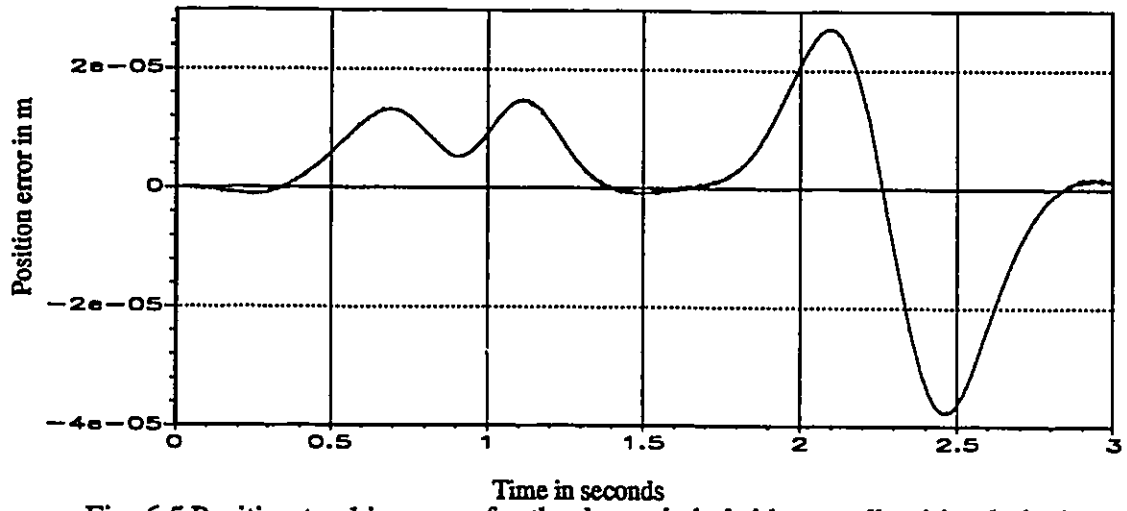

Fig. 6.5 Position tracking error for the dynamic hybrid controller (simulation)

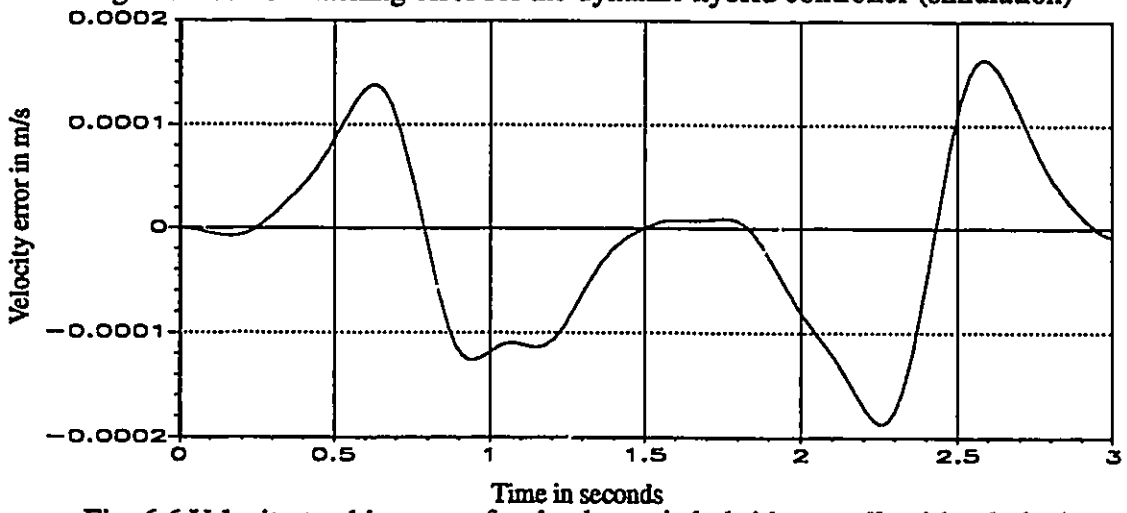

Fig. 6.6 Velocity tracking error for the dynamic hybrid controller (simulation)

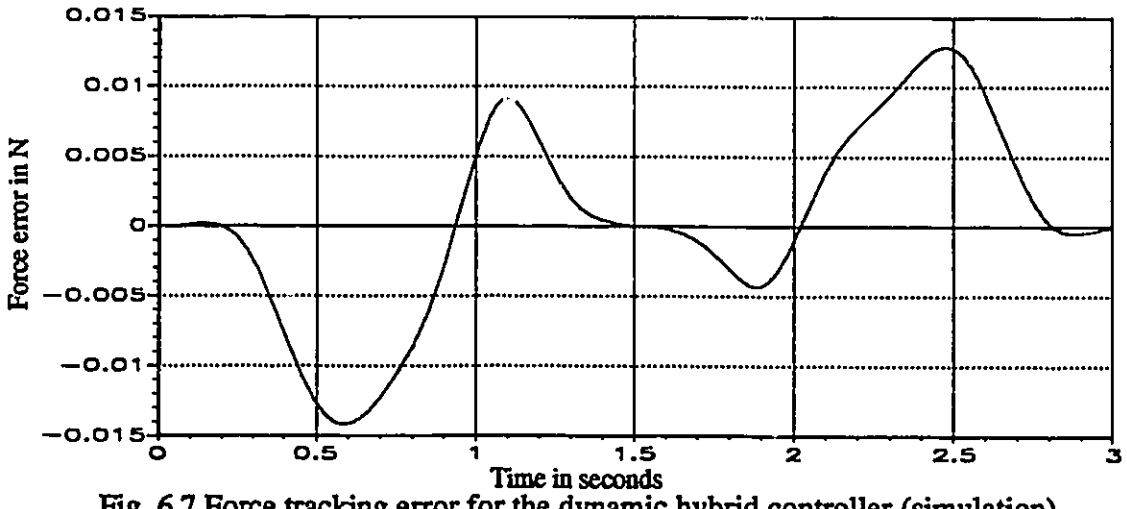

Fig. 6.7 Force tracking error for the dynamic hybrid controller (simulation)

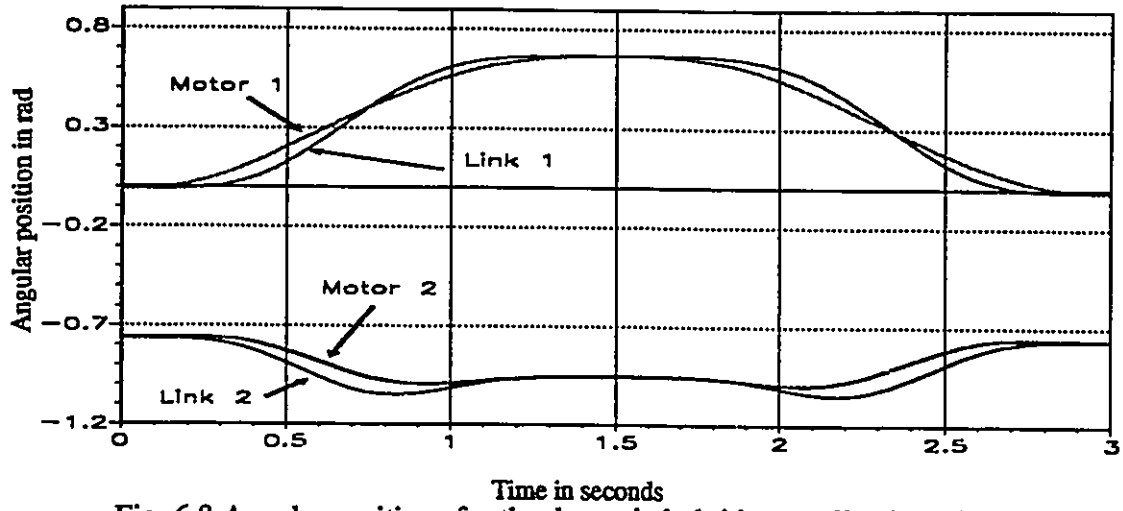

Fig. 6.8 Angular positions for the dynamic hybrid controller (simulation)

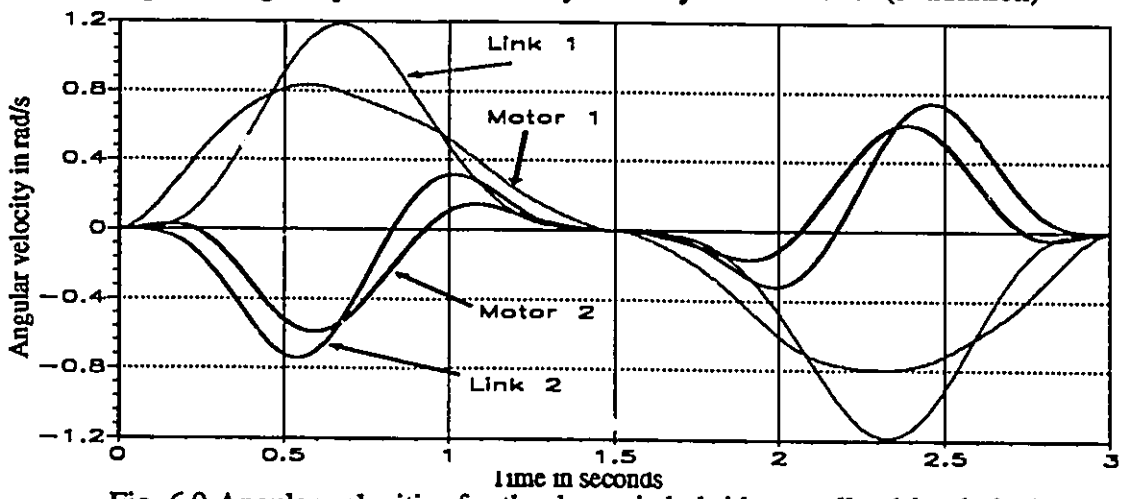

Fig. 6.9 Angular velocities for the dynamic hybrid controller (simulation)

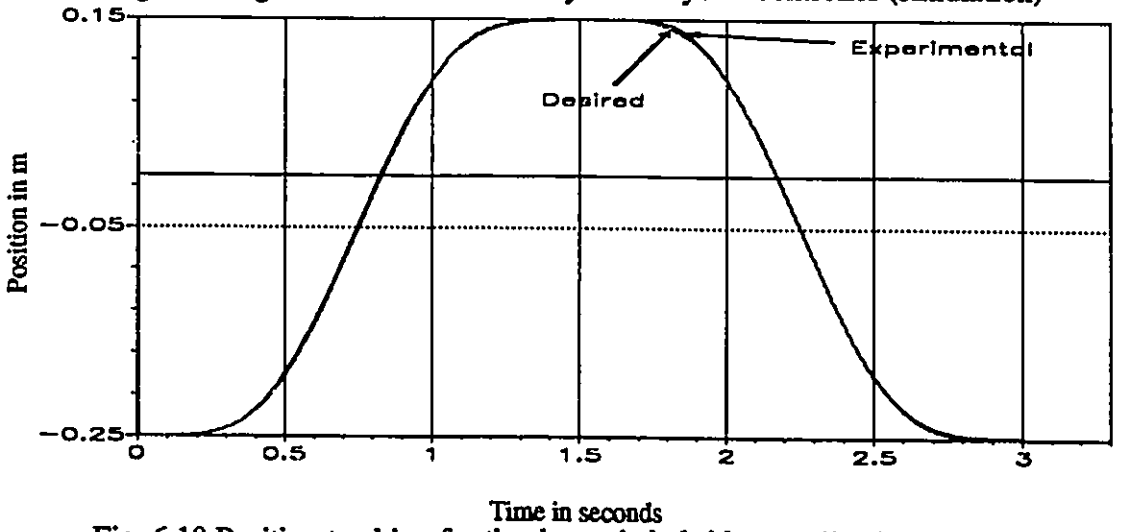

Fig. 6.10 Position tracking for the dynamic hybrid controller (experimental)

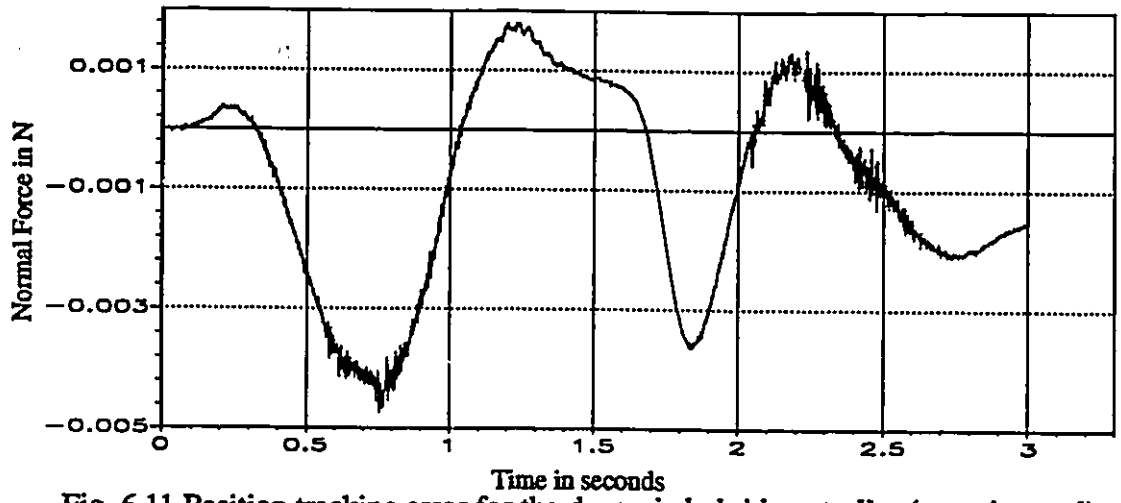

Fig. 6.11 Position tracking error for the dynamic hybrid controller (experimental)

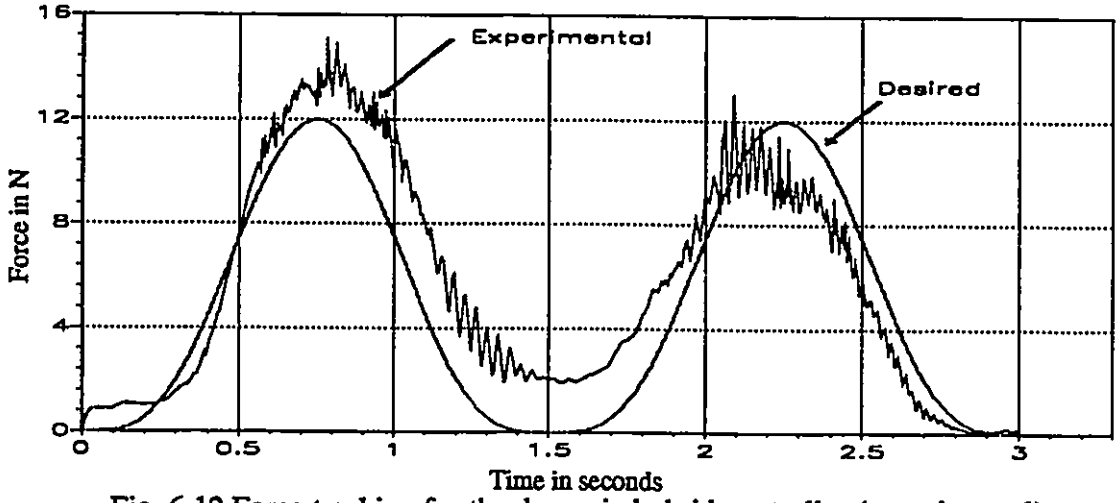

Fig. 6.12 Force tracking for the dynamic hybrid controller (experimental)

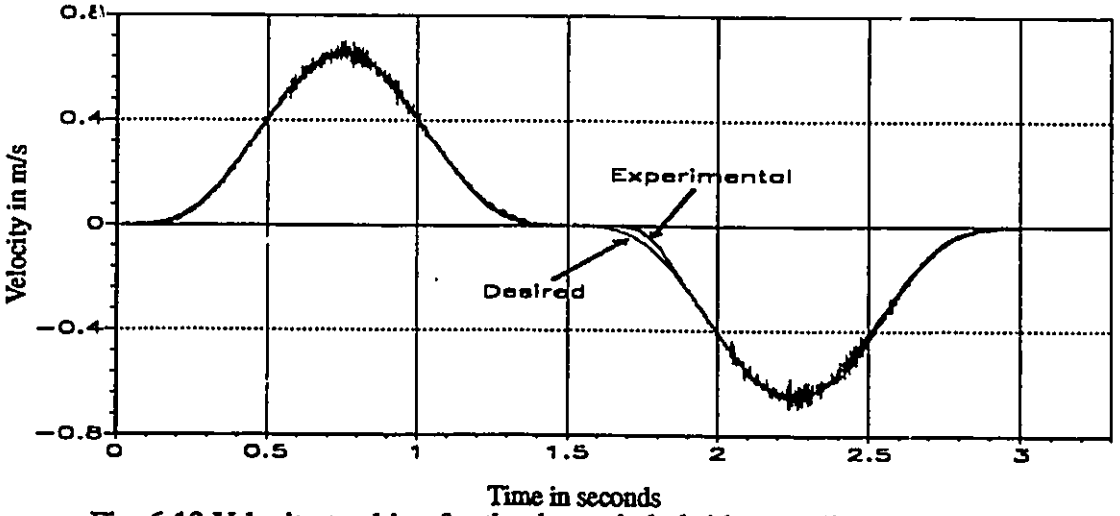

Fig. 6.13 Velocity tracking for the dynamic hybrid controller (experimental)

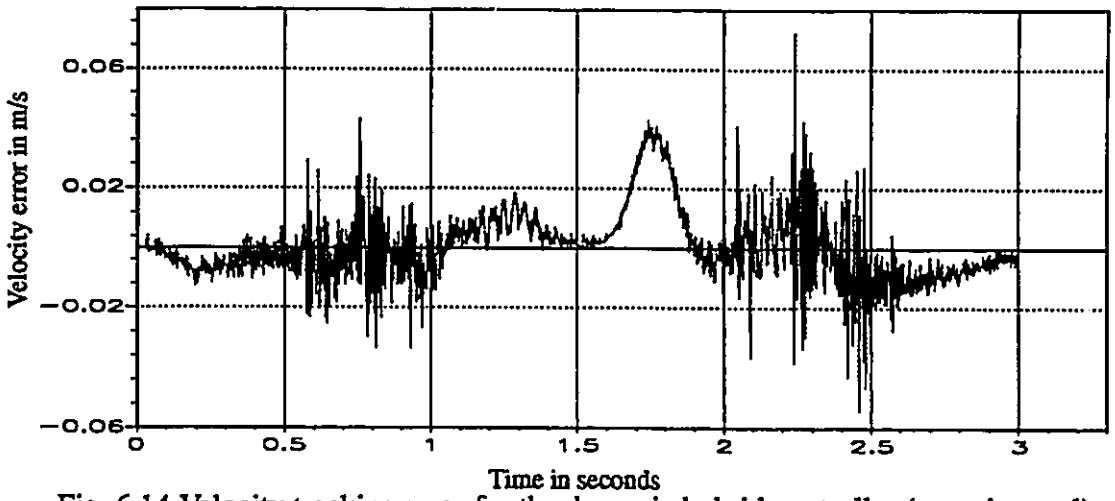

Fig. 6.14 Velocity tracking error for the dynamic hybrid controller (experimental)

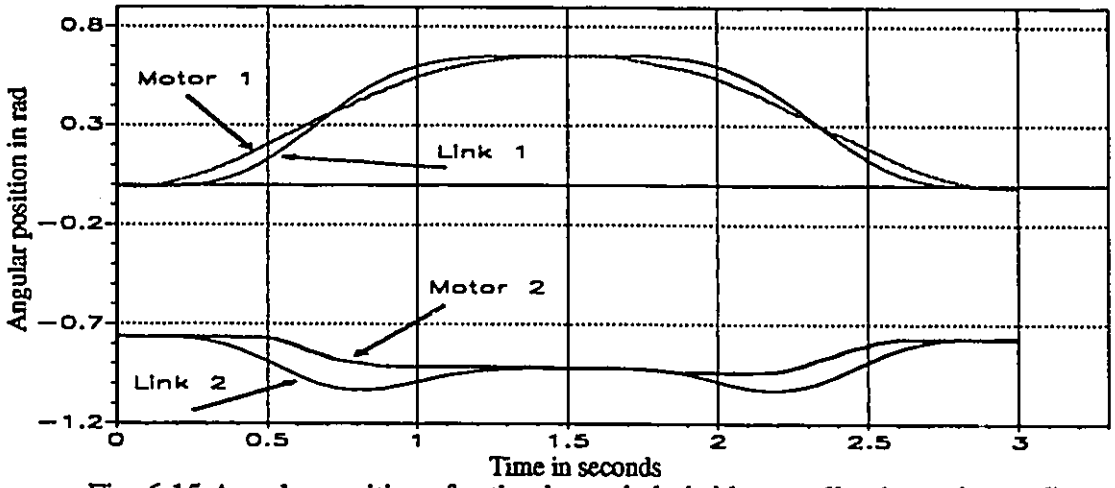

Fig. 6.15 Angular positions for the dynamic hybrid controller (experimental)

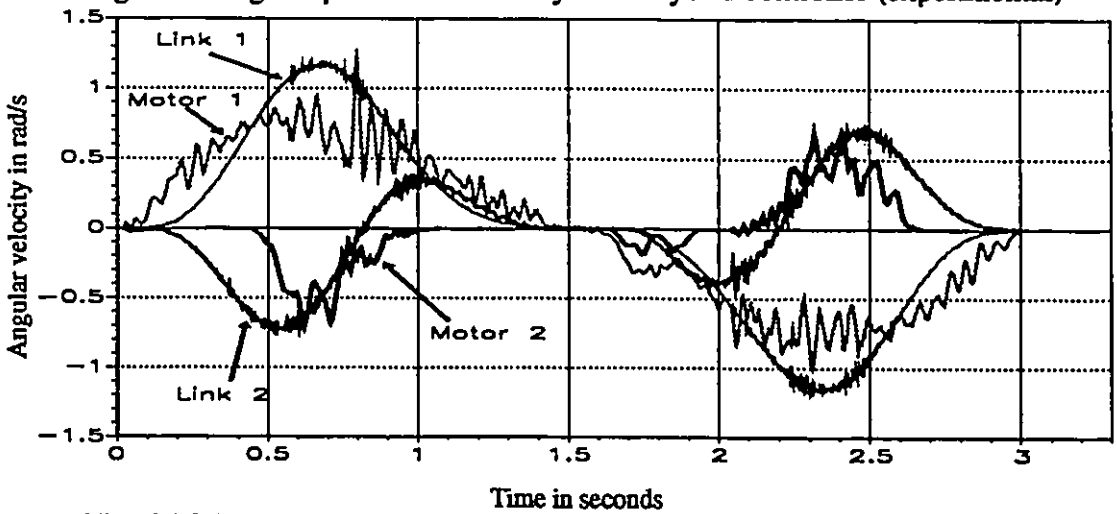

Fig. 6.16 Angular velocities for the dynamic hybrid controller (experimental)

6.3 IMPEDANCE CONTROL

6.3.1 Basic Concept

A nonlinear feedback impedance control approach is presented to control the position and/or force of flexible joint robot manipulators interacting with a compliant environment. The development is based on the feedback linearization of the fourth order model presented in Chapter 5. A desired cartesian target impedance is designed for the end–point of the flexible joint robot. The design of the target impedance is based on the characteristics of flexible joint robots. The desired impedance specifies a desired relationship between the normal force and the position tracking in the same direction. A nonlinear feedback control law is designed to linearize the system and impose the target impedance for the end–point of the robot in the Cartesian space. The same controller is used when the manipulator is performing a free (unconstrained) motion and when it is interacting with a compliant environment. Also, the inputs to the system in both unconstrained and compliant motions are the end–point position and its derivatives. During unconstrained motion, the robot end–point tracks the end–point trajectory, while in compliant motion, the desired end–point trajectory is used to regulate the normal force according to the specified target impedance. If the dynamic model of the environment is known, the robot parameters are known, and the angular positions and velocities of the links and motors are measured, then the proposed nonlinear feedback controller is able to linearize the system and impose the specified target impedance for the end–point of the flexible joint robot manipulator. As a result, the end–point would accurately track a desired trajectory in the position directions while regulating the forces according to the specified target impedance in the force directions.

6.3.2 Desired Target Impedance

Impedance control aims at changing the actual dynamic behavior of the system to the desired behavior. It is clear, by inspecting the robot model given in equation 5.3.12, that the dominant behavior of the system along each degree of freedom is that of a fourth order system. Consequently, a reasonable target impedance would also be a fourth order in each degree of freedom. The target impedance specified is based on the behavior of an ideal single link flexible joint robot (two degrees of freedom system). Consider the ideal single link robot with a flexible joint shown in figure 6.17.

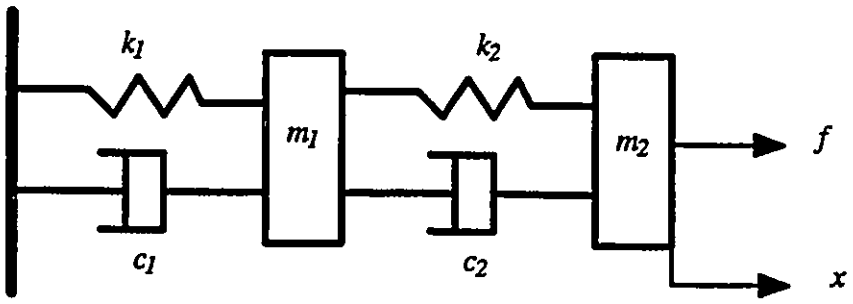

Fig. 6.17 An ideal single link flexible joint robot

The transfer function between the displacement x and the force f is given by:

$$\frac{X(s)}{F(s)} = \frac{a_0 + a_1 s + a_2 s^2}{b_0 + b_1 s + b_2 s^2 + b_3 s^3 + b_4 s^4} \qquad (6.3.1)$$

where:

$a_0 = k_1 + k_2$
$a_1 = c_1 + c_2$
$a_2 = m_1$
$b_0 = 2k_2^2 + k_1 k_2$
$b_1 = (k_1 + k_2)c_2 + (c_1 + c_2)k_2 + 2k_2 c_2$
$b_2 = m_1 k_2 + m_2(k_1 + k_2) + (c_1 + c_2)c_2 + c_2^2$
$b_3 = m_1 c_2 + m_2(c_1 + c_2)$
$b_4 = m_1 m_2$

The desired target impedance of a fourth order n degrees of freedom system is chosen according to the transfer function given by equation 6.3.1. In the time domain, it is given by:

$$a_{p0}(X_d - X) + a_{p1}(\dot{x}_d - \dot{X}) + a_{p2}(\ddot{X}_d - \ddot{X}) + a_{p3}(\overset{3}{X}_d - \overset{3}{X}) + a_{ap4}(\overset{4}{X}_d - \overset{4}{X})$$
$$= a_{f0}F + a_{f1}\dot{F} + a_{f2}\ddot{F} \qquad (6.3.2)$$

where X_d and X are the nominal desired and the actual trajectories of the end effector in the reference frame. The coefficients $a_p's$ and $a_f's$ are constant positive diagonal matrices designed to specify the target impedance. For the i^{th} degree of freedom, the desired impedance in the frequency domain is given by:

$$\frac{\bar{X}_i(s)}{F_i(s)} = \frac{a_{f0i} + a_{f1i}s + a_{f2i}s^2}{a_{p0i} + a_{p1i}s + a_{p2i}s^2 + a_{p3i}s^3 + a_{p4i}s^4} \qquad (6.3.3)$$

where $\bar{X}_i(s) = X_{di}(s) - X_i(s)$ is the difference between the desired nominal and the actual positions in the reference frame. The proposed target impedance is different from that proposed by Hogan [39,40,41] for rigid robots in two respects. First, for rigid robots, it is adequate to choose the target impedance to be of the second order, while for flexible joint robots, which is modelled as a fourth order system, a fourth order target impedance for the end–point is required. Secondly in the original development by Hogan [39] and subsequent implementation by Wlassich [120] only the nominal equilibrium position of the end–point (X_d in equation 6.3.2) was used in designing the target impedance. Other designs, which include the rate of the change of the commanded position, allow flexibility in executing the contact task. This is because the force, to be regulated, is not only proportional to the desired stiffness but to the desired damping and inertia and hence more parameters are available to regulate the force. The target impedance should adequately reflect the real dynamic behavior of the robot. The m_1, m_2, k_1, k_2, c_1 and c_2 can be designed to allow the target impedance to have the desired dynamic characteristics, i.e. the natural frequencies and damping ratios. Another approach would be to design the $a_p's$ and $a_f's$ to allocate the two zeros and four poles as desired. The allocation of the two zeros and four poles of the target impedance allows flexi-

bility in design. As all the coefficients of the target impedance given by equation 6.3.2 are design parameters one can apply linear control design methodologies. Moreover, the problem can be reduced to that of designing a second order system by cancelling the two zeros by two poles.

6.3.3 The Nonlinear Feedback Controller

In this section, a nonlinear feedback controller is designed to impose the desired target impedance for the end–point of the flexible joint robot manipulator. A suitable approach to achieve the target impedance is the feedback linearization described and tested in Chapter 5. The controller utilizes the feedback linearizable fourth order model given by equation 5.3.12 and the inverse kinematics described in appendix B. Substituting for the fourth derivative of the link angular position vector from equation B.18 into the fourth order feedback linearizable model given by equation 5.3.12 we get:

$$M\,J^{-1}\,[\,(\overset{4}{X}) - a_q\,] + h_p\,(q,\dot{q},\ddot{q},\overset{3}{q}) + h_f(q,\dot{q},\ddot{q},F,\dot{F}) + N\,J^T\,\ddot{F} \quad = \tau \qquad (6.3.4)$$

The goals of the control law are to linearize the nonlinear system given by the above equation by cancelling the nonlinear terms $h_p\,(q,\dot{q},\ddot{q},\overset{3}{q})$, $h_f\,(q,\dot{q},\ddot{q},F,\dot{F})$, a_q, and $N\,J^T\,\ddot{F}$ and to impose the target impedance given by equation 6.3.3 for each degree of freedom of flexible joint manipulators end–point. Thus, the control law is designed as:

$$\tau \;=\; \hat{M}\,J^{-1}\,[\,(\overset{4}{X^*}) - \hat{a}_q] + \hat{h}_p\,(q,\dot{q},\ddot{q},\overset{3}{q}) + \hat{h}_f\,(q,\dot{q},\ddot{q},F,\dot{F}) \;+\; \hat{N}\,J^T\,\hat{\ddot{F}} \qquad (6.3.5)$$

where $\overset{4}{X^*}$, is 6×1 vector of new input to the system. Solving the equation of the target impedance for $\overset{4}{X}$ and equating with the new input $\overset{4}{X^*}$, the following results:

$$\overset{4}{X}^{*} = [\ a_{p4}{}^{-1}(a_{p0}(X_d - X) + a_{p1}(\dot{X}_d - \dot{X}) + a_{p2}(\ddot{X}_d - \ddot{X}) + a_{p3}(\overset{3}{X}_d - \overset{3}{X}) + a_{p4}\overset{4}{X}_d - (a_{f0}F + a_{f1}\hat{\dot{F}} + a_{f2}\hat{\ddot{F}})\ ) - a_q] \qquad (6.3.6)$$

Thus the overall control law is given by:

$$\tau = \hat{M}\, J^{-1}\ [\ a_{p4}{}^{-1}(a_{p0}\bar{X} + a_{p1}\bar{\dot{X}} + a_{p2}\bar{\ddot{X}} + a_{p3}\overset{\bar{3}}{X} + a_{p4}\overset{4}{X}_d - (a_{f0}F + a_{f1}\hat{\dot{F}} + a_{f2}\hat{\ddot{F}})) - \hat{a}_q\ ] + \hat{h}_p\ (q, \dot{q}, \ddot{q}, \overset{3}{q}) + \hat{h}_f\ (q, \dot{q}, \ddot{q}, F, \dot{F}) + \hat{N}\, J^T\, \hat{\ddot{F}} \qquad (6.3.7)$$

The same assumption, regarding the robot parameters, as in the joint space implementation and the dynamic hybrid controller, is adopted. The angular positions and velocities of the motors and links are measured in addition to the contact force vector. Finally, the environment is assumed to be accurately modelled as a stiffness element. Thus, the control law given by 6.3.6 when applied to the flexible joint robot model interacting with a compliant environment would result in achieving the desired target impedance for the end–point of the robot. In directions where the flexible joint robot is interacting with a compliant environment the controller regulates the relationship between the contact force and the positional difference and its derivatives according to the specified impedance in those directions. However, in directions where the robot end–point is performing free motions, the controller aims at tracking the specified trajectory as the fourth order impedance specified in those directions. Thus, the impedance controller can perform the three robotic tasks of contact and free motions and transition to/from contact with an external object.

The impedance controller is different than the dynamic hybrid controller in a number of aspects. First, the impedance controller aims at regulating the relationship between the contact force and the positional difference between the commanded and actual positions of the end–point in the same direction while the dynamic hybrid controller aims at direct control of the contact force. Second, the impedance controller requires cancelling the second

derivative of the contact force before imposing the target impedance while the dynamic hybrid controller requires the force and its derivative to specify desired characteristics for the force control subsystem. Thus, one expects the impedance controller to be more difficult to implement. However, if one succeeds in implementing the impedance controller it can result in better stability conditions than the dynamic hybrid controller due to the ability of the former to perform contact and non–contact tasks. Finally, it is recognized that the impedance controller depends on position tracking in order to achieve force tracking. Thus, the impedance controller can be considered as a modified position controller.

6.3.4 Implementation Issues

The task chosen to evaluate the impedance control approach for flexible joint robots consists of both contact and free motions. The task is best described in reference to figure 6.1. The robot starts from point A and is commanded to perform 0.3 m contact motion with the straight wall in 1.5 seconds. The commanded motion in the X direction is meant to achieve a desired contact force based on an estimated stiffness model of the contact wall. The robot is to move 0.05 m away from the wall in the X direction followed by 0.3 m in the negative Y direction and finally to return to the initial point. The free motion is to be performed in another 1.5 seconds. Figures 6.18 to 6.24 shows the desired position, velocity and force trajectories in both X and Y directions.

As the steel wall is not perfectly rigid, it is appropriate to model it as a stiffness element. The model can then be used to estimate the contact force and its first two derivatives which are required for feedback. The dynamic hybrid controller was used to evaluate the stiffness of the wall. The contact force and the incremental position and its first two derivative were recorded, then a third order polynomial in the incremental position was chosen to model the environment stiffness in the normal direction as follows:

$$F = K_{a0} + K_{a1}\,\delta x + K_{a2}\,\delta x^2 + K_{a3}\,\delta x^3 \qquad (6.3.8)$$

Estimates of the coefficients K_{a0}, K_{a1}, K_{a2} and K_{a3} were obtained by using the least squares technique. The first and second derivatives of the contact force can be evaluated by differentiating equation 6.3.8 to give:

$$\dot{\hat{F}} = K_{a1} + (2\,K_{a2}\,\delta x + 3\,K_{a3}\,\delta x^2)\dot{\delta x} \qquad (6.3.9)$$

$$\ddot{\hat{F}} = (2\,K_{a2}\,\delta x + 3\,K_{a3}\,\delta x^2)\ddot{\delta x} + (2\,K_{a2} + 6\,K_{a3}\,\delta x)\dot{\delta x}^2 \qquad (6.3.10)$$

The accuracy of the estimated derivatives of the contact force is dependent on the accuracy of the estimated stiffness and the measured position, velocity, and acceleration. Several measurements were performed in order to obtain accurate estimates of the polynomial coefficients. Experiments showed that the estimation is very sensitive to the initial position of the end–point and the amplitude of the contact force. Figure 6.25 shows plots of the measured and estimated force using the third order polynomial stiffness. The procedures followed to implement the impedance nonlinear feedback controller are very similar to those used in the dynamic hybrid control algorithm with exception of estimating of the first and second derivatives the contact force.

6.3.5 Simulation Results

The impedance control algorithm was simulated to evaluate its performance during compliant and free motion tasks. In the simulations, the full nonlinear model of the flexible joint robot is used. In addition, all the practical conditions regarding the measurements and estimations required by the nonlinear feedback control law are considered. Specifically, the angular positions and angular velocities of the motors and links are directly available while the angular acceleration and jerk are computed using the state transformation equations. The environment is modelled as a linear stiffness element. This model is combined with the robot dynamic model to generate the contact force and further to estimate its first and second deriv-

atives. The target impedance is completely specified by allocating the two zeros at –20.0 rad/s and the four poles at –37.0 rad/second.

Figures 6.26 to 6.31 show simulation results. The nonlinear controller managed to linearize the system and to impose the target impedance. The tracking errors of the positions, velocities, and contact force clearly demonstrate the excellent performance of the impedance controller in performing both contact and free motions. The same controller was used to perform both contact and free motions which is considered a great advantages over other controllers aimed at force or position control separately. The transition to/from the contact tasks is crucial to the tracking performance of the impedance controller. This is because in contact tasks the contact force greatly affects the dynamics of the system while in free motion the manipulator's own dynamics dominates. The controller succeeded in eliminating the effect of the flexible joints and achieving stable and acceptable tracking for the force and position of the end–point of the flexible joint robot.

6.3.6 Experimental Results

The impedance controller was implemented on the experimental flexible joint robot at a sampling frequency of 1 KHz. The conditions of the measurements and estimations are as described in the simulation results section. The robot parameters obtained from the frequency response identification were used in implementing the impedance control algorithm. The task is similar to that described in section 6.3.4 except for the desired normal force. The gains are specified by choosing the two zeros at –20 rad/second and the four poles at –37 rad/second. The experimental results are shown in figures 6.32 to 6.41. Figures 6.32 and 6.33 show plots of the position tracking and the corresponding error in the Y–direction. Figures 6.34 and 6.35 show plots of the position tracking and the corresponding error in the X–direction. Velocity tracking and its corresponding error for both the X– and Y–directions are shown in figures 6.36 to 6.39. The desired and measured normal force trajectories are

shown in figure 6.39. Finally, the end–point position tracking in the X–Y plan is shown in figure 6.41.

The experimental results of the impedance controller show that the controller managed to decouple the system in the reference frame, to track the position trajectory and to regulate the normal force according to the specified impedance. However, the performance is not as good as that achieved by the dynamic hybrid controller. The main reason for this is that the impedance nonlinear feedback controller depends on the elimination of the contact force second derivative which is very sensitive to the contact environment model and the end–point velocity and acceleration measurements. These results are not very good as one can classify the impedance controller as a position control system rather than a force controller. In conclusion, the impedance controller performed the compliant and free motions properly. Inaccurate environment model cannot drive the impedance controller unstable but results in a slightly different force trajectory than expected. A very accurate model of the contact environment is a must in order to achieve perfect force tracking.

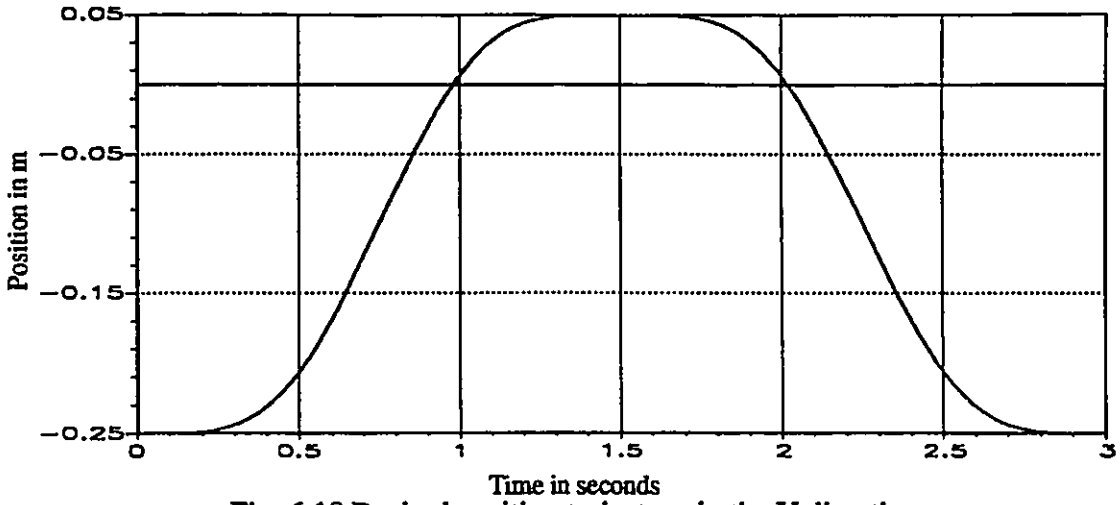

Fig. 6.18 Desired position trajectory in the Y direction

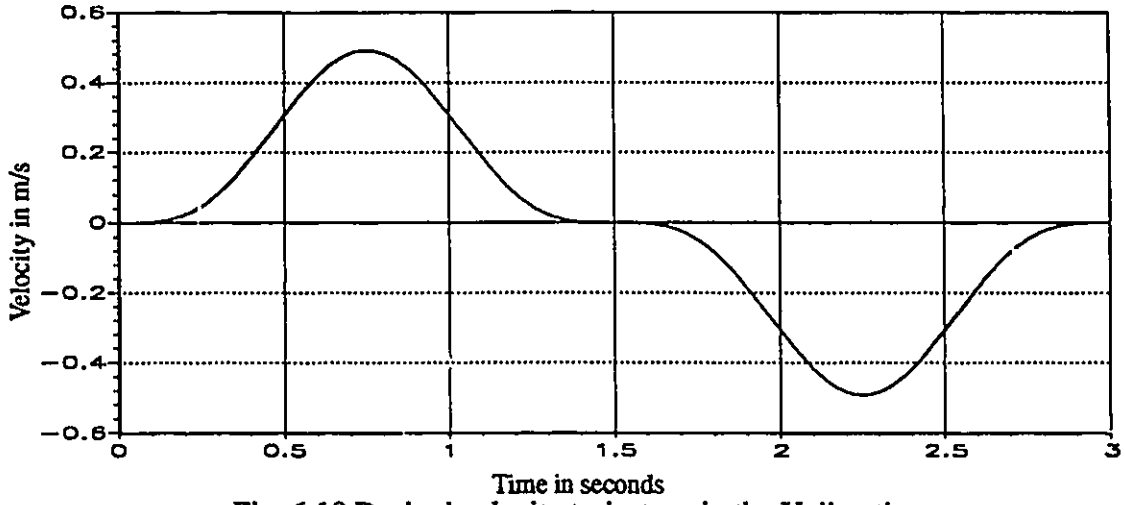

Fig. 6.19 Desired velocity trajectory in the Y direction

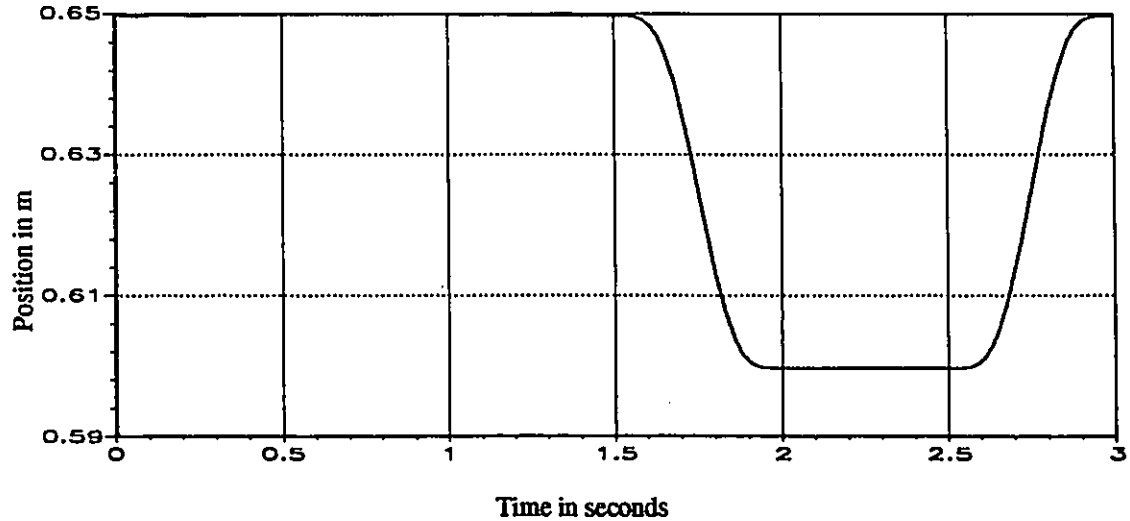

Fig. 6.20 Desired position trajectory in the X direction

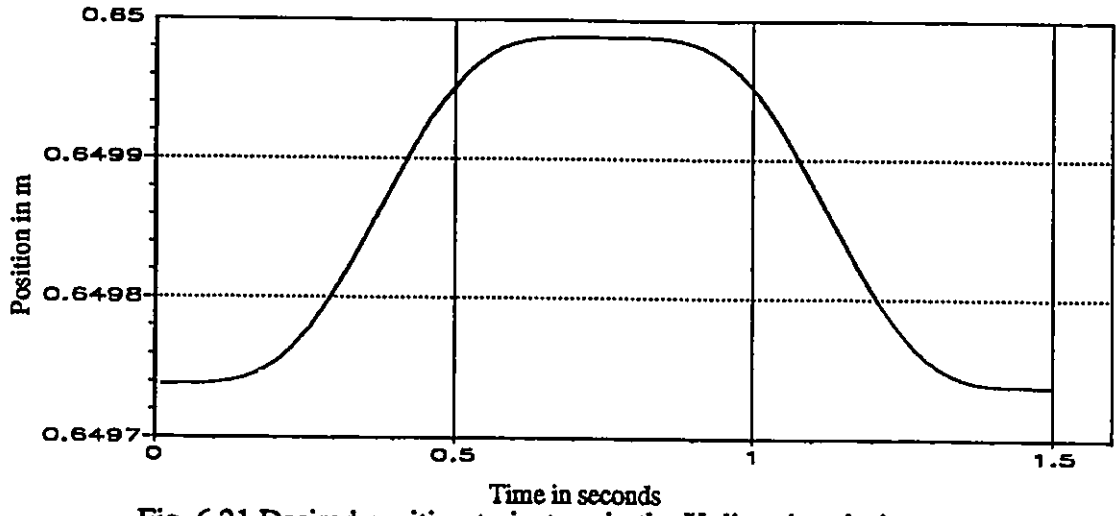

Fig. 6.21 Desired position trajectory in the X direction during contact

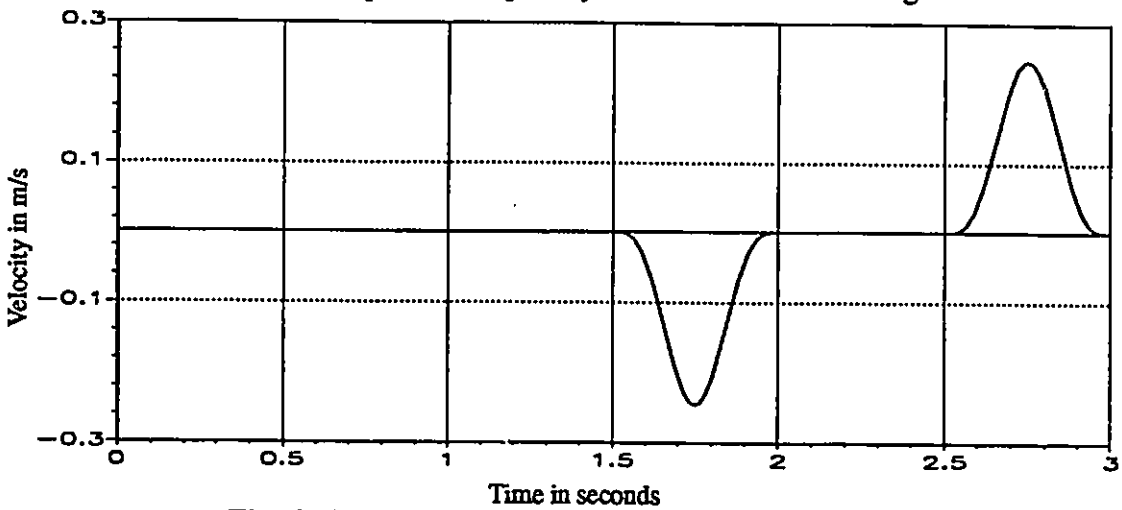

Fig. 6.22 Desired velocity trajectory in the X direction

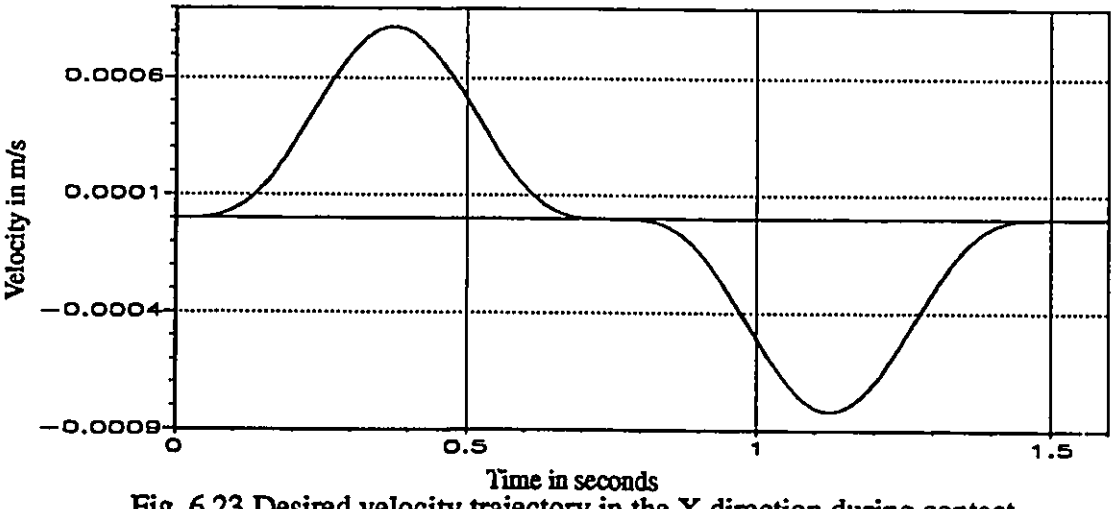

Fig. 6.23 Desired velocity trajectory in the X direction during contact

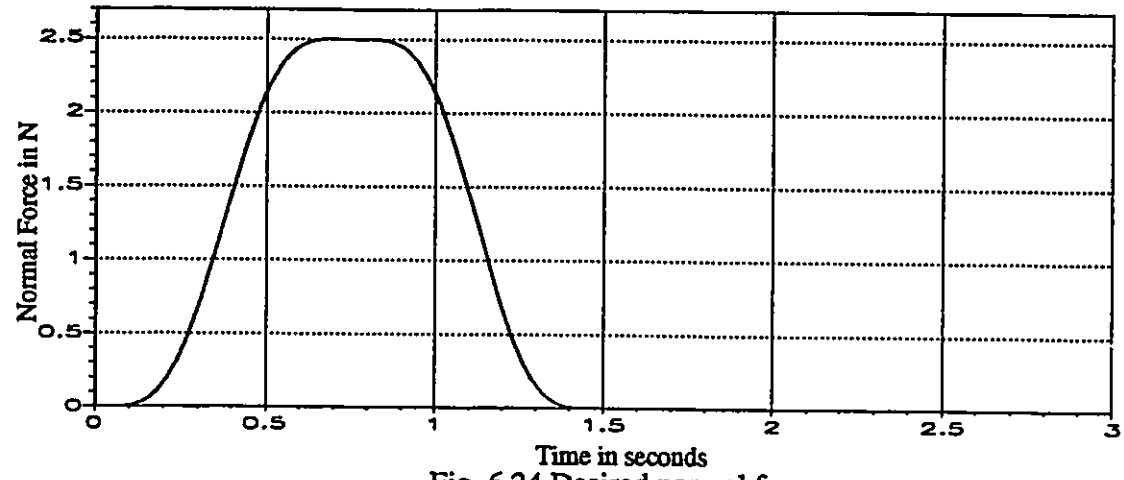

Fig. 6.24 Desired normal force

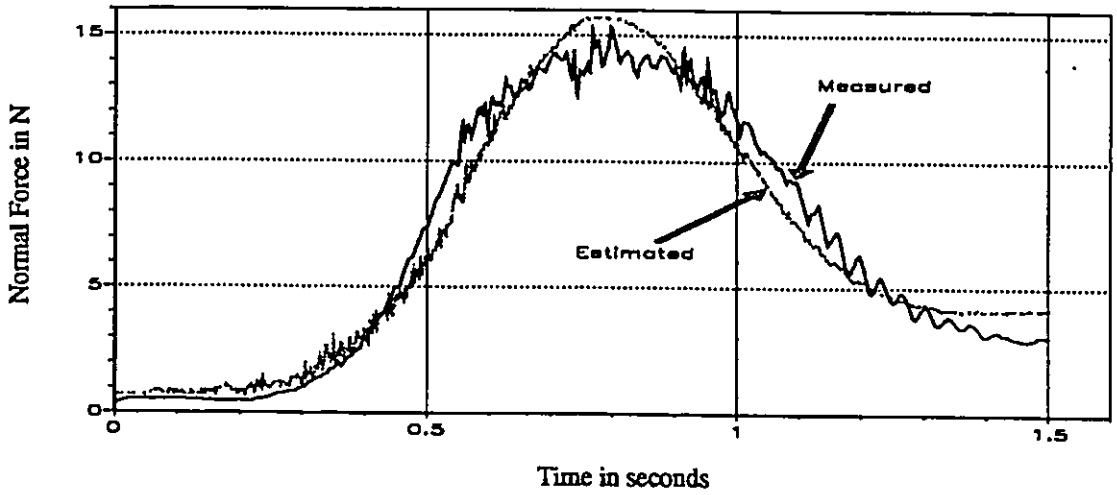

Fig. 6.25 Measured and estimated force trajectories

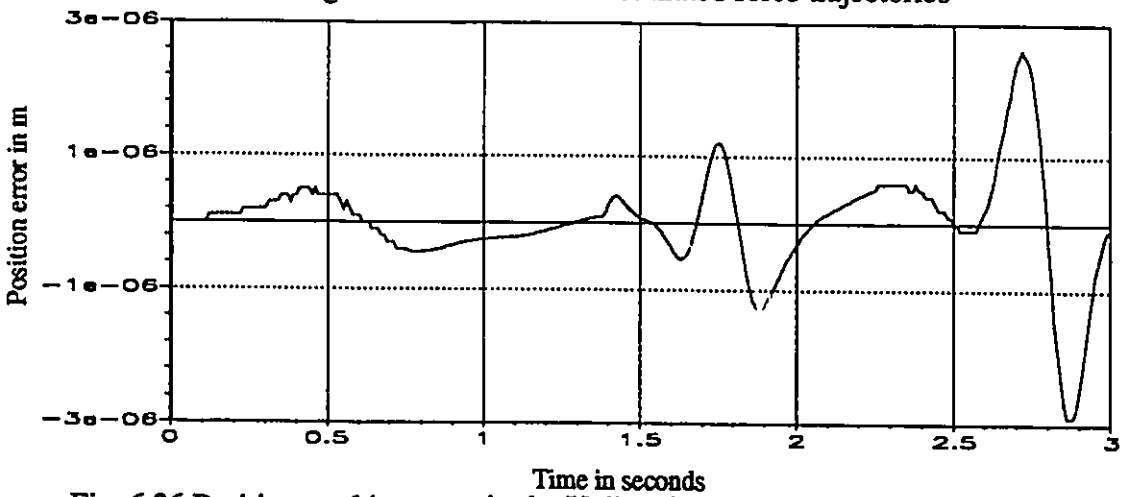

Fig. 6.26 Position tracking error in the Y direction for the impedance controller (simulation)

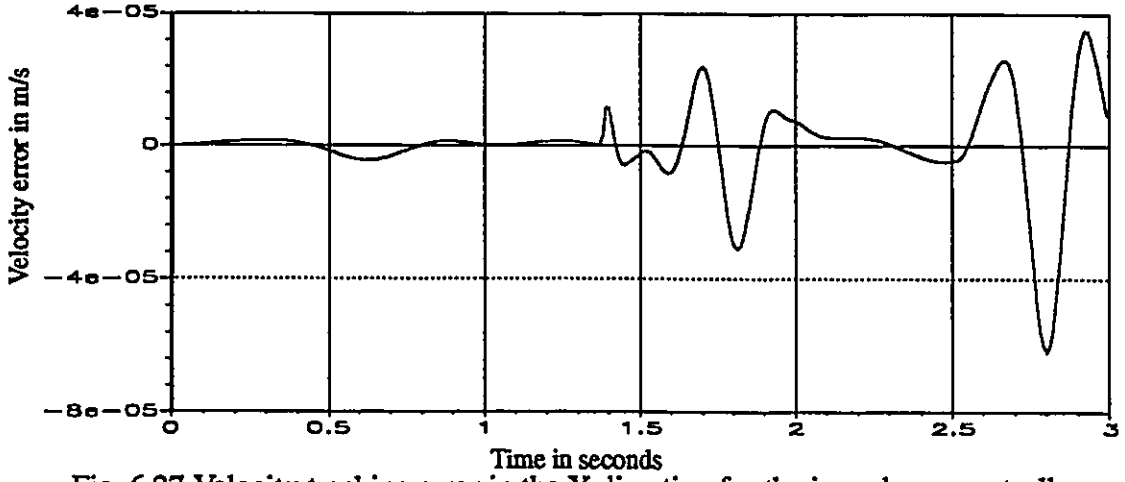

Fig. 6.27 Velocity tracking error in the Y direction for the impedance controller (simulation)

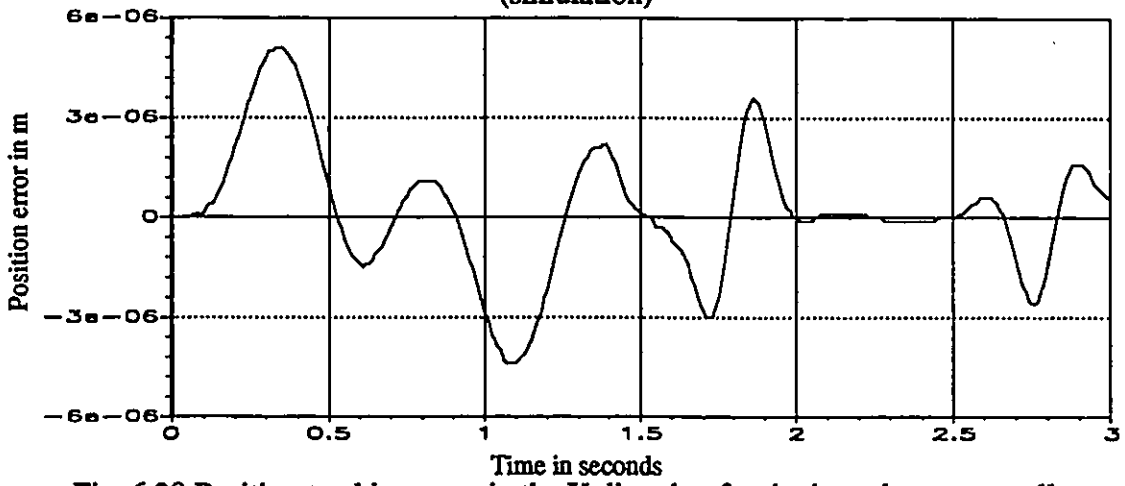

Fig. 6.28 Position tracking error in the X direction for the impedance controller (simulation)

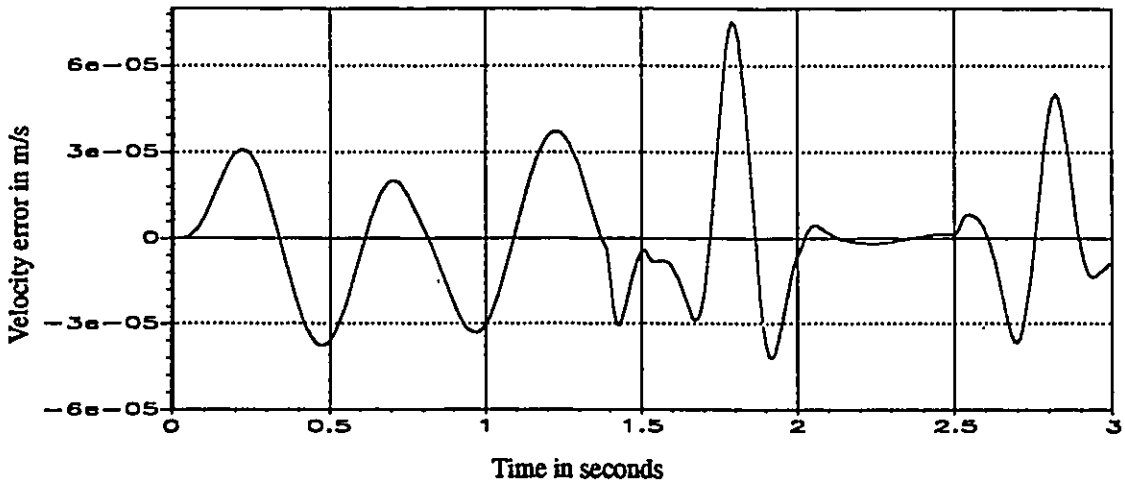

Fig. 6.29 Velocity tracking error in the X direction for the impedance controller (simulation)

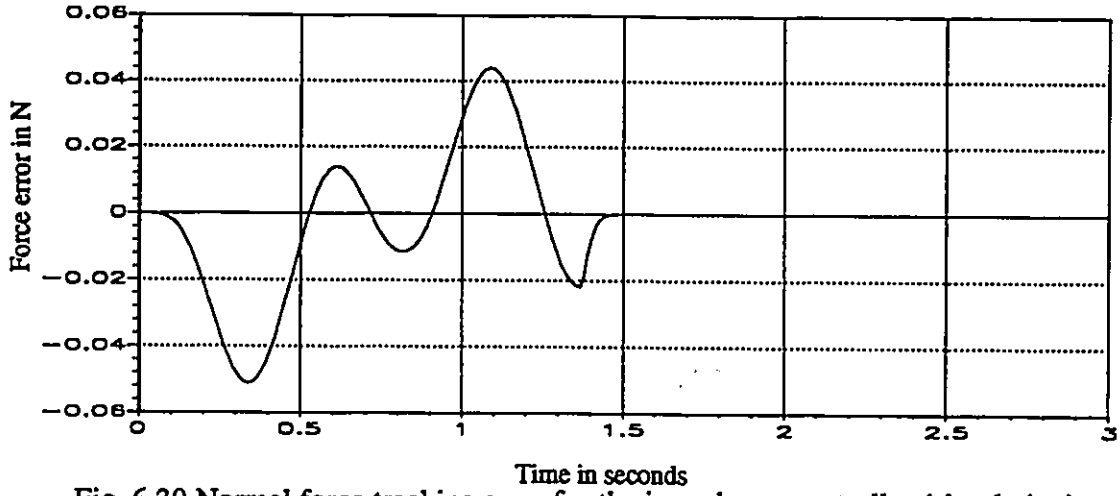

Fig. 6.30 Normal force tracking error for the impedance controller (simulation)

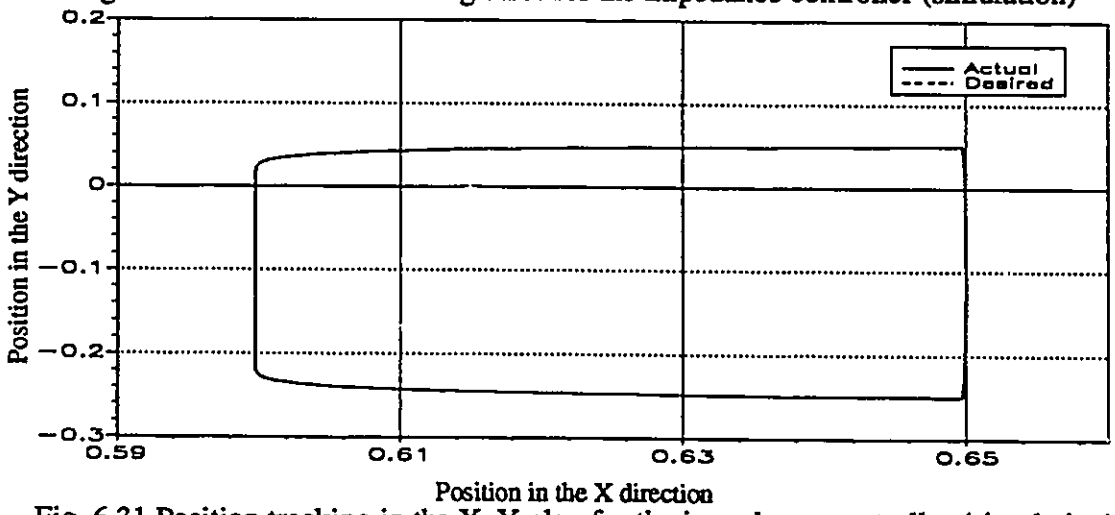

Fig. 6.31 Position tracking in the X–Y plan for the impedance controller (simulation)

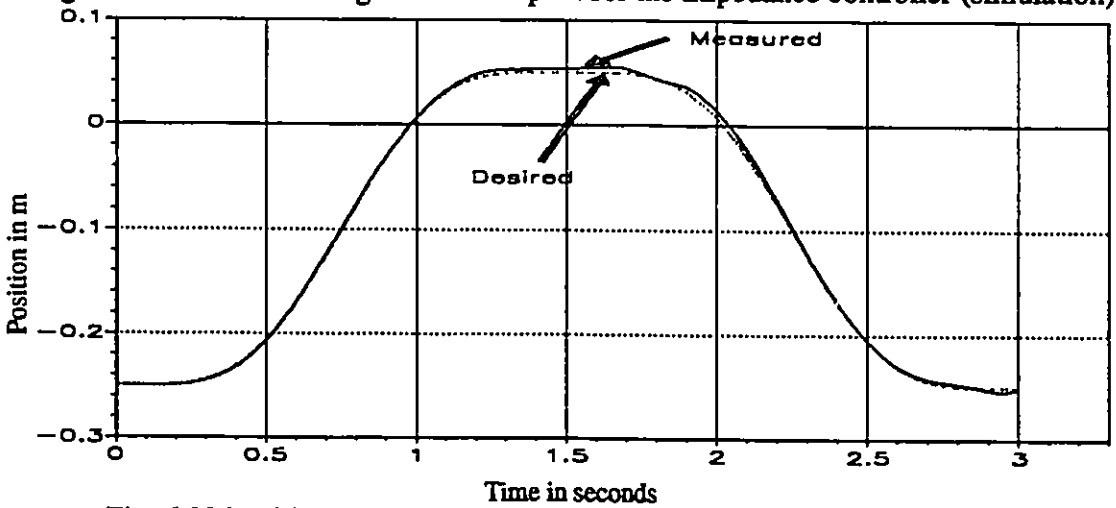

Fig. 6.32 Position tracking in the Y direction for the impedance controller (experimental)

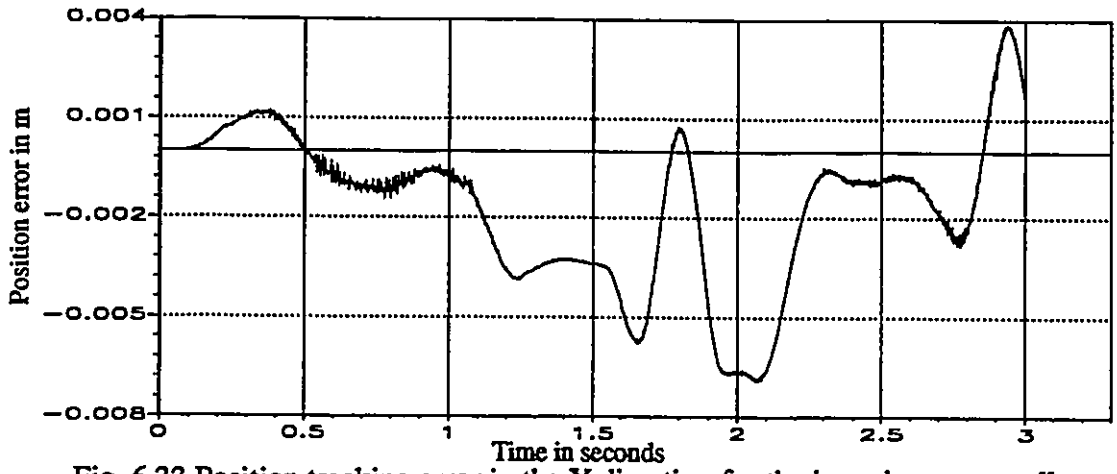

Fig. 6.33 Position tracking error in the Y direction for the impedance controller (experimental)

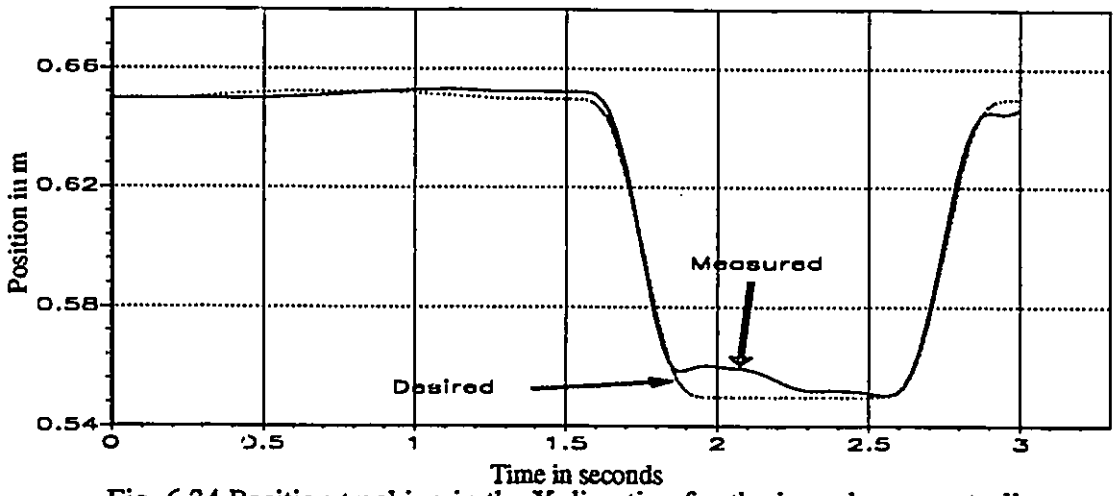

Fig. 6.34 Position tracking in the X direction for the impedance controller (experimental)

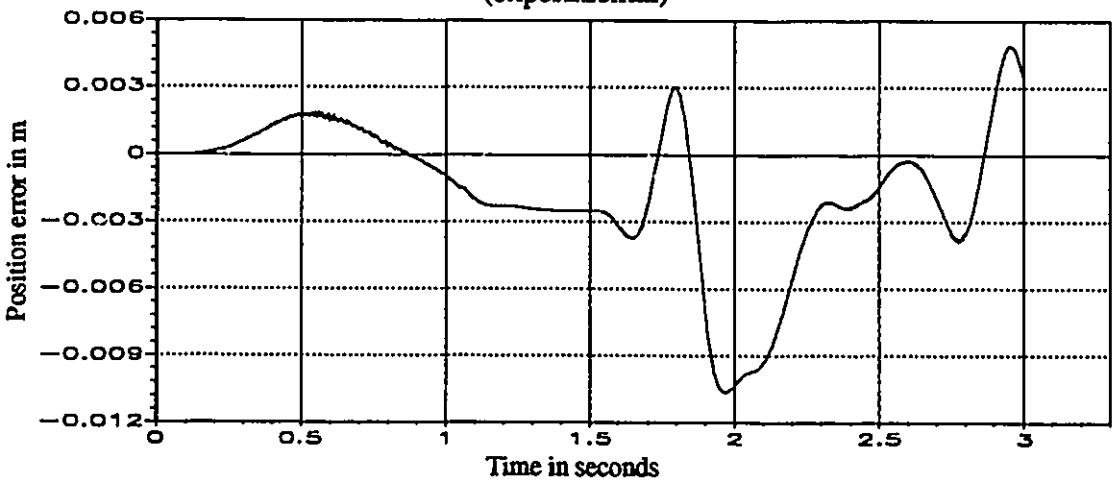

Fig. 6.35 Position tracking error in the X direction for the impedance controller (experimental)

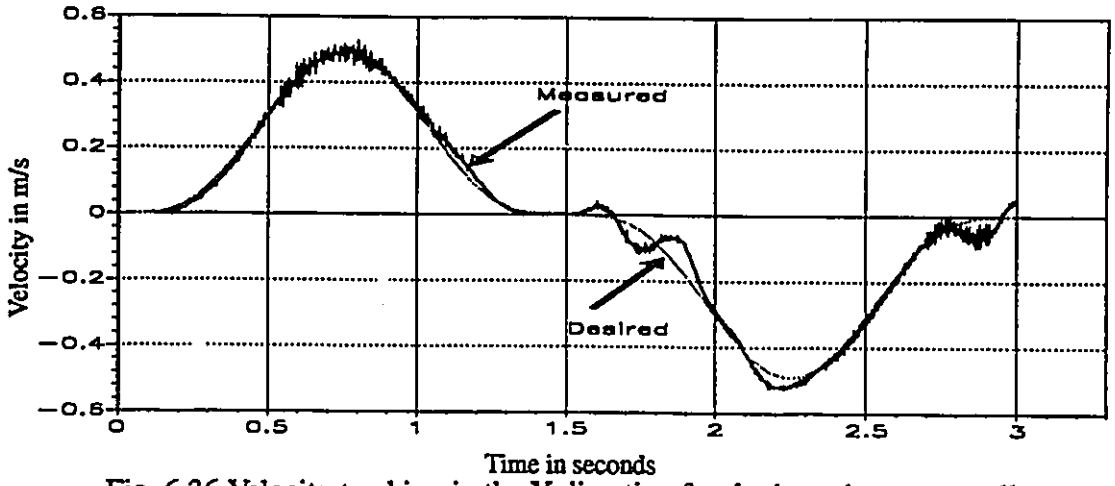

Fig. 6.36 Velocity tracking in the Y direction for the impedance controller (experimental)

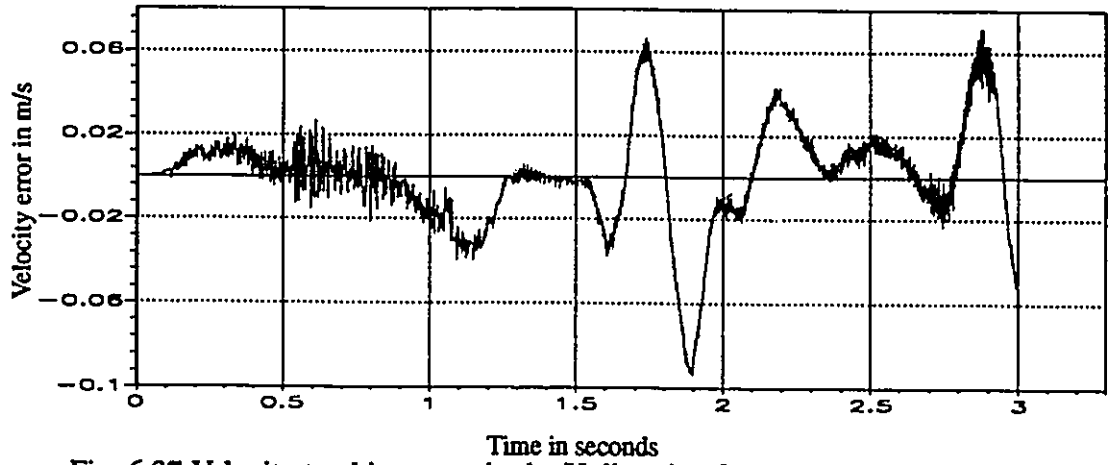

Fig. 6.37 Velocity tracking error in the Y direction for the impedance controller (experimental)

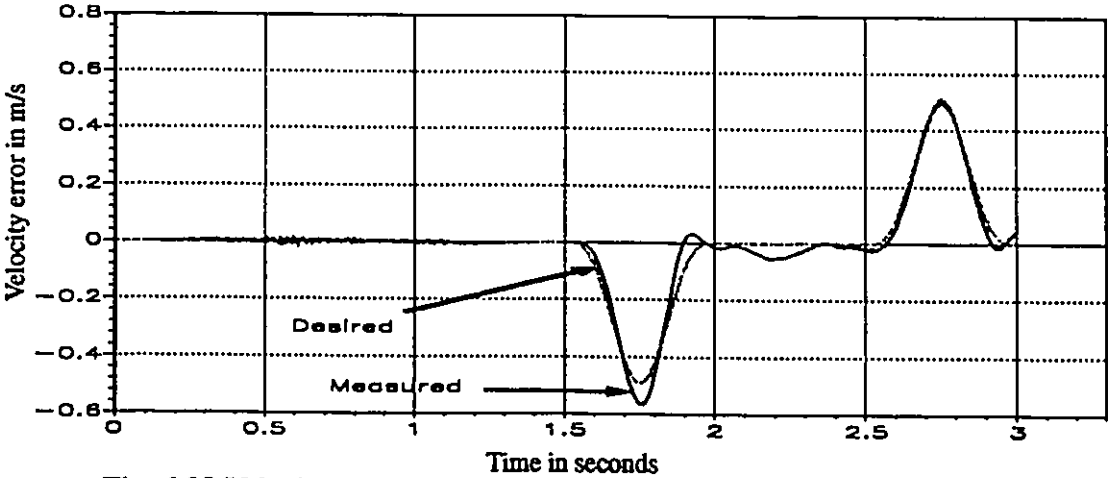

Fig. 6.38 Velocity tracking in the X direction for the impedance controller (experimental)

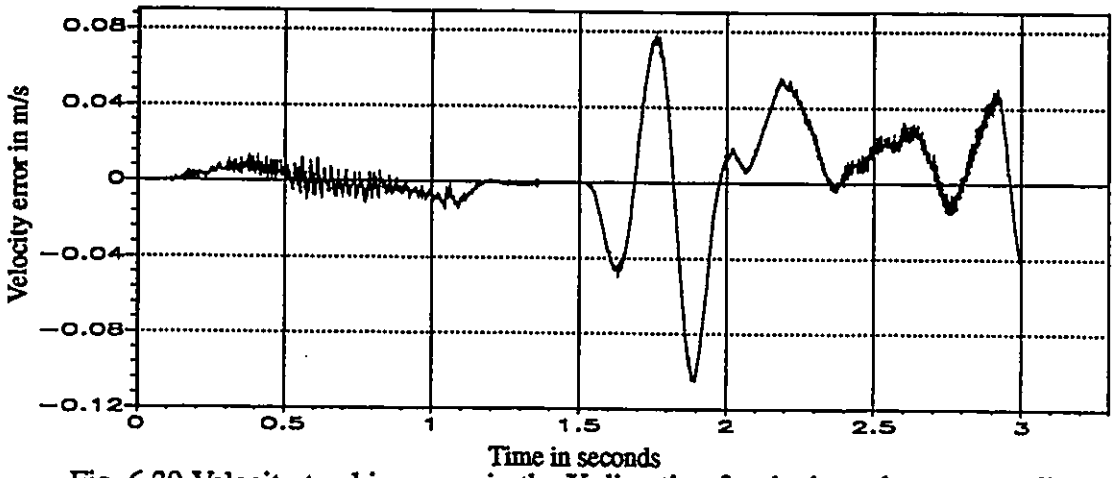

Fig. 6.39 Velocity tracking error in the X direction for the impedance controller (experimental)

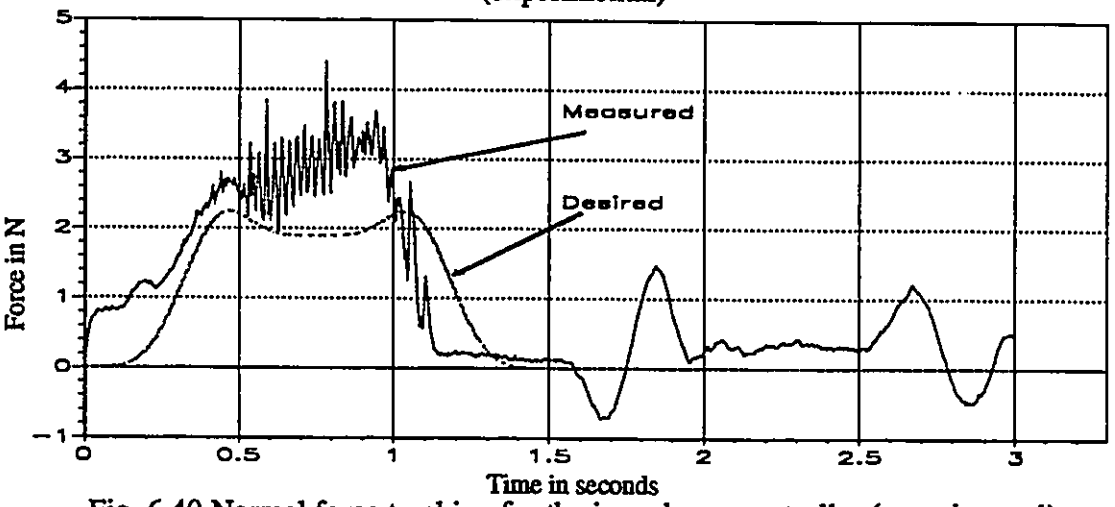

Fig. 6.40 Normal force tracking for the impedance controller (experimental)

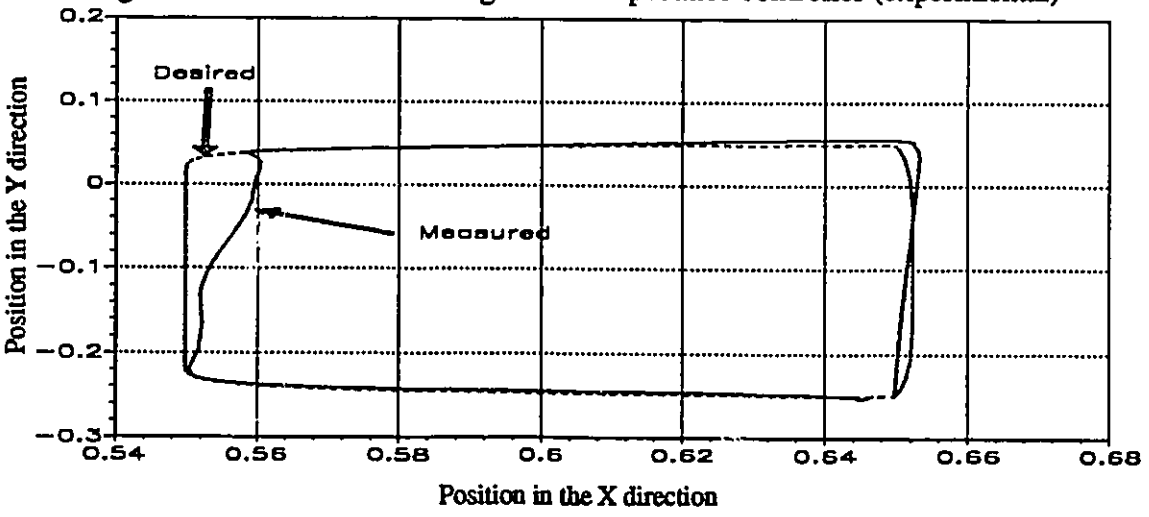

Fig. 6.41 Position tracking in the X–Y plan for the impedance controller (experimental)

6.4 SUMMARY

In this chapter two different position and force control approaches for flexible joint robot manipulators were developed, simulated, and implemented on the experimental flexible joint robot manipulator. Both approaches are based on the feedback linearization principle. The first approach, the dynamic hybrid control, deals with the rigid environments. The nonlinear feedback control law requires the knowledge of the robot parameters, measurements of the angular positions and velocities and the contact forces, and description of the constraint surface in order to linearize and decouple the system then impose desired characteristics for the formed position and force subsystems. The experimental results indicate superior performance in achieving both position and force tracking for flexible joint manipulators. The second approach, the impedance control, aims at regulating the relationship between the contact force and the difference between the commanded and actual position of the end–point. The control law requires the contact force and its first and second derivatives in addition to the angular position and velocities of the links and motors in order to impose a desired target impedance for the end–point of the flexible joint manipulator. The experimental results indicate reasonable success of the impedance controller in regulating the contact force and tracking position trajectories.

CHAPTER 7

ROBUST AND ADAPTIVE POSITION AND FORCE CONTROL

In this chapter, three different position and force control schemes are presented. These controllers deal with the problem of tracking position and force trajectories for flexible joint robot manipulators taking into account parametric uncertainty. A robust sliding mode controller, an adaptive cascade controller, and an adaptive feedback linearization controller have been developed, simulated, and experimentally tested.

7.1 INTRODUCTION

The problem of designing control laws which can achieve position and force tracking for flexible joint manipulators in the presence of parametric uncertainty is considered in this chapter. The following solutions are presented; a robust sliding mode controller, an adaptive cascade controller, a robust nonlinear sliding mode observer, and an adaptive feedback linearization controller. Several important issues need clarification before describing these control schemes. First, the effect of taking joint flexibilities of the manipulator into account while constructing the dynamic model resulted in a new model. In the flexible joint manipulator model, the rigid dynamics (the link subsystem) are connected to the flexible dynamics (the motor subsystem) by the joint stiffness. Thus, the model has double the degrees of freedom of its equivalent rigid manipulator. In addition, the control inputs (motor torques) are not related to the variables to be controlled (link position and tip force). Second, the problem of force trajectory tracking is more difficult than pure position tracking because;

i) the variable to be controlled, in this case, is faster than in the position control case, and ii) the force control is more crucial to the stability of the system than the position control. Third, parametric uncertainty is considered. Efforts are focused on model imprecision caused by parameters while assuming, in the working conditions of the controller, that there are no unstructured uncertainties. This assumption, related to the unstructured uncertainties or unmodelled dynamics, is justified by analogy to industrial robots for which only joint flexibilities cause resonance frequencies in, or close to, the controller operating bandwidth. Resonant frequencies caused by link flexibilities are far outside the controller bandwidth. Thus, joint flexibilities dominate the dynamics in this range.

Both robust and adaptive control attempt to accomplish the same objective of controlling a system under uncertainty, however, the method of achieving this objective differs. Robust control is a fixed controller designed to achieve performance specifications over an expected range of uncertainty while adaptive control incorporates some on–line parameter estimation algorithm and modification of the controller gains. Thus, one can expect an adaptive controller to produce ever–decreasing tracking errors from trail to trail since the controller is learning by on–line updating of the parameters while a robust controller is expected to produce repetitive tracking errors because it does not learn from past experience. Both robust and adaptive control are considered in this chapter. This problem is attacked as follows:

1. A robust sliding mode controller which aims at maintaining the perfect performance achieved by the dynamic hybrid controller presented in Chapter 6 in the presence of bounded uncertainty in the manipulator parameters.

2. An adaptive cascade controller which consists of two adaptive loops, the first is for the rigid dynamics and the second is a MRAC (Model Reference Adaptive Control) for the flexible dynamics.

3. In dealing with the problem more rigorously, a robust sliding mode observer is developed for the feedback linearizable model.

4. Finally, an adaptive feedback linearization controller is designed and combined with the robust observer.

7.2 ROBUST SLIDING MODE CONTROL

7.2.1 Basic Concept

The sliding mode control methodology is based upon the remark that, "it is much easier to control first order systems than to control general n^{th} order systems". A notational simplification is introduced which allows n^{th} order problems to be replaced by equivalent first order problems. It is then easy to show that, for the transformed problems, "perfect" performance can be, in principle, achieved in the presence of arbitrary parameter inaccuracies. The performance is obtained at the price of extremely high control activity. For practical applications, the control law can be modified to achieve an effective trade–off between tracking performance and parametric uncertainty. The fundamental principles of the sliding mode control approach can be found in [115,98,103]. This approach has found successful application to rigid robots [123,99].

As explained in the development of the dynamic hybrid control in Chapter 6, the decoupled fourth order feedback linearizable model possesses properties making it possible to linearize and decouple the system and impose desired characteristics for each of the force and position subsystems. In the ideal case, the proposed control law results in achieving the exponentially stable error dynamics described by equation 6.2.30. However, in case of parametric uncertainty, there will be a mismatch in the closed loop system which can be described by:

$$\dot{Z} = A_1 Z + B_1 \delta(t) \qquad (7.2.1)$$

where $\delta(t)$ is the overall mismatch in the closed loop caused by parametric uncertainty in estimating:1) the transformed state elements $\ddot{q}$ and $\overset{3}{q}$, 2) the decoupling matrices M and N, and 3) the nonlinear vectors required for linearization the nonlinear terms $h_p\ (q, \dot{q}, \ddot{q}, \overset{3}{q})$ and $h_f\ (q, \dot{q}, \ddot{q}, F, \dot{F})$ and the kinematic transformations a_q, a_x and a_f. In other words, when the robot parameters are uncertain, equations 6.2.20 to 6.2.23 do not hold and, thus, the true error dynamics is given by equation 7.2.1 instead of equation 6.2.30. However, the disturbance in the closed loop satisfies the matching conditions making it possible to compensate for the disturbance effects by an additional control activity. Sliding mode control is applied in order to achieve and maintain good tracking performance in the presence of the disturbance in the closed loop caused by parametric uncertainty. First, sliding surfaces are defined for the position and force subsystems. A nominal control law is then designed which achieves perfect tracking for the undisturbed system. Finally, the control law is modified by adding a switching term based on the sign of the error measure in the position and force subsystems and the bounds of the disturbance vector. It is shown that the composed control law results in achieving a desired tracking performance by forcing the position and force subsystems to reach and remain on their sliding surfaces.

7.2.2 Design of the Robust Controller

The design of the robust sliding mode controller to achieve position and force tracking for flexible joint robot manipulators in the presence of parameters uncertainty is presented in this section. The robust controller makes use of the fourth order feedback linearizable model and the constraint frame results. First, sliding surfaces for the position and force tracking errors in the constraint frame are defined as follows:

$$s_{pi} = (\frac{d}{dt} + \lambda_{pi})^4 \int_0^t z_{pi}\, dr \qquad i = 1,2,...6-m \qquad (7.2.2)$$

$$s_{fi} = (\frac{d}{dt} + \lambda_{fi})^2 \int_0^t z_{fi}\, dr \qquad i = 6-m+1,...6 \qquad (7.2.3)$$

where z_{pi} and z_{fi} are the i^{th} end–effector position and force tracking errors in the constraint frame and λ_{pi} and λ_{fi} are positive scalar constants. The basic idea is to design the control torques which force the system to reach and remain on the sliding surfaces. Thus, it is required to look for the control law which will result in achieving the following sliding conditions:

$$\dot{s}_{pi} = 0 \qquad i = 1,2,...6-m \qquad (7.2.4)$$

$$\dot{s}_{fi} = 0 \qquad i = 6-m+1,...6 \qquad (7.2.5)$$

meaning that the position and tracking errors converge to zero. Thus, the control law which satisfies the sliding conditions 7.2.4 and 7.2.5, achieves the goal of position and force tracking. Constructing the sliding conditions 7.2.4 and 7.2.5, according to the definitions of the position and force surfaces defined by equations 7.2.2 and 7.2.3 results in:

$$\dot{s}_{pi} = \overset{4}{z}_{pi} + 4\lambda_{pi}\overset{3}{z}_{pi} + 6\lambda_{pi}^2\ddot{z}_{pi} + 4\lambda_{pi}^3\dot{z}_{pi} + \lambda_{pi}^4 z_{pi} = 0 \qquad i = 1,2,...6-m \qquad (7.2.6)$$

$$\dot{s}_{fi} = \ddot{z}_{fi} + 2\lambda_{fi}\dot{z}_{fi} + \lambda_{fi}^2 z_{fi} \qquad i = 6-m+1,...6 \qquad (7.2.7)$$

The vectors S_p, S_f, and S are defined as follows:

$$S_p = [s_{p1}, s_{p2}, ...s_{p6-m}]^T$$

$$S_f = [s_{f6-m+1}, s_{f6-m+2}, ...s_{f6}]^T$$

$$S = [S_p, S_f]^T$$

The decoupled fourth order model given by equation 6.2.18 can be rewritten to augment the

position and force in the constraint frame in one vector as follows:

$$H(q)\begin{bmatrix} \overset{4}{P} \\ \ddot{f} \end{bmatrix} + h_p(q,\dot{q},\ddot{q},\overset{3}{q}) + h_f(q,\dot{q},\ddot{q},F,\dot{F}) + M J^{-1}[R^{-1}a_x - a_q] + N J^T a_f = \tau \qquad (7.2.8)$$

where $H(q)$ is a new matrix, the first $6-m$ columns are the first $6-m$ columns of the matrix $M J^{-1} R^{-1}$ and the other m columns are the matrix $N J^T L$. By solving the sliding conditions, equations 7.2.6 and 7.2.7, for the position fourth derivative and the force second derivative and substituting into decoupled model, equation 7.2.8, the following control law results:

$$\tau = H(q)\begin{bmatrix} \overset{4}{P}^d + 4\lambda_p \overset{3}{z}_p + 6\lambda_p^2 \ddot{z}_p + 4\lambda_p^3 \dot{z}_i + \lambda_p^4 z_p \\ \ddot{f}^d + 2\lambda_f \dot{z}_f + \lambda_f^2 z_f \end{bmatrix} + h_p(q,\dot{q},\ddot{q},\overset{3}{q}) + h_f(q,\dot{q},\ddot{q},F,\dot{F}) + M J^{-1}[R^{-1}a_x - a_q] + N J^T a_f \qquad (7.2.9)$$

The above control law, when applied to the constrained flexible joint robot manipulator, results in satisfying the sliding conditions and hence position and force tracking is achieved. However, in the case of parametric uncertainty, the above control law cannot be obtained. The best approximation of the above control law is that which has the same structure as the ideal control law given by equation 7.2.9 evaluated using the best known approximation of the robot parameters. This approximate control law is thus given by:

$$\hat{\tau} = \hat{H}(q)\begin{bmatrix} \overset{4}{P}^d + 4\lambda_p \overset{\wedge\,3}{z}_p + 6\lambda_p^2 \hat{\ddot{z}}_p + 4\lambda_p^3 \dot{z}_i + \lambda_p^4 z_p \\ \ddot{f}^d + 2\lambda_f \dot{z}_f + \lambda_f^2 z_f \end{bmatrix} + \hat{h}_p(q,\dot{q},\ddot{q},\overset{3}{q}) + \hat{h}_f(q,\dot{q},\ddot{q},F,\dot{F}) + \hat{M} J^{-1}[R^{-1}\hat{a}_x - a_q] + \hat{N} J^T \hat{a}_f \qquad (7.2.10)$$

The above control law is similar to the dynamic hybrid control law except that the former uses the estimated robot parameter. In order to satisfy the sliding conditions 7.2.4 and 7.2.5

despite the uncertainty in the robot parameters, $\hat{\tau}$ is modified by adding a term discontinuous across each of the surfaces $S_p = 0$ and $S_f = 0$. Thus the overall control law is given by:

$$\tau = \hat{\tau} - \hat{H}(q)\, K_d\, sgn(S) \qquad (7.2.11)$$

where K_d is a diagonal matrix of positive constant elements and $sgn(S)$ is a vector defined by:

$$\begin{aligned} sgn(S) &= [sgn(S_p),\ sgn(S_f)]^T \\ sgn(S_p) &= [sgn(s_{p1}), sgn(s_{p2}), \ldots sgn(s_{p6-m})]^T \\ sgn(S_f) &= [sgn(s_{f6-m+1}),\ sgn(s_{f6-m+2}), \ldots\ sgn(s_{f6})]^T \end{aligned} \qquad (7.2.12)$$

where sgn is the sign function which is defined by

$$\begin{aligned} sgn(x) &= +1 \qquad \text{if } x > 0 \\ sgn(x) &= -1 \qquad \text{if } x < 0 \end{aligned} \qquad (7.2.13)$$

It remains to design the switching gain matrix K_d and to ensure the availability of the sign vector in 7.2.11. The design of the gain matrix K_d proceeds as follows. First, the control law given by equation 7.2.10 can be rearranged in a way which enables computing an upper bound for the disturbance as follows:

$$\tau = \hat{H}(q) \begin{bmatrix} \overset{4}{P}{}^d + 4\lambda_p \overset{3}{z}_p + 6\lambda_p{}^2 \ddot{z}_p + 4\lambda_p{}^3 \dot{z}_i + \lambda_p{}^4 z_p \\ \ddot{f}^d + 2\lambda_f \dot{z}_f + \lambda_f{}^2 z_f \end{bmatrix} + \hat{g}(q, \dot{q}, \ddot{q}, \overset{3}{q}, F, \dot{F}) +$$
$$\hat{H}(q)\, \delta(\overset{3}{z}_p, \dot{z}_p, \hat{\overset{3}{z}}_p, \hat{\ddot{z}}) - \hat{H}(q)\, K_d\, sgn(S) \qquad (7.2.14)$$

where

$$\begin{aligned} \hat{g}(q, \dot{q}, \ddot{q}, \overset{3}{q}, F, \dot{F}) &= \hat{h}_p(q, \dot{q}, \ddot{q}, \overset{3}{q}) + \hat{h}_f(q, \dot{q}, \ddot{q}, F, \dot{F}) \\ &\quad + \hat{M} J^{-1} [\, R^{-1} \hat{a}_x - a_q \,] + \hat{N} J^T \hat{a}_f \end{aligned} \qquad (7.2.15)$$

$$\delta(\overset{3}{z}_p, \ddot{z}_p, \overset{\wedge}{\overset{3}{z}}_p, \overset{\wedge}{\ddot{z}}_p, \dot{z}_f, \overset{\wedge}{\dot{z}}_f) = \begin{bmatrix} 4\lambda_p(\overset{\wedge}{\overset{3}{z}}_p - \overset{3}{z}_p) + 6\lambda_p{}^2(\overset{\wedge}{\ddot{z}}_p - \ddot{z}_p) \\ 2\lambda_f\,(\overset{\wedge}{\dot{z}}_f - \dot{z}_f) \end{bmatrix} \qquad (7.2.16)$$

Also, the following term is defined:

$$\xi = \begin{bmatrix} \overset{4}{P}{}^d + 4\lambda_p \overset{\wedge}{\overset{3}{z}}_p + 6\lambda_p{}^2 \overset{\wedge}{\ddot{z}}_p + 4\lambda_p{}^3\,\dot{z}_i + \lambda_p{}^4\,z_p \\ \ddot{f}^d + 2\lambda_f\,\dot{z}_f + \lambda_f^{\,2}\,z_f \end{bmatrix} \qquad (7.2.17)$$

Finally, the matrix $H(q)$ is transformed to a multiplicative form as follows:

let $\tilde{H} = H - \hat{H}$ and $\Delta = H^{-1}\,\tilde{H}$ then $\hat{H} = \tilde{H} + H = H(H^{-1}\tilde{H} + I) = H(D + I)$. The sliding conditions are modified as:

$$\dot{s}_{pi} \leq -\eta_i \qquad i = 1, 2, \ldots 6 - m \qquad (7.2.18)$$

$$\dot{s}_{fi} \leq -\eta_i \qquad i = 6 - m + 1, \ldots 6 \qquad (7.2.19)$$

where $\eta_i, i = 1, 2, \ldots 6$ are strictly positive constants. The above sliding conditions can be written in the following vector form:

$$\dot{S}_p \leq -\eta_p \qquad (7.2.20)$$

$$\dot{S}_f \leq -\eta_f \qquad (7.2.21)$$

where:

$$\eta_p = [\eta_{p1}, \eta_{p2}, \ldots \eta_{p6-m}]^T$$

$$\eta_f = [\eta_{f6-m+1}, \eta_{f6-m+2}, \ldots \eta_{f6}]^T$$

Then conditions 7.2.20 and 7.2.21 can be combined to give:

$$\dot{S} \leq -\eta \qquad (7.2.22)$$

where $\eta = [\eta_p, \eta_f]^T$.

The above sliding condition states that the squared distance measured by S^2 decreases along the trajectories. Thus, it constrains trajectories to point toward the surface S. When the con-

trol law given by equation 7.2.14 is applied to the fourth order feedback linearizable model given by equation 7.2.8 the following error dynamics results:

$$H\ (q)\ \dot{S} = H\ (q)\ \gamma(t)\ - H(D + I)\ K_d\ sgn(S) \qquad (7\ .\ 2\ .\ 23)$$

where

$$\gamma(t)\ = -\ (H^{-1}\ \tilde{g}\ (q, \dot{q}, \ddot{q}, \overset{3}{q}, F, \dot{F})\ + (D + I)\ \ \delta(\overset{3}{z}_p, \dot{z}_p, \overset{\wedge}{\overset{3}{z}}_p, \overset{\wedge}{\ddot{z}}_p)\ \ + D\ \xi\ ) \qquad (7\ .\ 2\ .\ 24)$$

It can be seen that if the gain matrix K_d is designed to satisfy the following inequality:

$$(D + I)K_d \geq \eta + \gamma(t) \qquad (7\ .\ 2\ .\ 25)$$

then the sliding conditions given by equations 7.2.20 and 7.2.21 are satisfied and thus:

$$\frac{1}{2}\frac{d}{dt}\ S^2\ \leq\ -\ \eta\ |\ S\ | \qquad (7\ .\ 2\ .\ 26)$$

The remaining issues are to determine the upper bound of the disturbance $\gamma(t)$ and to investigate the knowledge of the sign of the sliding surfaces since both the angular acceleration and jerk are not measured but computed from the state transformation. The analysis is based on the following two properties.

1. <u>The state transformation</u>

The new state obtained by transforming the original system to the feedback linearizable form is bounded. The state transformations given by equations 5.3.15 , in the presence of parametric uncertainty, can be written in the following form:

$$\begin{aligned} \hat{x}_3 &= T_3(y_1, y_2, y_3, \hat{\Theta}) \\ \hat{x}_4 &= T_4(y_1, y_2, y_3, y_4, \hat{\Theta}) \end{aligned} \qquad (7\ .\ 2\ .\ 27)$$

Thus the error in the transformed state can be quantified as

$$\begin{aligned} \|\, x_3 - \hat{x}_3 \,\| &= \|\, T_3(y_1, y_2, y_3, \Theta)\ - T_3(y_1, y_2, y_3, \hat{\Theta})\ \| \leq J_{T3}\ (y)\ \|\, \tilde{\Theta}\,\| \\ \|\, x_4 - \hat{x}_4 \,\| &= \|\, T_4(y_1, y_2, y_3, y_4, \Theta) - T_4(y_1, y_2, y_3, y_4, \hat{\Theta})\,\| \leq J_{T4}\ (y)\ \|\, \tilde{\Theta}\,\| \end{aligned} \qquad (7\ .\ 2\ .\ 28)$$

where J_{T3} (y) and J_{T4} (y) are the Jacobians of the transformations $T_3(y_1, y_2, y_3, \hat{\Theta})$ and $T_4(y_1, y_2, y_3, y_4, \hat{\Theta})$ evaluated with respect to Θ, respectively. Θ is the true robot parameters vector, $\hat{\Theta}$ is the estimated robot parameters vector and $\tilde{\Theta} = \Theta - \hat{\Theta}$. The Jacobians are bounded because the uncertainty in the parameters vector is bounded and the transformations are continuous in the parameters vector. Thus, there exist some positive constants σ_{x3} and σ_{x4} such that

$$\begin{aligned} \| x_3 - \hat{x}_3 \| &= \sigma_{x3} \\ \| x_4 - \hat{x}_4 \| &= \sigma_{x4} \end{aligned} \qquad (7.2.29)$$

The above relations ensure directly that:

$$\begin{aligned} \| \ddot{z}_p - \hat{\ddot{z}}_p \| &= \sigma_3 \\ \| \overset{3}{z}_p - \hat{\overset{3}{z}}_p \| &= \sigma_4 \end{aligned} \qquad (7.2.30)$$

where σ_3 and σ_4 are positive constants. The above equations state that the difference between the true and estimated state vector is bounded. This can be described based on the physical interpretation of the parametric uncertainty in the manipulator parameters. The new state vector, computed using the state transformation and the estimated parameters vector, can be recognized as a true state vector of some different manipulator but still finite. For example, when the true mass of one of a link is 2.0 Kg, and the best known estimate is 1.0 Kg, this represents a 50% uncertainty, one may consider that there are two robots with different parameters yet for both manipulators two different transformed state vectors can be computed. The computed state vectors are bounded since the uncertainty is bounded. Knowing that the force and it first derivatives are continuous functions of the state x and the robot parameters Θ, then, following the same analysis for the angular acceleration and jerk, one can derive an upper bound for the force first derivative. Equation 6.2.17 can be written as:

$$\dot{f}_f = T_f(y_1, y_2, y_3, \Theta)$$
$$\hat{\dot{f}}_f = T_f(y_1, y_2, y_3, \hat{\Theta}) \qquad (7.2.31)$$

thus:

$$\| \dot{f}_f - \hat{\dot{f}}_f \| = \| T_f(y_1, y_2, y_3, \Theta) - T_f(y_1, y_2, y_3, \hat{\Theta}) \| \leq J_{Tf}(y) \| \tilde{\Theta} \| \qquad (7.2.32)$$

where $J_{Tf}(y)$ are the Jacobians of the transformations $T_f(y_1, y_2, y_3, \hat{\Theta})$ evaluated with respect to Θ. The fact that the robot parameters are bounded resulted in the existence of upper bounds for the estimated states. These two properties ensure the existence of an upper bound for the disturbance vector $\gamma(t)$, thus enabling design of the switching gain matrix K_d which satisfies the inequality given by equation 7.2.25.

2. The sliding surface properties

The bounds on the state transformation error can be combined with the properties of the sliding surface to obtain a range in which the sliding mode control can be applied to the problem. This requires the introduction of the boundary layer concept. In practical applications, the discontinuous control law generates very high control activity which should be avoided. As a result, the objective of the surface converging to zero is replaced by having the surface remain within certain limits which define the boundary layer thickness. The thickness of the boundary layer is reflected into accuracy on the tracking errors. Outside the boundary layer the discontinuous control is applied while inside the boundary layer the control is interpolated as:

$$\tau = \hat{\tau} - K_d sat(S/\phi_s) \qquad (7.2.33)$$

where ϕ_s is a scalar positive constant which defines the boundary layer thickness and *sat* is the saturation function defined by:

$$sat(x) = x \qquad x \leq 1$$
$$sat(x) = sgn(x) \qquad x > 1 \qquad (7.2.34)$$

Thus, instead of aiming at $S = 0$, it is aimed at having $\| S \| \leq \phi_s$. If the robot parameters are uncertain but the state vector of the transformed system is available then the choice of boundary ϕ_s is arbitrary in the sense that the only limitation is that of eliminating chattering. However, in cases where some elements of the state vector are estimated, other limitations exist on the minimum achievable boundary layer thickness. The relationship between the minimum boundary layer thickness and the maximum error in S, caused by parametric uncertainty, is derived. Each of the true surfaces defined by equations 7.2.2 and 7.2.3 can be decomposed into an estimated part, and a measured part, as follows:

$$S = S_u + S_n \qquad (7.2.35)$$
$$\hat{S} = \hat{S}_u + S_n \qquad (7.2.36)$$

where:

$$S_u = \begin{bmatrix} \dddot{z}_p + 4\lambda_p \ddot{z}_p \\ \dot{z}_f \end{bmatrix} \quad , \quad \hat{S}_u = \begin{bmatrix} \hat{\dddot{z}}_p + 4\lambda_p \hat{\ddot{z}}_p \\ \hat{\dot{z}}_f \end{bmatrix} \qquad \text{and}$$

$$S_n = \begin{bmatrix} 6\lambda_p^2 \dot{z}_p + 4\lambda_p^3 z_p + \lambda_p^4 \int_0^t z_p \\ 2\lambda_f \dot{z}_f + \lambda_f^2 \int_0^t z_f \end{bmatrix}$$

Subtracting equation 7.2.36 from 7.2.35 the following results:

$$S - \hat{S} = \delta_s(t) \doteq \begin{bmatrix} (\dddot{z}_p - \hat{\dddot{z}}_p) + 4\lambda_p (\ddot{z}_p - \hat{\ddot{z}}_p) \\ (\dot{z}_f - \hat{\dot{z}}_f) \end{bmatrix} \qquad (7.3.37)$$

By using the properties of the state transformation given by equation 7.2.30, and of the force first derivative expression given by equation 7.2.32, the following upper bound for the error

in S is obtained:

$$\| S - \hat{S} \| = \| S_u - \hat{S}_u \| = \| \delta_s(t) \| \leq \sigma_s \qquad (7.2.38)$$

where

$$\sigma_s \geq \| \frac{\sigma_4 + 4\lambda_p \sigma_3}{\sigma_f} \| \qquad (7.2.39)$$

By inspecting the bound on the sliding surfaces given by equation 7.3.38, it is clear that the boundary layer ϕ_s cannot be smaller than σ_s, thus the limitation on the boundary layer thickness is given by:

$$S \leq \phi_s \geq 2\,\sigma_s \qquad (7.2.40)$$

It is possible to force the true surface S to remain inside the above boundary layer since $\hat{S}$ is known. Equation 7.3.37 can be written as:

$$S = \hat{S}_u + \delta_s(t) \qquad (7.2.41)$$

Outside the boundary layer $\hat{S} > \sigma_s$ then $sgn(S) = sgn(\hat{S})$ and thus the discontinuous control can force the system to sliding conditions inside the boundary layer. Inside the boundary layer $S < 2\,\sigma_s$ and $\hat{S} < \sigma_s$ which enable approximating S by $\hat{S}$.

7.2.3 Simulation Results

The above robust controller was simulated to evaluate its performance in achieving position and force tracking in the presence of parametric uncertainty. The task used in the simulation is the same as that used in the dynamic hybrid controller. Parametric uncertainty is introduced in rigid dynamics inertia matrix of the robot manipulator model. The inertia parameters known to the controller are the nominal values while true inertia is increased by adding a 0.98 Kg mass at the centre of mass of the second link. The position and force surfaces are defined by $\lambda_p = 25$ and $\lambda_f = 60$. The boundary layer thickness is defined by $\phi_p \leq 2.0$ and $\phi_f \leq 5.0$. Figures 7.1 to 7.3 shows plots of the position, velocity and force

tracking errors. The figures indicate that the robust controller is working within the sliding surface. As a result, the controller achieved tracking for both position and force trajectories according to the accuracy dictated by the boundary layer thickness, despite the unknown inertia load introduced in the model.

7.2.4 Experimental Results

The robust controller was implemented on the experimental flexible joint robot at a sampling frequency of 1 KHz. The task used is the same as that used in simulation and described in section 6.2.5.1. Parametric uncertainty was introduced by adding a 0.98 Kg steel block at the centre of mass of the second link. The robust controller used nominal inertia parameters obtained from the frequency response identification. The position and surfaces were defined by $\lambda_p = 25$ and $\lambda_f = 60$. The boundary layer thickness chosen was based on the performance of the dynamic hybrid controller, i.e. the bounds on the surfaces s_p and s_f were computed using experimental tracking trajectories. It was found that $s_p < 50.0$ and $s_f < 80.0$. Thus, in the experiment, the robust controller aims at forcing the sliding surfaces to stay within the bounds mentioned on the position and force surfaces. The angular positions and velocities of the motors and links are measured while the angular acceleration, jerk, and force first derivative are computed as before. Figures 7.4 and 7.5 show plots of the position and velocity tracking errors. Figure 7.6 exhibits plots of the desired and measured normal force. These figures indicate that the robust sliding mode controller managed to achieve an excellent position and force tracking performance despite the 0.98 Kg mass added to the second link. Computation of the sliding surfaces showed that they remained within the defined boundary layers.

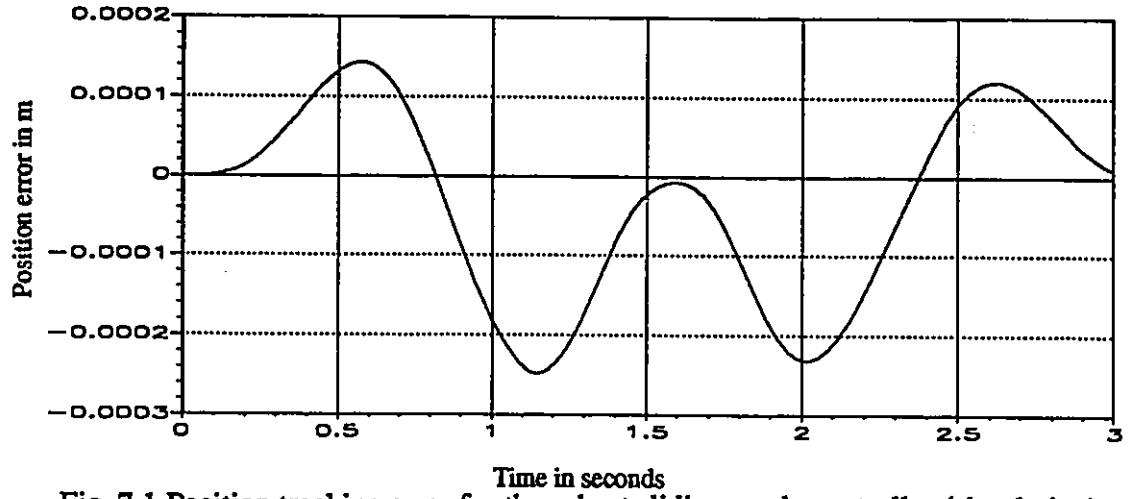

Fig. 7.1 Position tracking error for the robust sliding mode controller (simulation)

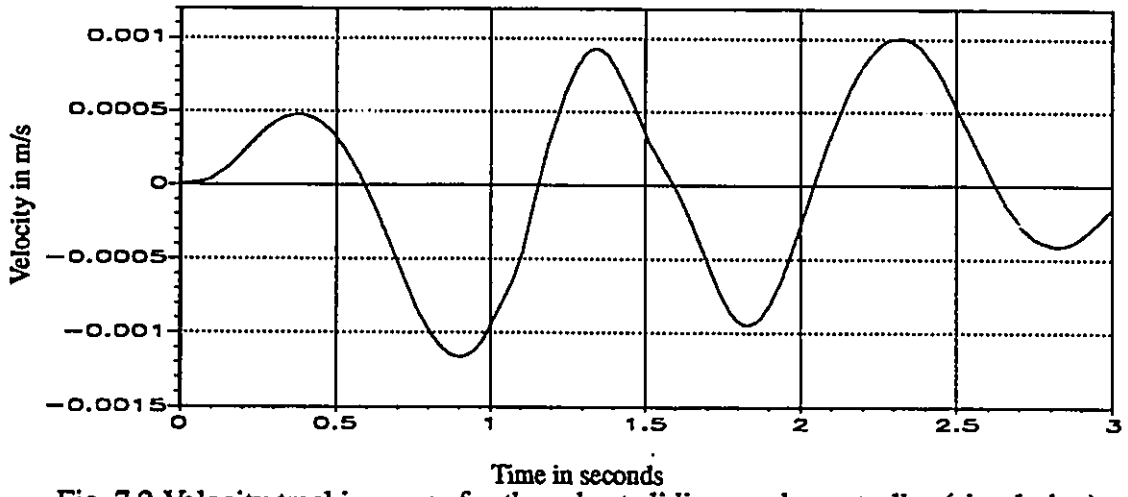

Fig. 7.2 Velocity tracking error for the robust sliding mode controller (simulation)

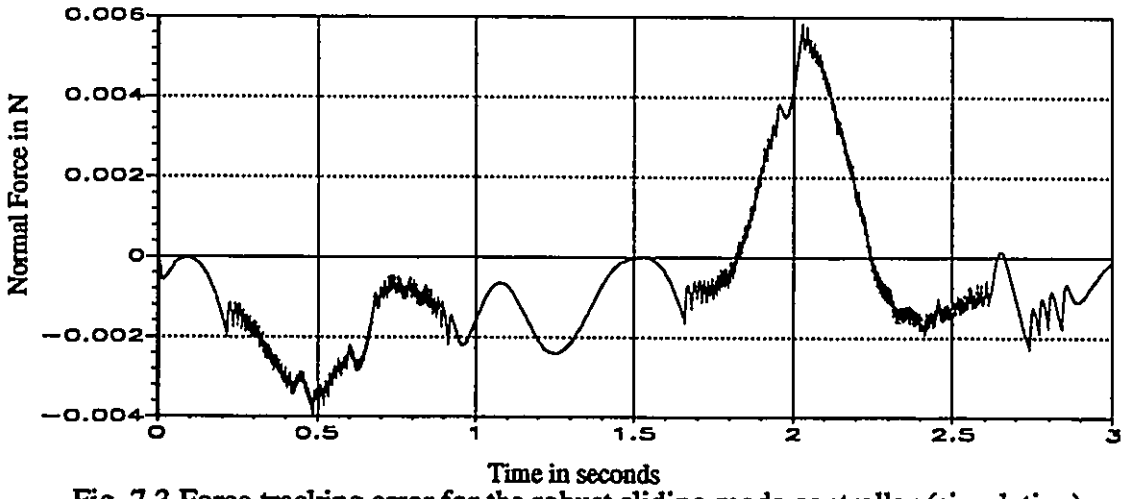

Fig. 7.3 Force tracking error for the robust sliding mode controller (simulation)

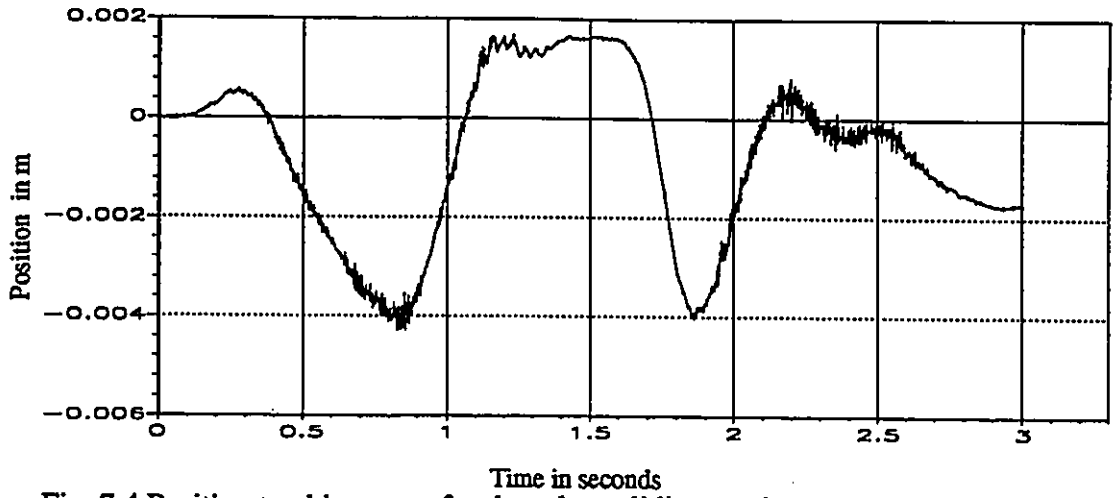

Fig. 7.4 Position tracking error for the robust sliding mode controller (experimental)

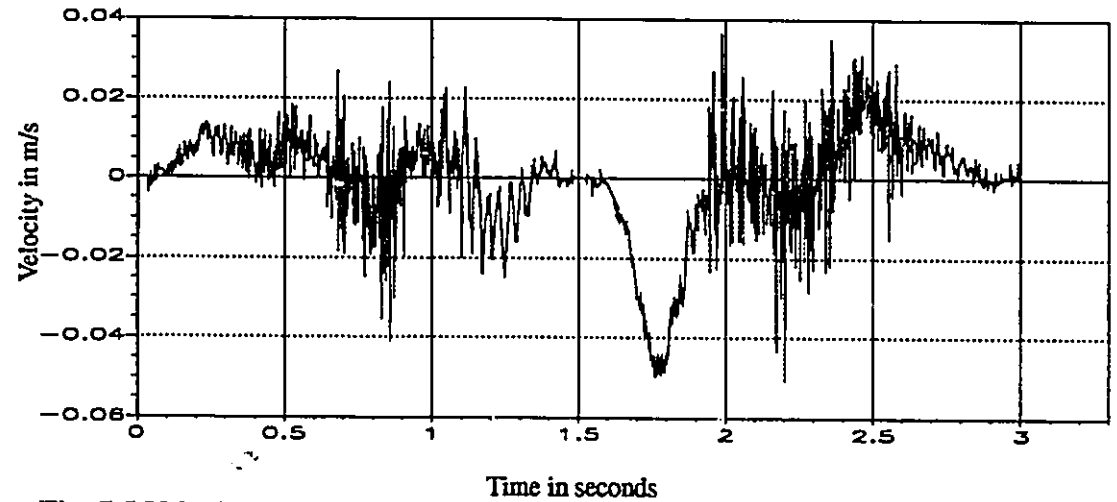

Fig. 7.5 Velocity tracking error for the robust sliding mode controller (experimental)

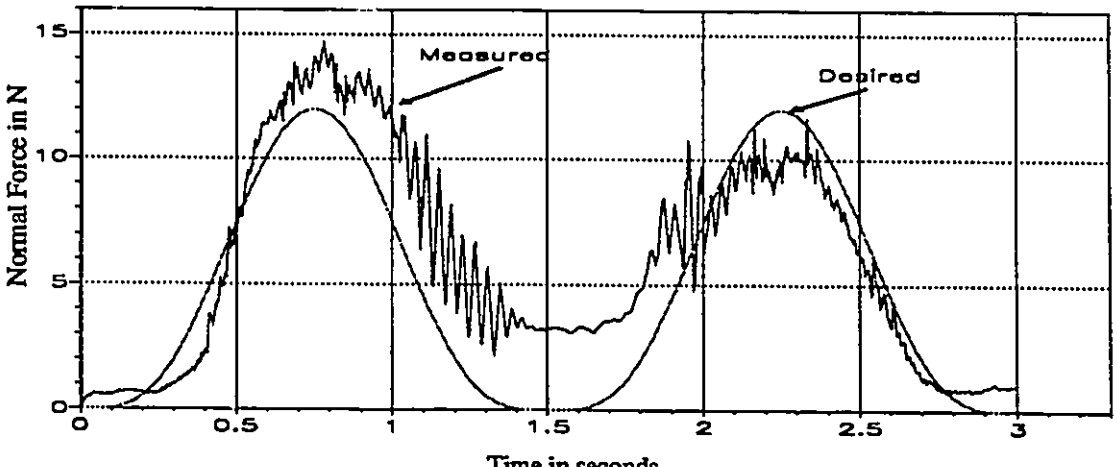

Fig. 7.6 Force trajectory tracking for the robust sliding mode controller (experimental)

7.3 ADAPTIVE CASCADE CONTROL

This section describes the design of an adaptive cascade controller for flexible joint robot manipulators to achieve position and force tracking in the presence of parametric uncertainty. A strategy based on cascade control is presented combining a direct adaptive control scheme for the link control with a Model Reference Adaptive Control (MRAC) for the joints. Simulation and experimental results are presented.

7.3.1 Basic Concept

The basic idea of the cascade control in order to achieve tracking can be described as follows. Given a system of the form [116]

$$\dot{x}_1 = f_1(x_1, x_2, t) \qquad (7.3.1)$$
$$\dot{x}_2 = f_2(x_1, x_2, t) + B_2(x_1, x_2, t)U \qquad (7.3.2)$$

where vector x_1 is required to track a desired trajectory $x_1{}^d(t)$. The cascade control design regards the vector x_2 as a control variable for the subsystem 7.3.1 and, as such, a desired function $x_2{}^d(t)$ to be designed is assumed to exist in order to achieve the tracking goal. Then the control input U is designed so that x_2 tracks $x_2{}^d(t)$. Thus, this allows x_1 to track the desired trajectory $x_1{}^d(t)$. It can be seen, as in section 7.3.2, that a flexible joint robot manipulator has identical structure to the system described in equations 7.3.1 and 7.3.2. A flexible joint robot manipulator model can be decomposed into two subsystems; the links subsystem and the motors subsystem. An adaptive controller can be designed for the links subsystem with the objective of having the end–point to track some position and force trajectories by using the motor angular position as the control variable. Then, a Model Reference Adaptive Controller (MRAC) is designed for the motors subsystem with the objective of forcing the motor to track the designed angular position obtained from the links subsystem adaptive controller, despite the disturbance caused by the inaccuracy of the motors subsystem parameters.

Hsu and Guanther [44] proposed cascade control for position control of flexible joint robots in the joint space. For the link subsystem, they suggested using Slotine and Li's adaptive algorithm [102], then they proposed two variable structure controllers for the motors subsystem. In the cascade controller presented here, a direct adaptive controller, as that developed by Craig [17], is proposed for the links subsystem. The reason for adopting Craig's algorithm, rather than Slotine and Li's, is that the latter requires very high control activity which, even with the boundary layer design, makes it more difficult for the motors subsystem controller to track the designed angular position. For the motors subsystem, a Model Reference Adaptive Controller (MRAC) meets the necessary conditions for implementation over the variable structure control as the variable structure controller requires not only the desired angular position but also the angular velocity, which is not available. On the other hand, Model Reference Adaptive Control (MRAC) can be designed to achieve good performance with only the designed angular position given as the reference trajectory.

7.3.2 Design of the Adaptive Cascade Controller

Consider the model of an n–link flexible joint robot manipulator, similar to that of the experimental two–link flexible joint manipulator, given by:

$$D(q)\,\ddot{q} + C(q,\dot{q}) + B_l\,\dot{q} - K(q_m - q) = -J^T F \qquad (7.3.3)$$

$$I_m\,\ddot{q_m} + B_m\,\dot{q_m} + F_c + K(q_m - q) = \tau \qquad (7.3.4)$$

By inspecting the model given by the above equations, it becomes clear that the link dynamics 7.3.3 and the motor dynamics 7.3.4 are statically coupled by the elastic torques $\tau_e = K(q_m - q)$. The vector τ_e represents the torque transmitted between links and motors. Thus, one can write the link dynamics as:

$$D(q)\,\ddot{q} + C(q,\dot{q}) + B_l\,\dot{q} = -J^T F + \tau_e \qquad (7.3.5)$$

and so the system given by equations 7.3.5 and 7.3.4 is of the form 7.3.1 and 7.3.2. Thus, following the cascade control approach one can define τ_e as the elastic torque required to

achieve stable tracking of the position and force trajectories of the end–point. Once τ_e has been designed, the desired motors angular positions can be obtained as:

$$q_m{}^d = K^{-1}\tau_e + q \qquad (7.3.6)$$

Next, the motor tracking error vector is defined as $\tilde{q}_m = q_m - q_m{}^d$, thus the links subsystem equation can be written as:

$$D(q)\,\ddot{q} + C(q,\dot{q}) + B_l\,\dot{q} = -J^T F + K\,\tilde{q}_m + \tau_e \qquad (7.3.7)$$

The term $K\,\tilde{q}_m$ is considered as a disturbance acting on the link dynamics system since the exact elastic torque cannot be generated. In summary, the overall system of a flexible joint robot is described by equations 7.3.7 and 7.3.4. Control τ_e is designed according to Craig's algorithm for rigid robots, for the system given by equation 7.3.7, while a Model Reference Adaptive Control (MRAC) scheme, based on the development by Landau [63] and Stoten [109], is applied for motors given by equation 7.3.4. The cascade controller structure can be illustrated as in figure 7.7. As shown in the structure of the cascade controller, a low–pass

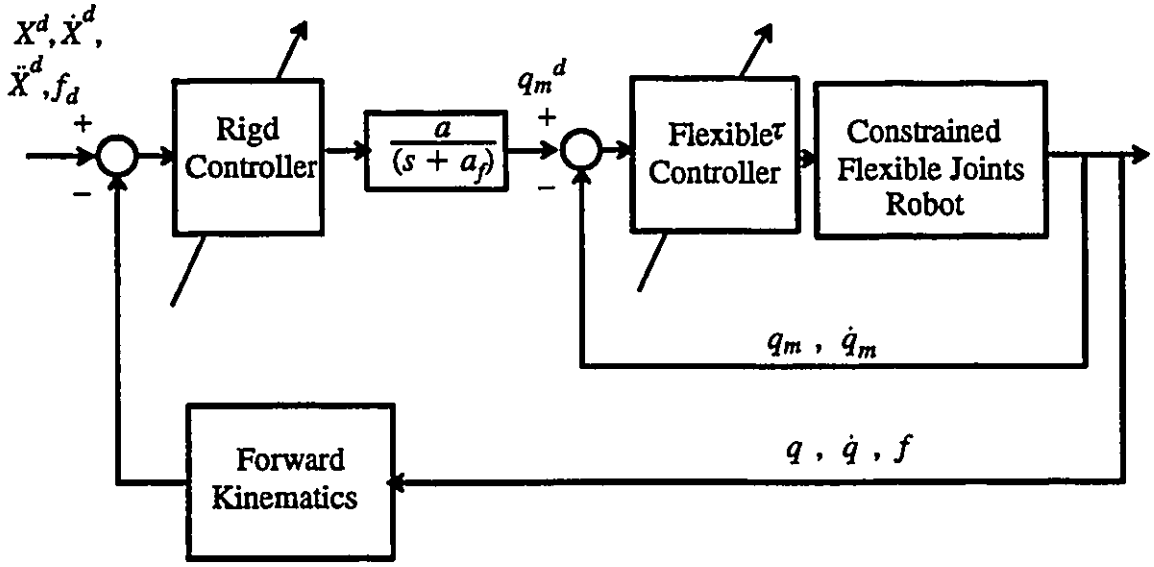

Fig. 7.7 The Cascade controller for the flexible joint robot

first order filter is introduced between the rigid and the flexible controllers. The purpose of

incorporating the low–pass filter is to remove undesirable noise, while estimating the desired angular position vector, from propagation in the flexible controller. The low–pass filter is included in the experimentation but not in the simulation.

7.3.2.1 Adaptive Dynamic Hybrid Control of the Link Dynamics

In this section, the design of a direct adaptive controller for the link subsystem is described. The contact with a rigid environment as described in sections 6.2.2 and 6.2.3 is considered. The object is to design the control inputs, τ_e in this case, in order that the end–point tracks the desired position and force trajectories in the presence of parametric uncertainty in the link dynamics. Given equation 7.3.7 of the link subsystem, the link angular acceleration and the contact force are transformed into the constraint frame. The resulting decoupled model is given by:

$$D(q)\, J^{-1}[\, R^{-1}(\, \ddot{X}_t - \dot{R}\, \dot{X}\,) - \dot{J}\, \dot{q}] + C(q,\dot{q}) + B_l\, \dot{q} + J^T L f = \tau_e \quad (7.3.8)$$

Next, the linear parametrization property for the link subsystem is utilized. This property states that the parameters of the link subsystem appear linearly in the link dynamics. Thus:

$$\tilde{D}(q)\, J^{-1}[\, R^{-1}(\, \ddot{X}_t - \dot{R}\, \dot{X}\,) - \dot{J}\, \dot{q}] + \tilde{C}(q,\dot{q}) + \tilde{B}_l\, \dot{q} = \psi_l \tilde{\Theta}_l \qquad (7.3.9)$$

where $\phi_l \in R^{n \times r}$ is a matrix of known functions called the regressor matrix, and $\Theta_l \in R^r$ is a vector of the link subsystem parameters (see section 7.4.3). The terms with the tilde bar represents the difference between the true and estimated values for considered terms as follows:

$$\begin{aligned}
\tilde{D}(q) &= D(q) - \hat{D}(q) \\
\tilde{C}(q,\dot{q}) &= C(q,\dot{q}) - \hat{C}(q,\dot{q}) \\
\tilde{B}_l &= B_l - \hat{B}_l \\
\tilde{\Theta}_l &= \Theta_l - \hat{\Theta}_l
\end{aligned} \qquad (7.3.10)$$

A computed torque control term for the position subsystem and a PI control term for the force subsystem are proposed, thus the control law for the link subsystem is given by:

$$\tau_e = \hat{D}(q)\, J^{-1}[\, R^{-1}(\, \ddot{X}_t^{*} - \dot{R}\, \dot{X}\,) - \dot{J}\, \dot{q}] + J^T L f^{*} + \hat{C}(q,\dot{q}) + \hat{B}_l\, \dot{q} \quad (7.3.11)$$

where $\ddot{X}^{*}_{t} = \begin{bmatrix} \ddot{P}^{*} \\ 0 \end{bmatrix}$, $\ddot{P}^{*}$ $(6-m)$ x 1 vector of new input to the position subsystem and f^{*} is m x 1 vector of new inputs to the force subsystem. The outer loop inputs are designed as follows:

$$\ddot{P}^{*} = \ddot{P}^{d} + K_{p1}(\dot{P}^{d} - \dot{P}) + K_{p0}(P^{d} - P) \quad (7.3.12)$$

$$f^{*} = K_{fp} f^{d} + K_{fI} \int_0^t (f^{d} - f) \quad (7.3.13)$$

where K_{p0} and K_{p1} are $(6-m)$x$(6-m)$ constant positive diagonal matrices and K_{fI0} and K_{fP} are mxm constant positive diagonal matrices. The application of the control law given by equation 7.3.11 with the outer loop designed as in equations 7.3.13 and 7.3.14 on the link dynamics given by equation 7.3.8 with the linear parametrization model given by equation 7.3.9 results in the following error dynamics:

$$\hat{H}_l\,(q) \begin{bmatrix} \ddot{e}_p + K_{p1}\dot{e}_p + K_{p0}e_p \\ K_{fP}\, e_f + K_{fI} \int_0^t e_f dr \end{bmatrix} = \psi_l\, \bar{\Theta}_l \quad (7.3.14)$$

where $H_l(q)$ is a new matrix, the first $6-m$ columns are the first $6-m$ columns of the matrix $D(q)\; J^{-1}\; R^{-1}$ and the other m columns are the matrix $N\; J^T\; L$. The error dynamics can be written in the following state space form:

$$\dot{Z}_r = A_r\, Z_r + B_r\, \phi_l\, \bar{\Theta}_l \quad (7.3.15)$$

where

$$Z = [z_{r1}\; z_{r2}\; z_{r3}]^T \equiv \left[e_p\; \dot{e}_p \int_0^t e_f dr \right]^T$$

$$\text{and} \quad A_r = \begin{bmatrix} 0 & I & 0 \\ -K_{p0} & -K_{p1} & 0 \\ 0 & 0 & -K_{fP}^{-1} K_{fI} \end{bmatrix} \quad B_1 = \begin{bmatrix} 0 & I_p \\ I_p & 0 \\ 0 & K_{fP}^{-1} \end{bmatrix} \quad \phi_l = \hat{H}_l^{-1}(q)$$

Next, an adaptation law is designed for the link dynamics to ensure the global stability of the system given by equation 7.3.16 using Lyapunov stability criterion. Choose the following Lyapunov function candidate:

$$V_l = Z_l^T P_l Z_l + \tilde{\Theta}_l^T \Gamma^{-1} \tilde{\Theta}_l \qquad (7.3.16)$$

where P_l is a symmetric positive definite solution of the Lyapunov equation:

$$A_l^T P_l + P_l A_l = -Q_l \qquad (7.3.17)$$

Γ is a symmetric and positive definite gain matrix and Q_l is a positive definite matrix. Then, the time derivative of V_l along the trajectories of the system 7.3.16 is given by:

$$\dot{V}_l = -Z_l^T Q_l Z_l + 2\,\tilde{\Theta}^T [\phi_l^T B_1^T Z^l + \Gamma_l \dot{\Theta}_l] \qquad (7.3.18)$$

Inspecting the above expression for $\dot{V}_l$ suggests that one should choose a parameter updating law which makes the second term zero, namely:

$$\dot{\tilde{\Theta}}_l = -\Gamma \psi_l^T B_1^T P_l Z_l \qquad (7.3.19)$$

Since the parameters vector Θ_l is constant then $\dot{\tilde{\Theta}}_l = \dot{\hat{\Theta}}_l$. Thus the parameter update law is given by:

$$\dot{\hat{\Theta}}_l = -\Gamma \psi_l^T B_1^T P_l Z_l \qquad (7.3.20)$$

The above choice of the adaptation law results in the following:

$$\dot{V}_l = -Z_l^T Q_l Z_l \leq 0 \qquad (7.3.21)$$

Therefore, the system is stable and the state Z_l converges to zero. Since Z_l is a vector of the

position, velocity, and force tracking errors, its convergence to zero implies directly that these tracking errors converge to zero as the time approaches infinity.

To ensure that the matrix $\hat{H}_l(q)$ is non–singular, one has to restrict each of the estimated parameters to lie between some upper and lower bounds by augmenting the update law 7.3.20 with the following reset conditions:

$$\begin{aligned} \hat{\Theta}_{li} &= \Theta_{li\max} \qquad \text{if} \quad \hat{\Theta}_{li} \geq \Theta_{li\max} \\ \hat{\Theta}_{li} &= \Theta_{li\min} \qquad \text{if} \quad \hat{\Theta}_{li} \leq \Theta_{li\min} \end{aligned} \tag{7.3.22}$$

where $\Theta_{li\max}$ and $\Theta_{li\min}$ are the upper and lower bounds of the parameter Θ_{li}, respectively. Since the regression matrix ψ_l depends on the angular acceleration which is not measured in our case, the technique used by many researchers regarding the implementation of the adaptive computed torque is adopted. The angular accelerations are estimated from the velocity signals using the following first order filter:

$$\ddot{q}_l = \frac{s}{\tau_a s + 1}\, \dot{q}_l \tag{7.3.23}$$

where s is the Laplace transformation operator and τ_a is the filter time constant. By choosing τ_a to be very small, the following approximation can be made:

$$\ddot{q}_{lc} \approx s\, \dot{q}_l \approx \ddot{q}_l \tag{7.3.24}$$

7.3.2.2 Model Reference Adaptive Control of the Motors

In this section, a MRAC is designed for the motor subsystem. The objective is to have the motors track the desired angular position vector which is obtained from the direct adaptive control of the link subsystem, in the presence of parametric uncertainty in the motors dynamics.

First, the motors subsystem is transformed to the following state space form:

$$\dot{x}_p = A_p\, x_p + B_p\, \tau + \mathfrak{D}(t) \qquad (7.3.25)$$
$$y_p = C_p\, x_p \qquad (7.3.26)$$

where $x_p = \left[x_{p1} \;\; x_{p2}\right]^T = [\; q_m \;\; \dot{q}_m \;]^T$

$$A_1 = \begin{bmatrix} 0 & I \\ -I_m^{-1} K & -I_m^{-1} B_m \end{bmatrix} \qquad B_1 = \begin{bmatrix} 0 \\ -I_m^{-1} \end{bmatrix} \qquad C_p = I$$

and $\mathfrak{D}(t)$ is a disturbance vector acting on the system. This disturbance combines the effects of inaccurate plant parameters and, of special significance is the Coulomb friction vector. The following standard linear state feedback control law is designed:

$$\tau = -K_g\, x_p + K_{gr}\, r \qquad (7.3.27)$$

where $r \in R^n$ is the reference input (the desired motor angular position vector). When the linear control law of equation 7.3.27 is applied to the system given by equation 7.3.25 the following closed loop results:

$$\dot{x}_p = (\, A_p - B_p\, K_g \,)\, x_p + B_p\, K_{gr}\, r + \mathfrak{D}(t) \qquad (7.3.28)$$

A reference model of the same dimensions as the system given by equations 7.3.25 and 7.3.26 is chosen. The reference model is given by:

$$\dot{x}_m = A_m\, x_m + B_m\, r \qquad (7.3.29)$$
$$y_m = C_m\, x_m \qquad (7.3.30)$$

Subtracting the controlled system, equation 7.3.28, from the reference model, equation 7.3.25, results in the following error equation:

$$\dot{x}_e = A_m\, x_e + (\, A_m - A_p + B_p\, K_g \,)\, x_p + (\, B_m - B_p\, K_{gr} \,) + \mathfrak{D}(t) \qquad (7.3.31)$$

Inspecting the above equation, it is clear that if the three terms are zero, i.e.

$$A_m - A_p + B_p\, K_g = 0 \qquad (7.3.32)$$
$$B_m - B_p\, K_{gr} = 0 \qquad (7.3.33)$$

and $\mathfrak{D}(t) = 0$ then the error equation reduces to:

$$\dot{x}_e = A_m\, x_e \qquad (7.3.34)$$

which implies that the vector x_e converges to zero as the time approaches infinity. As a result, the plant output tracks the reference model output. Equations 7.3.32 and 7.3.33 can be satisfied by solving for the gain matrices to yield:

$$K_g = B_p{}^{+} (A_m - A_p) \qquad (7.3.35)$$
$$K_{gr} = B_p{}^{+} B_m \qquad (7.3.36)$$

where $B_p{}^{+} = (B_p{}^T B_p)^{-1} B_p{}^T$ is the pseudo inverse of B_p. Evaluation of conditions 7.3.32 and 7.3.33 according to 7.3.35 and 7.3.36 results in:

$$(I - B_p B_p{}^{+}) (A_m - A_p) = 0 \qquad (7.3.37)$$
$$(I - B_p B_p{}^{+}) B_m = 0 \qquad (7.3.38)$$

Landau [63] defines the above two equations as Ezberger's conditions.

The choice of the reference model proceeds as follows. First, A_m is designed to be the closed loop system matrix. Specific characteristics can assigned to the closed loop system using pole placement method. Second, B_m is designed based on the desired steady state properties, i.e. $\dot{x}_m \Rightarrow 0$ as the time approaches infinity. Thus:

$$\bar{x}_e = - A_m{}^{-1} B_m \bar{r} \qquad (7.3.39)$$

where the over bar denotes the steady state vectors. As a result, the steady state output of the system is given by:

$$\bar{y} = - C A_m{}^{-1} B_m \bar{r} \qquad (7.3.40)$$

which leads to the following expression for the reference model input matrix:

$$B_m = - A_m C^{+} \qquad (7.3.41)$$

Next, to ensure the stability of the system in the presence of the disturbance caused by parametric uncertainty, an adaptation loop is introduced and designed. The linear control law given by equation 7.3.27 is modified to be:

$$\tau = - (K_g + \delta K_g) x_p + (K_{gr} + \delta K_{gr}) r \qquad (7.3.42)$$

where δK_g and δK_{gr} are two adaptive gain matrices of the same dimensions as K_g and K_{gr}. The objective is to design the adaptive gain matrices δK_g and δK_{gr} such that the system, motor subsystem, follows the reference model in the presence of disturbance $\mathcal{D}(t)$ caused by parametric uncertainty. The design of the adaptive loop is formulated based on the development by Landau [63] and the application to rigid robots joint tracking by Stoten [109]. The design is based on the hyperstability principle by Popov [86]. One can include the disturbance in the error dynamics given in equation 7.3.34 together with the modified control law to yield:

$$\dot{x}_e = A_m\, x_e + \mathcal{D}(t) - B_p\, (\, \delta K_g\, x + \delta K_{gr}\, r\,) \qquad (7.3.43)$$

Let:

$$\mathcal{W}(t) = \delta K_g\, x + \delta K_{gr}\, r \qquad (7.3.44)$$

Thus, the error dynamics is reduced to:

$$\dot{x}_e = A_m\, x_e + \mathcal{D}(t) - B_p\, \mathcal{W}(t) \qquad (7.3.45)$$

Then, the following error output vector y_e is introduced:

$$y_e = C_e\, x_e \qquad (7.3.46)$$

Thus, the complete closed loop error dynamics can be represented by the following figure

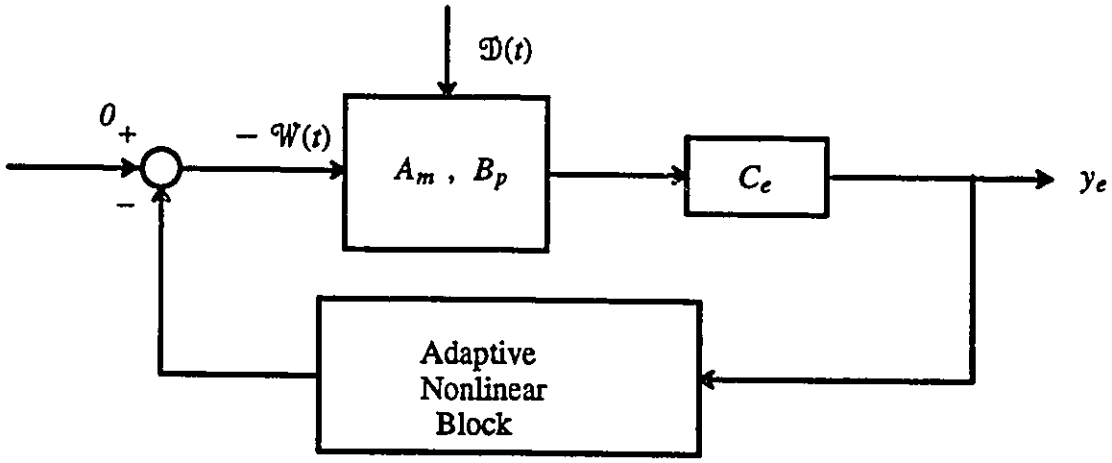

Fig. 7.8 Nonlinear system (The Hyperstability problem)

It is clear that the error dynamics are represented by the linear forward block described by

$\{A_m\ ,\ B_p\ ,\ C_e\}$ and the nonlinear adaptive feedback block. Popov [86] studied such a system and one of the main conclusions is that if $\{A_m\ ,\ B_p\ ,\ C_e\}$ is a hyperstable block and the adaptive block is synthesized to satisfy the following inequality:

$$\int_{t0}^{t1} y_e^T(t)\ \mathcal{W}(t)\ dt\ \geq\ -\gamma^2 \qquad ,\ \forall\ \ t_1 \geq t_0 \tag{7.3.47}$$

Then x_e asymptotically converges to zero. The hyperstability problem is solved by an effective choice of the C_e. First, find the solution of the following Lyapunov equation:

$$A_m^T\ P_2 + P_2\ A_m = -\ Q_m \tag{7.3.48}$$

where Q_m is a positive definite matrix, then construct C_e as:

$$C_e = B_p{}^T\ P_2 \tag{7.3.49}$$

Landau [63] presented a solution to satisfy Popov's inequality by updating the adaptive gain matrices δK_g and δK_{gr} according to the following PI implementation:

$$\delta K_g = \int_0^t \alpha_g\ y_e(t)\ x_p{}^T(t)\ dt\ + \beta_g\ y_e(t)\ x_p{}^T(t) \tag{7.3.50}$$

$$\delta K_{gr} = \int_0^t \alpha_{gr}\ y_e(t)\ r^T(t)\ dt\ + \beta_{gr}\ y_e(t)\ r^T(t) \tag{7.3.51}$$

where $\alpha_g\ ,\ \alpha_{gr}\ ,\beta_g$ and β_{gr} are positive constant scalar parameters.

7.3.2.3 Stability of the Connected System

The overall controlled system is represented by equations 7.3.15 and 7.3.45. The system is stable if $\dot{Z}_l \Rightarrow 0$ and $\dot{x}_e \Rightarrow 0$ as $t \Rightarrow \infty$. The stability problem is simplified if the disturbance term $K\ \tilde{q}_m$ acting on the link subsystem is bounded. Thus, proceeding with the motor subsystem, the control law given by 7.3.42 with adaptation algorithm given by equations 7.50 and 7.3.51 ensures that the motor subsystem follows the reference model i.e. $\dot{x}_e \Rightarrow 0$ as $t \Rightarrow \infty$. Finally, given that the disturbance $K\ \tilde{q}_m$, acting on the links subsystem

is uniformly bounded together with the link subsystem control law given by equation 7.3.11 and adaptation law 7.3.20, ensures that the $\dot{Z}_l \Rightarrow 0$ as $t \Rightarrow \infty$. This directly implies that the end–point tracks the desired position and force trajectories.

7.3.3 Simulation Results

Figures 7.9 to 7.14 show the simulation results of the adaptive cascade controller. The task used in the simulation is the same as that used in the dynamic hybrid controller case. Parametric uncertainty is introduced in the inertia matrix of the rigid dynamics subsystem as described in the robust controller section simulation. Nominal model parameters obtained from the frequency response identification were used to design the reference model. For the rigid dynamics, the control law is defined by $\omega_p = 25.0, \omega_{fp} = 10.0$, $\omega_{ff} = 1000.0$, and $\zeta_p = \zeta_f = 1.0$. The reference model is chosen to be the nominal model under the linear controller. The gain matrices are designed by using the pole placement technique, and the closed loop poles for the reference model are [–50,–60,–50,–60].

Figures 7.9 to 7.11 show plots of the position, velocity, and force tracking errors, verifying that the rigid dynamics controller managed to achieve position and force tracking in the presence of the introduced parametric uncertainty. Figure 7.12 shows the update history of the inertia parameters indicating that the estimated parameters approach their true values. Figure 7.13 shows plots of the angular position tracking errors which indicate that the motor subsystem under the MRAC accurately tracked the desired angular position vector generated by the the rigid dynamics adaptive controller. Finally, figure 7.14 shows how accurately the plant output (motors angular positions) followed the reference model output.

7.3.4 Experimental Results

The adaptive cascade controller was implemented on the experimental flexible joint adaptive controller at a sampling frequency of 500 Hz. Parametric uncertainty was

introduced in the rigid dynamics by adding the C–shape steel block as described in the robust sliding mode controller experiment section. The task is similar to that used in the dynamic hybrid controller except that the controller is applied only in the first path (1.5 seconds trajectory from point A to point B in figure 6.1). The rigid dynamics controller is defined by $\omega_p = 15.0$, $\omega_{fp} = 1.0$, $\omega_{fl} = 750.0$ and $\zeta_p = \zeta_f = 1.0$. The reference model is chosen to be the nominal motors subsystem under a Linear Quadratic Regulator. This design allowed more flexibility by specifying the weight matrices which resulted in a better experimental performance than that obtained by only placing the closed loop poles.

Experiments showed that the adaptive cascade control is stable for a wide range of the reference model closed loop poles and succeeded in tracking the desired position and force trajectories. However, there is a limitation on the rigid dynamics controller bandwidth imposed by the motors tracking and stability performances. This limitation was anticipated since by increasing the position and force bandwidth, generating a faster desired trajectory vector is implied , which, in turn, makes the task of the motors subsystem controller more difficult. Perfect tracking of the end–point position and force trajectories can be achieved in principle, only if the motors subsystem controller tracking error is zero. This is impossible since the input torque controlling the rigid dynamics is generated through the second order system of the motors. Figures 7.15 to 7.19 show plots of one experiment. The force trajectory tracking is acceptable. However, position tracking is not as good as that obtained using feedback linearization controllers. It is clear that this position tracking performance is a result of applying a slow position controller. Increasing the position controller bandwidth beyond $\omega_p = 15.0$ resulted in instability. Figure 7.17 shows the inertia parameters update. The estimated parameters are approaching their true values. Figure 7.18 and 7.19 indicate that the MRAC succeeded in accurately tracking the desired angular position.

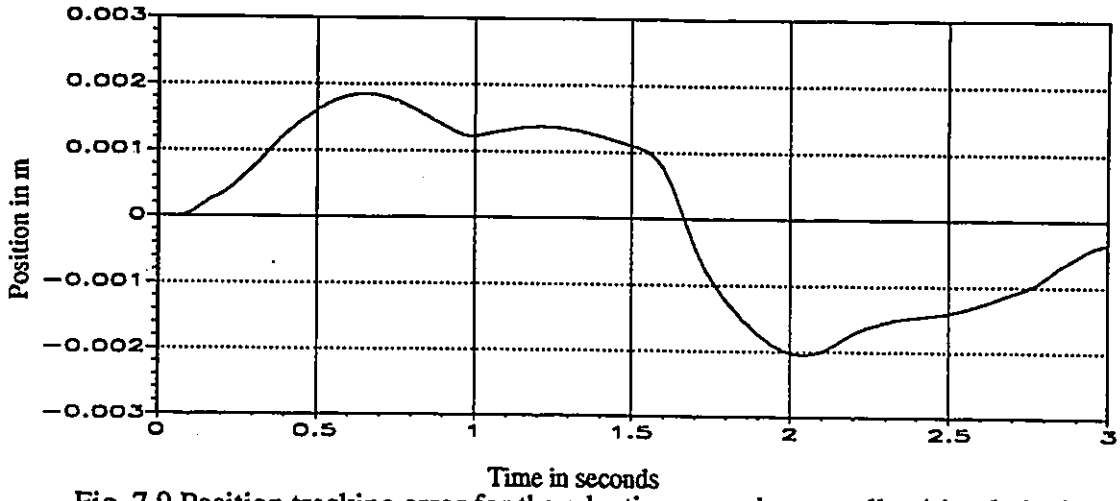

Fig. 7.9 Position tracking error for the adaptive cascade controller (simulation)

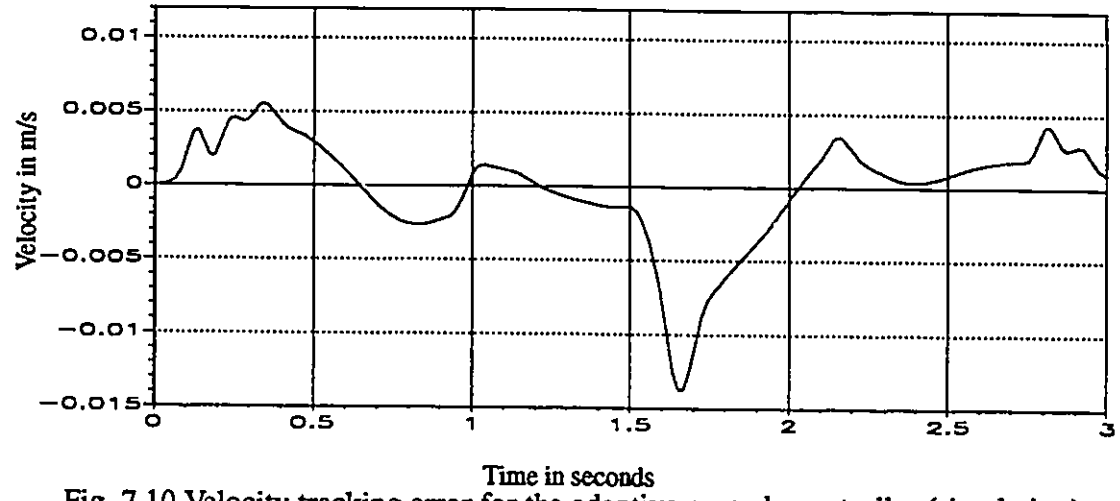

Fig. 7.10 Velocity tracking error for the adaptive cascade controller (simulation)

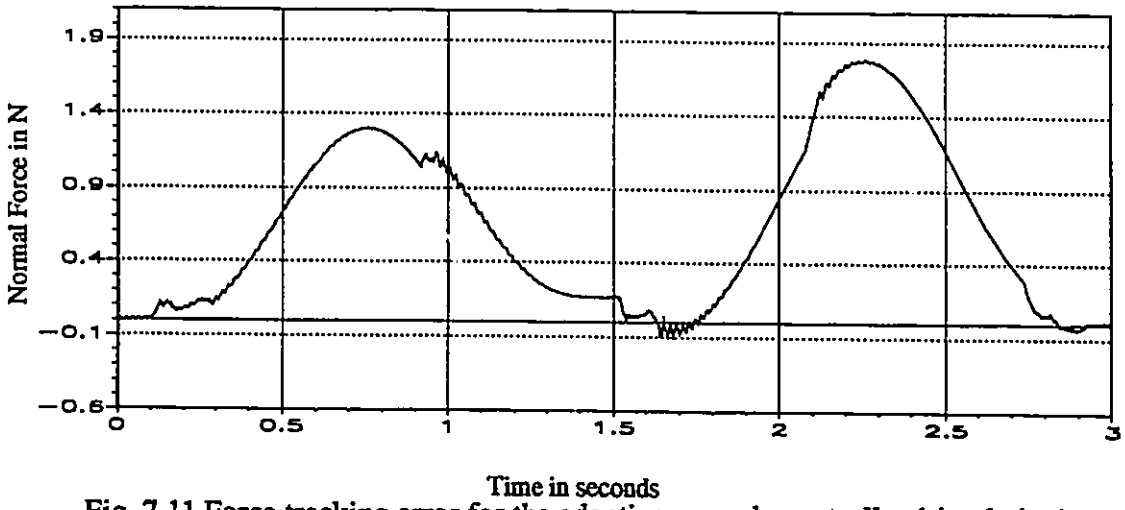

Fig. 7.11 Force tracking error for the adaptive cascade controller (simulation)

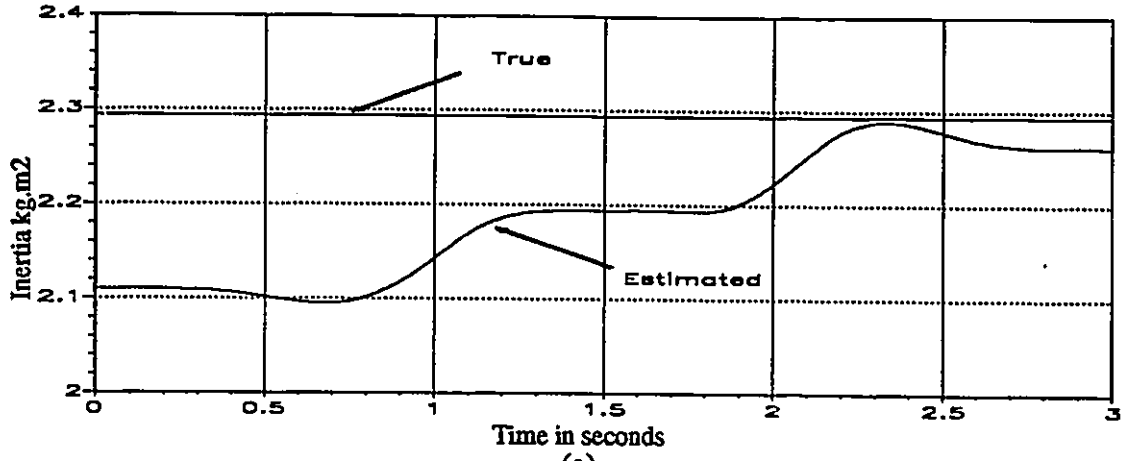

(a)

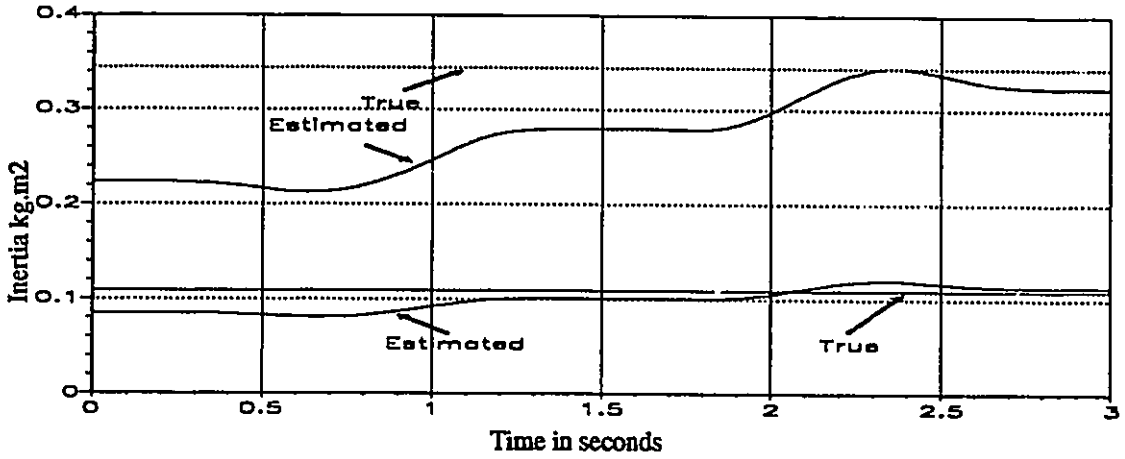

(a)

Fig. 7.12 Parameter estimation for the adaptive cascade controller (simulation)
(a) First parameter (b) Second and Third parameters

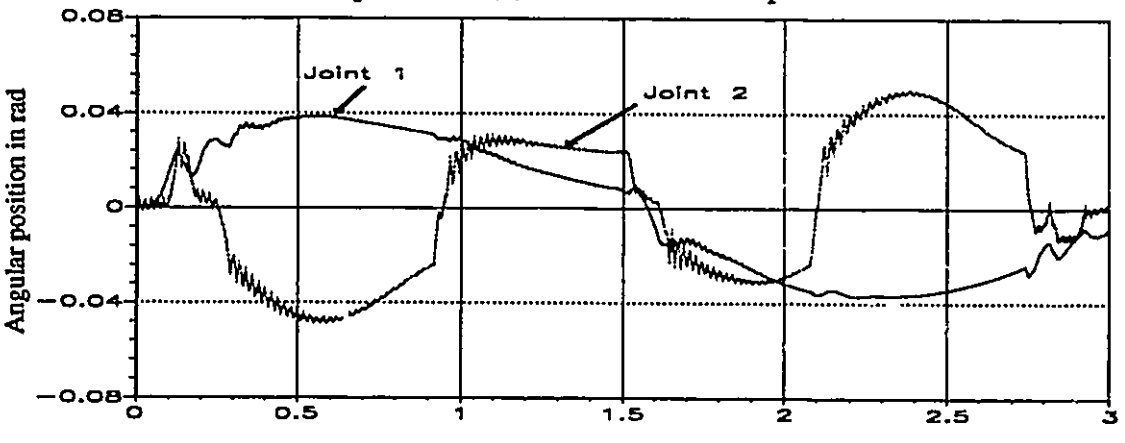

Fig. 7.13 Angular position tracking error for the adaptive cascade controller (simulation)

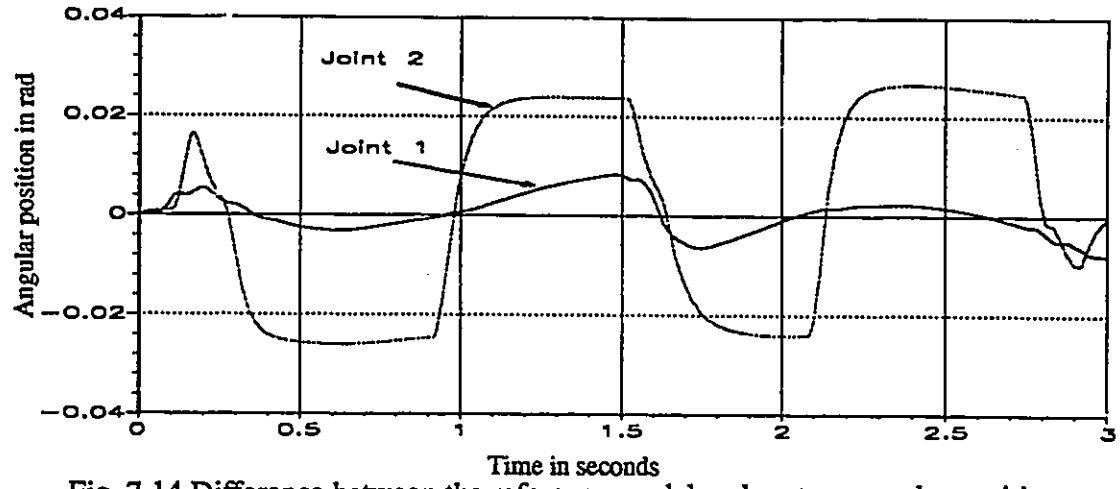

Fig. 7.14 Difference between the reference model and motors angular positions for the adaptive cascade controller (simulation)

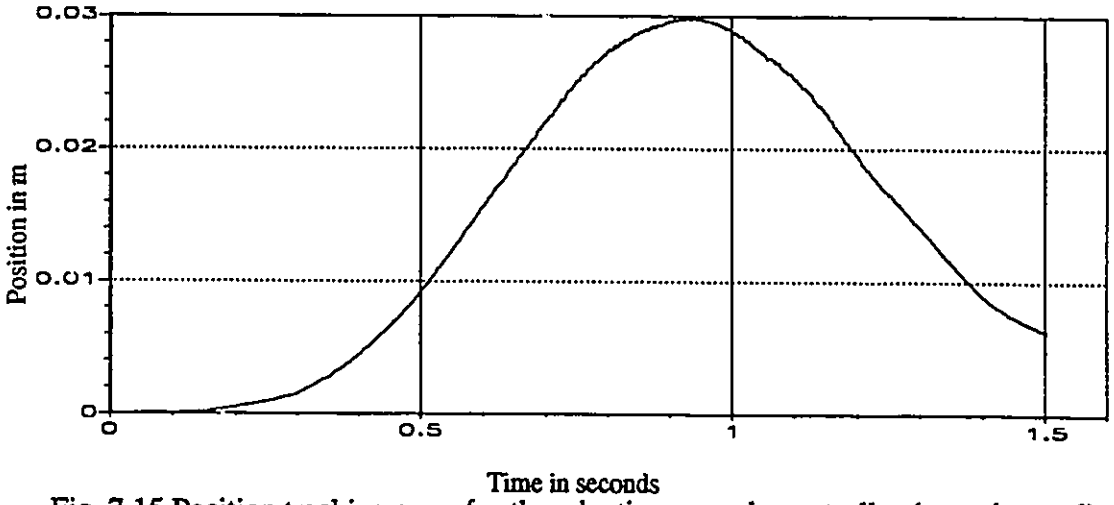

Fig. 7.15 Position tracking error for the adaptive cascade controller (experimental)

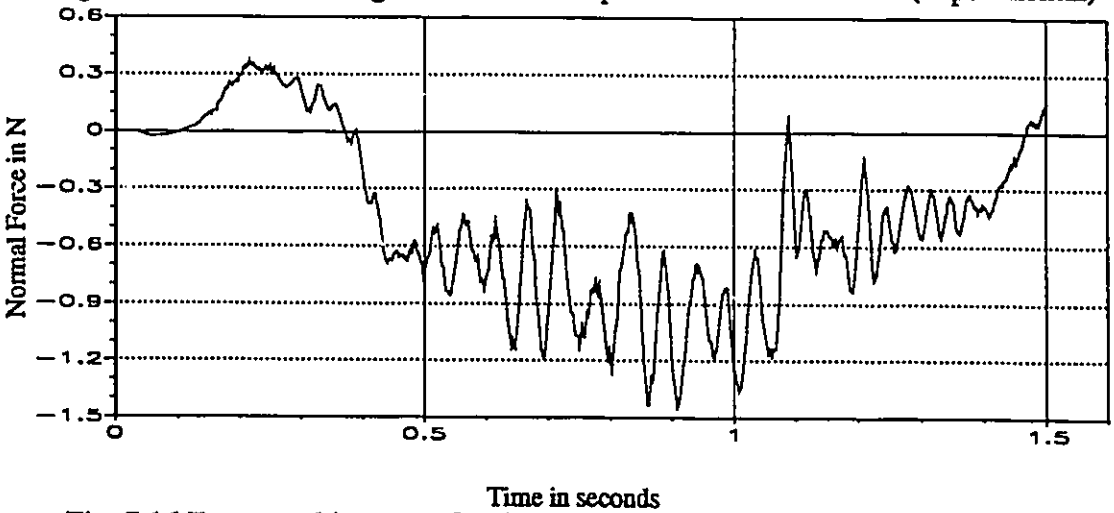

Fig. 7.16 Force tracking error for the adaptive cascade controller (experimental)

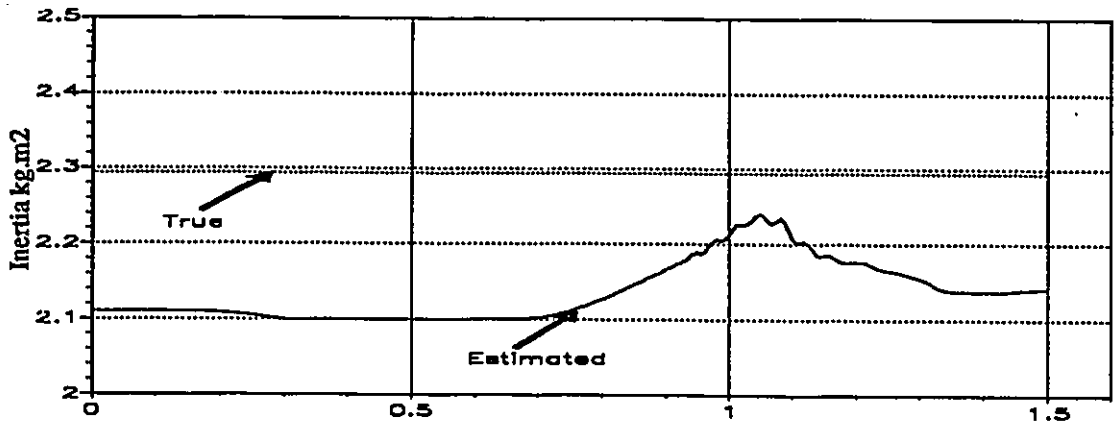

(a)

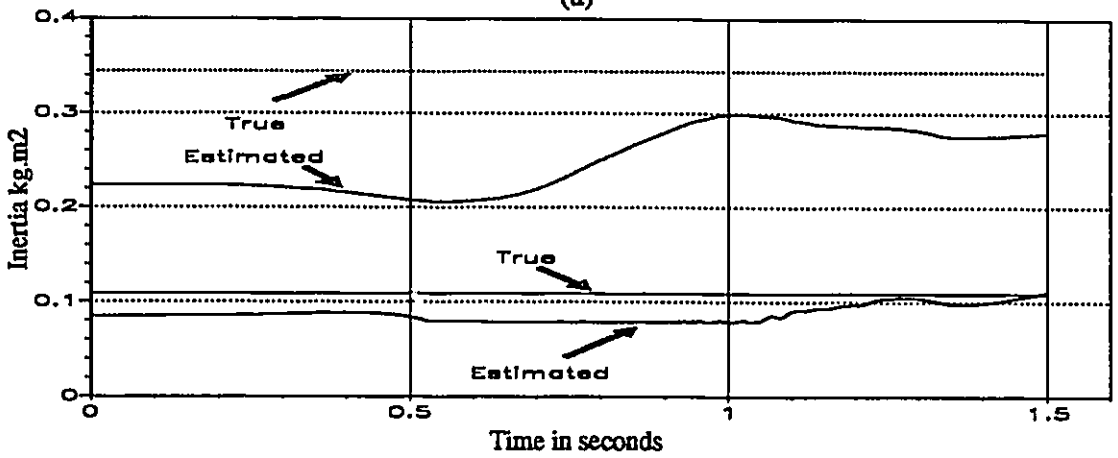

(b)

Fig. 7.17 Parameter estimation for the adaptive cascade controller (experimental)
(a) First parameter (b) Second and Third parameter

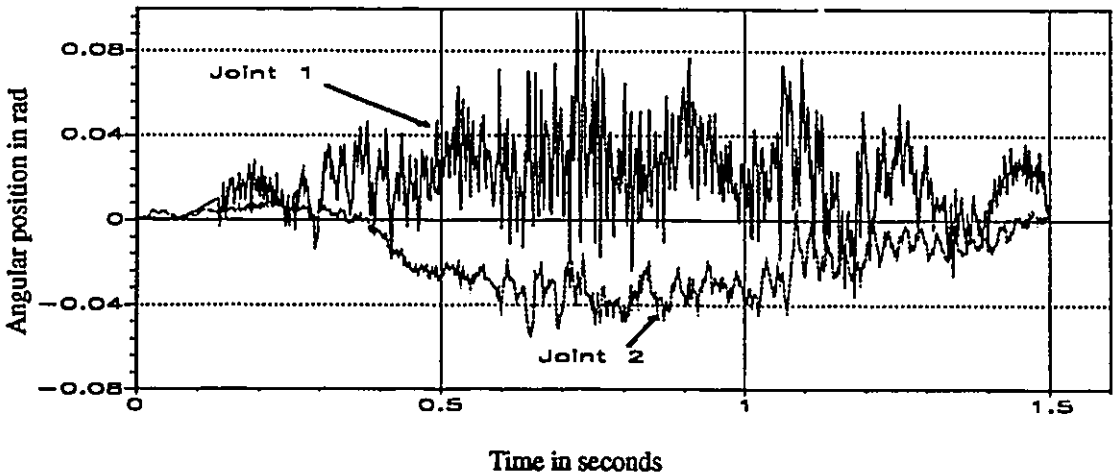

Fig. 7.18 Angular position tracking error for the adaptive cascade controller (experimental)

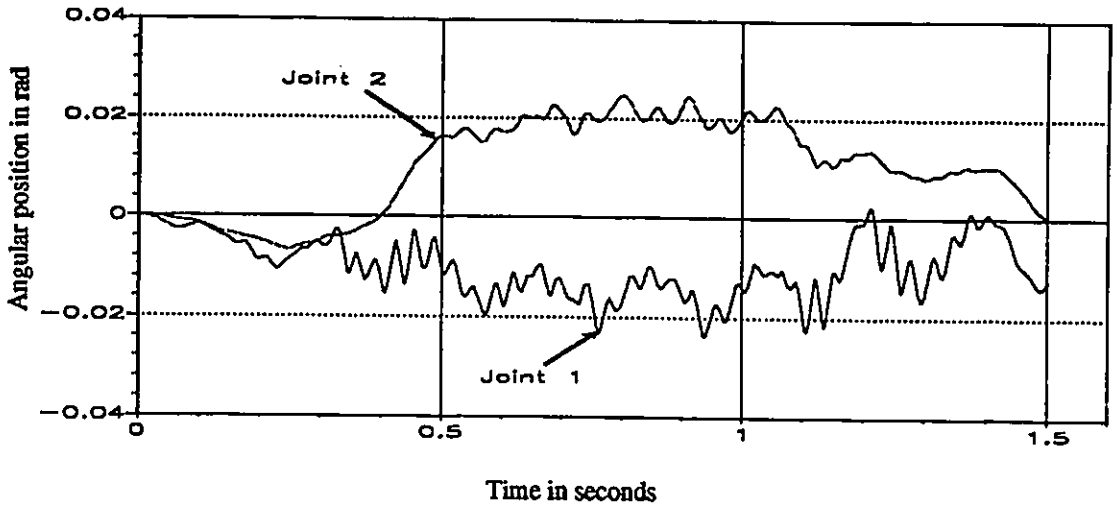

Fig. 7.19 Difference between the reference model and motors angular positions for the adaptive cascade controller (experimental)

7.4 ADAPTIVE FEEDBACK LINEARIZATION CONTROL

7.4.1 Basic Concept

The problem tackled in this section is position and force trajectories tracking taking into account parametric uncertainty and the estimation of the state for feedback. As discussed earlier, the flexible joint manipulator model is feedback linearizable by means of coordinate transformation and nonlinear feedback. Linear control techniques can then be used to specify a desired dynamic performance for the resultant linear system. Thus, there are two stages: 1) state transformation and nonlinear feedback to obtain the equivalent linear system in the inner loop, 2) linear controller design using linear state feedback to control the equivalent linear system. When the robot parameters are uncertain the exact linear system cannot be obtained. This leads to two fundamental approaches in order to control the system. First, using state transformation with the application of parameter adaptation in order to asymptotically linearize the system. There has been progress in the formulation of this problem for pure–feedback linearizable systems. Nam and Arapostathis [82] proposed a model reference adaptive scheme which requires a linear parametrization model for the feedback linearizable system. Sastry and Isidori [91] used input–output linearization assuming the linearities to be Lipschitz–continuous. An important issue in designing adaptive control algorithms for feedback linearizable systems is that both the state transformation and the control variables are functions of the system state and the uncertain parameters. Adaptive control algorithms of this class are very complex for practical implementations.

An alternative approach is to employ a robust observer for the feedback linearizable system. In relation to rigid robots, some advances have been made to include the effect of using a nonlinear observer to estimate the velocities used in the feedback. An approach for controlling rigid robot in the joint space using only joints position measurement was pres-

ented in [10]. The velocity used in the feedback is estimated using a sliding mode observer. A variable structure control algorithm was presented in [125] for controlling rigid robots in the joint space using a model–based observer for velocity estimate. Only [9] presented an adaptive control approach for joint tracking when the robot parameters are uncertain and a sliding observer is used. The parameter adaptation and state observation were performed simultaneously.

The adaptive control developed in this section is described as follows. First, a robust nonlinear sliding mode observer is designed for the feedback linearizable system. A linear parametrization model of the original system is constructed. A nonlinear feedback control law is then designed which uses the estimated state and parameters. The error dynamics were formulated in a way which includes constraint dynamics and allows the design of a parameter updating law. Finally, the coupling between the observer and the controller is considered. The conditions under which the overall closed loop system, composed of the robot, the observer, the controller and the adaptation law, is stable, are obtained. The structure of this adaptive controller is illustrated by figure 7.20.

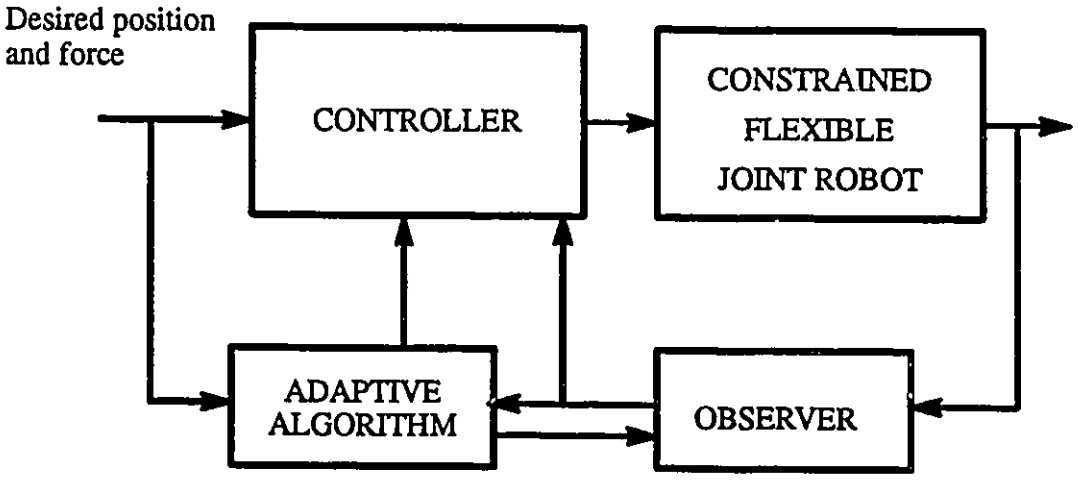

Fig. 7.20 Structure of the Adaptive Control Approach

7.4.2 Robust Nonlinear Sliding Mode Observer

In the model–based control, the links angular accelerations and jerks are computed from the dynamic model. When the robot parameters are uncertain , a sliding mode observer is proposed [100]. The sliding observer is based on the concept of the attractive manifold, which consists of defining a hyper surface (as a function of the observation errors) and determining the conditions such that the manifold is attractive. Once the error trajectories reach this hyper surface, a switching error based action makes the observation errors approach zero.

The fourth order system given by equation 5.3.13 can be decomposed and written in the following form:

$$\left.\begin{aligned} \dot{x}_1 &= C x_2 \\ \dot{x}_2 &= A_2\, x_2 + f_2(x_1, x_2) \\ y_1 &= x_1 \end{aligned}\right\} \qquad (7.4.1)$$

where

$$x_1 = q \quad , x_2 = [\, \dot{q} \;\; \ddot{q} \;\; \overset{3}{q} \,]^T$$

$$A_2 = \begin{bmatrix} 0 & I & 0 \\ 0 & 0 & I \\ 0 & 0 & 0 \end{bmatrix}, \quad C = [\, I \;\; 0 \;\; 0 \,]$$

$$f_2(x_1, x_2) = M(q)^{-1} \left(\tau - N(q)\, J^T \ddot{F} - h_p\, (q, \dot{q}, \ddot{q}, \overset{3}{q}) h_f(q, \dot{q}, \ddot{q}, F, \dot{F}) \right)$$

where the fact that the force and its derivatives are functions of the state $x = [x_1, x_2]^T$ has been used from equations 6.2.16 and 6.2.17. The nonlinear function $f_2(x_1, x_2)$ is continuous in x_2 and has a Lipschitz constant defined by the following inequality:

$$\| f_2(x_1, x_2) - f_2(x_1, \hat{x}_2) \| < \mu_x \| x_2 - \hat{x}_2 \| \qquad (7.4.2)$$

The observer is given by:

$$\left.\begin{aligned}\dot{\hat{x}}_1 &= C\hat{x}_2 - \Gamma_1\,\tilde{x}_1 - K_1\,sgn\,(\tilde{x}_1)\\ \dot{\hat{x}}_2 &= A_2\,\hat{x}_2 + f_2(\hat{x}_1,\hat{x}_2) - \Gamma_2\,\tilde{x}_1 - K_2\,sgn\,(\tilde{x}_1)\end{aligned}\right\} \qquad (7.4.3)$$

where

$$\begin{aligned}\tilde{x}_1 &= \hat{x}_1 - x_1\\ \tilde{x}_2 &= \hat{x}_2 - x_2\end{aligned}$$

where Γ_1, Γ_2, K_1, and K_2 are positive definite constant diagonal matrices, $\Gamma_1 = diag\,[\,\gamma^i{}_1]$, $\Gamma_2 = diag\,[\,\gamma^i{}_2]$, and $K_1 = diag\,[\,\lambda^i{}_2]$. This is different from the design in [100] in that the switching term gains are constant. The error equations can be obtained by subtracting the system given by equation 7.4.1 from the observer 7.4.3 and are given by:

$$\left.\begin{aligned}\dot{\tilde{x}}_1 &= C\tilde{x}_2 - \Gamma_1\,\tilde{x}_1 - K_1\,sgn\,(\tilde{x}_1)\\ \dot{\tilde{x}}_2 &= A_2\,\tilde{x}_2 + f_2(x_1,\hat{x}_2) - f_2(x_1,x_2) - \Gamma_2\,\tilde{x}_1 - K_2\,sgn\,(\tilde{x}_1)\end{aligned}\right\} \qquad (7.4.4)$$

The hyper plane $\tilde{x}_1$ is attractive within the following set:

$$\tilde{x}_2{}^i - \gamma_1{}^i\,\hat{x}_1{}^i - \lambda_1{}^i < 0\;;\;\tilde{x}_1{}^i > 0\;\forall\, i = 1,2\;..\,n$$
$$\tilde{x}_2{}^i - \gamma_1{}^i\,\hat{x}_1{}^i - \lambda_1{}^i > 0\;;\;\tilde{x}_1{}^i < 0\;\forall\, i = 1,2\;..\,n$$

Note that one can always start with $\hat{x}_1(0) = x_1(0)$, because the initial position is directly available from the encoder. Therefore at $t=0$, $\tilde{x}_1(0) = 0$ which when introduced in 7.4.4 gives sufficient conditions for the invariance of $\tilde{x}_1$ that is $\|\,\tilde{x}^i{}_2\,\| < \lambda^i{}_1$ for all $t > 0$. Thus, the equivalent dynamics on the reduced–order manifold is given by:

$$\dot{\tilde{x}}_2 = (A_2 - K_2\,K_1{}^{-1}\,C)\,\tilde{x}_2 + f_2(x_1,\hat{x}_2) - f_2(x_1,x_2) \qquad (7.4.5)$$

Choose the following Lyapunov function candidate: $V_2 = \tilde{x}_2{}^T\,P_2\,\tilde{x}_2$, where P_2 is positive definite symmetric matrix satisfying the Lyapunov equation:

$$(A_2 - K_2 K_1^{-1} C)^T P_2 + P_2 (A_2 - K_2 K_1^{-1} C) = - Q_2 \qquad (7.4.6)$$

where Q_2 is a positive definite symmetric matrix. The derivative of V_2 along the trajectories of 7.4.5 is given by:

$$\dot{V}_2 = \tilde{x}_2^T [(A_2 - K_2 K_1^{-1} C)^T P_2 + P_2 (A_2 - K_2 K_1^{-1} C)] \tilde{x}_2 + 2 \tilde{x}_2^T P_2 [f_2(x_1, \hat{x}_2) - f_2(x_1, x_2)] \qquad (7.4.4)$$

It can be seen using 7.4.2 that:

$$\dot{V}_2 \leq - \lambda_{\min}(Q_2) \| \tilde{x}_2 \|^2 + 2 \mu_x \lambda_{\max} (P_2) \| \tilde{x}_2 \|^2 \qquad (7.4.8)$$

where $\lambda_{\min}(Q_2)$ and $\lambda_{\max}(P_2)$ are the minimum and maximum eigenvalues of Q_2 and P_2, respectively. If $\lambda_{\min}(Q_2) > 2 \mu_x \lambda_{\max} (P_2)$, then $\dot{V}_2$ is negative definite and hence $\tilde{x}_2 \Rightarrow 0$ as $t \Rightarrow \infty$. Now, it is clear that the gain matrix K_2 can be designed to ensure the stability of the reduced–order manifold. The procedure developed by Raghavan and Hedrick [87] can be used to design K_2 to ensure the stability of the reduced–order manifold. The idea is to transform the stability condition to a condition on solving a Riccati equation.

7.4.3 Linear Parametrization Model

It is possible to construct a linear parametrization model for the links subsystem [1,59,60] and further used in [43,65]. In addition, a linear parametrization for the motor subsystem can be constructed. The models ar given by the following two equations:

$$\Psi_l \Theta_l + K(q - q_m) + J^T F = 0 \qquad (7.4.9)$$

$$\Psi_m \Theta_m - K(q - q_m) = \tau \qquad (7.4.10)$$

where Θ_l, Θ_m, Ψ_l, and Ψ_m are the links parameters vector, the motor parameters vector, a matrix which its elements are functions of the link position, velocity, and acceleration, and a matrix which its elements are functions of the motor velocity and acceleration. By inspecting the equations of motion, 5.3.7 and 5.3.8, or 7.4.9 and 7.4.10, one can see that each of the links and motors subsystems are coupled by the stiffness force due to joint flexibility. Recog-

nizing that this coupling force is internal, then the two subsystems can be combined by solving either of the two equations for the stiffness force vector and substituting into the other. Therefore, one can augment the two linear parametrization models together to yield one model that describes the flexible joint robot. This model is given by the following equation:

$$\Psi \Theta + J^T F = \tau \qquad (7.4.11)$$

where Θ is a vector of the links and motors parameters and Ψ is a regression matrix, which is a function of the links position, velocity, and accelerations, and the motors velocity, and acceleration. The link velocity and acceleration are obtained from the observer, while the motor velocity and acceleration can be obtained by numerical differentiation as proposed and tested in [59,60,13].

7.4.4 Adaptive Controller

The control law of the dynamic hybrid control approach given by equation 6.2.19 when using the estimated parameters and observed state is described by the following equation:

$$\tau = \hat{M} J^{-1} [R^{-1} (\overset{4}{X}^*_t - \hat{a}_x) - \hat{a}_q] + \hat{h}_p (q, \dot{q}, \ddot{q}, \overset{3}{q}) + \hat{h}_f (q, \dot{q}, \ddot{q}, F, \dot{F}) + \hat{N} J^T (L \ddot{f}^* + \hat{a}_f) \qquad (7.4.12)$$

The new inputs $\overset{4}{P}^*$ and $\ddot{f}^*$ are designed as given by equations 6.2.26 and 6.2.28 using the estimated states. Applying the above control law to the fourth order feedback linearizable model given by equation 6.2.18, after some algebraic operations and the use of the linear parametrization model given by equation 7.4.11, the following closed loop results:

$$\hat{M}\, J^{-1}\, [\, R^{-1}\, (\, \overset{4}{\hat{e}}_p + K_{p3}\overset{3}{\hat{e}}_p + K_{p2}\ddot{\hat{e}}_p + K_{p1}\dot{\hat{e}}_p + K_{p0}\hat{e}_p\,)\,]$$
$$+\ \hat{N}\, J^T\, (\, L\, (\ddot{\hat{e}}_f + K_{f1}\dot{\hat{e}}_f + K_{f0}\hat{e}_f) \;=\; \hat{\Psi}\,\tilde{\Theta} + \tilde{\Psi}\,\tilde{\Theta} \qquad (7.4.13)$$

where $\hat{e}_p = P^d - \hat{P}$ and $\hat{e}_f = f^d - \hat{f}$, $\hat{P}$ is the estimated position in the tangential direction of the constraint and $\hat{f}$ is the estimated force normal to the constraint. $\tilde{\Psi} = \Psi - \hat{\Psi}$, $\hat{\Psi}$ where $\hat{\Psi}$ is the estimated regression matrix. Inspecting the closed loop system given by equation 7.4.13, one can see that the right hand side represents the error due to the mismatch in both the parameters and state. Specifically, $\hat{\Psi}\,\tilde{\Theta}$ is the error in the closed loop due to parametric uncertainty, and $\tilde{\Psi}\,\Theta$ is the error due to observation of the state. The constraint frame can be used to combine the position vector in the tangential direction and the force vector in the normal direction into a new vector Z. The closed loop of equation 7.4.13 can be written as:

$$H(q)\begin{bmatrix} \overset{4}{\hat{e}}_p + K_{p3}\overset{3}{\hat{e}}_p + K_{p2}\ddot{\hat{e}}_p + K_{p1}\dot{\hat{e}}_p + K_{p0}\hat{e}_p \\ \ddot{e}_f + K_{f1}\dot{e}_f + K_{f0}e_f \end{bmatrix} = \quad \hat{\Psi}\,\tilde{\Theta} + \quad \tilde{\Psi}\,\Theta \qquad (7.4.14)$$

The above system can be transformed to the following state space form:

$$\dot{Z} \;=\; A_1\,\hat{Z} \;+\; B_1\,\hat{\Phi}\,\tilde{\Theta} \;+\; B_1\,\tilde{\Phi}\,\Theta \qquad (7.4.15)$$

where

$$\hat{Z} = \begin{bmatrix} \hat{z}_1 & \hat{z}_2 & \hat{z}_3 & \hat{z}_4 & \hat{z}_5 & \hat{z}_6 \end{bmatrix}^T \equiv \begin{bmatrix} \hat{e}_p & \dot{\hat{e}}_p & \ddot{\hat{e}}_p & \overset{3}{\hat{e}}_p & \dot{\hat{e}}_f & \hat{e}_f \end{bmatrix}^T \quad \text{and} \quad \Phi \;=\; \hat{H}^{-1}(q)\,\Psi$$

By transforming the error vector from the constraint frame into the joint space, the above system can be written in the following form:

$$\dot{Z} \;=\; A_1\,Z \;+\; B_1\,\hat{\Phi}\,\tilde{\Theta} \;+\; B_1\,\tilde{\Phi}\,\Theta \;+\; B_3\,g_1(x_1, x_2, \hat{x}_2)\tilde{x}_2 \qquad (7.4.16)$$

where $B_3\ A_1\ g_1(x_1, x_2, \hat{x}_2)\ \tilde{x}_2$ represents the transformation of the vector $\hat{Z} - Z$ as a function of the error in the joint space. Choose the following Lyapunov function candidate: $V_1 = Z^T\ P_1\ Z + \tilde{\Theta}^T\ \Gamma^{-1}\ \tilde{\Theta}$, where P_1 is positive definite symmetric matrix satisfying the Lyapunov equation:

$$A_1^T\ P_1 + P_1\ A_1 = -\ Q_1 \qquad (7.4.17)$$

Q_1 is a positive definite symmetric matrix and Γ is a symmetric positive definite gain matrix. Choosing the following adaptation law:

$$\dot{\hat{\Theta}} = -\ \Gamma\ \Phi^T\ B_1{}^T\ P_1\ \hat{Z} \qquad (7.4.18)$$

Noting that all the robot parameters are constant in time, then, the derivative of V_1 along the trajectories of 7.4.16 is given by:

$$\dot{V}_1 = -\ Z^T\ Q_1\ Z + 2\tilde{\Theta}^T \hat{\Phi}^T\ B_1{}^T P_1\ g_1(x_1, x_2, \hat{x}_2)\tilde{x}_2 +$$

$$2\ [\Theta^T \tilde{\Phi}^T\ B_1{}^T + \tilde{x}_2^T\ g_1{}^T(x_1, x_2, \hat{x}_2)\ A_1{}^T B_3{}^T\ ] P_1 Z \qquad (7.4.19)$$

Now, the stability of the overall closed loop can be analyzed using the introduced Lyapunov functions V_1 and V_2.

Lemma: Application of the control law given by equation 7.4.12, the sliding observer given by equation 7.4.3 and initialized such that $\tilde{x}_1(t) = 0$ remains attractive, and the adaptation law given by equation 7.4.18, ensures that the augmented state vector defined by $\mathcal{Z}(t) = [Z\ \tilde{x}]^T$ converges to zero as t approaches infinity.

Proof: the closed–loop analysis is performed on the basis of the reduced–order manifold dynamics 7.4.5 and the tracking error dynamics 7.4.16, i.e.

$$\dot{Z} = A_1\ Z + B_1\ \hat{\Phi}\ \tilde{\Theta} + B_1\ \tilde{\Phi}\ \Theta + B_3\ A_1\ g_1(x_1, x_2, \hat{x}_2)\tilde{x}_2 \qquad (7.4.20)$$

$$\dot{\tilde{x}}_2 = (A_2 - K_2\ K_1{}^{-1}\ C)\ \tilde{x}_2 + f_2(x_1, \hat{x}_2) - f_2(x_1, x_2) \qquad (7.4.21)$$

Introducing the following Lyapunov function

$$V = V_1 + V_2 = \mathcal{Z}(t)^T \begin{bmatrix} P_1 & 0 \\ 0 & P_2 \end{bmatrix} \mathcal{Z}(t) + \tilde{\Theta}^T \Gamma^{-1} \tilde{\Theta} \qquad (7.4.22)$$

the time derivative of V is given by:

$$\dot{V} = \mathcal{Z}(t)^T Q \mathcal{Z}(t) + 2 [\tilde{\Theta}^T \hat{\Phi}^T B_1^T P_1 g_1(x_1, x_2, \hat{x}_2) + [f_2(x_1, \hat{x}_2) - f_2(x_1, x_2)] P_2$$
$$+ 2[\Theta^T \tilde{\Phi}^T B_1^T + \tilde{x}_2^T g_1^T(x_1, x_2, \hat{x}_2) A_1^T B_3^T] P_1 Z \qquad (7.4.23)$$

where $Q = \begin{bmatrix} Q_1 & 0 \\ 0 & Q_2 \end{bmatrix}$

Let q_{10} and q_{20} be the minimum eigenvalues of Q_1 and Q_2, and p_{10} and p_{20} be the maximum eigenvalues of P_1 and P_2, respectively. Introducing the following properties:

1– $\| \Theta^T \tilde{\Phi}^T B_1^T \| \leq \delta_1 \| \tilde{x}_2 \|$

2– $\| \tilde{x}_2^T g_1^T(x_1, x_2, \hat{x}_2) A_1^T B_3^T \| \leq \delta_2 \| \tilde{x}_2 \|^2$

3– $\| \tilde{\Theta}^T \hat{\Phi}^T B_1^T P_1 g_1(x_1, x_2, \hat{x}_2) \| \leq \delta_3 \| \tilde{x}_2 \|$

4– $\| f_2(x_1, x_2) - f_2(x_1, \hat{x}_2) \| < \mu_x \| \tilde{x}_2 \|$

where δ_1, δ_2 and δ_3 are positive scalar constants, then equation 7.4.23 can be written as:

$$\dot{V} \leq - [\| Z \| \| \tilde{x}_2 \|] [\mathcal{H}] \begin{bmatrix} \| z \| \\ \| \tilde{x}_2 \| \end{bmatrix} \qquad (7.4.24)$$

where

$$\mathcal{H} = \begin{bmatrix} q_{10} & -(\delta_1 + \delta_2) p_{10} \\ -(\delta_1 + \delta_2) p_{10} & q_{20} - \mu_x p_{20} + \delta_3 p_{10} \end{bmatrix}$$

Finally, equation 7.4.24 can be written as:

$$\dot{V} \leq - \lambda_{\min}(\mathcal{H}) \| \mathcal{Z}(t) \| \qquad (7.4.25)$$

where $\lambda_{min}(\mathcal{H})$ is the smaller eigenvalue of $\mathcal{H}$. It is necessary to have $\lambda_{min}(\mathcal{H}) > 0$ for all $t > 0$ to ensure the closed loop stability. The following two conditions are required to satisfy the above condition:

$$q_{20} - \mu_x p_{20} + \delta_3 p_{10} > 0 \qquad (7.4.26)$$

$$q_{10} (q_{20} - \mu_x p_{20} + \delta_3 p_{10}) - (\delta_1 + \delta_2)^2 p_{10}^2 > 0 \qquad (7.4.26)$$

Assuming that the observer and controller gains can be chosen to satisfy the above two conditions, then the closed loop system will be stable and the state vector $\mathcal{Z}(t)$ will approach zero as the time approaches infinity.

7.4.5 Simulation Results

The adaptive feedback linearization controller with the robust sliding mode observer was simulated to evaluate its performance in achieving position and force tracking in the presence of parametric uncertainty. The task used in the simulation is the same as that used in the dynamic hybrid controller except that the adaptive algorithm is applied in the first path (1.5 seconds trajectory from point A to point B in figure 6.1). Parametric uncertainty was introduced in the rigid dynamics by adding the C–shape steel block as described in the robust sliding mode controller experiment section. The controller is defined by $\omega_p = 22.0$, $\omega_f = 80.0$, and $\zeta_p = \zeta_f = 1.0$. The sliding mode observer is defined by $\lambda^1{}_1 = 0.025$, $\lambda^2{}_1 = 0.025$ and the poles of $(A_2 - K_2 K_1^{-1} C)$ are placed at [–2.0,–2.0,–2.0]. Figure 7.21 to 7.23 show plots of the position, velocity, and force tracking errors. Figure 7.24 shows the estimation of the inertia parameters which indicate that the estimated parameters approach their true values. Figure 7.25 and 7.26 show the observer error in the angular positions and velocities for joint 1 and joint 2. The plots indicate that the observer is working within the sliding conditions. As a result, the angular velocity error remained less than 0.025 rad/s which can be noted from figures 7.27 and 7.28 for the first and second joint, respectively.

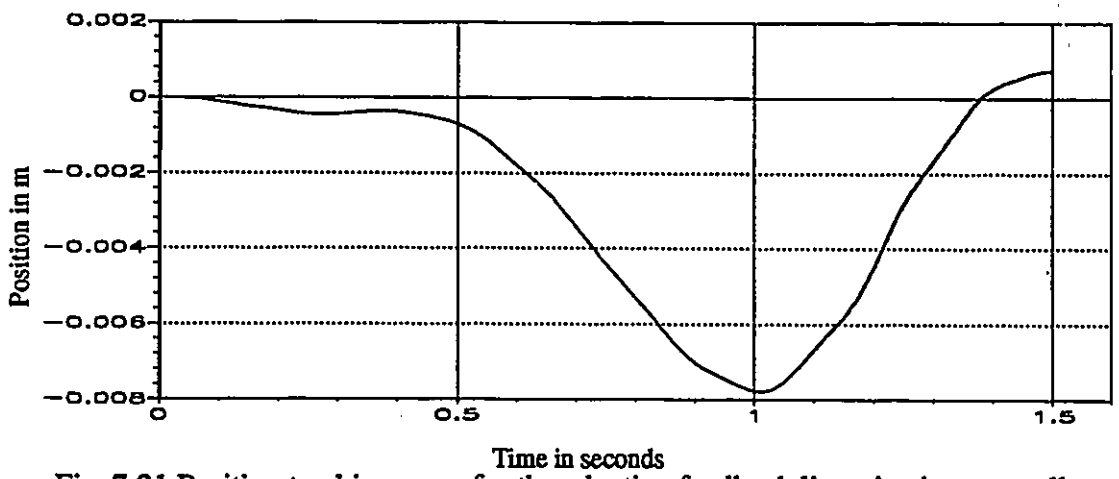

Fig. 7.21 Position tracking error for the adaptive feedback linearization controller with the robust sliding mode observer (simulation)

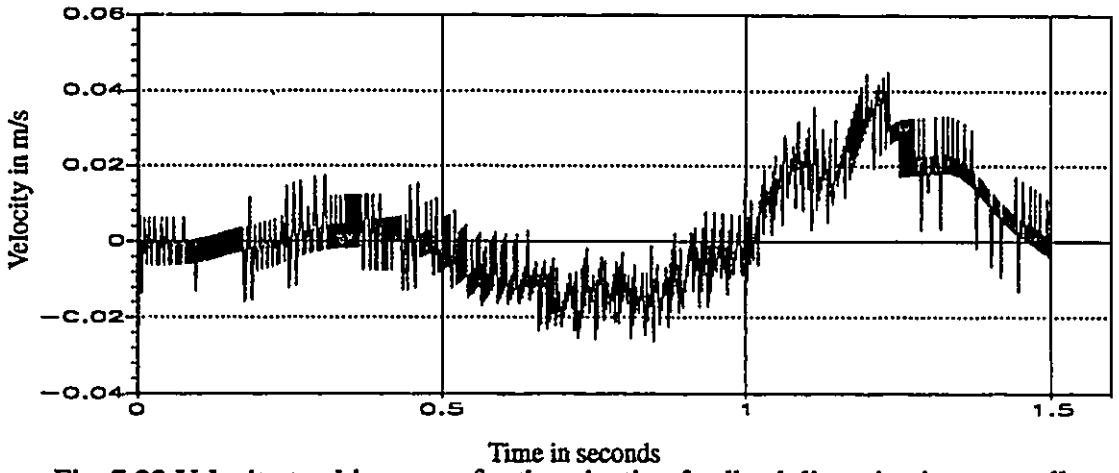

Fig. 7.22 Velocity tracking error for the adaptive feedback linearization controller with the robust sliding mode observer (simulation)

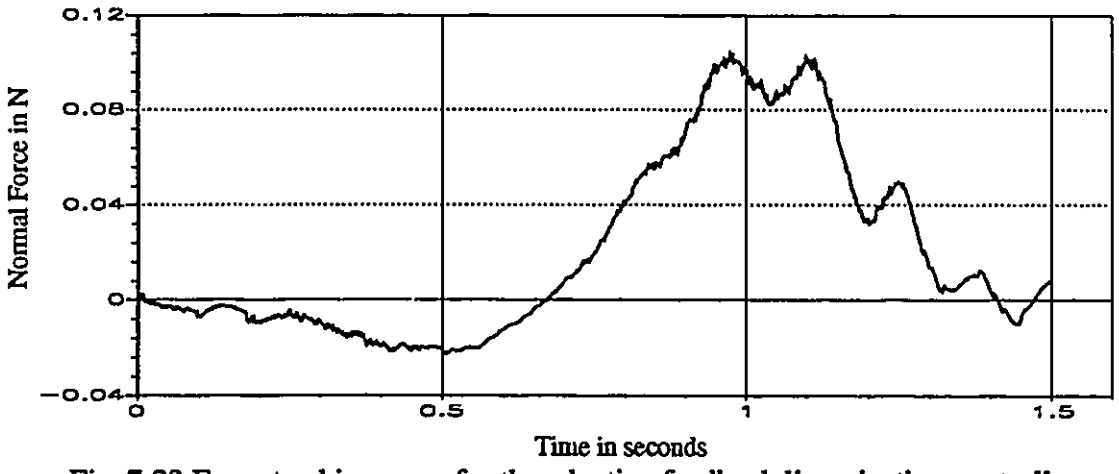

Fig. 7.23 Force tracking error for the adaptive feedback linearization controller with the robust sliding mode observer (simulation)

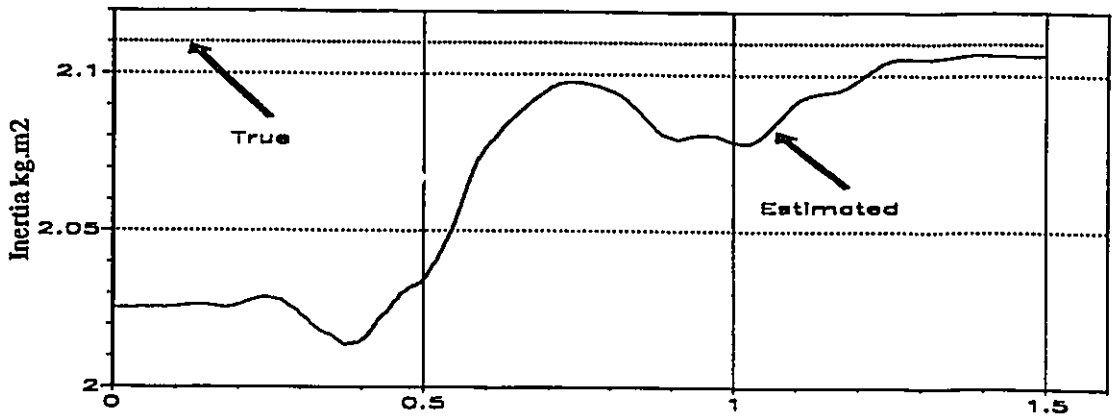

(a)

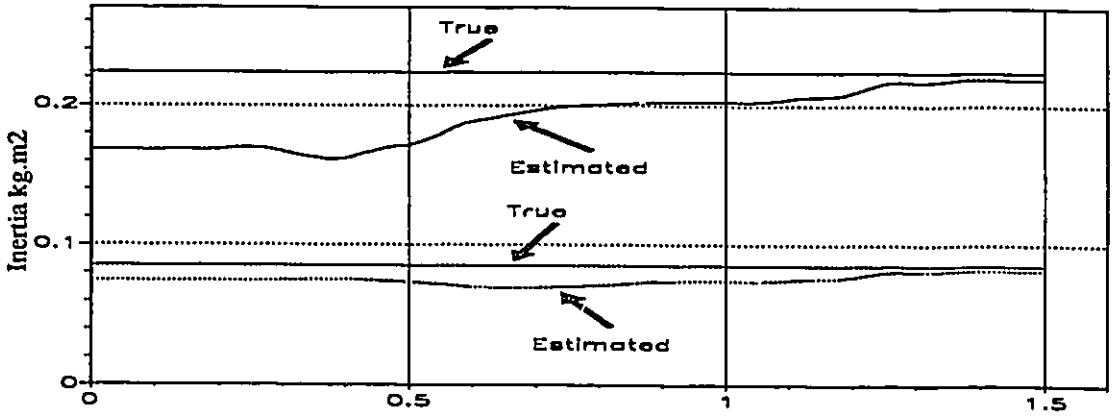

(b)

Fig. 7.24 Parameter estimation for the adaptive feedback linearization controller with the robust sliding mode observer (simulation)
(a) First parameter (b) Second and Third parameters

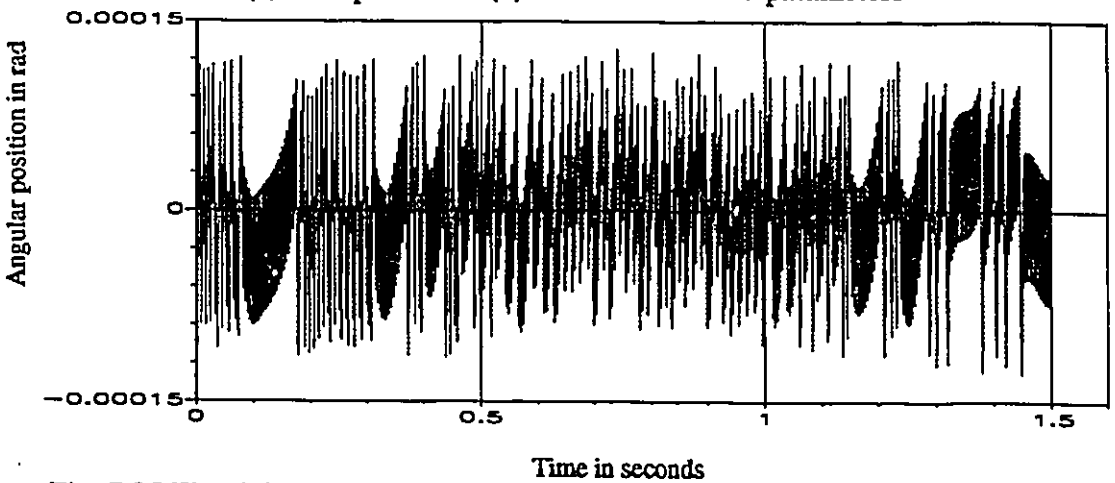

Fig. 7.25 First joint angular position observer error for the adaptive feedback linearization controller with the robust sliding mode observer (simulation)

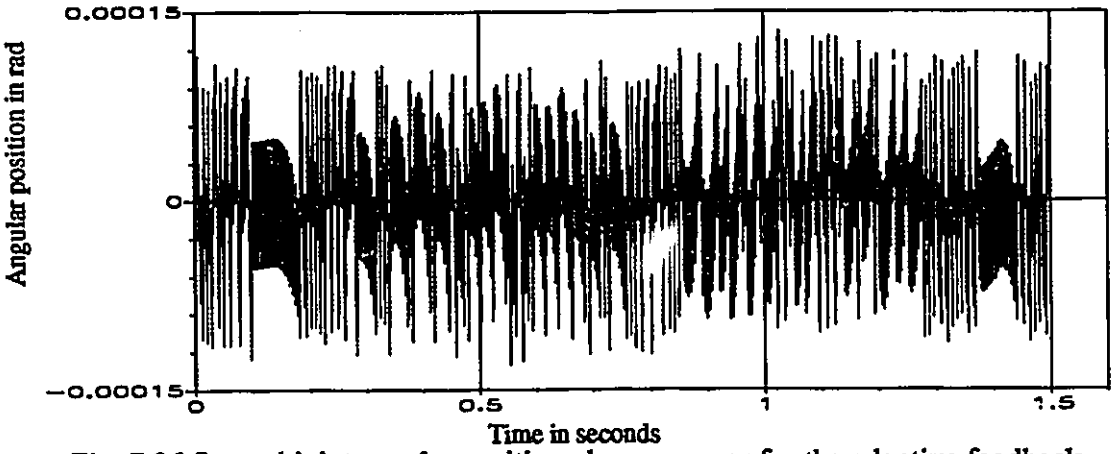

Fig. 7.26 Second joint angular position observer error for the adaptive feedback linearization controller with the robust sliding mode observer (simulation)

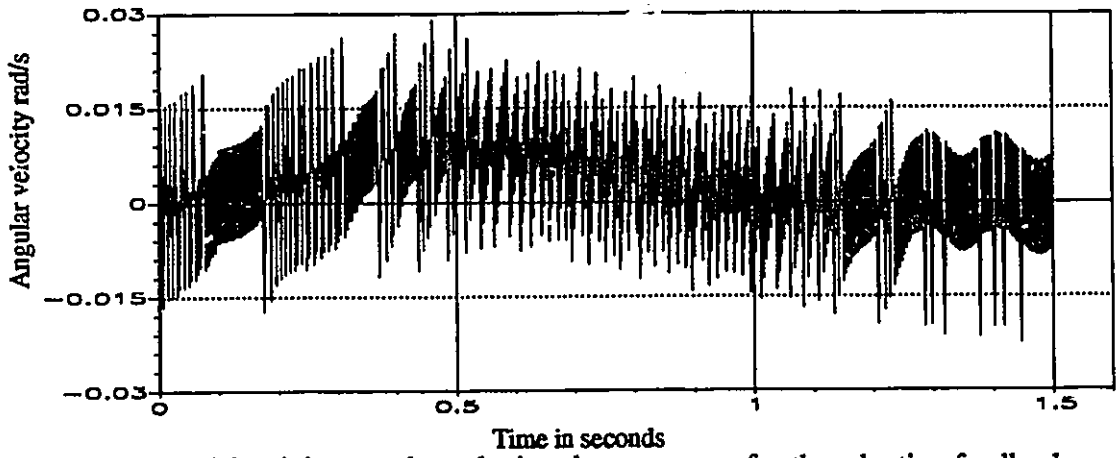

Fig. 7.27 First joint angular velocity observer error for the adaptive feedback linearization controller with the robust sliding mode observer (simulation)

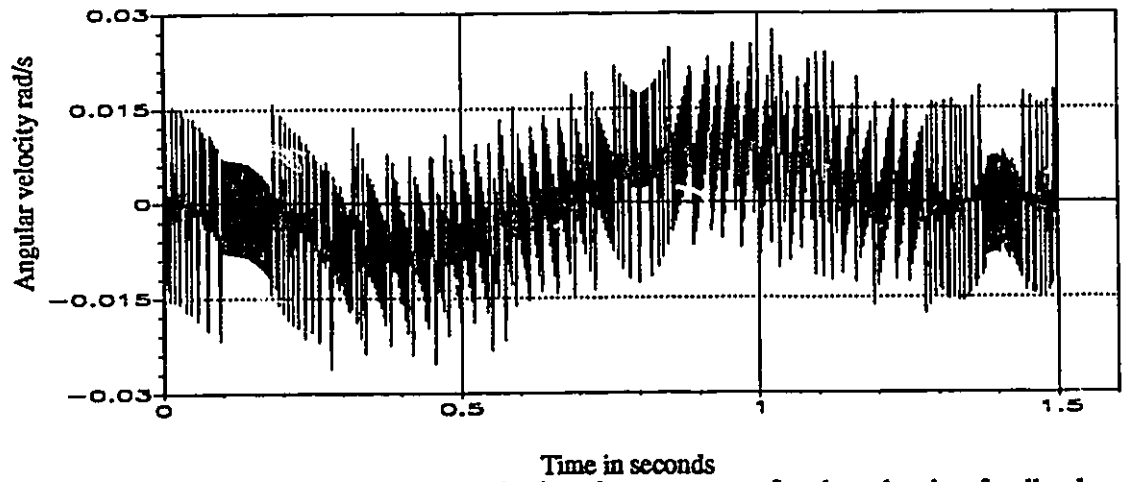

Fig. 7.28 Second joint angular velocity observer error for the adaptive feedback linearization controller with the robust sliding mode observer (simulation)

7.5 SUMMARY

In this chapter, the problem of position and force tracking for flexible joint robot manipulator in the presence of parametric uncertainty was considered. Three different control algorithms were designed as solutions to the problem.

1. A robust sliding mode controller was designed, simulated, and implemented on the experimental flexible joint robot manipulator. The problem was formulated, using the feedback linearizable model and the constraint frame, in a way which enabled determination of the upper bound of the disturbance caused by parametric uncertainty. This enabled design of the discontinuous control term. Analysis showed that the minimum achievable boundary layer thickness has a lower bound due to the estimation of the state vector using the original system state. This controller requires the measurements of the original state (motors and links angular positions and velocities) and the contact force. Simulation and experimental results indicated excellent performance of the controller in tracking both position and force trajectories in the presence of parametric uncertainty.

2. An adaptive cascade controller was designed, simulated, and implemented on the experimental flexible joint robot. Cascade control allowed reducing the problem to that of controlling two second order systems. A direct adaptive controller was designed for the rigid system while a MRAC controller was designed for the flexible system. Simulation results indicated a good performance in tracking both position and force trajectories in the presence of parametric uncertainty in both the links and the motors systems. The experimental results indicated acceptable force tracking with slow response in position tracking although the links adaptive controller maintained stability despite the parametric uncertainty. Moreover, the motors system, under the MRAC, managed to closely follow the reference model. The limitation on the position subsystem bandwidth, to allow the motors to perform its tracking task and to ensure stability, is the main reason for the obtained performance.

3. An adaptive feedback linearization control algorithm with a robust sliding mode observer was designed and simulated. The robust sliding mode observer is designed for the feedback linearizable system to ensure the availability of the state for feedback. The adaptive controller consists of a nominal control law, similar to the dynamic hybrid controller, using the estimated states and parameters. The problem was formulated in a way which enabled designing the update law and analyzing the stability of the system. The conditions to ensure the stability of the overall system, composed of the robot, the observer, controller, and the adaptation law, were obtained. Simulation results indicated a good performance in tracking the position and force trajectories by estimating of the state and parameters of the system. Due to time constraint, the adaptive feedback linearization algorithm was not implemented on the experimental robot.

CHAPTER 8

CONCLUSION

This chapter is divided into four sections: Introduction, Summary, Discussion and Conclusions and Future Research.

8.1 INTRODUCTION

A fundamental limitation to achieving high performance control in robotic manipulators are the lightly–damped drive system resonances. The common practice of using sensors collocated with the actuators with PID controller limits the controller bandwidth to one–half the cantilever frequency of the manipulator. The links positioning accuracy is very limited when only positioning control of the actuators is performed because of the imperfect joints, gears and drive trains. To increase the positioning accuracy for this design, it is only possible to increase the structural vibration frequencies by increasing the rigidity of the structure and the drive system.

Force control is essential when the robot manipulator performs contact tasks. In this case, the effect of the drive system resonances is more crucial than in pure position control as the joint flexibility limits the control bandwidth and causes control instability.

The main objective of the research was to control both end–point position and force trajectories while taking into account the drive system flexibility. The research approach proposed to attack this problem had the following features:

1. Employment of sensors to measure the links angular positions and the end–point contact forces, in addition to measuring of the motors angular positions.

2. Adoption of the full nonlinear model describing the drive system flexibility and the contact forces when interacting with rigid and compliant environments.
3. Ensuring high resolution measurements and a high sampling rate for successful digital implementation of the continuous nonlinear control algorithms.
4. Development of control algorithms to achieve high accuracy end–point position and force trajectories tracking. In parallel with the control development, the following issues were considered:

    a. Make thoroughly comprehensive benefits from two areas related to the considered problem: i) position control of flexible joint robots and ii) force control of rigid robots.

    b. Ensure the performance of the control system in case of disturbance caused by parametric uncertainty in the system.

8.2 SUMMARY

An experimental two–link robot manipulator with flexible joints was designed and built to test the developed control algorithms. Two preliminary controllers were designed and tested and five position and force control algorithms were developed and tested. The control algorithms are divided into four groups:

A. Preliminary Controllers

B. Model--based Controllers

C. Robust Controllers

D. Adaptive Controllers.

A– Preliminary controllers

1. PD controller

A collocated PD controller was designed, simulated and implemented. Simulation and ex-

perimental results indicated the inadequacy of this controller for controlling of the rigid dynamics.

2. Feedback linearization in the joint space

A fourth order feedback linearizable model of the flexible joint robot manipulator was constructed and analyzed. Based on the full nonlinear model, a nonlinear feedback linearization controller was designed, simulated and implemented. Simulation and experimental results indicated excellent tracking performance.

B– Model–Based Controllers

After gaining confidence in the performance of the feedback linearization, two different model–based controllers were developed, simulated and implemented.

1. Dynamic hybrid controller

This controller deals with the contact with rigid environments. The control law requires knowledge of robot parameters, measurements of the angular positions and velocities of the links and motors and the contact forces, and description of the constraining surface. With these requirements fulfilled, the controller linearizes and decouples the system, then imposes desired characteristics for each of the decoupled position and force subsystems. Simulation and experimental results indicated superior performance in achieving both position and force trajectories tracking.

2. Impedance controller

This controller deals with the contact with compliant environments. The controller aims at regulating the relationship between the contact force and the difference between the commanded and actual end–point positions. The control law requires the knowledge of the robot parameters, measurements of the angular positions and velocities of the links and motors and the contact forces, and a model describing the contact environment. With these requirements fulfilled, the controller linearizes the system then imposes a desired fourth order target im-

pedance for the end–point in the cartesian space. Simulation and experimental results indicated the ability of the impedance controller to regulate the contact forces, tracking position trajectories, and switching between contact and free motions.

The development of these two control approaches served as basis for formulating the problem for consideration of robust and adaptive control.

C– Robust Controllers

A robust controller based on the concept of sliding mode control was designed, simulated and implemented. The problem was formulated, using the feedback linearizable model and the constraint imposed by the contact environment, in a way to determine the upper bound of the disturbance caused by parametric uncertainty. In addition, the effect of parametric uncertainty on the computing of the unmeasured state elements of the feedback linearizable system was included in the design and analysis of the sliding mode controller. The controller requires the measurements of the angular positions and velocities of the links and the motors and the contact force. Simulation and experimental results indicated excellent performance in tracking the position and force trajectories in the presence of parametric uncertainty.

D– Adaptive Controllers

1. Adaptive cascade controller

An adaptive cascade controller was designed, simulated and implemented. It consists of a direct adaptive controller for the rigid dynamics and a Model Reference Adaptive Controller (MRAC) for the flexible dynamics. Simulation results indicated good performance in controlling both position and force in the presence of parametric uncertainty. Experimental results indicated good performance in force tracking and slow, but stable, response in position tracking. The rigid dynamics controller maintained stability despite the introduced parametric uncertainty and the parameter adaptation loop was able to approach the true parameters.

The MRAC controller performed its task of tracking the desired angular position. The limitation on the position control bandwidth, to ensure stability and tracking by the motors, was responsible for the slow response.

2. Adaptive feedback linearization controller

An adaptive feedback linearization algorithm with a robust sliding mode observer was designed and simulated. The robust observer is designed for the feedback linearizable system to ensure the availability of the state for feedback in case of uncertainty in the robot parameters. The adaptive control law has the structure of the dynamic hybrid control law but uses estimated states and parameters. The problem was formulated to enable designing of an adaptation law and the analysis of the stability of the overall system. Simulation results indicated good performance in tracking position and force trajectories by robust estimation of the state vector and the updating of the robot parameters

8.3 DISCUSSION AND CONCLUSIONS

The feedback linearization can result in a better stability and tracking performance in comparison with the collocated control (PD) and cascade control approaches. This is because collocated control lacks the advantages of sensing and controlling the rigid dynamics which are connected to the collocated system by the joints flexibilities. The cascade control approach requires instantaneous response from the actuator system, thus it cannot practically achieve stability and tracking as that of the feedback linearization. Two modifications were considered to enhance the cascade controller performance: i) running the flexible dynamics controller faster than the rigid dynamics controller and ii) evaluating or predicating the desired motor angular velocity and not just the position. The first modification resulted in enhancing the cascade controller performance when the flexible dynamics controller was running at twice the speed of the rigid dynamics controller. However, higher sampling ratios did not introduce further improvements. This modification was not implemented on the exper-

imental robot because it reduces the sampling rate to less than 300 Hz. The second modification considered requires the angular acceleration and force first derivative. This alternative was avoided based on the fact that two of the main objectives while developing the cascade controller are to avoid the higher order requirements used in the feedback linearization and the simplicity of the cascade controller it introduces by controlling two second order systems instead of a fourth order system.

Feedback linearization is the most suitable for flexible joint robot manipulators in comparison with singular perturbation and cascade control. The feedback linearization deals with the full dynamically coupled nonlinear system. Thus, it enables controlling not only the rigid dynamics but also the flexible dynamics simultaneously. Because the system is pure–feedback linearizable, controlling the linearizable system is sufficient to ensure stability and interaction between the flexible and rigid dynamics. In addition, feedback linearization application is not limited to specific flexibility characteristics. It managed to achieve the tracking objective for some nonlinearity in the joint flexibility which was evident during the identification process. The two developed model–based position and force controllers made use of all advantages of the feedback linearization properties and the established force control approaches for rigid robots in a basic structure frame work. In principle, the only limitation of these controllers are the measurement accuracy and the computation speed. Thus, perfect position and force tracking can be achieved. In addition, the formulation enables considering other problems related to feedback linearization, namely: i) the need for the full state for feedback and maintaining stability and tracking performance in the presence of parametric uncertainty.

In dealing with these two problems, two controllers were developed. The robust sliding mode controller, by taking into account the error introduced in computing the state of the feedback linearizable system and the error in cancelling the nonlinearities (both are

errors caused by parametric uncertainty), established a way of maintaining the stability and tracking performance in the presence of parametric uncertainty. The design uses the basic property that the uncertainty in the robot parameters is bounded. The limitation found on the minimum achievable boundary layer thickness together with actuator characteristics used to specify the sliding surface bandwidth form a basic relation for specifying position and force tracking accuracies. The developed robust sliding mode observer is very useful for feedback linearization algorithms as it provides accurate estimation of the unmeasured states of the feedback linearizable system when the robot parameters are uncertain. The design makes use of the Lipschitz–continuity of the feedback linearizable system nonlinearity and the property that the contact forces are not independent variables. The second alternative in dealing with the problem was the development of an adaptive feedback linearization algorithm. This algorithm is combined with the robust observer and uses a linear parametrization model of the original system. The formulation enabled designing adaptation law similar to the case of second order systems and using the estimated states. In addition, the formulation enabled obtaining specific conditions to ensure the stability of the combined system. The problem needs more efforts to design a systematic procedures to design the observer and controller gains to satisfy the stability conditions.

Finally, noncollocated measurement is a primary requirement in order to control robots which exhibit joint flexibility problems. The presented control approaches by use of the noncollocated sensing and control achieved stability and tracking performance similar to that of rigid robots.

8.4 FUTURE RESEARCH

There are a number of issues related to the problem of controlling position and force of flexible joint robots that need investigation:

1. Impedance control

Approach for the design of the target impedance parameters for a variety of contact tasks with different requirements.

2. Position control mode

Development and modification of current position and force control algorithms for application using the direct drive motors in the position mode. To achieve this goal, the high positioning accuracy of the motors may be combined with other controllers.

3. Adaptive control with robust observer

More analysis is required for the adaptive feedback linearization regarding satisfaction of the stability conditions and experimental testing.

4. Industrial robots

Industrial robots need to be equipped with sensors to provide measurements of the links position. In addition, the application of the developed control algorithms to industrial robots is required.

REFERENCES

[1] An, C. H. , Atekson, C. G., and Hollerbach J. M., "Model–Based Control of Robot Manipulator", The MIT Press, Cambridge, MA, 1988.

[2] An, C. H. and Hollerbach, J. M., "The Role of Dynamic Models in Cartesian Force Control of Manipulators" , Int. J. of Robotics Research, Vol. 8, No. 4, pp. 51–71, August, 1989.

[3] Asada, H. and Youcef–Toumi, K., "Direct–Drive Robots: Theory and Practice", The MIT Press, Cambridge, MA, 1987.

[4] Assurance Technologies Inc., "Installation and Operations Manual F/T", NC, 1992.

[5] Bejzey, A. K., "Robot Arm Dynamics and Control", Proc. of the IEEE Conf. on Robotics and Automation, St. Louis, MO, pp. 960–970, March, 1985.

[6] Berger, R. M., "The Control of a Two Link, Flexible Joint Manipulator", M.E. thesis, Mechanical Engineering Department, McMaster University, Ont., December, 1989.

[7] Book, W. J., "Modelling, Design and Control of Flexible Manipulator Arms: A Tutorial Review", Proc. of the 29th IEEE Conf. on Decision and Control, pp. 500–506, Honolulu, HI, 1990.

[8] Cannon, R. H., and Schnitz, E., "Initial Experiments on the End–Point Control of a Flexible One–Link Robot", Int. J. of Robotics Research, Vol. 3, No. 8, pp. 681–685, 1987.

[9] Canudas de Wit, C. and Fixot, N., "Adaptive Control of Robot Manipulators via Velocity Estimated Feedback", Advanced Robot Control, Proc. of the Int. Workshop on Nonlinear and Adaptive Control: Issues in Robotics, pp. 69–82, France, November, 1990.

[10] Canudas de Wit, C., Fixot, N., Astrom, K. J., "Trajectory Tracking in Robot

Manipulators via Nonlinear Estimated State Feedback", IEEE Trans. on Robotics and Automation, Vol. 8, No. 1, pp. 138–144, February, 1992.

[11] Canudas de Wit, C. and Slotine, J.–J. E., "Sliding Observers for Robot Manipulators", Automatica, Vol. 27, No. 5, pp. 859–864, 1991.

[12] Carusone, J., and d'Eleuterio, G., "Experiments in the Control of Structurally Flexible Manipulators with the Radius Facility", Proc. of the Second Joint Japan–USA Conference on Adaptive Structures, 1991.

[13] Chiou, B. C. and Shahinpoor, M., "The Effects of Joint and Link Flexibilities on the Dynamic Stability of Force Controlled Robot Manipulators", Proc. of the IEEE Conf. on Robotics and Automation, Scottsdale, AZ, pp. 398–403, May, 1989.

[14] Christian, A. D. and Seering, W. P., "Initial Experiments with a Flexible Robot", Proc. of the IEEE Conf. on Robotics and Automation, Cincinnati, OH, pp. 722–727, May 1990.

[15] Christien, A. D., "Design and Implementation of a Flexible Robot", Technical Report, No. AI–TR 1153, Artificial Intelligence Laboratory, Massachusetts Institute of Technology, 1989.

[16] Compumotor Division, Parker Hannifin Corporation, "Dynaserv DM & DR User Guide", CA, 1991.

[17] Craig, J., "Adaptive Control of Mechanical Manipulators" Addison–Wesley Publishing Company, Inc., MA, 1988.

[18] De Luca, A., "Dynamic Control of Robots with Joint Elasticity" , Proc. of the IEEE Conf. on Robotics and Automation, Philadelphia, PA, pp. 152–158, April, 1988.

[19] De Luca, A. , Isidori, A., Nicolo, F., "Control of Robot Arm with Elastic Joints via Nonlinear Dynamic Feedback", Proc. of the 24th IEEE Conf. on Decision and Control, Ft. Lauderdale, FL, pp. 1671–1678, December, 1985.

[20] De Luca, A., Manes, C., and Nicolo, F., "A Task Space Decoupling Approach to

Hybrid Control of Manipulators", IFAC 2nd Symposium on Robot Control (SYRCO'88), Karlsruhe, Germany, pp. 541–546, October, 1988.

[21] dSPACE digital signal processing and control engineering GmbH, Paderborn, Germany, DSP–CITpro Hardware Version 1.0, 1990.

[22] ElMaraghy, W. H., ElMaraghy, H. A., Zaki, A., Massoud, A., "Design and Control of Robots with Flexibilities", To appear in the CIRP, Singapore, 1994.

[23] ElMaraghy, W. H., ElMaraghy, H. A., Zaki, A., Massoud, A., "A Study on the Design and Control of Robot Manipulators with Flexibilities", To appear in the IFAC 4th Symposium on Robot Control (SYRCO'94), Italy, 1994.

[24] ElMaraghy, H. and John, B., "An Investigation into the Compliance of SCARA Robots, Part I: Analytical Model and Part II: Experimental and Numerical Validation" Trans. of the ASME J. of Dynamic Systems, Measurements and Control, Vol. 110, pp. 18–30, March, 1988.

[25] ElMaraghy, A., and Massoud, Atef T., "Adaptive Dynamic Hybrid Position and Force Control of Flexible Joint Robot Manipulators", The Third Int. Symposium on Experimental Robotics, Kyoto, Japan, pp. 59–67, October, 1993.

[26] Eppinger, D. and Seering, W. P., "Understanding Bandwidth Limitations in Robot Force Control", Proc. of IEEE Conf. on Robotics and Automation, Raleigh, NC, pp. 904–909, April, 1987.

[27] Eppinger, S. D. and Seering, W. P., "Three Dynamic Problems in Robot Force Control", Proc. of IEEE Conf. on Robotics and Automation, Scottsdale, AZ, pp. 392–397, May, 1989.

[28] Ficolo, A., Marino, R., and Nicosia, S., "A Singular Perturbation Approach to the Dynamic Control of Elastic Robots", In the Proc. of the 21st Ann. Allerton Conf. on Comm., cont., and comp, Monticello, IL, University of Illinois at Urbana–Champaign, October, 1983.

[29] Ficolo, A., Marino, R., and Nicosia, S., "A Composite Control Strategy for a Weakly Elastic Robots", In the Proc. of the 21st Ann. Allerton Conf. on Comm., cont., and comp, Monticello, IL, University of Illinois at Urbana–Champaign, October, 1983.

[30] Forrest–Barlach, M. G. and Babcock, S. M., "Inverse Dynamics Position Control of Complaint Manipulators", IEEE Trans. on Robotics and Automation, Vol. RA–3, No. 1, pp. 75–83, February, 1987.

[31] Freund, E. , "A Nonlinear Control Concept for Computer Controlled Manipulators", Proc. of the IFAC Symposium Multivariable Tech. Sys., Tokyo, pp. 395–403, 1977.

[32] Ghorble, F., Hung, J. Y., and Spong, M. W., "Adaptive Control of Flexible Joint Manipulators", IEEE Control System Magazine, pp. 9–13, December, 1989.

[33] Good, M. C., Sweet, L. M., and Strobel, K. L., "Dynamic Models For Control System Design of Integrated Robot and Drive Systems", Trans. of the ASME J. of Dynamic Systems, Measurements and Control, Vol. 107, pp. 53–59, March, 1985.

[34] Han, Y. , "Adaptive Tracking in Feedback Linearizable Systems", Ph.D. Thesis, Electrical Engineering, McMaster University, Hamilton, Ont., 1992.

[35] Han, Y., Sinha, N. K., and Elbestawi, M. A., "Simulation of adaptive controller for constrained manipulator with joint flexibility", Proc. of the 34th Midwest symposium on circuits and systems, CA, May, 1991.

[36] Henrichfreise, H., "The Control of an Elastic Manipulator Device Using DSP", Proc. of the American Control Conf., Atlanta, GA, pp. 1029–1035, June, 1988.

[37] Hernandez, J. and Barbot, J–P., "Feedback Control with Observers for Flexible Joint Manipulators", The European Control Conf., The Netherlands, 1993.

[38] Hong, X., "Robust Impedance Control of Robotic Manipulator", M. Eng. thesis, Electrical Engineering, McMaster University, Hamilton, Ont., 1990.

[39] Hogan, N., "Impedance Control: An Approach to Manipulation: Part I– Theory, Part II– Implementation, Part III– Applications", Trans. of the ASME J. of Dynamic

Systems, Measurements and Control,Vol. 107, pp.1–24, March, 1985.

[40] Hogan, N., "Stable Execution of Contact Tasks Using Impedance Control", Proc. of the IEEE Conf. on Robotics and Automation, Raleigh, NC, pp. 1047–1054, April, 1987.

[41] Hogan, N., "On the Stability of Manipulators Performing Contact Task", IEEE Trans. on Robotics and Automation, Vol. 4, No. 6, pp. 677–686, December, 1988.

[42] Hollars, M. G., "Experiments in End–Point Control of Manipulator with Elastic Drives", Ph. D. thesis, Department of Aeronautics and Astronautics, Stanford University, Stanford, CA 94305, May, 1988.

[43] Hsu, P., Bodson, M., Sastry, S. , and Paden, B., "Adaptive Identification and Control for Manipulators without Using the Joints Accelerations", Proc. of the IEEE Conf. on Robotics and Automation, Raleigh, NC, pp. 1210–1215, April, 1987.

[44] Hsu, L. and Guenther, R. "Variable Structure Adaptive Cascade Control of Multi–Link Robot Manipulators with Flexible Joints: the case of arbitrary uncertain flexibilities", Proc. of the IEEE Conf. on Robotics and Automation, Atlanta, GA, pp. 340–345, May, 1993.

[45] Hung J. Y. " Robust Control Design of Flexible Joint Robot Manipulator " Ph. D. thesis, Department of Electrical and Computer Engineering, University of Illinois at Urbana–Champain, IL, 1989.

[46] Integrated System Inc., "MATRIXx v. 3.1 and xmath v. 1.1", CA, 1992.

[47] Jankowski, K. P. and ElMaraghy, H. A., "Dynamic Control of Flexible Joint Robots with constrained End Effector", IFAC 4th Symposium on Robot Control, (SYROCO'91), Vienna, Austria, pp. 345–350, 1991.

[48] Jankowski, K. P. and ElMaraghy, H. A., "Dynamic decoupling for Hybrid Control of Rigid–Flexible–Joint Robots", IEEE Trans. on Robotics and Automation, Vol. 8, No. 5, pp. 519–533, October, 1992.

[49] Jankowski, K. P. and ElMaraghy, H. A., "Inverse Dynamics and Feedforward Controllers for High Precision Position/Force Tracking of Flexible Joint Robots", Robotica, Vol. 12, pp. 227–241, 1994.

[50] Jankowski, K. P. and Van Brussel, "An Approach to Discrete Inverse Dynamics Control of Flexible Joint Robots", IEEE Trans. on Robotics and Automation, Vol. 8, No. 5, pp. 651–658, October, 1992.

[51] Kang, C. G., Kao, W. W., and Boals, M., "Modellig Identification and Simulation of a Two Link SCARA Manipulator", Proc. of the winter Annual Meeting of the ASME, Chicago, IL, pp. 393–407, 1988.

[52] Kazerooni, H. "Robust, Nonlinear Impedance Control for Robotic Manipulators", Proc. of the IEEE Conf. on Robotics and Automation, Philadelphia, PA, pp. 741–750, April, 1988.

[53] Kazerooni, H., Sharidan, T. B., and Houpt, P. K., "Robust Compliant Motion Control for Manipulators", IEEE Trans. on Robotics and Automation, Vol. RA–2, No. 2, pp. 83–105, June, 1986.

[54] Khalil, H. K., "Nonlinear Systems", Macmillan Pub. Company, New York, 1992.

[55] Khatib, O., "A Unified Approach for Motion and Force Control of Robot Manipulators: The Operational Space Formulation", IEEE Trans. on Robotics and Automation, Vol. RA–3, No. 1, pp. 43–53, February, 1987.

[56] Khatib, O. and Burdick, J., "Motion and Force Control of Robot Manipulators", Proc. of the IEEE Conf. on Robotics and Automation, San Francisco, CA, pp. 1381–1386, April, 1986.

[57] Khorasani, K., "Nonlinear Feedback Control of Flexible Joint Manipulators : A Single Link Case Study", IEEE Trans. on Automatic Control, Vol. 35, No. 10, pp. 1145–1149, October, 1990.

[58] Khorasoni, K. and Spong, M., "Invariant Manifolds and Their Application to Robot

Manipulators with Elastic Joints", Proc. of the IEEE Conf. on Robotics and Automation, St. Louis, MO, pp. 978–983, March, 1985.

[59] Khosla, P. "Estimation of the Robot Dynamics Parameters: Theory and Application", IEEE Trans. on Robotics and Automation, Vol. 3, No. 1, pp. 35–41, 1988.

[60] Khosla, P. K. and Kanade, T., "Parameter Identification of Robot Dynamics", Proc. of the 24th Conf. on Decision and Control, Ft. Landerdale, FL, pp. 1754–1760, December, 1985.

[61] Kiranski, N., Timcenko, A., and Vukobrakovic, M., "Position Control of Robot Manipulators with Elastic Joints Using Force Feedback", J. of Robotic Systems, Vol. 7, No. 4, pp. 535–554, 1990.

[62] Krishnan, H. and McClamroch, N. H., "A new Approach to Position and Contact Force Regulation in Constrained Robot Systems", Proc. of the IEEE Conf. on Robotics and Automation, Cincinnati, OH, pp. 1344–1349, May, 1990.

[63] Landau, Y. D., "Adaptive Control: The Model Reference Approach", Marcel Dekker, Inc., New York, 1979.

[64] Lee, K. Y., De La Torre, H. J., and Beekman, R. W., "Decoupled Nonlinear Robotic Control with Series Compliance and Bounded Inputs", Proc. of the 28th IEEEConf. on Decision and Control, Tampa, FLA, pp. 712–715, December, 1989.

[65] Li, W., and Slotine, J. –J. E., "Parameter Estimation Strategies for Robotic Applications", Proc. of the Winter Annual Meeting of the ASME, DSC–Vol. 6, pp. 213–218, Boston, MA, December, 1987.

[66] Lin, L. –C. and Yuan, K., "Control of Flexible Joint Robots via External Linearization Approach", J. of Robotic Systems, Vol. 7, No. 1, pp. 1–22, 1990.

[67] Lin, P. L. and Wu, Y. C., "Identification of Multi Input Multi Output Linear Systems From Frequency Response Data", Trans. of the ASME J. of Dynamic Systems, Measurements and Control, Vol. 104, pp. 58–64, March, 1982.

[68] Lin, S.– H., Tosunoglu, S. , and Tesar, D., "Control of Multi–Link Robotic Manipulator with Compliant Joints", Proc. of the Winter Annual Meeting of the ASME, San Francisco, CA, DSC–Vol 14, pp. 299–307, December, 1989.

[69] Mario, R., and Nicosia, S., "On the Control of Robots with Elastic Joints", Proc. of the American Control Conf., Boston, MA, pp. 69–70, June, 1985.

[70] Marino, R. and Spong, M. W., "Nonlinear Control Techniques for Flexible Joint Manipulators : A Single Link Case Study", Proc. of the IEEE Conf. on Robotics and Automation, San Francisco, CA, pp. 1030–1036, April, 1986.

[71] Mason, M., "Compliance and Force Control for Computer Controlled Manipulators", IEEE Trans. on Systems, Man, and Cybernetics, Vol. SMC–11, No. 6, pp. 418–432, June, 1981.

[72] Massoud, Atef T. and ElMaraghy, Hoda A., "Design, Dynamics, and Identification of a Flexible Joint Robot Manipulator", The IASTED Int. Conf. on Robotics and Manufacturing, Oxford, England, pp. 72–75, September, 1993.

[73] Massoud, Atef T., "Mechanical Design of An Experimental Flexible Joint Robot Manipulator", Flexible Manufacturing Centre Report, McMaster University, Hamilton, Ont., 1992.

[74] Massoud, Atef T., "User's Manual for The Experimental Robot Real–Time Control System", Flexible Manufacturing Centre Report, McMaster University, Hamilton, Ont., 1993.

[75] Massoud, Atef T. and ElMaraghy, Hoda A., "Impedance Control for Flexible Joint Robot Manipulators", Proc. of the Canadian Society for Mechanical Engineering Forum, Montreal, pp. 630–640, June, 1994.

[76] McClamroch, N. H. and Wang, D., "Feedback Stabilization and Tracking of Constrained Robots", IEEE Trans. on Automatic Control, Vol. 33, No. 5, pp 419–426, May, 1988.

[77] Mills, J. K. , "Control of Robot Manipulators with Flexible Joints During Constrained Motion Task Execution", Proc. of the 28th IEEE Conf. on Decision and Control, Tampa, FL, pp. 1676–1681, December, 1989.

[78] Mills, J. K. and Goldenberg, A. A., "Force and Position Control of Manipulators During Constraint Motion Tasks", IEEE Trans. on Robotics and Automation, Vol. 5, No. 1, pp. 30 46, February, 1989.

[79] Misaws, E. A. and Hedrick J. K., "Nonlinear Observers – A state of the Art Survey" Trans. of the ASME J. of Dynamic Systems, Measurements and Control, Vol. 111, pp. 344–352, September, 1989.

[80] Morimoto, Y. "Dynamic Control of Flexible Robot Arm by Using the Modal Analysis", Proc. of the Winter Annual Meeting of the ASME, Boston, MA, DSC–Vol. 6, pp. 337–343, December, 1987.

[81] Mrad, F. T. and Ahmad, S., "Adaptive Control of Flexible Joint Robot Using Position and Velocity Feedback", Int. J. of Control, Vol. 55, No. 5, pp. 1255–1277, May, 1992.

[82] Nam, K., and Arapostathis, A., "A Model Reference Adaptive Control Scheme for Pure–Feedback Nonlinear Systems", IEEE Trans. on Automatic Control, Vol. AC–33, No. 9, pp. 803–811, 1988.

[83] Oakley, C. M., and Cannon, R. H., "Equations of Motion for an Experimental Planar Two–Link Flexible Manipulator", Proc. of the Winter Annual Meeting of the ASME, San Francisco, CA, DSC–Vol 14, pp. 267–278, December, 1989.

[84] Oakley, C. M., and Cannon, R. H., "Theory and Experiments in selecting Mode Shapes for Two–Link Flexible Manipulators", Proc. of the First Int. Symposium on Experimental Robotics, pp. 1–19, 1989.

[85] Pfeiffer, F., and Gelber, B., "A Multistage Approach on the Dynamics and Control of Elastic Robots", Proc. of the IEEE Conference on Robotics and Automation, Philadelphia, PA, pp. 2–7, April, 1988.

[86] Popov, V. M., "Hyperstability of Automatic Control Systems", Springer Verlag, NY, 1973.

[87] Raghavan, S. and Hedrick, J. K., "Observers Design for a Class of Nonlinear Systems", Int. J. of Control, Vol. 59, No. 2, pp. 515–528, 1994.

[88] Raibert, M. H. and Craig, J. J., "Hybrid Position/Force Control of Manipulators", Trans. of the ASME J. of Dynamic Systems, Measurements and Control, Vol. 102, pp. 126–133, June, 1981.

[89] Readman, M. C., and Bélanger, "Stabilization of Fast Modes of a Flexible–Joint Robot", Int. J. of Robotics Research, Vol. 11, No. 2, pp. 123–134, April, 1992.

[90] Riven, E., "Mechanical design of Robots", McGraw–Hill Book Co., NY, 1988.

[91] Sastry, S. S. and Isidori, A., "Adaptive control of Linearizable Systems", IEEE Trans. Automatic Control, Vol. AC–34, No. 11, pp. 1123–1131, 1989.

[92] Schoukens, J. and Pintelon, R., "Identification of linear systems a practical guide", Pergamon Press, Oxford, England, 1991.

[93] SDRC Structural Dynamics Research Corporation, Milford, OH. I–DEAS Solid Modelling User's Guide, 1991. Version VI.

[94] Sharon, A., Hogan, N., and Hardt, D. E., "Controller Design in the Physical Domain: Application to Robot Impedance Control", Proc. of the IEEE Conf. on Robotics and Automation, Scottsdale, AZ, pp. 552–559, May, 1989.

[95] Shin, K. G. and Lee, C.–P., "Compliant Control of Robot Manipulators with Resolved Acceleration", Proc. of the 24th IEEE Conf. on Decision and Control, Ft. Lauderdale, FL, pp.350–357, December, 1985.

[96] Sinha, N. K. and Kuszta, B., "Modelling and Identification of Dynamic systems", Van Nostrand Reinhold Electrical Computer Science and Engineering Series, NY, 1983.

[97] Sira–Ramrez, Hebertt and Spong, M. "Variable Structure Control of Flexible Joint manipulators", IEEE Trans. on Robotics and Automation, Vol. 3, No. 2, pp. 57–64,

1988.

[98] Slotine, J. J.–E., "Sliding Controller Design for Nonlinear Systems", Int. J. of Control, Vol. 40, No. 2, pp. 421–434, 1984.

[99] Slotine, J. –J. E., "The Robust Control of Robot Manipulators", Int. J. of Robotics Research, Vol. 4, No. 2, pp. 49–64, 1985.

[100] Slotine, J. –J. E., Hedrick, J. K. and Misawa, E. A., "Nonlinear State Estimation Using Sliding Observers", Proc. of the 25th IEEE Conf. on Decision and Control, Athens, Greece, pp. 332–339, December, 1986.

[101] Slotine, J. –J. E. and Li, W., "Adaptive Strategies in Constrained Manipulation " Proc. of the IEEE Conf. on Robotics and Automation, Raleigh, NC, pp. 595–601, March, 1987.

[102] Slotine, J. –J. E. and Li, W., "On the Adaptive Control of Robot Manipulator Robotics: Theory and Applications", The winter Annual Meeting of the ASME, DSV 3, pp. 51–56, Anaheim, CA, December, 1986.

[103] Slotine, J. –J. E. and Li, W., "Applied Nonlinear Control" Prentice–Hall, Englewood Cliffs, NJ, 1991.

[104] Spong, M., "Modeling and Control of Elastic Joint Robots", Trans. of the ASME J. of Dynamic Systems, Measurements and Control, Vol. 109, No. 4, pp. 310–319, December, 1987.

[105] Spong, M.,"On the Force Control Problem of Flexible Joints Manipulators", IEEE Trans. on Automatic Control, Vol. 34, No. 1, pp. 107–111, January, 1989.

[106] Spong, M., Lewis, F. L., and Abdallah, C. T., "Robot Control", IEEE Press, Piscataway, NJ, 1993.

[107] Spong, M. W. and Vidyasagar, M., "Robot Dynamics and Control", John Wiley & Sons, Inc., NY, 1989

[108] Stoica, P. , "A test for Whiteness ", IEEE Trans. on Automatic Control, Vol. AC–22,

pp. 992–993, 1977.

[109] Stoten D.P., "Model Reference Adaptive Control of Manipulators", Research Studies Press Ltd., England, 1990.

[110] Su, R. , "On the Linear Equivalents of Nonlinear System", Systems and Control Letters, Vol. 2, pp. 48–52 1981.

[111] Sweet, L. M. and Good, M. C., "Re–Definition of the Robot Motion Control Problem: Effects of Plant Dynamics, Drive System, Constraints and User Requirements", Proc. of 23rd IEEE Conf. on Decision and Control, Las Vegas, NV, pp. 724–732, December, 1984.

[112] Sympolics, Inc., "MACSYMA", v. 13, U.S.A., 1988.

[113] Tomei, P., Nicosia, S., and Ficola, A., "An Approach to the Adaptive Control of Robots Elastic at Joints", Proc. of the IEEE Conf. on Robotics and Automation, San Francisco, CA, pp. 552–558, April, 1986.

[114] Uhlik, C. R., "Experiments in High–Performance Nonlinear and Adaptive Control of a Two–Link Flexible–Drive–Train Manipulator", Ph. D. thesis, Department of Aeronautics and Astronautics, Stanford University, Stanford CA 94305, May 1990.

[115] Utkin, V. I., "Variable Structure Systems with Sliding Modes", IEEE Trans. on Automatic Control, Vol. AC–22, No. 2, pp. 212–222, 1977.

[116] Utkin, V. I., "Discontinuous Control Systems: State of Art in Theory and Applications", IFAC 10th World Congress on Automatic Control, Munich, Vol. 1, pp. 74–94, 1987.

[117] Vukobratovich, M. and Nakamura, Y., "Force and Contact Control in Robotic Systems, A Historical Perspective and Current Technologies", Proc. of the IEEE Conf. on Robotics and Automation, Tutorial S5, Atlanta, GA, May, 1993.

[118] Whitney, D. E., "Historical Perspective and State of the Art in Robot Force Control", Int. J. of Robotics Research, Vol. 6, No. 1, pp. 3–14, 1987.

[119] Widmann, G. R. and Ahmad, S., "Control of Industrial Robot with Flexible Joints", Proc. of the IEEE Conf. on Robotics and Automation, Raleigh, NC, pp. 1561–1566, April, 1987.

[120] Wlassich, J., "Nonlinear Force Feedback Impedance Control ", M.S.M.E., Department of Mechanical Engineering, Massachusetts Institute of Technology, MA, February, 1986.

[121] Yoshikawa, T., "Dynamic Hybrid Position Force Control of Robot Manipulators– Description of Hand Constraints and Calculation of Joint Driving Forces", IEEE Trans. on Robotics and Automation, Vol. RA–3, No. 5, pp. 386–392, October, 1987.

[122] Yoshikawa, T., "Dynamic Hybrid Position Force Control of Robot Manipulators– Controller Design and Experiment", IEEE Trans. on Robotics and Automation, Vol. 4, No. 6, pp. 699–705, December 1988.

[123] Young, K. –K. D., "Controller Design for Manipulators Using the Theory of Variable Structure Systems", IEEE Trans. on Systems, Man, and Cybernetics, Vol. 8, No. 2, pp. 101–109, 1978.

[124] Zaki, A., and ElMaraghy, W. H., "An Overview of the Experimental Facility for the Study of Flexible Manipulators at UWO", Proc. of the Canadian Society for Mechanical Engineering Forum, Montreal, pp. 641–652, June, 1994.

[125] Zhu, W.–h, Chen, H.–t., and Zhang, Z.–j., "A Variable Structure Robot Control Algorithm with an Observer", IEEE Trans. on Robotics and Automation, Vol. 8, No. 4, pp. 486–492, August, 1992.

APPENDIX A

THE EXPERIMENTAL FLEXIBLE JOINT ROBOT

This appendix describes the mechanical structure, actuators and sensors of the experimental flexible joint robot manipulator.

A.1 The Mechanical Manipulator

Details of the mechanical design can be found in [73]. An overview of the mechanical components of the manipulator is shown by a diagrammatic sketch in figure A.1. The design was made very compact by using the center holes of the two direct drive motors. The construction of the two joints is similar, except that in the second joint the motor is reversed (the stator upwards), to maintain the two links rotation in a common horizontal plane. A stationary shaft, located in the center of the motor hole, is used to hold the stator leaving space for coupling the load to the outer–type rotor. To ensure free rotation of the rotors, two tapered roller bearings were coupled to the load around the center shaft. Joint flexibility is introduced between the rotor and the load side by means of two identical helical torsional springs. Figure A.2 shows the first joint to illustrate the mounting of the springs. This design provided compact construction and enables application of wide range flexibility by changing the springs. The springs were custom–designed by Associated Springs Operations. Table A.1 summaries the springs specifications for both joints during the design stage. The angular positions of the motors are provided by built–in encoders, while the links angular positions are measured by two external encoders located above the flexible joints. The links have rectangular cross sections and are made of aluminum. Table A.2 summarizes the links cross sections dimen-

sions.

Table A.1 Springs parameters

Parameter	Joint 1	Joint 2
No. of springs	2	2
Wire diameter (mm)	8.71	5.53
Mean diameter (mm)	100.0	64.0
No. of coils	1.7714	1.7789
Spring stiffness (N.m/rad)	99.067	25.51
Joint stiffness (N.m/rad)	198.135	50.303
Max. torque (N.m)	100.0	30.0
Max. deflection (degrees)	28.9	34.1
Max. stress (MPa)	1.287	0.963

Table A.2 Links cross sections

Parameter	Link 1	Link 2
Width (mm)	100.0	60.0
Depth (mm)	60.0	48.0
Wall thickness (mm)	3.0	12.0

A.2 The Actuators

The robot is powered by two direct drive motors manufactured by Compumotor. The motor sizes were chosen based on dynamic analysis to achieve high acceleration and meet the force control requirements. The maximum torque of the first and second motors are 100 and 30 N.m respectively. This Dynaserv DM series model consists of a brushless direct drive motor, encoder, microprocessor drive (servo controller), and 10 foot motor to drive cable. The motor can be controlled in one of three modes:

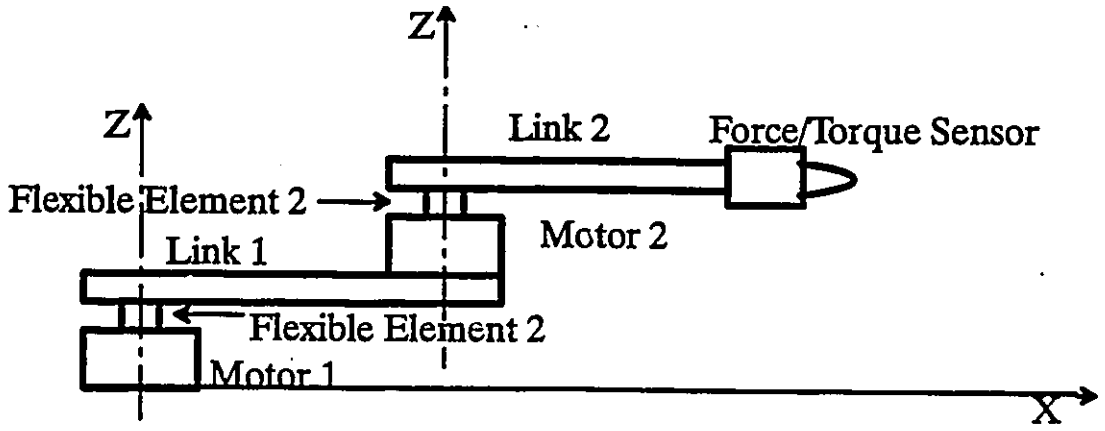

Fig. A.1 An overview of the two–link manipulator

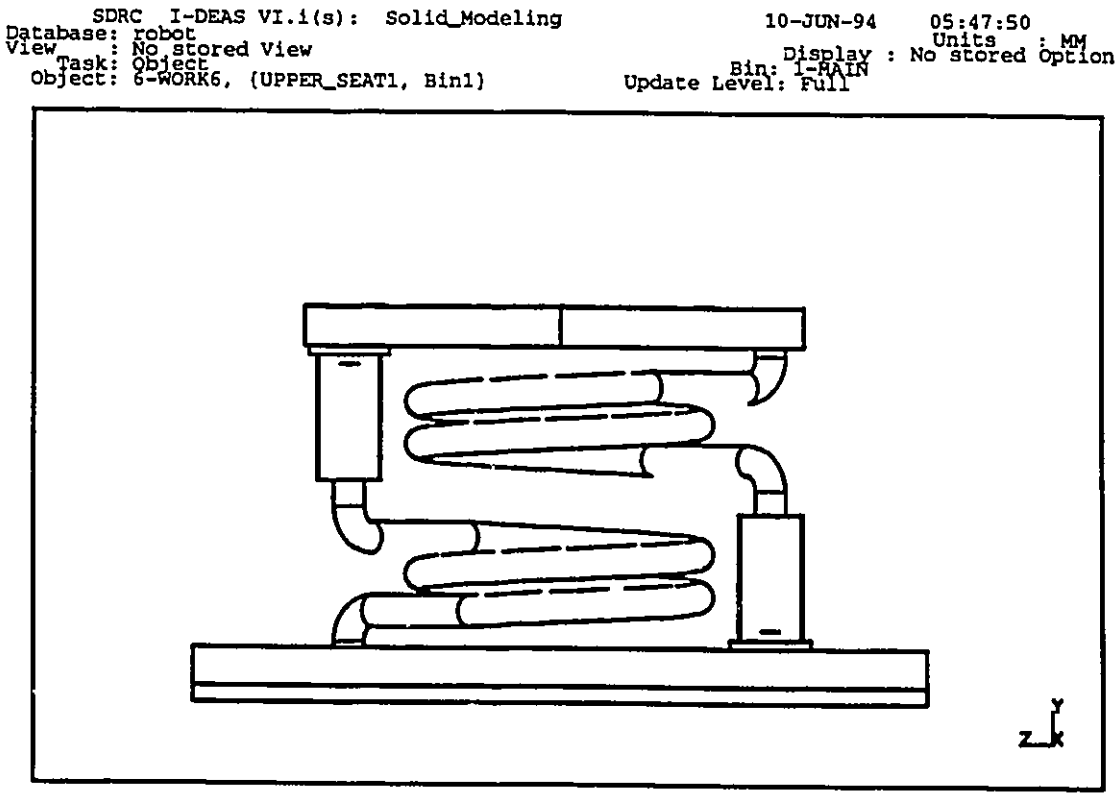

Fig. A.2 First joint flexible construction

1. Position mode ➧ I–PD or P with 150 ns width minimum pulse.

2. Velocity mode ➧ analog ±8 volt

3. Torque mode ➧ analog ±8 volt

In the torque mode, which is used in all reported experiments, none of the servo gains are active. The current flowing to the motor is controlled according to a current command voltage (±8 volt) from the higher level controller. Table A.3 summarizes the motor specifications.

Table A.3 Motors specifications

	DM1100A	DM1030B
Peak torque (N.m)	100.0	30.0
Rated speed (rps)	1.0	2.0
Rotor inertia (kg.m^2)	0.119	0.015
Max. steps/rev.	1024000	655360
Motor weight (kg)	19.0	7.5
Axial compression load (lbs)	8800	6600
Axial tension load (lbs)	4400	2200

A.3 The sensors

The robot is equipped with four encoders and a force/torque sensor. The two encoders, built in the direct drive motors, provide angular positions of the motors. The links angular positions are measured by two external encoders located after the flexible joints. Table A.4 summarizes the encoder specifications.

Table A.4 Encoders specifications

	Motor 1	Motor 2	Link 1	Link 2
Pulses/rev	1024000	655360	32000	32000
Output Speed (KHz)	A/B 750	A/B 750	A/B 100	A/B 100

The force/torque sensor manufactured by Assurance Technologies Inc. (ATI), it is the metric model 130/10 with its F/T controller. The controller converts the strain gauge data to Cartesian force/torques outputs. Communications can be performed through the serial I/O, the discrete I/O, the optional parallel I/O, or the optional analog Output. In the current configuration, the optional analog output is used. This option enables faster communication and sampling speeds. The "fast mode" of the analog output allows a speed of 1.9 KHz when reading 3 axes and 1.0 KHz when reading the 6 axes. In addition, raw gauge data is available at 2.5 KHz. A start–up macro is used to initialize the system, set the communication, and set the bias for the 6 axes. The following table summarizes the force/torque sensor specifications.

Table A.5 Force/Torque Sensor specifications

	Model 130/10
Sensing ranges Force (N) Torque (N.m)	 ±130 ±10
Resolution Fx,Fy (N) Fz (N) Tx,Ty,Tz (N.m)	 0.1 0.2 0.005
Stiffness Kx,Ky (N/m) Kz (N/m) Ktx,Kty (N.m/rad) Ktz (N.m/rad)	 8.8E6 17E6 10E3 16E3
Transducer weight (grams)	175

APPENDIX B

KINEMATICS

This appendix contains a description of the kinematics for the experimental two–link flexible joint robot manipulator. Included are: a description of the coordinate frames used, the kinematic and inverse kinematic relations, and the relations for the velocities, accelerations, jerks and jerk first derivatives expressed in the different frames. Finally, the appendix concludes with a description for the measured force transformations.

B.1 Coordinate Frames

As described in Chapter 4, there are four different coordinate frames used in describing the kinematics of the manipulator. These four frames are:

1. The reference frame X, Y, Z
2. The joint space q_1, q_2, q_{m1}, q_{m2}
3. The force sensor frame X_f, Y_f, Z_f
4. The constraint frame X_t, Y_t, Z_t

B.2 Transformations between the Joint Space and the Reference Frame

Since the manipulator is planar, only two coordinates are sufficient to describe any point in the mechanism as given by the following vectors:

– for the joint space $q = [q_1, q_2]^t$

– for the task space $X_r = [x_r, y_r]^t$

– for the constraint frame $X_t = [x_t, y_t]^t$

– for the force sensor, the three coordinates are required because the measured forces are not in the plane of motion.

- The Forward Kinematics

$$X_r = L(q) \tag{B . 1}$$

where

$$L(q) = \begin{bmatrix} l_1 \cos q_1 + l_2 \cos(q_1 + q_2) \\ l_1 \sin q_1 + l_2 \sin(q_1 + q_2) \end{bmatrix}$$

- Inverse Kinematics

The transformations between the reference frame coordinates and the joint space coordinates are generally not unique. As shown in figure B.2, two different sets of joints angles yield the same end–point position for the two–link manipulator. However, the correct set can be determined by tracing the sign of the second link angle. A closed form inverse kinematics solution exists and is best described algorithmically by:

$$\cos(q_2) = \frac{x_r^2 + y_r^2 - l_1^2 - l_2^2}{2 l_1 l_2} \tag{B . 2}$$

$$sin\ (q_2) = \pm \sqrt{1 - \cos(q_2)} \tag{B . 3}$$

$$q_2 = atan2\ (sin\ (q_2), \cos(q_2)) \tag{B . 4}$$

$$T_1 = x_r\ (l_2 \cos(q_2) + l_1) + y_r l_2 \sin(q_2) \tag{B . 5}$$

$$T_2 = y_r\ (l_2 \cos(q_2) + l_1) - x_r l_2 \sin(q_2) \tag{B . 6}$$

$$\cos(q_1) = \frac{T_1}{\sqrt{T_1^2 + T_2^2}} \tag{B . 7}$$

$$sin(q_1) = \frac{T_2}{\sqrt{T_1^2 + T_2^2}} \tag{B . 8}$$

$$q_1 = atan2\ (sin\ (q_1), \cos(q_1)) \tag{B . 9}$$

- Velocity and higher order derivatives transformations

The velocity, acceleration, jerk and jerk first derivative are required to be transformed from the joint space to the reference frame. These transformations can be obtained directly by differentiating the forward kinematic relation given by equation B.1 to yield:

$$\dot{X}_r = J\,\dot{q} \tag{B . 10}$$

$$\ddot{X}_r = J\,\ddot{q} + \dot{J}\,\dot{q} \tag{B . 11}$$

$$\overset{3}{X}_r = J\,\overset{3}{q} + 2\,\dot{J}\,\ddot{q} + \ddot{J}\,\dot{q} \tag{B . 12}$$

$$\overset{4}{X}_r = J\,\overset{4}{q} + 3\,(\dddot{J}\,\ddot{q} + \dot{J}\,\overset{3}{q}) + \overset{3}{J}\,\dot{q} \tag{B . 13}$$

where J is the manipulator Jacobian and is given by:

where

$$J = \begin{bmatrix} -l_1 \sin q_1 - l_2 \sin(q_1 + q_2) & -l_2 \sin(q_1 + q_2) \\ l_1 \cos q_1 + l_2 \cos(q_1 + q_2) & l_2 \cos(q_1 + q_2) \end{bmatrix}$$

- Inverse velocity and higher order derivatives transformations

The inverse of the above forward transformations requires only the inverse of the manipulator Jacobian. Thus:

$$\dot{q} = J^{-1}\,\dot{X}_r \tag{B . 15}$$

$$\ddot{q} = J^{-1}\,[\ddot{X}_r - \dot{J}\,\dot{q}] \tag{B . 16}$$

$$\overset{3}{q} = J^{-1}\,[\,\overset{3}{X}_r - 2\,\dot{J}\,\ddot{q} - \ddot{J}\,\dot{q}\,] \tag{B . 17}$$

$$\overset{4}{q} = J^{-1}[\overset{4}{X}_r - 3\,(\dddot{J}\,\ddot{q} + \dot{J}\,\overset{3}{q}) - \overset{3}{J}\,\dot{q}] \tag{B . 18}$$

B.3 Transformations between the Force Sensor Frame and the Reference Frame

The transformation of the measured forces from the force sensor frame to the reference frame is performed through two successive kinematic transformations. The first trans-

formation is to rotate the components of F_{xm} and F_{ym} about the force sensor axis Z_f into the plane of the manipulator motion as follows (see figure B.3):

$$\begin{bmatrix} F_{xm} \\ F_{ym} \end{bmatrix} = \begin{bmatrix} \cos a_1 & -\sin a_1 \\ \sin a_1 & \cos a_1 \end{bmatrix} \begin{bmatrix} F_{xf} \\ F_{yf} \end{bmatrix} \qquad (B.19)$$

The second transformation is to rotate the planar components of the measured forces into the reference frame about the reference frame axis Z axis as follows (see figure B.4):

$$\begin{bmatrix} F_y \\ F_x \end{bmatrix} = \begin{bmatrix} \cos a_2 & -\sin a_2 \\ \sin a_2 & \cos a_2 \end{bmatrix} \begin{bmatrix} F_{zf} \\ F_{xm} \end{bmatrix} \qquad (B.20)$$

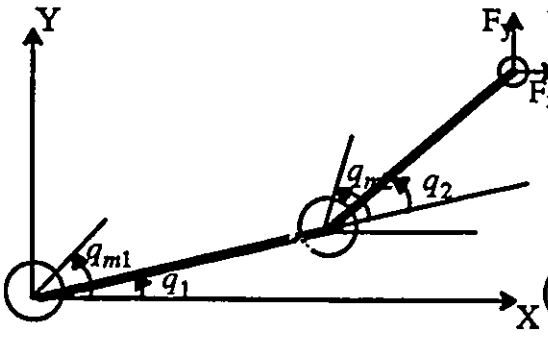

Fig. B.1 Coordinates of the experimental robot kinematics

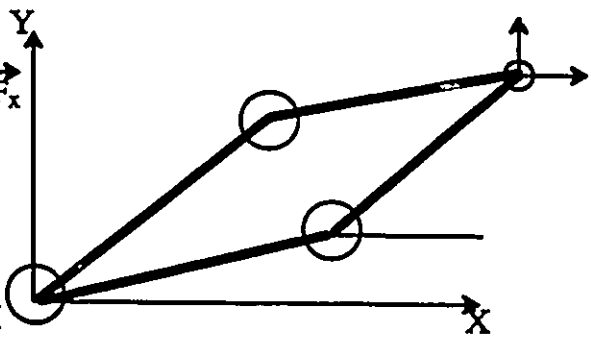

Fig. B.2 Inverse kinemtics configurations

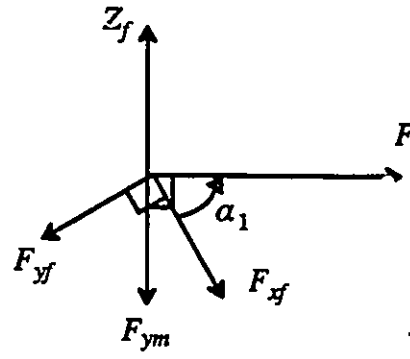

Fig. B.3 Forces first rotation

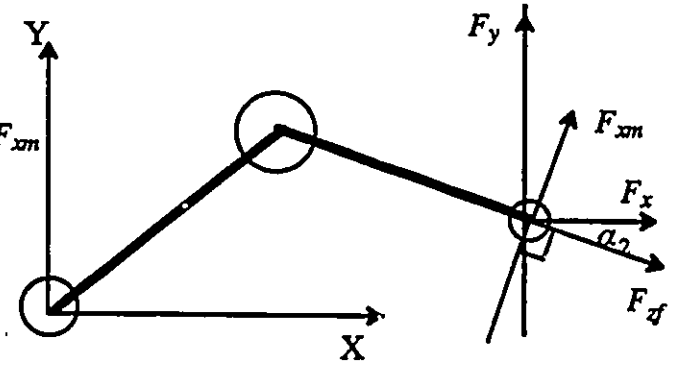

Fig. B.4 Forces second rotation

APPENDIX C

VELOCITY ESTIMATION AND FILTERING

In this appendix, an algorithm describing the computation of the angular velocities of the links and motors using the encoder measured position is described. Also, a first order filter used in conjunction with the velocity estimation is described.

C.1 Velocity Estimation

After considering several velocity estimation techniques used in experimental robotic systems, the Gear's algorithm was chosen as it provides the velocity estimation with zero–delay. When using five points approximation, the algorithm is given by:

$$\dot{q}_k = c_f \left(c_0\, q_k + c_1\, q_{k-1} + c_2\, q_{k-2} + c_3\, q_{k-3} + c_4\, q_{k-4} \right) \qquad (C.1)$$

where

Δt is the sampling period

$$c_f = \frac{1}{12\,\Delta t} \quad , \quad c_0 = 25.0 \quad , \quad c_1 = -48.0$$

$$c_2 = 36.0 \quad , \; c_3 = -16.0 \quad \text{and} \quad c_4 = 3.0$$

C.2 Filtering

Experimental observations suggested the application of a first order filter to enhance the velocity estimate by removing undesirable high frequency components. A simple low–pass first order filter is chosen, it is given by:

$$G_f(s) = \frac{s}{s + a_f} \qquad (C.2)$$

where a_f is the cut–off frequency which is chosen to be 125.0 rad/s.